APPLICATION OF COMPUTERS

IN FATIGUE ANALYSIS

January 1985

Turan DIRLIK

Ph.D. Thesis submitted to

Department of Engineering

University of Warwick

Coventry, England

ACKNOWLEDGEMENTS

I am most sincerely grateful to Dr. F. Sherratt, not only for providing the research subject and for his most generous advice and guidance, but also for his never-ending encouragement and patience with me throughout my years as a student.

I also wish to thank Mr. A. Redhead, the Chief Technician, for his expert advice and help over many practical issues, and for his kind and friendly interest in my work.

I wish to express my sincere gratitude to Miss L. H. Heah, for her unwavering moral support and faith in me.

Lastly, I am much indebted to Mrs. C. Gow for typing this thesis at such short notice and to Miss N. Gvero for additional assistance.

SUMMARY

The availability of minicomputers and microprocessors, at a reasonable cost, has provided a significant stimulus in a critical appraisal of fatigue testing and analysis methods. This thesis reviews and extends some of the recent fatigue analysis methods. Two major areas investigated in detail are cycle counting methods and methods for prediction of fatigue life to crack initiation.

The three recent counting methods, range-pair, Wetzel's and rainflow, which avoid the distortion and inaccuracy from which the traditional cycle counting methods suffer, are described and compared with each other to find out the similarities and differences between them. It is shown that if a service loading history starts and ends at an extreme peak, then all the three methods give an identical count. All relevant methods for the description of measured service histories are reviewed critically in connection with fatigue life assessment, service history regeneration and simulation.

Confidence in the rainflow method for better fatigue life predictions and increased use of analytical methods like Finite Element analysis offering frequency domain information about a component have initiated a search for a link between rainflow counting and the power spectral density of a stationary and ergodic random process. Using a Monte Carlo approach and digital simulation techniques, the thesis presents a link in the shape of a closed-form expression which defines the probability density function of rainflow counted ranges for any given power spectral density. A closed-form expression for the distribution of ordinary ranges is also presented.

Methods of predicting fatigue crack initiation life under variable amplitude loading are reviewed. From the basic ingredients of the local-strain approach, various life prediction procedures are assembled methodically with regard to how the local stress and strain are determined for a given load level, how the local stress and strain are linked to the life, and how the mean stress effect is accounted for.

Predictions made by these methods are compared with the published test data; however predictions are compared mostly within themselves in order to highlight the differences between methods. It is shown that under certain circumstances, some methods give very erroneous results. A sensitivity analysis is carried out to examine how sensitive various methods are to changes in the material properties. A new procedure of determining the material properties from the experimental data is proposed.

CONTENTS

CHAPTER 1

INTRODUCTION

Fatigue in materials is the process by which repeated application of a load, less than the one needed to break a component by a single application, eventually leads to the mechanical failure of that component. At the microscopic level the process generally depends on crystal imperfections, which are increased in number by repeated straining and at the same time collected to preferred sites. Eventually this slip-driven process creates a major discontinuity in the crystal, which continues to grow and becomes a crack, propagating then by an opening and closing mechanism linked to principal tensile stresses.

Many researchers have aimed at clarifying the major factors and mechanisms relevant to fatigue failure, ranging from investigations on the atomic scale of 10^{-7}mm to those on the scale of a few metres on engineering structures. The research on a near-atomic scale by physicists and metallurgists has as yet produced little knowledge which can be usefully employed in practical engineering designs. Recent progress in both understanding and designing against fatigue has emerged by investigations at more appropriate levels of physical scale, mainly by using empirical laws.

Engineers have been faced with the problem of predicting when fatigue will occur in a component, since cyclic loading first caused

unexpected metal failures in the railway industry in the middle 1800's[1]*. In the early days of fatigue analysis, it was widely believed that there existed some critical level of stress below which no damage was done to the specimen. Finding this fatigue limit, or endurance limit was then the main target of fatigue tests, and good design kept all applied stresses below this so that no damage would occur. Although there are still some structures designed with the safe-life method, recent years have seen radical changes of emphasis in the design of engineering components. In an increasing number of cases it is no longer commercially acceptable to manufacture products which are functional but overdesigned. The conflicting requirements of maintaining the demand on reliability imposed by the consumer-oriented society and the drive for an economic design place considerable pressure on traditional design techniques. The objective in the development of a modern design approach for critically-stressed components is the accurate assessment of the damage caused by the elements of the service history.

The simplest way of getting fatigue data about a component is to put it in a test machine which will load it repeatedly until it breaks. Recording of the number of cycles to failure, N_f, at different levels of stress amplitude, S, yields the basic form of fatigue data which is universally referred as the S/N curve. Normally the test load in obtaining S/N curves is sinusoidal. However, there are very

---

*Numbers in brackets designate References at the end of each chapter.

few cases where the service load can be so easily described, like eccentric masses rotating at a constant speed. In all other cases, the description of the fatigue loading environment is a complex problem. The difficulty is in foreseeing the future range of service loads which the unit is expected to survive.

For many years the experimental procedures used to investigate the fatigue performance of structural materials and configurations have almost exclusively been limited to artificial and much simplified loadings. Fatigue testing has profited greatly from recent innovations in equipment technology. For example, the introduction of the modern electrohydraulic testing machines has made it possible to meet more complex experimental requirements, to produce a much better simulation of the actual service conditions. Another big step in understanding the fatigue phenomenon has been the introduction of computers into fatigue testing and analysis.

Applications of computers in fatigue are quite numerous. Typical application ranges cover structural and materials testing, data acquisition and reduction, and the bulk of computer usage, cumulative damage calculations. Computers do not only replace conventional single purpose devices, but offer new possibilities for the performance and organization of fatigue testing. In addition to providing a variety of program waveforms, including a realistic simulation of actual service conditions, a computer can monitor test variables such as load, strain, temperature, and also ensures that the test conditions are maintained. While certainly not a 'cure all' for many problems and complexities

associated with fatigue performance evaluation, when properly implemented, computers can effectively extend testing facilities, improve efficiency and quality of data acquisition and analysis procedures. Computers offer an attractive approach to fatigue in terms of capability, versatility, reliability, accuracy and cost. The recent advances in manufacturing technology have brought down the size and cost of processors to very modest levels giving added impetus to the application of computers in fatigue.

The increasing availability of minicomputers and microprocessors and associated peripherals at a relatively low cost makes it necessary to re-evaluate approaches to fatigue testing and analysis. Obviously it is beyond the scope of this research to cover the whole range of computer based applications, however the principal ways in which computers might assist in fatigue analysis are investigated. Since the trend is towards improved realism, fatigue performance analysis is likely to remain a complex activity and a computer approach may be the only way of meeting the ever increasing demands on reliability and economy.

Cumulative damage calculations occupy a dominant sector of fatigue analysis; hence the bulk of computer applications in fatigue lie in this area. In order to achieve a high level of structural reliability, fatigue life predictions have to be made at several stages of the design and development process. An important aspect of the development of fatigue resistant structures is the ability to predict component life and thus anticipate possible problems. Good agreement

between predicted fatigue lives and actual fatigue lives obtained from tests gives a greater confidence in a design and may eliminate the need for retesting improved designs.

Due to increased research activities of the past a large amount of fatigue data was produced and offered for design applications. To show the extent of this interest Watson and Rebbeck[1] record 7000 papers published on the subject in the last 20 years, in 1975. Considering the 180-year long history of fatigue research, the vast amount of papers published and the diversity of interests, the formidable task of literature survey is not attempted here. Readers may find various state-of-the-art surveys in the literature. Swanson[2] describes randomized sequence constant amplitude and actual random load fatigue testing, acoustic fatigue and random load crack propagation. Schijve[3] looks at the problems in aircraft structures and materials - fatigue damage and interaction effects, crack propagation under flight simulation loading. Dowling[4] discusses some of the failure prediction methods for complicated stress-strain histories, and mean stress and load-sequence effects. The same effects are reviewed by Nelson[5] from a fracture mechanics point of view: prediction methods of fatigue crack growth. In more recent papers, Morrow and Socie[6] trace the historical evolution of the local stress-strain approach for predicting the fatigue life of components in service. Haibach[7] also reviews some basic types of fatigue data available for use with existing procedures and emphasizes the practical need of different approaches in making fatigue assessment. Sherratt[8], in a series of 4 articles, provides a survey of the

current position on fatigue life estimation methods, points to parts of traditional design which are still in use, and gives enough details of the new methods - fracture mechanics, local stress-strain approach and vibration - to allow engineers to use them properly.

The literature dealing with metal fatigue and cumulative damage contains much new knowledge bearing on improved life prediction techniques. From a practical point of view, it is not sufficient to be aware of the fatigue phenomenon, to know about the parameters affecting the fatigue properties of materials and structures. It is one thing to observe and register a manifestation and another to express this knowledge in the pragmatic terms needed to put it to work making in-service life predictions.

The situation does not become easier due to various fatigue life prediction procedures recommended in the literature, such as the nominal stress approach requiring conventional S/N data, the local stress-strain approach requiring strain-life data, the fracture mechanics approach requiring cyclic stress-strain and crack propagation data. Furthermore, each of these procedures exists in several modifications, differing in terms of accuracy and/or in terms of simplicity in application. Considering the diversity of interests, such as the design of aircraft, ground vehicles, bridges, off-shore structures, and numerous type of materials used, it is not surprising that no generally accepted procedure for predicting fatigue performance has been accepted up to now. Nor does it seem possible to indicate

such a universal procedure in the future. Selection of the appropriate procedure of fatigue life estimation depends to a large extent on the level of input information available. Life predictions made by new procedures need to be reconciled both with experience and with simpler, long established methods.

In many cases, the present commonly used methods are adequate; if this was not so, it would not be possible to design against fatigue at all. However, since fatigue is the commonest cause of component failure, there are evidently still problems to be solved. Just as present methods are the result of a series of modifications to the earlier ones, so improved techniques will come about by incorporating those new ideas which are relevant and useful. Fatigue research has to be considered as attempting to solve parts of these problems, making small additions and changes to established techniques, so that the user has available to him methods which are valid for an ever widening range of problems. Starting from this philosophy, only one, but quite an important one, aspect of fatigue analysis, namely fatigue life estimation, was concentrated on in this research. This subject was further narrowed down to exclude the crack propagation part of fatigue life estimation, because it was deemed that fracture mechanics is a major area of research on its own right. Therefore, the term 'fatigue life estimation' used in this thesis refers to, unless otherwise stated, prediction of fatigue life to crack initiation.

In any cumulative damage calculation, including the fracture mechanics approach, there is a stage where the load history has to be

reduced into discrete cycles which can then be used to calculate their damaging effect. Three widely used cycle counting methods are described in detail in Chapter 2. Their use and limitations, and a comparison of them with the other simpler cycle counting methods are discussed not only from a damage calculation point of view, but also from a service history regeneration and simulation point of view.

Since its introduction 10 years ago, the rainflow cycle counting method has been shown to be superior and yields the best fatigue life estimates. In Chapter 3, a link is proposed between fatigue life estimation based on rainflow range distributions and the power spectral density of a stationary and ergodic random process. The link is in the form of a distribution function of rainflow-counted ranges for a given power spectral density. Using a Monte Carlo approach and digital simulation methods, probability density functions of rainflow ranges are obtained for various power spectra, and from observed data a closed-form expression for the rainflow-range probability density functions is proposed. As a by-product of this study, probability density functions of ordinary ranges - the distance between consecutive peaks and troughs - are also determined and a closed-form expression for the ordinary ranges is put forward.

After describing the traditional nominal stress methods of estimating fatigue life, in Chapter 4, the basic ingredients of a more recent approach, the local stress-strain method, are discussed. From these ingredients various life prediction procedures are assembled. The reasons why there are many ways of relating the local stress and

strain to the life using the same set of data are investigated, and the choices a would-be-user has to make are outlined methodically.

In Chapter 5, predictions using the methods described in Chapter 4 are compared with the well-documented test data published in the literature. However the predictions are compared mostly with each other in order to gain insight into the potential variability of the life prediction methods, to highlight the significance, utility and implication of various alternatives. The question of how sensitive the prediction methods are to variations in cyclic material properties and the effect of mean stresses on life calculations are analysed in detail.

Although relevant discussions and conclusions are included at the end of each chapter, overall implications of this research and directions for future improvement are outlined in Chapter 6.

REFERENCES

1. Watson, P., Rebbeck, R. G. "Modern Methods of Fatigue Assessment", Railway Engineering Journal, Ins. of Mech. Engrs., London, 1975

2. Swanson, S. R. "Random Load Fatigue Testing: State of the Art Survey", Materials Research and Standards, MTRSA, Vol. 8, No. 4 pp. 10-44, Apr. 1968

3. Schijve, J., "Cumulative Damage Problems in Aircraft Structures and Materials", The Aeronautical Journal of the Royal Aeronautical Soc., Vol. 74, pp. 517-532, June 1970

4. Dowling, N. E., "Fatigue Failure Predictions for Complicated Stress-Strain Histories", Journal of Materials, JMLSA, Vol. 7, No. 1, pp. 71-87, March 1972

5. Nelson, D. V., "Review of Fatigue Crack Growth Prediction Methods", Experimental Mechanics, Vol. 17, No. 2, Feb. 1977

6. Morrow, J., Socie, D. F., "The Evolution of Fatigue Crack Initiation Life Prediction Methods", Proc. of Fatigue '81 SEE Conference, held at Warwick University, England, March 1981

7. Haibach, E., "Fatigue Data for Design Appliations", Proc. of Fatigue '81 SEE Conference, held at Warwick University, England, March 1981

8. Sherratt, F., Reprint of 4 articles published in the Jr. of Soc. of Environmental Engineers, Dec. 1982, March, Sept., Dec., 1983
   i) "Fatigue Life Estimation: A Review of Traditional Methods"
   ii) "Fatigue Life Estimation Using Simple Fracture Mechanics"
   iii) Eaton, D., "Fatigue Life Estimation by Local Stress-Strain Methods"
   iv) "Vibration and Fatigue: Basic Life Estimation Methods"

CHAPTER 2

AN OVERVIEW OF CYCLE COUNTING AND RAINFLOW

An essential step in the prediction of the fatigue life of components or structures is the reduction of a service stress or strain history to a series of cycles or half-cycles, reversals. This process is known cycle counting and can be the source of large errors in the subsequent fatigue life calculation. There are three cycle counting methods widely used in recent years which avoid the distortion and inaccuracy from which the traditional methods suffer. These three methods produce similar, but not necessarily identical cycle counts for all types of service histories. Moreover, each of these methods exists in several variations. The choice of a particular method also depends on the purpose of cycle counting. The fundamental purpose of cycle counting is to extract cycles from a service history in order to calculate their damage contribution, however cycle counting methods are also used to delete small cycles from a service history for an accelerated test programme, and to obtain relevant information to generate loading signals for fatigue testing.

Although it has nothing to do with the cycle counting methods as such, a linear damage accumulation rule on which most of fatigue life prediction methods are based is presented first. After a brief description of some of the traditional cycle counting methods, the recent methods and their variations are examined in detail in order to highlight their differences and similarities. All the cycle counting methods are then reviewed critically to establish their limitations and applicability for the purposes for which they are intended.

2.1 Damage Accumulation: Miner's Rule

The basis of nearly all working methods for damage summation is surprisingly a simple hypothesis put forward first by Palmgren[1] in 1924, who proposed a linear damage law for the estimation of roller bearing life. The same idea was rediscovered later by Miner[2] in 1945, who applied it to the ordinary type of fatigue in structural components. This widely accepted Palmgren-Miner hypothesis, usually referred as Miner's Rule, assumes that if n_i cycles of load are applied to a component at a level of stress which would cause failure at N_i cycles in a constant amplitude test, then the fraction of life used is exactly proportional to n_i. Or it can be stated as that failure occurs when:

$$\sum \frac{n_i}{N_i} = 1 \qquad \text{Eq. 2.1}$$

Sometimes an arbitrary constant, generally less than 1., is substituted for unity on the right-hand side, hence an element of conservatism is introduced. There are many objections to this rule. The most obvious one is that to assume the first cycle of load applied to a virgin specimen does the same damage as a similar cycle applied near failure is an oversimplification. However the rule survives and has stood up to a good deal of use.

2.2 Cycle Counting

Whether one uses the nominal stress or the local stress-strain approach or the fracture mechanics analysis, there is bound to be a cycle counting part in each approach. The aim of the cycle counting is to reduce a complex load history into discrete cycles which can then be used to calculate their damaging effect.

Earlier reviews of counting methods[3, 4] have noted at least ten separate techniques which have been used to analyse an irregular load history. Some of the more notable ones are covered briefly below and illustrated in Fig. 2.1

Peak count:

All maximums above the mean and all the minimums below the mean are counted.

Mean crossing peak count:

Similar to peak count, only the largest peak between successive crossings of the mean is counted.

Level crossing count:

Only positive-going passes are registered at levels above the mean, and only negative-going pass below the mean. Counts at each level are cumulative.

Fatiguemeter count:

The fatiguemeter has been developed in aeronautics to record variations in acceleration. Similar to level crossing except that a count is accepted after the load crosses a preset

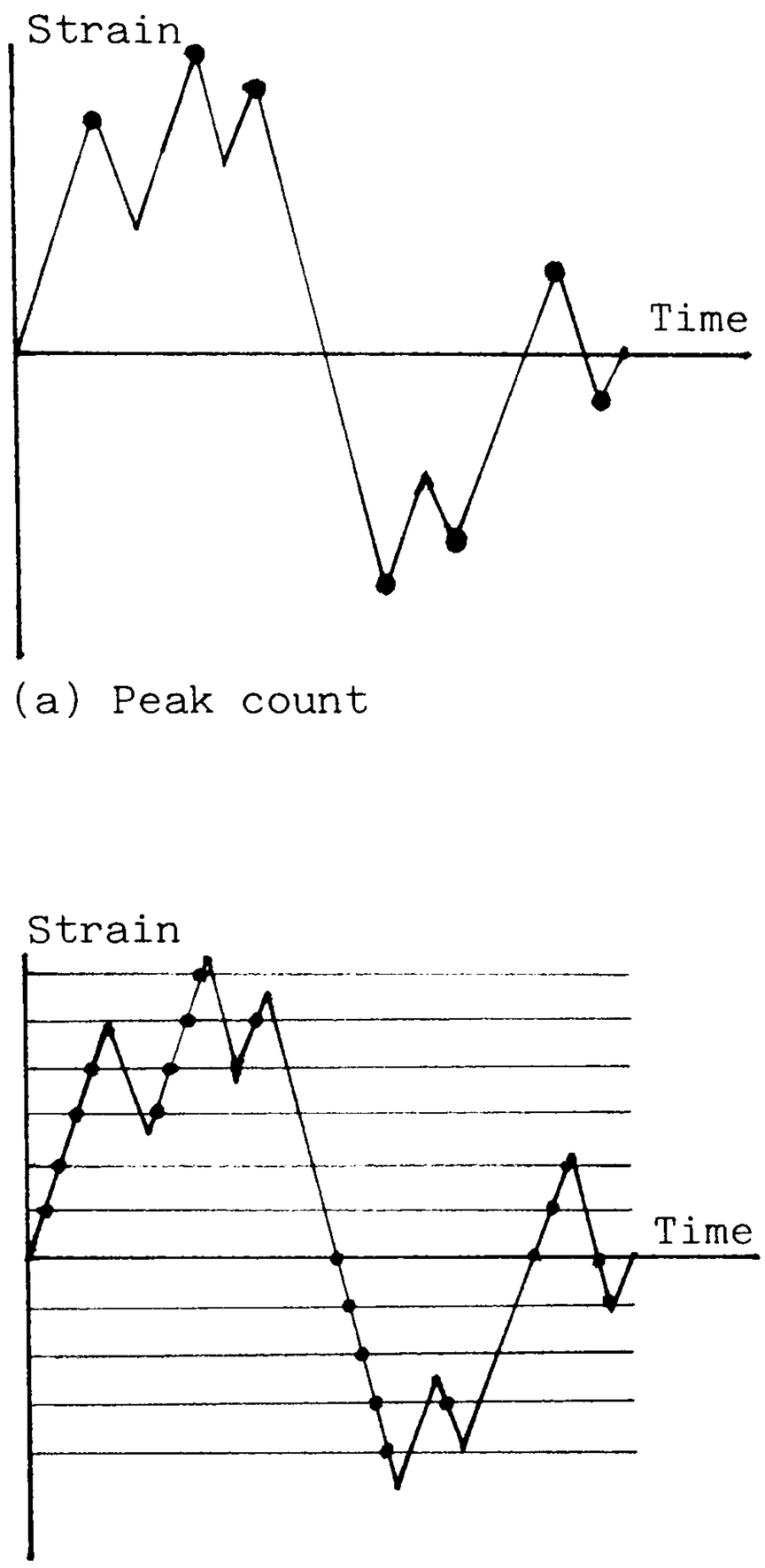

(a) Peak count

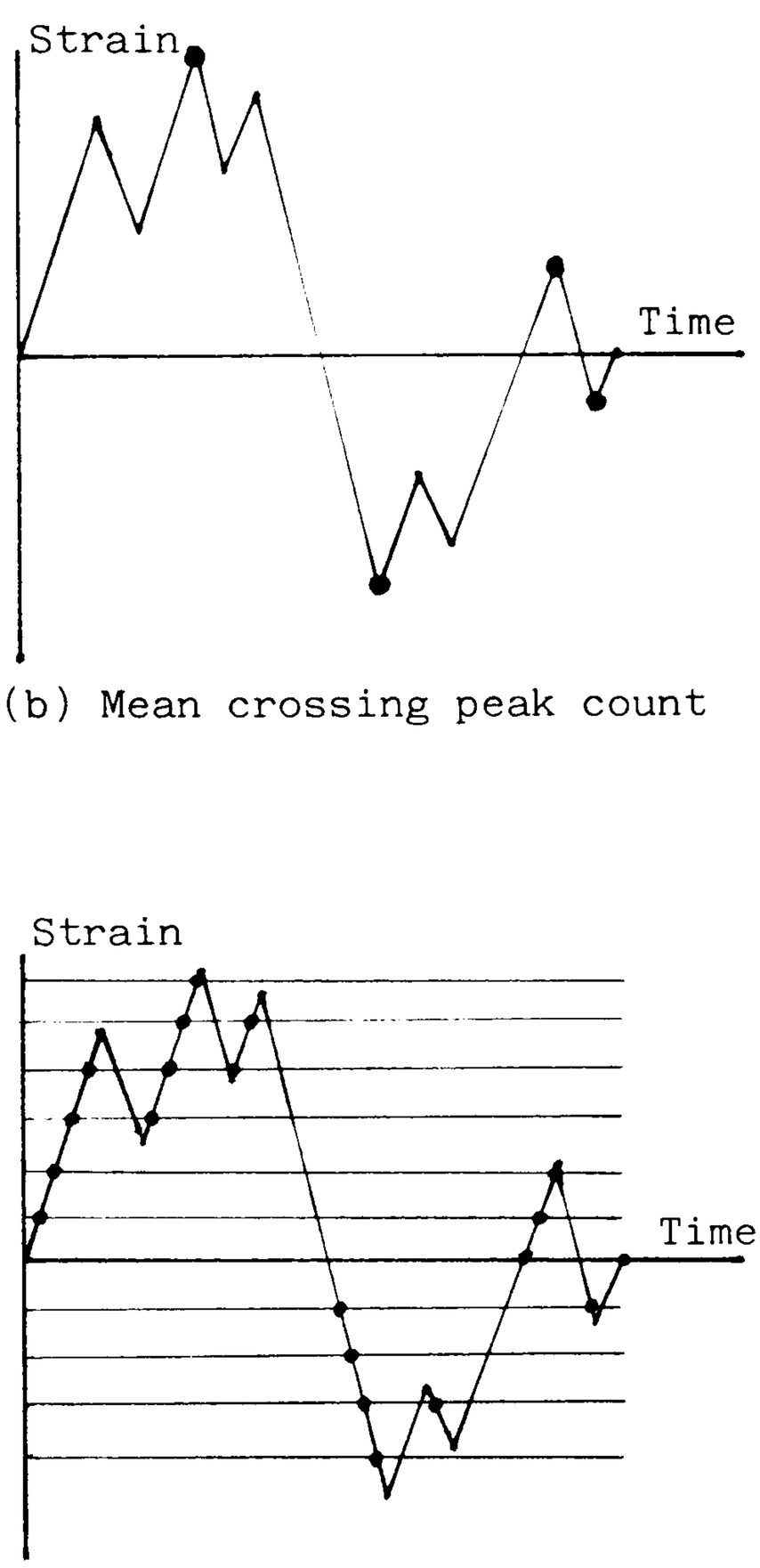

(b) Mean crossing peak count

(c) Level crossing count

(d) Fatiguemeter count

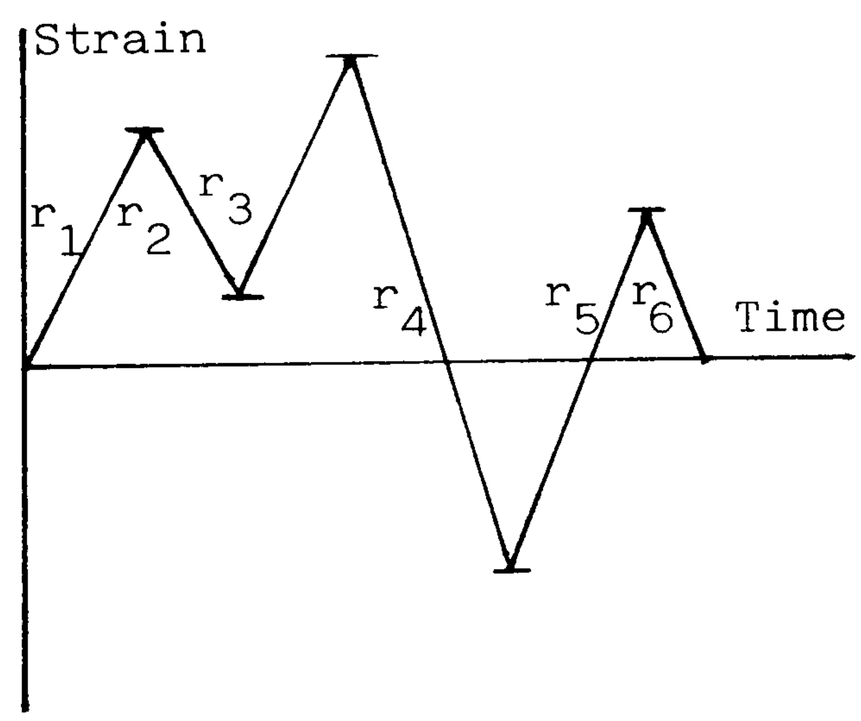

(d) Range count

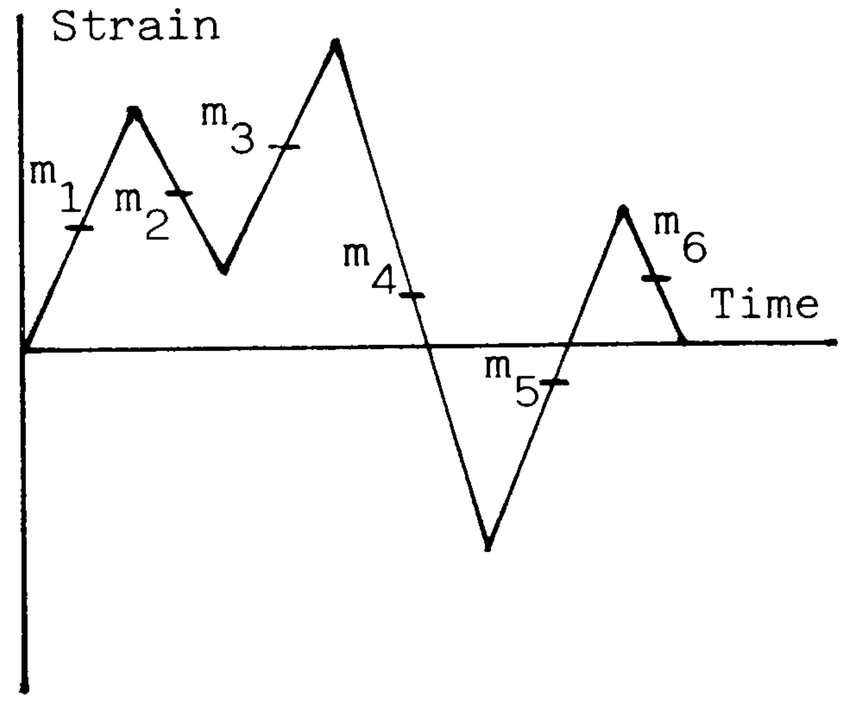

(f) Range-mean count

Figure 2.1 Some cycle counting methods

level in the downward direction. In this way small load variations, such as electrical noise, do not influence the count.

Range count:

Each range, i.e. the difference between successive peak and trough values is counted as a half cycle.

Range mean count:

Not only the value of the range, but the mean value of each range is also recorded.

However, the more recent reviews[5, 6, 7] concentrate on mainly three methods, range-pair, rainflow and Wetzel methods. The apparent reason for superiority of these methods is that they all define cycles as closed stress-strain hysteresis loops. The question "What is a cycle?" presents no problem when the loading is constant amplitude block programmes or narrow band histories. However, in the case of loadings shown in Figure 2.2, it is no longer so trivial a question. In the sequence shown in Figure 2.2(a), the small reversals do some fatigue damage that may or may not be significant compared to the damage done by the large cycle on which they are superimposed. Peak counting gives the same result for (a) and (b), but (b) is likely to be more damaging than (a). Mean crossing peak counting gives the same result for all the three cases which is non-conservative in situations where interrupting cycles become closer in amplitude to the large ones. The range and range-mean counting methods would record a series of low-amplitude cycles with

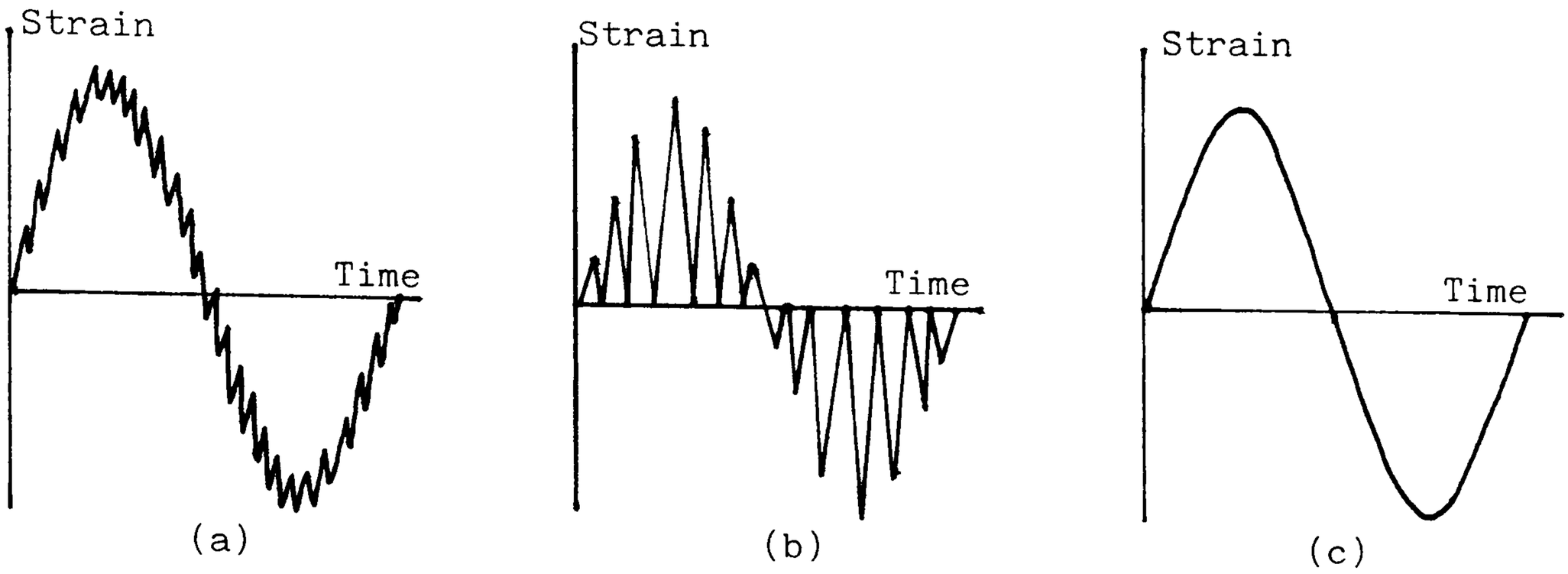

Figure 2.2 Some sequences causing problems for several counting methods[4].

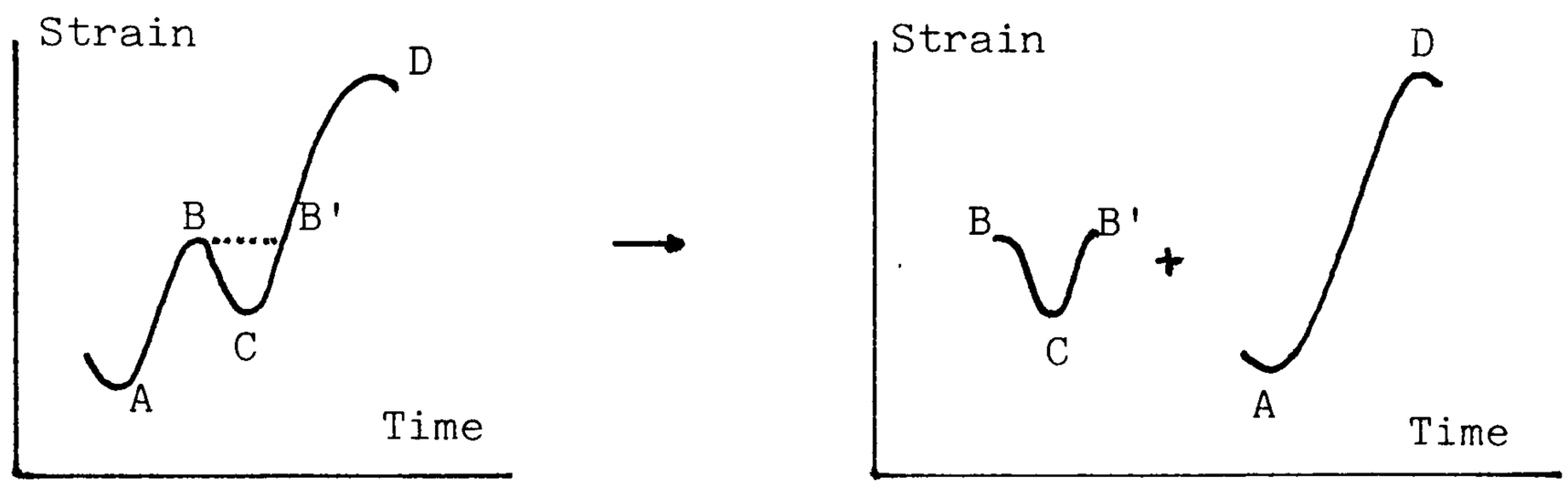

Figure 2.3 Interruption of a major cycle by a minor one.

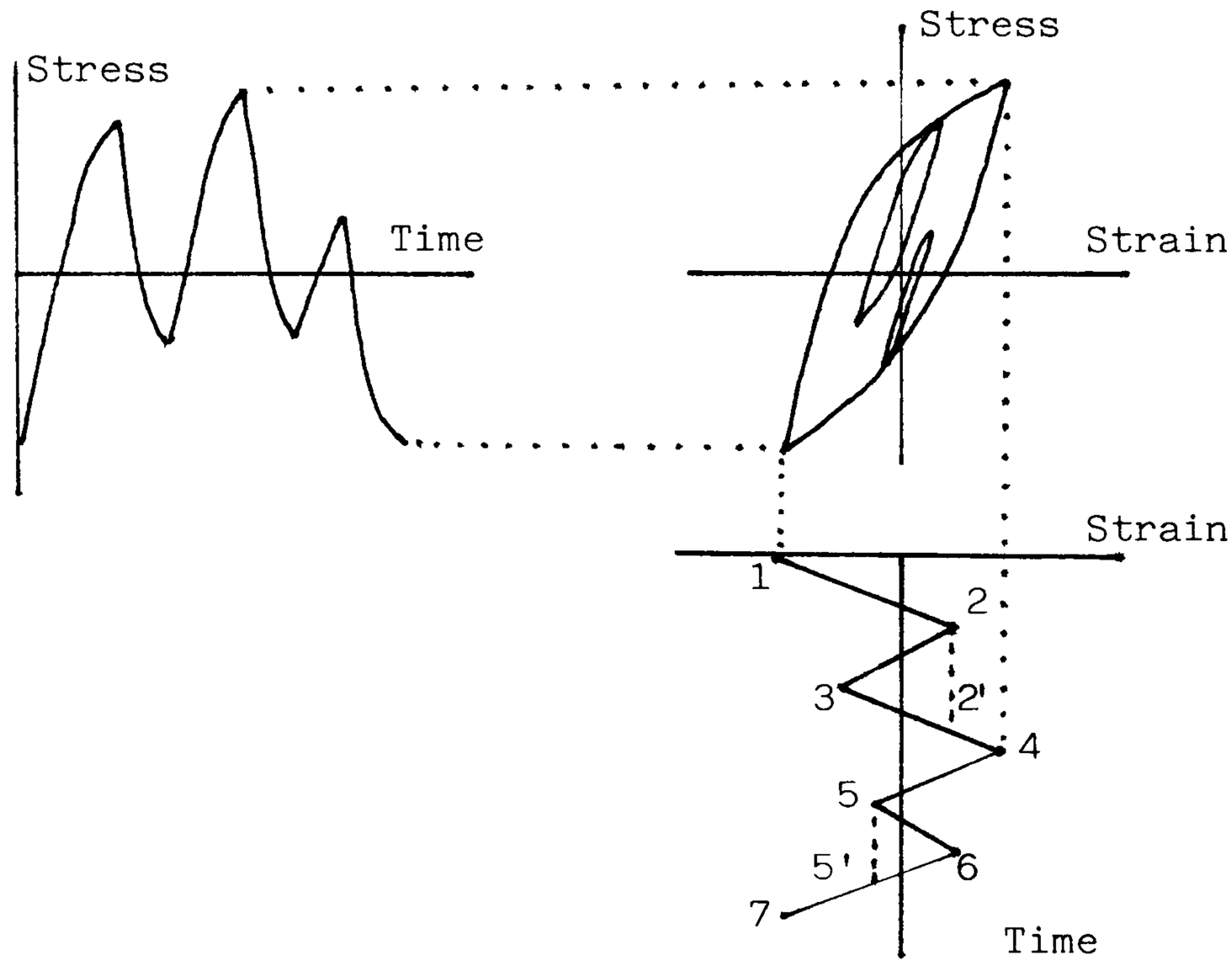

Figure 2.4 Stress and strain-time history and associated hysteresis loops.

gradually changing mean, for Figure 2.2(a) and (b), completely ignoring the existence of underlying waves of much greater amplitude and damage significance.

To show the extent of the effect of small cycle interruption the following data is extracted from the strain-life curve for Man-Ten steel[8], to predict the damage to the specimen subject to the history shown in Figure 2.3.

Let the amplitudes of AB, BC, CD and AD be 0.003, 0.001, 0.005 and 0.007 respectively, then the corresponding damage parameters i.e. reversals to failure can be extracted as 4.60×10^4, 4.61×10^6, 1.12×10^4 and 5.62×10^3 respectively from the strain-life curve. The damage calculated by an ordinary range method would be:

$$D_1 = D_{AB} + D_{BC} + D_{CD}$$

$$= \frac{1}{4.60 \times 10^4} + \frac{1}{4.61 \times 10^6} + \frac{1}{1.12 \times 10^4}$$

$$= \frac{1}{9000}$$

In other words, the specimen would fail after 9000 repetitions of such a waveform. On the other hand, if the same waveform is considered as one large half cycle AD interrupted by a small cycle BCB',then the damage would be:

$$D_2 = D_{AD} + 2 \times D_{BC}$$

$$= \frac{1}{5.62 \times 10^3} + \frac{2}{4.61 \times 10^6}$$

$$= \frac{1}{5600}$$

One way of handling the problem of small cycle interruption is to use a "gate level", "threshold" or "dead zone". It was found very early in the development of counting techniques that small amounts of noise on the record could lead to a count of a large number of small ranges. In order to avoid this a gate level was introduced, only ranges exceeding this preset level would be counted. For instance, as in Figure 2.3, had a gate greater than BC been used, then instead of three smaller ranges AB, BC and CD, only one large range AD would have been included. However, the choice of the gate level has posed a further problem, the paradox noted by many observers[5, 6, 9]. Decreasing the gate level, so that more events are counted, may result in less damage being calculated for a given loading waveform, as calculated above. Conversely, increasing the gate level may decrease the number of events counted but increase calculated damage. The only sensible approach to this problem is to try several gate levels and use the one which maximises the calculated damage, i.e., minimises the predicted life. This will give the most conservative life estimate possible with this method but this is not necessarily absolutely conservative.

There are three counting techniques mentioned earlier which

separate low and high amplitude cycles and record them in a physically meaningful way. These are range-pair, Wetzel and rainflow methods. The outstanding feature of these techniques is that counting is carried out on the basis of the stress-strain behaviour of the material considered. To exemplify this point, a brief complex strain-time and stress-time history and the stress-strain response are shown in Figure 2.4. The cycles that would be determined by these counting methods are identified by 1-4-7, 2-3-2', and 5-6-5'. Each of these cycles is a closed stress-strain hysteresis loop, consistent with those in constant amplitude tests on which life predictions are invariably based.

2.3 Range-Pair Count

There are at least two variations of this counting technique. Dowling's[5] interpretation of the range-pair counting method is that a strain range is counted as a cycle if it can be paired with a subsequent straining of equal magnitude in the opposite direction. Each peak is taken in order as the initial peak of a range, except that a peak is skipped if the part of the history immediately following it has already been paired with a previously counted range. If the initial peak of a range is a minimum, a cycle is counted between this minimum and the most positive maximum which occurs before the strain becomes more negative than the initial peak of the range. Conversely, if the initial peak is a maximum, a cycle is counted between this maximum and the most negative minimum which occurs before the strain becomes more positive than the initial peak.

Figure 2.5 illustrates the technique, the counted ranges are marked with long dashed lines and the paired ranges with short dashed lines. For example, a cycle is counted between peaks 2 and 3, peak 3 being the most negative minimum before the strain becomes more positive than peak 2. Similarly a cycle is counted between peaks 5 and 6, and the range between peaks 1 and 4 is paired with the range between peaks 4 and 7.

Livesey and Webber's[3] interpretation of the range-pair method is somewhat different in that counting is done by counters instead of pairing ranges. The full strain range is divided into equal levels, and each level is associated with a counter. Each maximum is treated as a positive range acting from the most minimum peak. All counters within this range are then cocked; those already cocked are unaffected. When a minimum detected the negative range is measured from the previous maximum. Counters within this range are triggered, thereby completing the counting action. When the absolute minimum is detected all cocked counters are triggered. The number of cycles at each strain range is obtained by subtracting the count at the next higher range from the count at the range in question.

The first reversal in Figure 2.6, starts in level-1, passes through levels-2 and 3 and stops in level-4. Hence counters 1-4 are cocked. The next reversal travels three levels triggering the first three counters. The reversal from peak 3 to peak 4 stops at level-5 which means that all counters are cocked; since counter 4 is already cocked, it is not affected. The remaining reversals are examined in

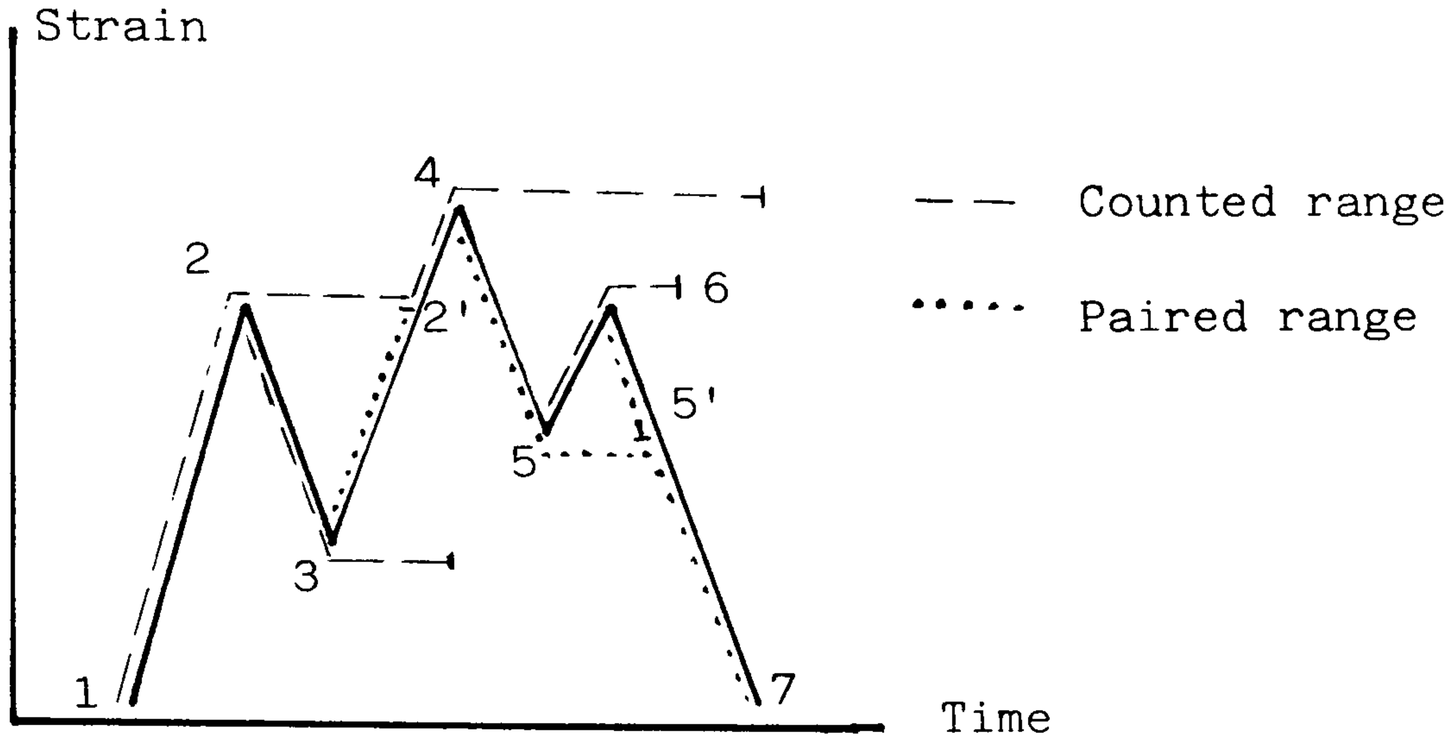

Figure 2.5 Example of range-pair counting method

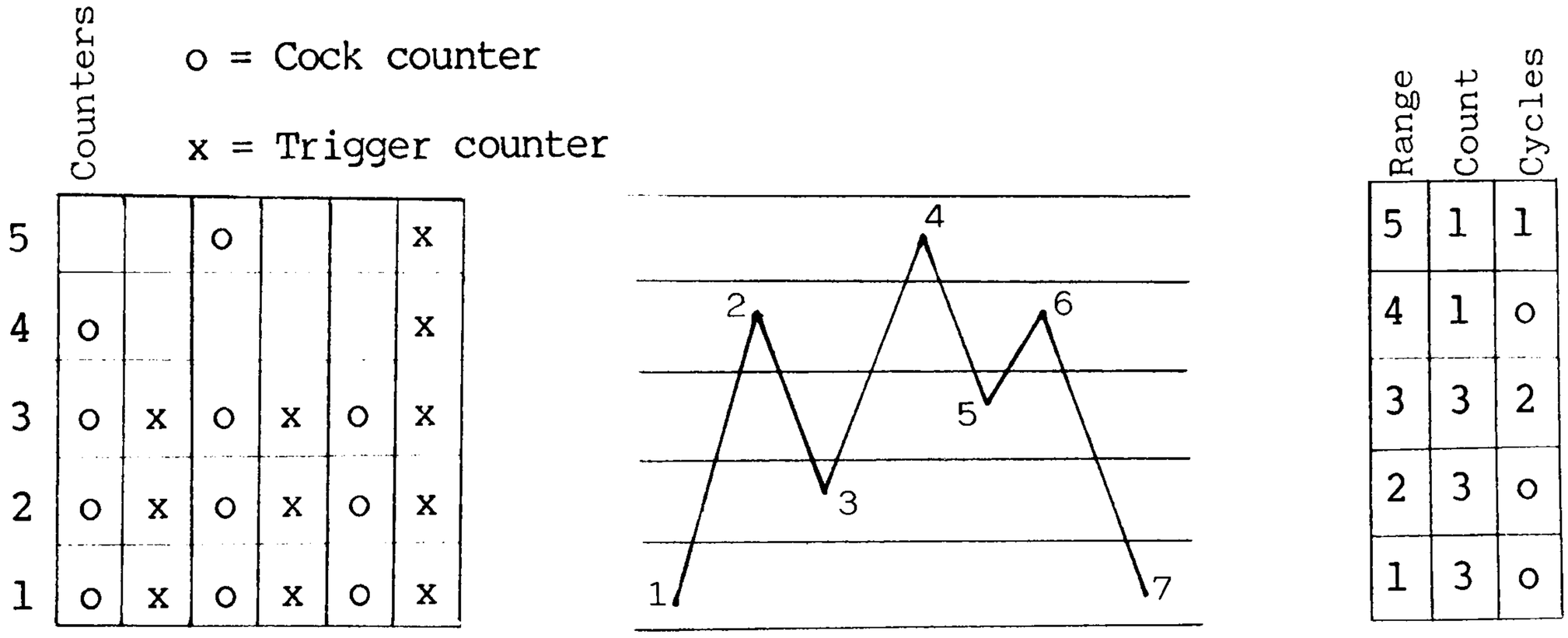

Figure 2.6 Range-pair counting by using counters.

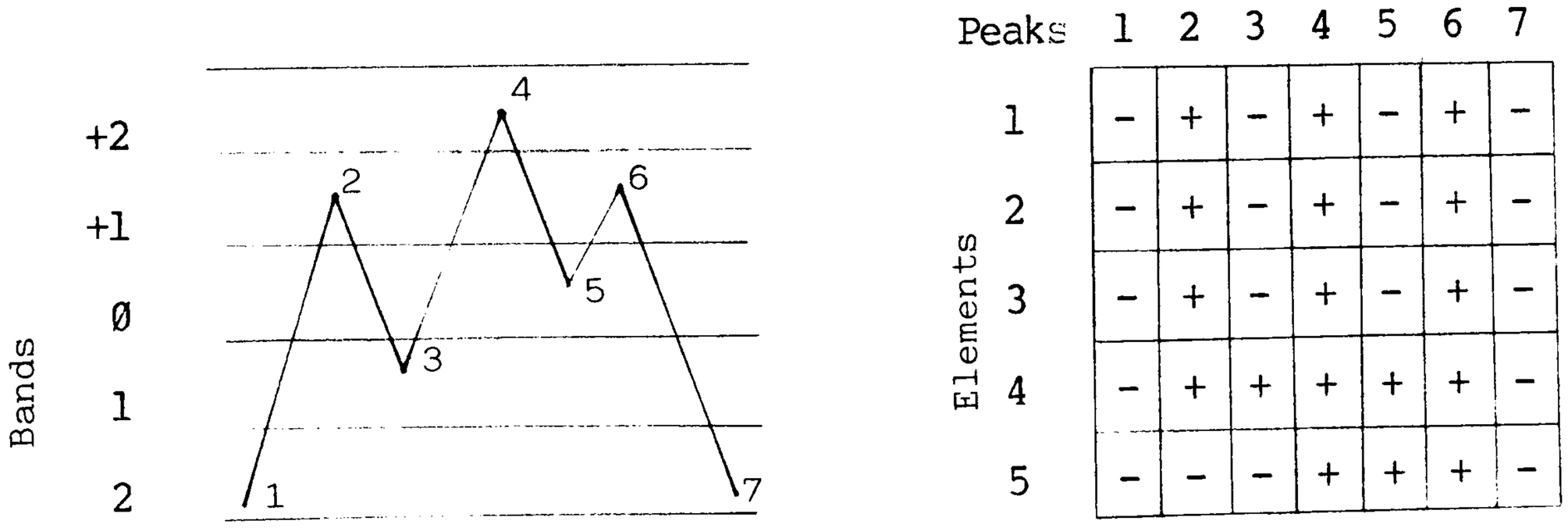

Figure 2.7 Counting of Fig. 2.5 by Wetzel's method.

the same way. Total number of triggering action at each level is counted. Then the number of cycles at each level is calculated, yielding one cycle that has a range of five levels, and two cycles of three levels.

2.4 Wetzel's Method

This counting technique developed by Wetzel[9] is very similar to the Livesey and Webber's interpretation of the range-pair method. The full strain range is divided into equal levels or "bands". Next, line segments or "elements" are used to define each reversal; the length of each element is equal to one band. The rules for using the elements follow: Starting from each reversal peak, as they occur in sequence, each element is used starting with the first, in order, to its full value if available. Each element has an "availability sign" to indicate if the element is available for the reversal under question. An element is available when its sign is opposite to the sign of the slope for the current reversal. It is likely that during the evaluation of a complex history several elements in a row may be skipped over until an available element is found. At a latter time in the analysis the skipped elements may again become available for use, but the decision comes at the instant of need.

Figure 2.7 demonstrates the application of the rules above to the same, brief history used before. The full range is divided into five bands. Since the history starts at the absolute minimum, all

the elements are initialized to (-). The first reversal, from peak 1 to peak 2, travels in the positive direction, passing through four bands. Hence the first elements are set to (+). The next reversal requires three (-) elements and changes the sign of the first three elements. The reversal from peak 3 to peak 4 needs four (+) elements. Examining the previous array reveals that elements 1,2 or 3 are available while element 4 is not available, for having the same sign. Therefore elements 1, 2 3 and 5 are set to (+), element 4 is skipped, and so on.

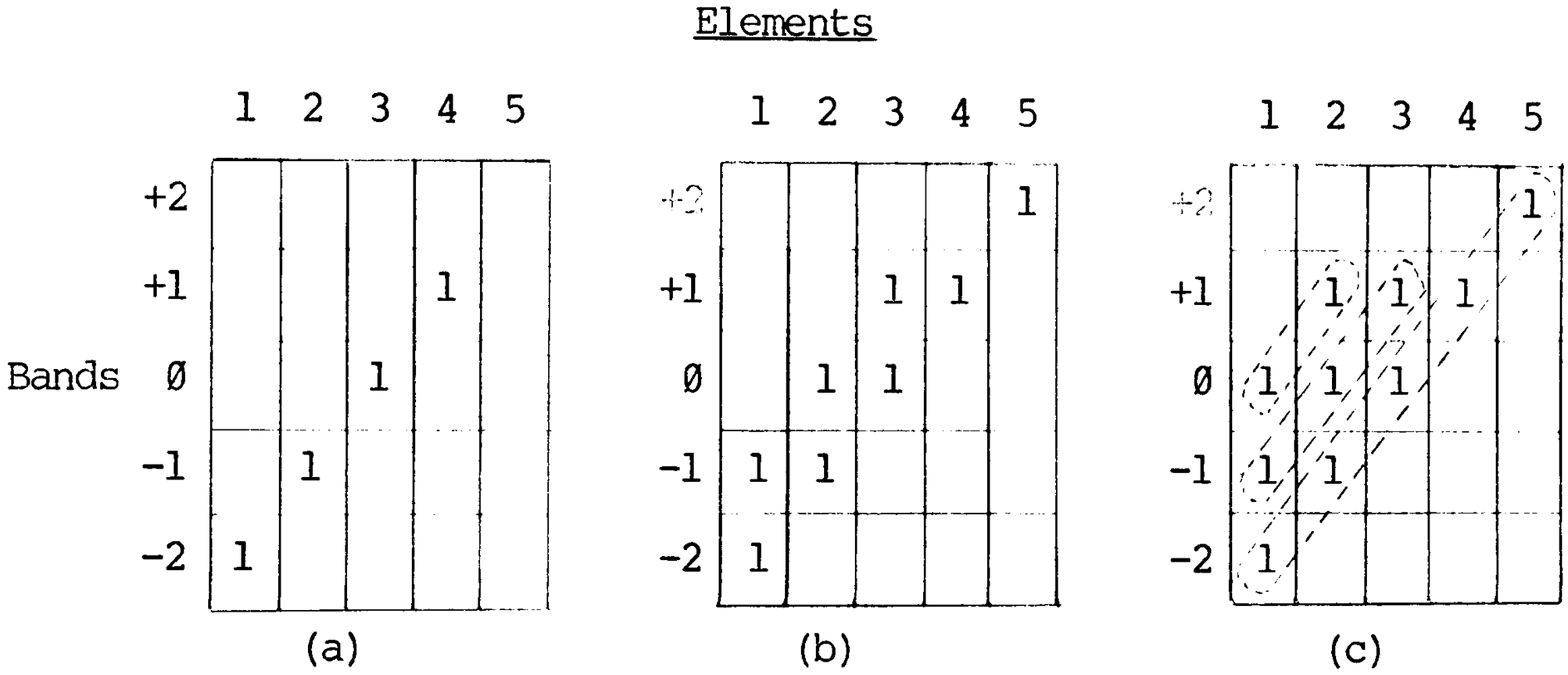

Figure 2.8 Band-Element matrix for Figure 2.7.

There are two ways of storing the necessary data to compile the cycle count. One is to construct two-dimensional band-element array to determine the number of cycles at each range as well as the mean values at each range. The other is to use a single sum array sacrificing the information about mean values. The first of these

ways is illustrated in Figure 2.8. If one starts at the largest absolute value in the history, and also ends at that value, for each tensile reversal there will occur an equal compressive reversal to complete the cycle. For this reason, one needs to enter into the band-element matrix only those elements used during the excursions in the same direction; in this case from a minimum to a maximum. Of the first reversal in Figure 2.7, band (-2) uses element 1, band (-1) uses element 2, band (Ø) uses element 3, and band (1) uses element 4. These data are now entered in the band-element matrix shown in Figure 2.8(a). During the next positive going excursion, from peak 3 to peak 4, band (-1) uses element 1, band (Ø) uses element 2, band (+1) uses element 3, and, remembering that element 4 is skipped, band (+2) uses element 5, and so on.

The data are removed from the matrix by constructing diagonals, starting from the largest one to the smaller diagonals, as shown in Figure 2.8(c). In this example, the largest diagonal describes a cycle which starts in band (-2) and ends in band (+2), i.e. a cycle with a range of five bands about a mean value of Ø. The next diagonal represents a cycle with a range of three bands and zero mean, the last cycle has a range of two bands and a mean value of Ø.5.

In the alternate version, a "sum" array is constructed by counting the number of sign changes for each element, as shown in Figure 2.9. The extraction of data from the array starts at the highest element, which contains non-zero count. Changing sign twice

Elements	Sum							
1	6		4		2		Ø	
2	6		4		2*		Ø	
3	4	→	2*	→	Ø	→	Ø	
4	2		Ø		Ø		Ø	
5	2*		Ø		Ø		Ø	

Figure 2.9 SUM array for Figure 2.7

is interpreted as two reversals or one full cycle. Hence the number of cycles at the highest element is found by dividing the count by two. Then the count at that level is subtracted from each value in the array.

The process is repeated for the next highest element containing non-zero count until zeros occur for every element. For this case, the history consists of one cycle with a range of five elements, one cycle with a range of three, and another one with a range of two elements.

The reader has probably noted that these two methods, Wetzel's method, and Livesey and Webber's version of the range-pair counting, are very similar in that both methods use the same logic. Elements in one method correspond to counters in the other. "An element is not available" means that a counter is already cocked or triggered, hence skipped, if it is within the counting range.

However, there is one major difference which makes the range-pair method give unreasonable results. In Wetzel's method, the ranges or "the number of bands to travel" are calculated as the difference between successive peaks for both tensile and compressive reversals. On the other hand, in the range-pair method the range of a tensile reversal is always calculated as the distance between that peak and the absolute minimum value. If a range was calculated between successive peaks instead and used to find the number of counters to be cocked or triggered, then the range-pair method would have given exactly the same result as Wetzel's method.

2.5 Rainflow Method

One of the most important developments in cycle counting has been the emergence of the rainflow method in the last decade. Since the first introduction to the West by Dowling[5] in 1972, the rainflow method has attracted much attention. It has been widely used by many investigators and shown by extensive experimental tests to be superior to all other counting techniques[5, 6, 7, 11, 12, 13,]. As a result, it has become a standard tool for fatigue life prediction packages. The apparent reason for this is that the rainflow method defines cycles as closed stress-strain hysteresis loops, without elaborate local stress-strain analysis.

There are three versions of the rainflow method which give identical cycle counts for all types of service histories. The first version, sometimes referred as Pagoda Roof method, uses the imaginary

rain flow on fictive multifarious overlapped pagoda roofs. Hence, the reason for generic names of "rainflow" and "pagoda-roof" is this analogy used by Matsuishi and Endo[10] in their original work. To illustrate the method, the strain-time history is plotted in Figure 2.10 so that the time axis is vertically downward, and the lines connecting the strain peaks are imagined to be a series of pagoda roofs.

Rainflow starts at the beginning of the strain-time history, and successively at the inside of every peak. The raindrops keep falling on the imaginary eaves to the lower roofs until one of the following conditions is met. Flow initiating at a peak drips down until it comes opposite a maximum more positive (minimum more negative) than the maximum (minimum) it started from. The flow also stops when it meets rain from a roof above. The the length of each rainflow is recorded as a half cycle range.

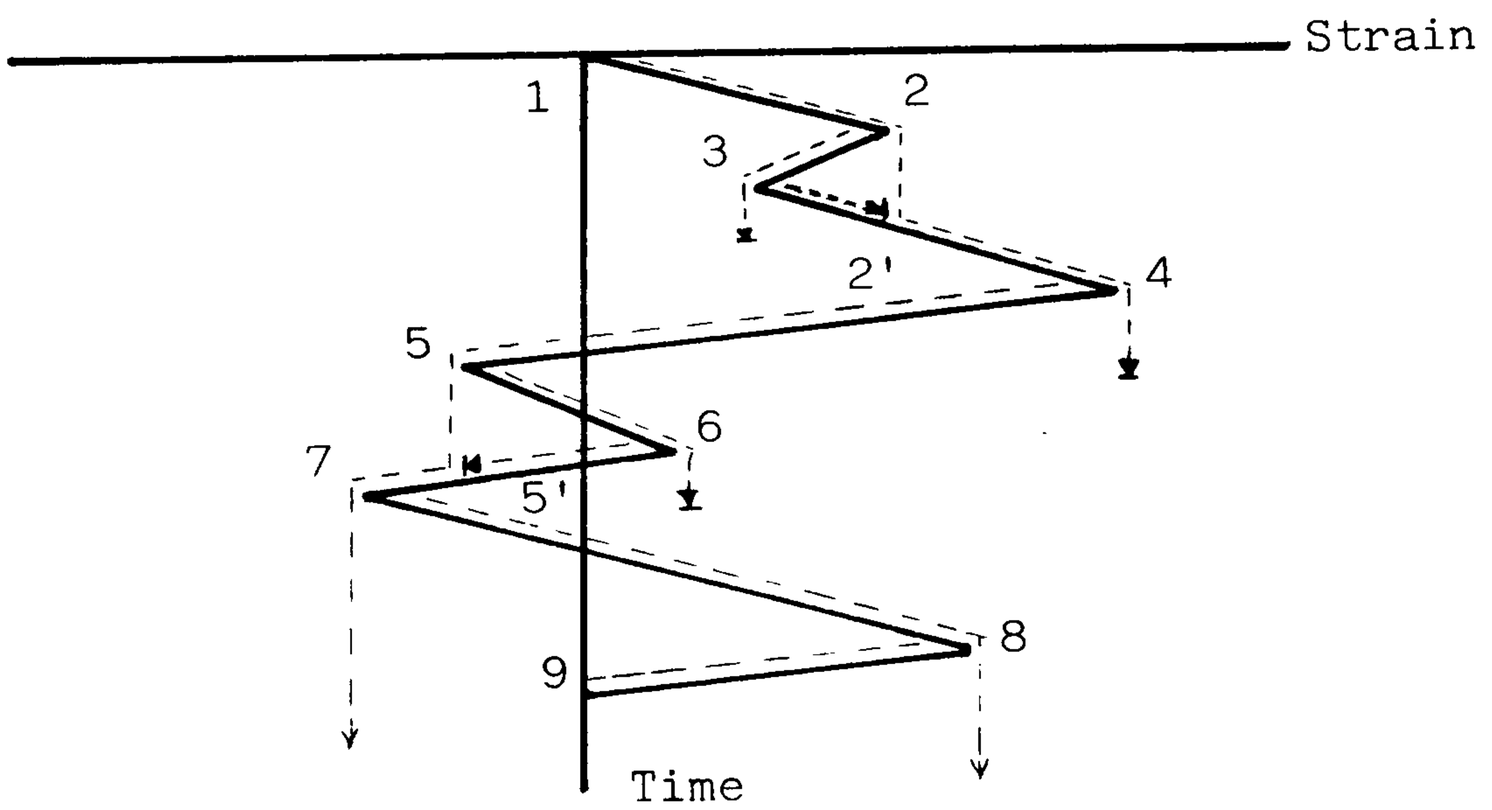

Figure 2.10 Example of pagoda-roof method

Figure 2.10 demonstrates the technique on a short strain-time history. Dashed lines represent the raindrops. For example the rain initiating at peak-1, a minimum, falls on peaks-2 and 4, and stops opposite peak-5, because peak-5 is more negative than peak-1. Hence the range from peak-1 to peak-4 is extracted as a half-cycle. Similarly peak-2 and peak-3 make one half-cycle, because the rain from peak-2 stops opposite peak-4 which is more positive than peak-2. However, the rain starting at peak-3 stops at 2' where it meets rain from the roof above. Note that when a half-cycle is extracted by the second condition, there already exists a corresponding half-cycle of equal magnitude extracted by the first condition, and two together make one full cycle. For example, range 2-3 and range 3-2' make a full cycle.

The second version, which is called Maximum-Minimum Procedure by the original authors[11], consists of repeated application of the following procedure:

1. The maximum and the minimum points of the whole strain-time history under consideration are determined. This action divides the history into three parts, the middle section between the extremum points, and the front and rear sections between the terminal points and the extremum points. The middle section is deferred to the next stage analysis.

2. For the front section, starting from the bounding extremum point a search is made towards the front terminal for the next opposite sign extremum point, i.e., if the extremum point is a

minimum, the next maximum point is searched towards the front terminal, or vice versa. Once again the section between the extremum points is deferred to the next stage analysis.

3. Step (2) is repeated until the front terminal is reached.

4. Steps (2) and (3) are repeated for the rear section.

The first application of this procedure to the total strain-time history gives half cycle ranges. Note that the ranges increase steadily until the maximum range bound by the absolute extremum points is reached, then they decrease steadily. When the standard procedure is applied again to the deferred sections, full cycle ranges are determined by picking up the ranges having even ordinal numbers. The ranges which are odd order are ignored. When the extremum points are searched at step (1) for the deferred sections, the terminal points which are maximum or minimum should be disregarded for the obvious reason.

Figure 2.11 shows the application of the maximum-minimum procedure to comparatively a longer strain-time history to clarify the rules. At step (1), peak-5 and peak-12 are located as the absolute minimum, MINØ and maximum, MAXØ of the whole history, respectively. Since the front section is bound by a minimum, the maximum of this section, FMAX1, is searched. Peak-2 is located at step (2). The front terminal is reached, hence step (3) is skipped. At step (4), the minimum of the rear section, RMIN1, is determined as peak-18. The end terminal is reached, hence the first application of the standard procedure is completed. The ranges between peaks 1-2,

2-5, 5-12, 12-13, 13-15 and 16-19 are counted as half cycles and shown by triangular marks , in Figure 2.12. The parts of the history between peaks 2-5, 5-12 and 13-18 are left to the second stage analysis. When the standard procedure is applied again, for example to the section between peak 13-18 the absolute minimum and maximum points for this section are searched. Peak-17 and peak-14 are located respectively. Since there are no more points left between these newly located extremum points and the terminal points, steps (2), (3), (4) are skipped. Hence the second stage analysis is completed for this section: it is divided into three ranges, between peaks 13-14, 14-17 and 17-18, and furthermore the part of history between peaks 14-17 is deferred to the next stage analysis. Then these ranges are ordered, and the ranges having odd or even orders are shown by marks X and O, respectively. Hence the range between peaks 14-17 is counted as one full cycle. The second stage analysis continues similarly for the rest of deferred sections from the first stage. The same procedure is applied repeatedly until all the deferred sections are exhausted.

The justification for the third version, Pattern Classification Procedure, of the rainflow count follows from material stress-strain behaviour. When a large range is interrupted by a smaller one, as in Figure 2.12(a) the range 1-4 is interrupted by the range 2-3, the interruption forms a closed stress-strain loop. Furthermore, the shape of the interrupted excursion on a stress-strain plot is the same as it would be if the interruption had not occurred. This has been called a "memory effect" in material

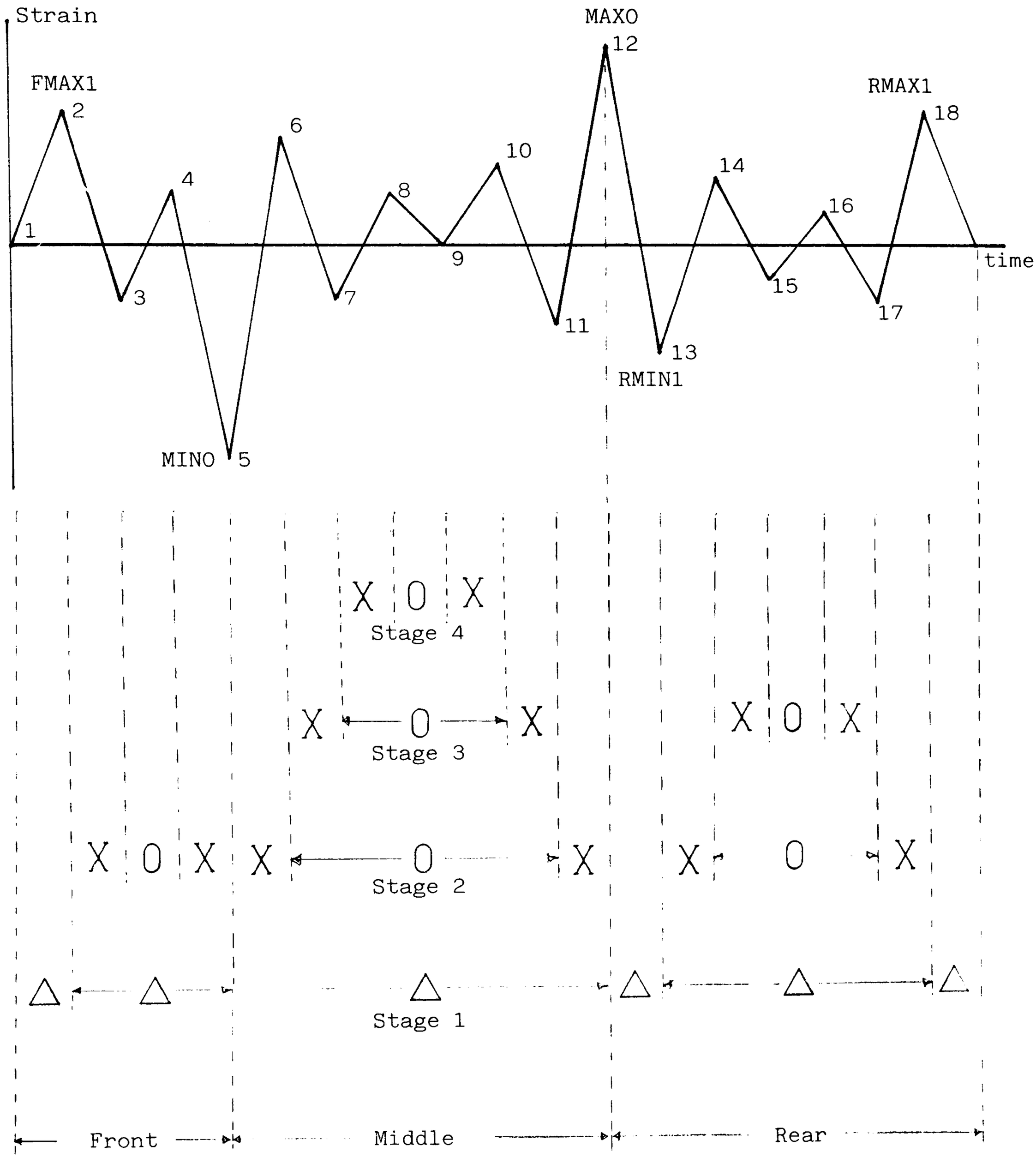

Figure 2.11 Rainflow Count using Maximum-Minimum Procedure

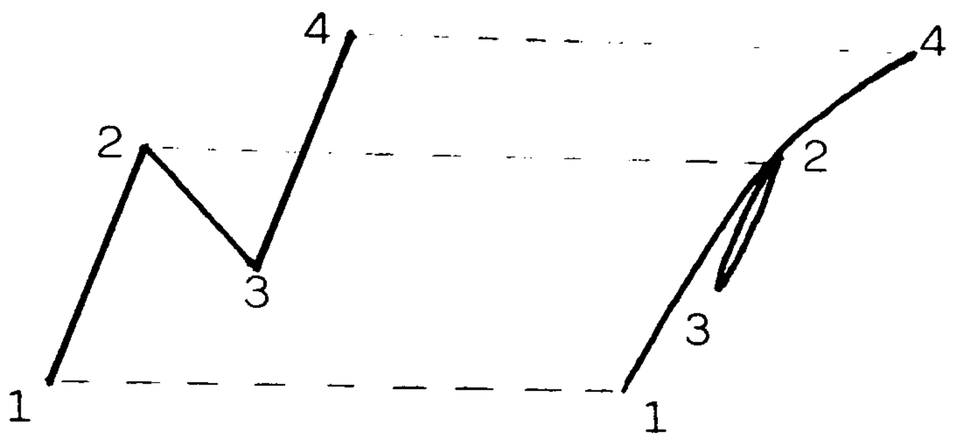

(a) D-I type

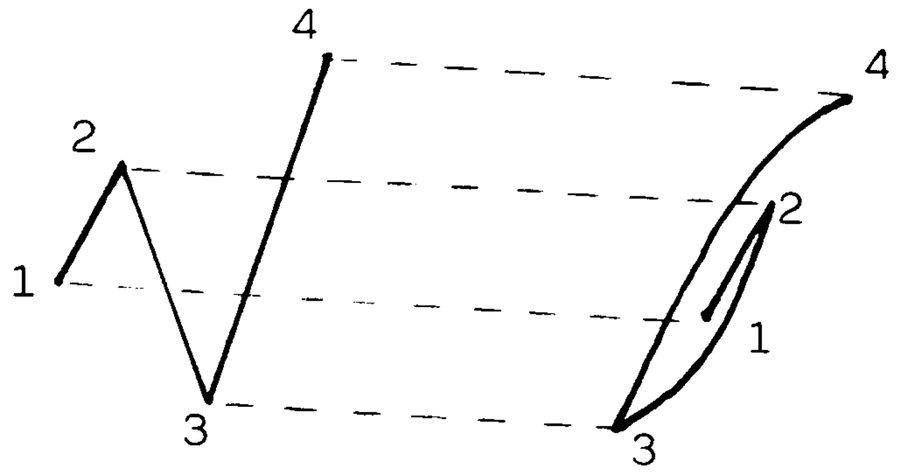

(b) I-I type

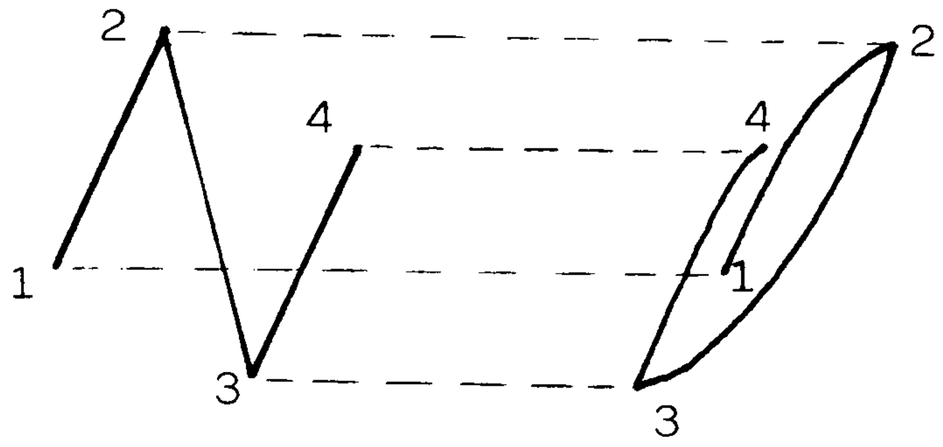

(c) I-D type

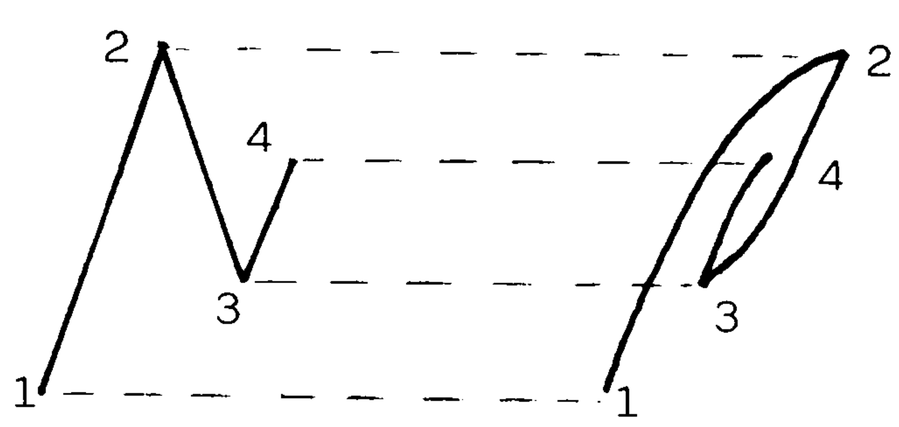

(d) D-D type

Figure 2.12 Four patterns of strain-time (left) and stress vs strain (right).

behaviour, the material "remembers" the stress-strain path it was following when interrupted and resumes this path when the interruption is over[9,14].

When four successive peaks of a strain-time history are considered, the pattern they form falls into one of the four types as shown in Figure 2.12. The type (a) shows that the second range, 2-3, is smaller than the first one, 1-2, and the third range, 3-4 is larger than the second one. Consequently this pattern is called decrease-increase, D-I type. The names of the other types follow similarly. As discussed earlier, D-I type corresponds to a large cycle interrupted by one closed hysteresis loop. The other patterns

form spiral type, sharp cornered, open hysteresis curves. This version of the rainflow count classifies three consequent ranges as one of the four patterns[11] shown in Figure 2.12., and the steps taken for each case are as follows:

In the case of D-I type, Figure 2.12(a), the interrupting range 2-3 is counted as one full cycle and removed. Accordingly the peaks 1 and 4 are connected and the next two peaks, 5 and 6, are considered to form a new pattern.

In the case of I-I type, Figure 2.12(b), the ranges 1-2 and 2-3 always correspond to one-half cycles irrespective of the following ranges. Hence peaks 3, 4, 5 and 6 are checked next.

In the case of I-D type, Figure 2.12(c), the first range 1-2 is always a half cycle. Hence peaks 2, 3, 4 and 5 are checked next.

In the case of D-D type, Figure 2.12(d), whether 3-4 will make a closed loop or not cannot be said without further information. Therefore the following peak is considered next, still retaining the information about the first peak.

When this technique is applied to the strain-time history in Figure 2.11, the first pattern 1-2-3-4 is I-D type, therefore the range 1-2 is counted as one half cycle. The next pattern 2-3-4-5 is D-I type, hence the range 3-4 is counted as one full cycle and removed. After connecting peaks 2 and 5, one gets 2-5-6-7 which is

D-D type. The next two patterns are also D-D type, hence retaining peaks 2, 5 and 6, the next pattern 7-8-9-10 is checked. It is D-I type, the range 8-9 is extracted as one full cycle. The remaining pattern 5-6-7-10 is still D-D type, therefore peak 11 is considered. 6-7-10-11 makes D-I type, the range 7-10 is extracted as one full cycle. This leaves 2-5-6-11, which is yet another D-D type. The next pattern 5-6-11-12 is D-I type, hence the range 6-11 is one full cycle, and so on. At the end of the count, 6 ranges, first increasing in magnitude, then decreasing steadily, are counted as half cycles and another 6 ranges as full cycles, as shown in Figure 2.13.

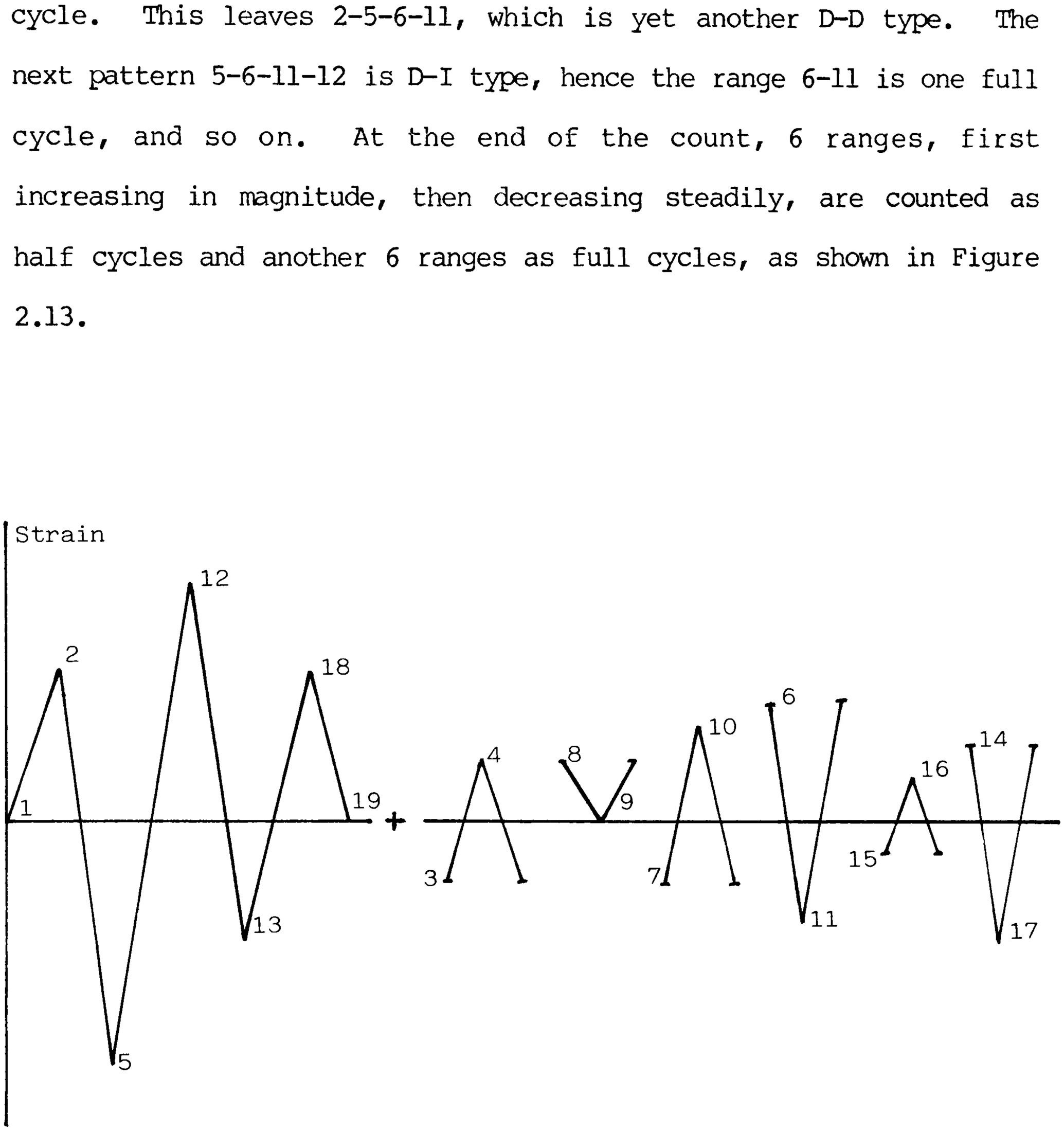

Figure 2.13 Decomposition of the strain history in Figure 2.12 into half cycles (left) and full cycles (right).

2.6 Overview of Cycle Counting Methods

Throughout their service life, machines, equipment, vehicles and buildings are subjected to loads, the majority of which fluctuate with time. When considering the effects of random loading, there are generally two aspects of the problem. The first is the damage significance of the load history on structural life, as measured by crack initiation and crack growth. The second and equally important aspect is the means by which the same fatigue damage may be produced using the simulation of service loads. In order to design structures safely without unnecessary expenditure of material and effort, it is necessary to have satisfactory techniques of analysing random data for both (1) damage assessment of service history and (2) service spectrum generation and simulation.

There are two fundamentally different approaches for this analysis, one in the time domain and the other in the frequency domain. The latter entails power spectrum analysis of the signal and knowledge of the frequency response characteristics of the system subject to the random loading. The power spectral presentation of a service history has been receiving more consideration because of the very important results obtained by S. O. Rice[15] who derived an equation to calculate the number of crossings of a level from the power spectrum of a stationary Gaussian process, which is equivalent to level crossing count in the time domain. By means of stationary or quasistationary Gaussian processes, a series of stress-time histories can be described with satisfactory accuracy as necessary for fatigue

life evaluation. Stress-time histories can be generated by means of random signal generators and filters or corresponding digital computer techniques which have the same statistical properties as the original ones.

The main reason why frequency domain analysis works is that the stresses resulting from environmental effects usually correspond to random vibrations and can be treated as continuous processes, for which the power spectral presentation seems to be suited. Typical examples are gusts of wind, sea waves, vibration or noise. The opposite to this represents stresses due to the usage of a structure, for example loading of a fork-lift truck, discontinuous processes for which the time averaging becomes questionable. Then one has to analyse the service history in the time domain to extract all the information relevant to the fatigue behaviour of the structure.

Ignoring fluctuations in frequency, which in most situations are too small in magnitude to have any significant effect on fatigue damage, there are three features of the random signal which might be expected to influence fatigue behaviour: amplitude, mean level and the sequence of the signal. Of numerous counting methods in this category, some notable ones are described in the earlier section.

The oldest and very widely used method to analyse a random signal is to count how often a defined event has occurred, for example, a peak, a range, or a crossing of a given level. The results are plotted as a histogram of level against cumulative occurrences or as commonly known, cumulative frequency, Figure 2.14.

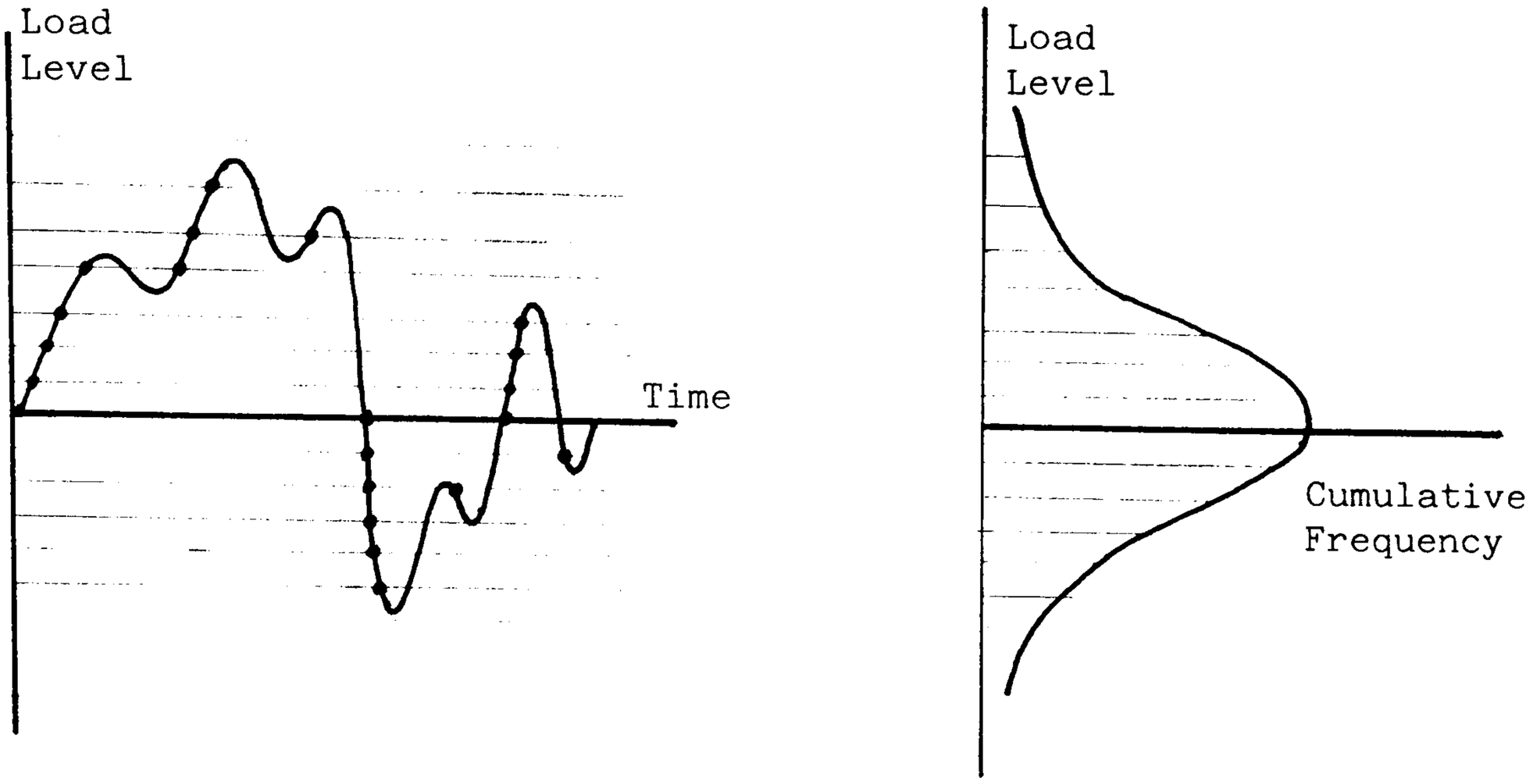

Figure 2.14 Load-Cumulative Frequency distribution for level crossing method.

Despite the known serious flaws in them, as a result of small cycles which either do not pass through the mean level or interrupt larger amplitude cycles, these methods have some advantageous features. The first is the ease with which data can be collected by means of simple automatic counting devices and interpreted graphically. Secondly, cumulative frequency distributions can be approximated in many cases by standardized distribution functions[16]. The introduction of standardized distributions facilitates the extrapolation of the results and the estimation of allowable stresses for design.

One logical step to improve one-parameter counting methods is

to count two events as one. In the peak-trough or range-mean counting, the waveform is divided into a succession of half-cycles, the peaks and their subsequent troughs, on the amplitude and mean values, are counted simultaneously. Presentation of overall data can be either a three dimensional graphical display, three axis being range, mean or peak, trough, and number of occurrences, or in the form of a numerical matrix. Although this counting technique retains details of fluctuations in both amplitude and mean, it still suffers from the fact that small excursions can completely mask the existence of underlying waves of much greater amplitude and damage significance, as shown in Figure 2.2 and 2.3. However, peak-trough counting method has been used extensively for the generation of standardized load sequences with stationary properties. If the peak-trough joint probability matrix is known, with a position along a row representing trough value, down a column representing peak value, then once a peak is chosen the possible values of next trough and their relative probabilities are given by the appropriate row in the matrix, Figure 2.15. Random selection process moves alternately along a row and down a column. A standardized loading sequence for fighter aircrafts, FALSTAFF[17], has been generated in this way where the peak-trough probability matrix was obtained from actual flight recordings. However, repeating a recorded history over and over again may not be the best way to test parts. It may, for instance, omit or exaggerate some sequence effects. Sherratt et al[18, 19] generated the random signals needed to drive servo-hydraulic and electro-magnetic rigs by applying one or two-dimensional random walk techniques to a joint peak-trough probability matrix.

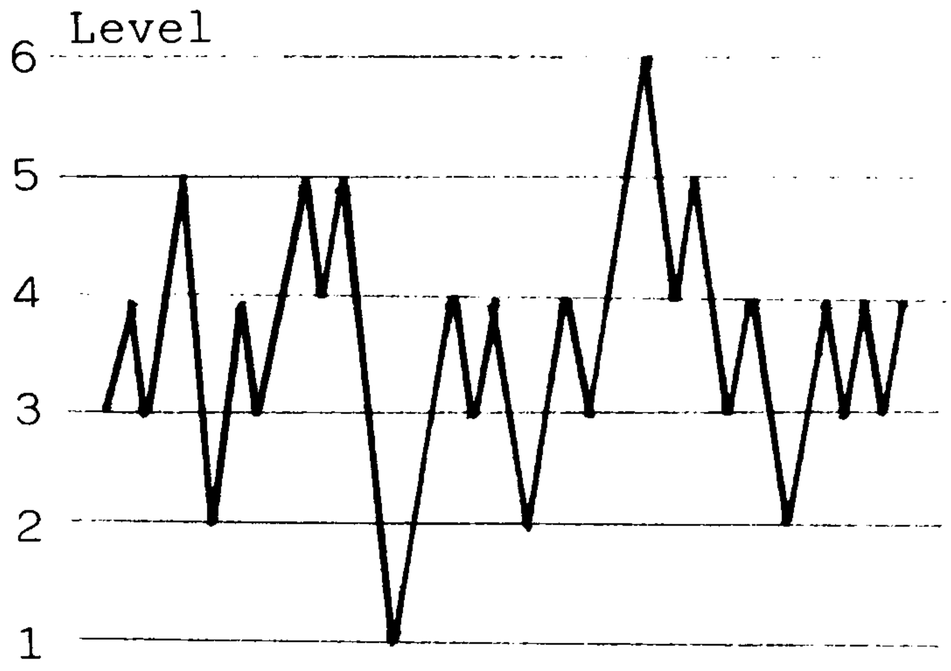

Trough

Peak		1	2	3	4	5	6
	1	X				1	
	2		X		2	1	
	3			X	6	1	
	4	1	3	5	X	1	1
	5			2	2	X	
	6			1			X

Figure 2.15 Peak-trough distribution matrix of a history segment.

If the cycle counting procedure is used as a part of the damage analysis to estimate the crack initiation life, then the rainflow and similar methods have features which make them superior to the other techniques considered earlier. They avoid the distortion and inaccuracy from which one-parameter or peak-trough methods suffer as a result of small cycles which either do not pass through the mean level or interrupt larger amplitude cycles. This is achieved without resort to arbitrary dead zones or reset levels. It may well be that some cycles are too small in magnitude to contribute any significant damage, they are nevertheless counted and recorded, and it is up to the user to eliminate these for the purpose of accelerated testing or gains in computing speed.

For repeating histories, the range-pair, the rainflow, and Wetzel's methods all give identical results, provided that the history starts at either the highest peak or the lowest trough. The reason for starting with an extreme point in the history is that no interruptions can exist outside the largest range determined by the highest peak and the lowest trough. If one ignores the transient effects which depend on the initial stress-strain co-ordinates and cyclic hardening or softening tendencies of the material, then repetitive application of the load history produces a stable, constant hysteresis looping pattern over most of the life of a typical fatigue specimen[9, 14]. Consequently starting at one of extreme points assures starting on a stress-strain path which, with possible interruptions, will terminate at the other, and return to the first after additional possible interruptions, as in Figure 2.4.

If a finite loading history is analysed to estimate the crack initiation life, then the requirement of starting of an extreme point does not create too much difficulty. When two consecutive blocks of any repeatedly applied history are considered, a new block may be conveniently defined between successive occurrences of the highest peaks or the lowest troughs, as in Figure 2.16.

However, for non-repeating, that is, open-ended, histories the aforesaid methods give different results. The rules described for the Wetzel's method are incomplete if at any time during the history the absolute value of load exceeds its value at the first peak. The second version of the rainflow method, maximum-minimum

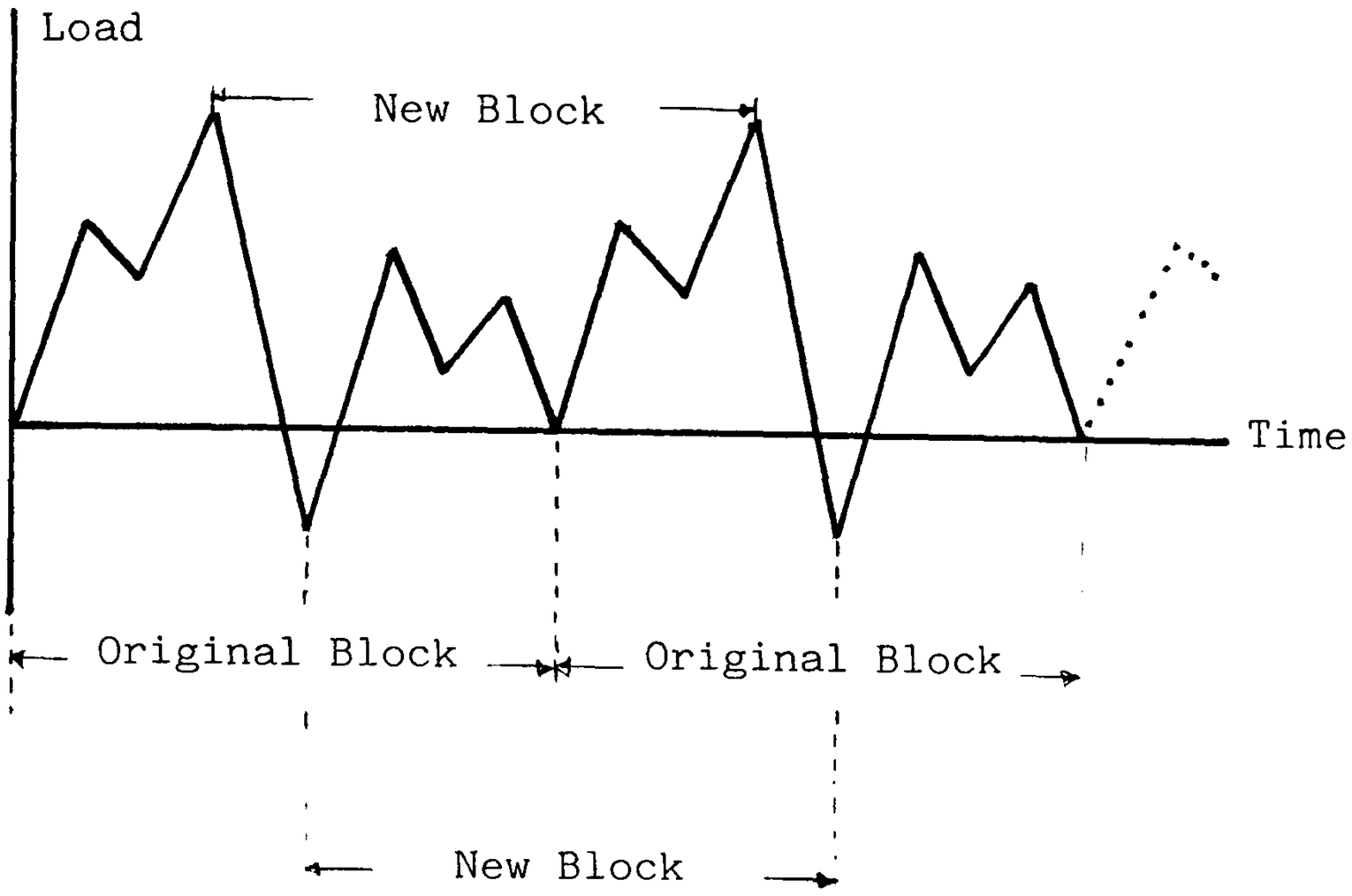

Figure 2.16 Repetition of a block history to define a new block.

procedure cannot be used either, because it requires the complete history to determine the absolute maximum and minimum points. The range-pair method counts a load range as a cycle if it can be paired with a subsequent loading of equal or <u>greater</u> magnitude in the opposite direction. This sort of counting completely ignores the existence of the sharp cornered spiral type stress-strain curve which does <u>not</u> form a closed loop when a metal is subjected to successively increasing or decreasing ranges of strain or stress[11]. The rainflow method counts these ranges as half-cycles. By matching unequal ranges and ignoring the remainder of the greater range, the range-pair method estimates less damage than the rainflow method. The difference may be significant in situations where there are only a few cycles to failure or where there are insignificant minor cycles

and most of the damage is done by a few major cycles. However, when the extreme point, which is the same type as the starting point, is reached, i.e. if the starting point is a peak then the highest peak, if it is a trough then the lowest trough is achieved, thereafter both counting methods give exactly the same result.

Although none of the three versions of the rainflow method is affected by the starting point as far as extracted cycles are concerned the third version, Pattern Classification Procedure is simplified considerably if the history starts at one of the extreme points. Since no other point exceeds the starting point, the four patterns in Figure 2.12 are reduced to two, namely D-D and D-I types. Then every newly examined point either extends a converging sequence, forming an extended converging sequence of any length during the search, or reduces the list by forming a closed hysteresis loop.

In Wetzel's counting method, if any history point occurs within a band, a full element and band are used. This procedure obviously leads to rounding errors, which are minimized by increased number of elements and bands. However as the number of bands is increased, computing time and storage space for the band array increases. If the purpose of counting is to extract cycles, this method becomes inefficient and uneconomic. The major advantage of this method is that it facilitates the simulation of local stress-strain response to a given nominal loading history.

2.7 Conclusions

It is rather hazardous to grade a cycle counting method on the basis of its ability to produce "better results" for one type of application only. In fatigue analysis, a cycle counting is needed for (a) on-line data acquisition and reduction to determine the loading environment, (b) regeneration and simulation of the service history, (c) truncation of smaller loads for accelerated testing, (d) estimation of crack initiation life, and (e) estimation of crack propagation life. Hence a cycle counting method ought to be chosen on the basis of what is expected out of the analysis. Cycle counting procedures need to be understood rather than merely followed.

- Frequency domain analysis techniques are well established in other areas of engineering and may be used in fatigue analysis to describe the loading environment, to measure and control the dynamic response of a test rig, and to regenerate and simulate the service history. Frequency domain techniques are particularly effective where loads that act upon a structure originate from the environment, for example, sea waves, gusts of wind, noise and vibration.

- One-parameter counting methods are simple to understand, easy to implement in hardware or software, convenient to display results graphically and interpret and extrapolate them.

- The peak-trough counting method may be used to regenerate standardized or random load sequences with stationary properties.

- For a given block of service history and ignoring the differences due to the use of discrete levels, if the block starts and ends at an extreme point, then the range-pair, Wetzel's, and the rainflow methods all give identical result.

- These methods are best suited for the use of estimating the crack initiation life, because they all extract cycles in a manner which is consistent with the stress-strain behaviour of the material considered.

- The choice of a counting method for predicting the crack growth largely depends on the growth model used.

REFERENCES FOR CHAPTER 2

1. Palmgren, A., "The Service Life of Ball Bearings", a Technical Translation, NASA TT F-13460.

2. Miner, M. A., "Cumulative Damage in Fatigue", ASME, Journal of Applied Mechanics, Sept. 1945.

3. Livesey, J., Webber, D., "Recording and Interpretation of Strain Measurements in Military Bridges", J.B.C.S.A. Conference, 1972.

4. Haas, T., "Loading Statistics as a Basis of Structural and Mechanical Design", Engineers Digest, Vol. 23, Nos. 3, 4 and 5, 1962.

5. Dowling, N. E., "Fatigue Failure Predictions for Complicated Stress-Strain Histories", Journal of Materials, JMLSA, Vol. 17, No. 1, March 1972.

6. Watson, P., Dabell, B. J., "Cycle Counting and Fatigue Damage" Proc. of SEE Symposium held at Warwick Uni., Feb. 1975.

7. Power, E. M., "The Analysis of Random Data for Fatigue Testing" Proc. of SEE Symp. held at Warwick Uni. Feb. 1975.

8. Tucker, L., Bussa, S., "The SAE Cumulative Fatigue Damage Test Program", SAE Paper No. 750038.

9. Wetzel, R. M., "A Method of Fatigue Damage Analysis", Ph.D. Thesis, University of Waterloo, Canada, 1971.

10. Matsuishi, M., Endo, T., "Fatigue of Metals Subjected to Varying Stress", Paper presented to Japan Soc. of Mech. Eng., Fukuoka, March 1968 (in Japanese).

11. Endo, T., Mitsunaga, K., Takahashi, K., Kobayashi, K. and Matsuishi, M., "Damage Evaluation of Metals for Random or Varying Loading", Proc. of Symp. on Mechanical Behaviour of Materials, Soc. of Material Science, Kyoto, Japan, Aug. 1974.

12. Endo, T., Anzai, H., "The On-Site Indication of Fatigue Damage under Complex Load", Proc. of SEECO '78 held at Warwick University, April 1978.

13. Nelson, D. V., Fuchs, H. O., "Predictions of Cumulative Damage Using Condensed Load Histories", SAE Paper No. 750045.

14. Martin, J. F., Topper, T. H., Sinclair, G. M., "Computer Based Simulation of Cyclic Stress-Strain Behaviour with Applications to Fatigue", Materials Research and Standards, MTRSA, Vol. 11 No. 2, Feb. 1977.

15. Rice, S. O., "Mathematical Analysis of Random Noise", Selected Papers on Noise and Stochastic Processes, edited by Nelson Wax, Dover Pbl. Inc., New York, 1958.

16. Buxbaum, O., "Random Load Analysis as a Link Between Operational Stress Measurement and Fatigue Life Assessment", ASTM, STP, 671, 1979.

17. FALSTAFF, Description of a Fighter Aircraft Loading Standard for Fatigue Evaluation, ICAF Doc. No. 839

18. Sherratt, F., Davall, P. W., "Advances in Computer Controlled Realistic Fatigue Testing", ASTM STP 613, 1976.

19. Sherratt, F., Edwards, P. R., "The Use of Small On-Line Computers for Random-Loading Fatigue Testing", Journal of Soc. of Environmental Engineers, Vol. 13-4, issue 63, Dec. 1974.

CHAPTER 3

LINK BETWEEN POWER SPECTRAL DENSITY AND FATIGUE LIFE BASED ON RAINFLOW

3.1 Introduction

Throughout their service life machines, equipment, vehicles, and buildings are subjected to loads, the majority of which vary with time. An important task in the estimation of the service life of a structure or a component is to analyse the operational loads in its different parts. These operational loads can seldom be characterized by a set of static forces. In most practical cases the loading is stochastic and may be a continuous random process, hence conventional statistical methods are needed to describe the operational loads. A common statistical function which describes the loads is the power spectral density.

The power spectral presentation of a stress-time history has been receiving more consideration as a result of increased used of Finite Element methods to analyse structures. Given a set of dynamic input forces, a Finite Element program will predict power spectral density plots at any point on a component or structure. Often the aim is to locate the critical areas and to see whether the proposed structure has potentially disastrous resonances. Once this has been done, a life estimate based on the most severely stressed location is useful, hence links between power spectral density and life estimation are needed.

The purpose of this study is to develop a life estimation procedure for a structural component subjected to a stationary and ergodic random stress process which in general can be wide band. The specific aim, given the power spectral density of operational loads, is to produce an expression which uses rainflow cycle counting to predict the fatigue life. Such a procedure could be useful in the design of components for which the loads that act upon them may originate from the environment, for example from gusts of wind; sea waves, noise, or road roughness.

3.2 Some Aspects of Random Loading

The theory of random processes is extensive, because so many physical systems are of this type. For a rigorous treatment of random processes, a knowledge of probability theory is necessary, and the subejct is covered in depth in the literature[1, 2]. However, some definitions and results are given here to base the discussion properly.

The ensemble is the entire history in time and amplitude of the random signal. A stationary random process is one in which the ensemble does not vary its statistical properties with time. An ergodic process is a stationary one in which one sample is representative of the ensemble. A correlation function provides a means of determining to what degree two functions are related. Given two functions $x(t)$ and $y(t)$, their correlation function $R_{xy}(\tau)$ is defined as:

$$R_{xy}(\tau) = \lim_{T\to\infty} \frac{1}{2T}\int_{-T}^{T} x(t)y(t+\tau)dt \qquad \textbf{Eq. 3.1}$$

An <u>autocorrelation function</u> shows how x(t) is correlated with itself as a function of τ, or time average of x(t) x $(t+\tau)$.

$$R_{xx}(\tau) = R(\tau) = \lim_{T\to\infty} \frac{1}{2T}\int_{-T}^{T} x(t)\,x(t+\tau)dt \qquad \textbf{Eq. 3.2}$$

<u>Power spectral density</u> describes the amount of average power contained in a band of frequencies, and is defined as:

$$G(w) = \lim_{T\to\infty} \frac{1}{2T}\left|\int_{-T}^{T} x(t)e^{-jwt}dt\right|^2 \qquad \textbf{Eq. 3.3}$$

The autocorrelation function and spectral density are a Fourier transform pair:

$$G(w) = \int_{-\infty}^{\infty} R(\tau)e^{-jw\tau}d\tau \qquad \textbf{Eq. 3.4}$$

$$R(\tau) = \frac{1}{2\pi}\int_{-\infty}^{\infty} G(w)e^{jw\tau}dw \qquad \textbf{Eq. 3.5}$$

The autocorrelation function and spectral density are further related[1]:

$$(-1)^n \frac{d^{2n}R(\tau)}{d\tau^{2n}} = \frac{1}{2\pi}\int_{-\infty}^{\infty} w^{2n}G(w)e^{jw\tau}dw \qquad \textbf{Eq. 3.6}$$

Defining the n^{th} moment of spectral density, m_n, as:

$$m_n = \frac{1}{2\pi}\int_{-\infty}^{\infty} w^n G(w)\ dw \qquad \textbf{Eq. 3.7}$$

then, with $\tau = 0$, eq.3.6 yields:

$$m_o = R(\emptyset) = \frac{1}{2\pi}\int_{-\infty}^{\infty} G(w)\ dw \qquad \textbf{Eq. 3.7.i}$$

$$m_2 = -R''(\emptyset) = \frac{1}{2\pi}\int_{-\infty}^{\infty} w^2 G(w)\ dw \qquad \textbf{Eq. 3.7.ii}$$

$$m_4 = R^4(\emptyset) = \frac{1}{2\pi}\int_{-\infty}^{\infty} w^4\ G(w)\ dw \qquad \textbf{Eq. 3.7.iii}$$

Eq.3.7.i may be re-written as:

$$\sigma_x^2 = \frac{1}{2\pi}\int_{-\infty}^{\infty} G(w)\,dw = \lim_{T\to\infty}\frac{1}{2T}\int_{-T}^{T} x^2(t)\,dt \qquad \textbf{Eq. 3.8}$$

Thus the total area of $G(w)/2\pi$ is nonnegative and equals the 'average power' of the process x(t), and its square root (the root-mean-square, rms), σ_x, is a common way of specifying the intensity of a process.

A narrow band process is a stationary random process whose spectral density G(w) has significant values only in a band of frequencies whose width is small compared to the magnitude of the centre frequency of the band. A wide band process has significant power terms over a wide range of frequencies. Fig. 3.1 shows these two types of processes and their time domain representations.

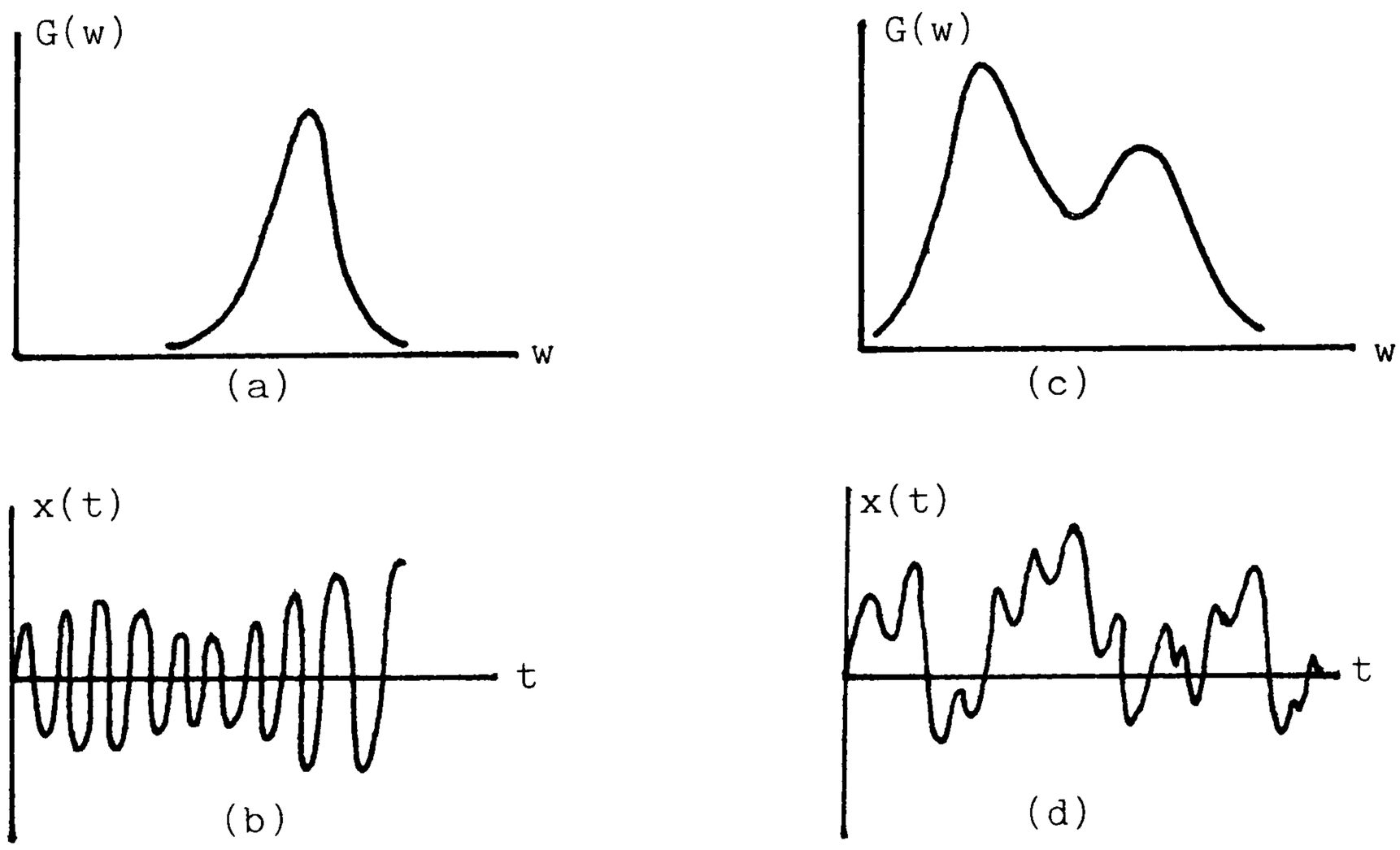

Fig. 3.1 Examples of two spectral density plots and their time-domain representation, narrow-band (a) and (b), wide band (c) and (d).

The amplitude probability density function, $p(\alpha)$, of a random process is a measure of how long the signal stays at a particular amplitude:

$$p(\alpha)d\alpha = \text{Prob } \{\alpha < x(t) < \alpha + d\alpha\} \qquad \textbf{Eq. 3.9}$$

In fatigue analysis, distribution of peaks or ranges is more important than the distribution of the signal itself . Peak or range probability density functions may be defined in the same way.

Two important density functions are:

Gaussian

$$p(\alpha) = \frac{1}{\sigma\sqrt{2\pi}} e^{-\alpha^2/2\sigma^2} \qquad \textbf{Eq. 3.10}$$

Rayleigh

$$p(\alpha) = \frac{\alpha}{\sigma^2} e^{-\alpha^2/2\sigma^2} \qquad \textbf{Eq. 3.11}$$

3.3 Description of the Problem

Two important parameters of a signal in fatigue life calculation are the range of a cycle and the number of cycles at all ranges. Once these two parameters are known, it is a straightforward matter to calculate damage or life by using an S/N curve for the material and the Palmgren-Miner rule. Hence a lot of work has been done to calculate zero crossings and level crossings, determine the expected number and spacing of peaks, and find the distribution of rises and falls in a continuous random process from the power spectral density.[1, 2, 3, 4, 5, 6] Some important results have been achieved and used for fatigue life estimation for the case of narrow band, stationary and ergodic random signals[7, 8, 9]. However, the situation for wide-band signals is much less satisfactory. There are

basically two reasons for the lack of progress for wide band signals. The first one is computational, the difficulty of determining a six-fold joint probability density and calculating the determinant of the matrix of correlation functions, which will have 36 elements made up of $R(\tau)$ and its derivatives[5]. The second and more important one is the difficulty of defining a 'cycle'. This does not create a problem in the case of a narrow-band signal, because the signal is varying slowly, like an amplitude modulated sine wave and it is reasonable to assume that each peak can be matched with a trough symmetrically placed below the mean, as in Fig. 1.b. However, if a peak is matched with the adjoining trough in the case of wide-band signal, Fig. 3.1.d, the interrupting small cycles conceal the presence of larger, much more damaging cycles. Fortunately, a consensus has emerged in the last decade that the rainflow counting is the answer to this problem, that it counts both large cycles and interrupting small cycles. It is the purpose of this study to predict the rainflow count from a power spectral density, for a stationary, ergodic random process.

3.3.1 Narrow-Band Case:

The theory behind the results presented below is discussed at some length in the literature[1]. The basic theory was first developed by S. O. Rice in his classic paper[4], and later applied to the fatigue problem by J. S. Bendat[2, 3].

Let $\underline{x}(t)$ be a Gaussian random variable with zero mean. Consider two time instances t and $t+\tau$. If $\underline{x}(t)\underline{x}(t+\tau)<\emptyset$, then the

number of zero crossings of the curve $\underline{x}(t)$ in the interval $(t, t+\tau)$ must be odd, Fig. 3.2. Furthermore, if τ is small then there will be only one zero crossings in an interval of length τ. Denoting by $p(\tau)$ the probability that there is only one zero crossing:

$$p(\tau) = \text{Prob}\ \{\underline{x}(t)\underline{x}(t+\tau) < \emptyset\} \qquad \textbf{Eq. 3.12}$$

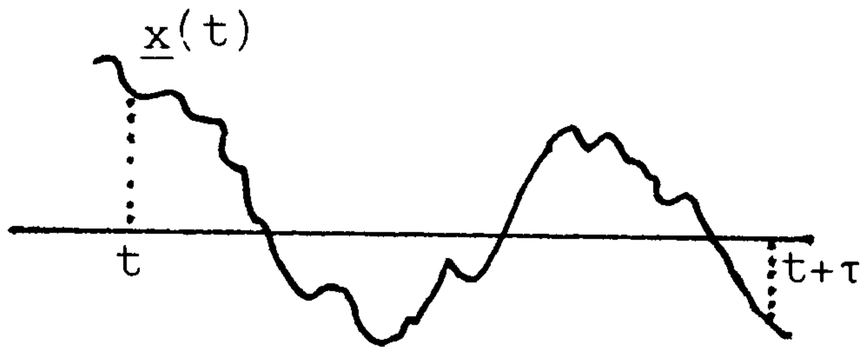

Fig. 3.2 Zero crossing problem

The probability function $p(\tau)$ and the autocorrelation function $R(\tau)$ of $\underline{x}(t)$ are linked as:

$$\cos[\pi p(\tau)] = \frac{R(\tau)}{R(\emptyset)} \qquad \textbf{Eq. 3.13}$$

Assume the derivative $R'(t)$ of $R(\tau)$ exists at the origin, then it must equal zero, since $R(\tau)$ is even. Expanding both the cosine function and $R(\tau)$ about the origin, keeping only the first two terms and neglecting higher power terms, Eq. 3.13 yields:

$$p(\tau) \simeq \frac{1}{\pi}\sqrt{-\frac{R''(\emptyset)}{R(\emptyset)}}\ \tau \qquad \textbf{Eq. 3.14}$$

Thus, for small τ, $p(\tau)$ is proportional to τ. Define a density λ_o as the expected number of zero crossings per unit time:

$$\lambda_o = \frac{1}{\pi}\sqrt{-\frac{R''(\emptyset)}{R(\emptyset)}} \qquad \textbf{Eq. 3.15}$$

Expressing R(Ø) and R" (Ø) in terms of the power spectrum, G(w), of $\underline{x}(t)$, Eq. 3.15 can be written as:

$$\lambda_o = \frac{1}{\pi}\sqrt{\frac{\int_{-\infty}^{\infty} w^2 G(w)\,dw}{\int_{-\infty}^{\infty} G(w)\,dw}} \qquad \textbf{Eq. 3.16}$$

The problem of determining the probability $q(\tau)$ that the process $\underline{x}(t)$ has an odd number of maxima in the interval $(t, t+\tau)$ can be reduced to the problem of zero crossings of $\underline{x}'(t)$. Assuming that τ is small enough so that there is only one peak or trough in the interval and defining a density μ as the expected number of peaks per unit time, a similar treatment of the problem yields:

$$\mu^2 = \frac{1}{(2\pi)^2}\,\frac{\int_{-\infty}^{\infty} w^4 G(w)\,dw}{\int_{-\infty}^{\infty} w^2 G(w)\,dw} \qquad \textbf{Eq. 3.17}$$

The probability $p_\alpha(\tau)$ that the given process $\underline{x}(t)$ intersects the line $\underline{x}(t) = \alpha$ in the small interval $(t, t+\tau)$ is given, in terms of the probability of zero crossings $p(\tau)$ and the autocorrelation function, as:

$$p_\alpha(\tau) = p(\tau)\; e^{-\alpha^2/2R(\emptyset)} \qquad \textbf{Eq. 3.18}$$

Define λ_α as the expected number crossings at the level α, then:

$$\lambda_\alpha = \lambda_o\, e^{-\alpha^2/2R(\emptyset)} \qquad \textbf{Eq. 3.19}$$

Note that, so far, no direct assumption is made concerning the shape of G(w). At this point, it is appropriate to define another term, the irregularity factor, γ, as the ratio of expected number of

zero crossings to expected number of peaks:

$$\gamma = \frac{\lambda_o}{\mu} = \sqrt{\frac{R''(\emptyset)^2}{R(\emptyset)R^4(\emptyset)}} \qquad \textbf{Eq. 3.20}$$

The factor γ lies in the range zero to unity. A system with a strong resonance at one frequency gives an irregularity factor approaching unity. Such a system has a load-time history which looks like an amplitude-modulated sine wave. There are practically no troughs above the signal mean, so that for any given level, α, the expected number of peaks above α, equals the expected number of positive-going level crossings of α. Thus, for a narrow band process, an estimate of the fraction of cycles having peaks greater than $\underline{x}(t) = \alpha$ is given by:

$$P_p(\alpha) = \text{Prob}\{\text{positive-going peak} > \alpha\}$$

$$= \frac{p_\alpha(\tau)}{p(\tau)} = e^{-\alpha^2/2R(\emptyset)} \qquad \textbf{Eq. 3.21}$$

It should be noted that the quantity $[1 - P_p(\alpha)]$, which defines the probability that a peak is less than α, is called the <u>distribution</u> function of peaks, and derivative of this quantity with respect to gives the peak probability <u>density</u> function:

$$P_p(\alpha) = \frac{\alpha}{R(\emptyset)} e^{-\alpha^2/2R(\emptyset)} \qquad \textbf{Eq. 3.22}$$

Thus, for the special case of a narrow band process, where the probability density function for the instantaneous amplitudes is the Gaussian function given in Eq. 3.1Ø, the resulting probability density function for the peak amplitudes, $P_p(\alpha)$, will be the Rayleigh function shown in Eq. 3.11.

3.3.2 Expected Fatigue Damage:

Consider a stationary stress process $\underline{s}(t)$ with zero mean, and a narrow band power spectral density, as in Fig. 3.3. A damage $\underline{D}(T)$ can be associated with a time interval T of $\underline{s}(t)$ by using the Palmgren-Miner rule. Clearly, this damage is also a random variable taking on different values for each sample stress history.

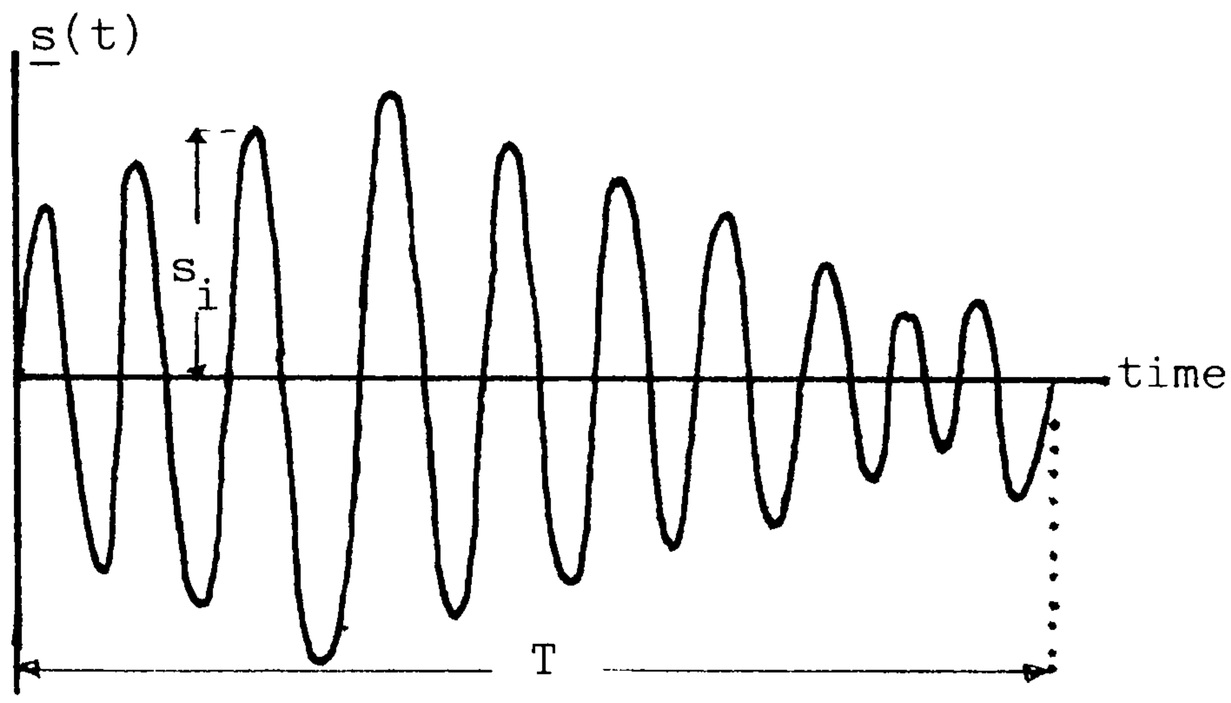

Fig. 3.3 Narrow band stress time history

Assuming the basic fatigue curve is $NS^b = K$, then the fatigue damage associated with the i^{th} peak, which has an amplitude S_i and assuming that it can be matched with a trough symmetrically placed below mean, is given by:

$$d_i = \frac{1}{K} S_i^b \qquad \textbf{Eq. 3.23}$$

In the interval T, the expected number of peaks N_p is estimated by:

$$N_p = \frac{\lambda_o}{2} T \qquad \textbf{Eq. 3.24}$$

where λ_o is the expected number of zero crossings per unit time. If the

damage accumulates linearly, then the total damage for the given time interval is:

$$D = \sum_{i=1}^{m} \frac{1}{K} S_i^b \qquad \textbf{Eq. 3.25}$$

Letting the instantaneous peak stress amplitude be α, then the expected values of d_i and D are determined by:

$$E(d_i) = \frac{1}{K} \int_0^{\infty} \alpha^b P_p(\alpha)\, d\alpha \qquad \textbf{Eq. 3.26}$$

$$E(D) = \frac{N_p}{K} \int_0^{\infty} \alpha^b P_p(\alpha)\, d\alpha \qquad \textbf{Eq. 3.27}$$

where $P_p(\alpha)$ is the peak probability density function. Substituting Eq. 3.22 in Eq. 3.27 gives:

$$E(D) = \frac{N_p}{K} \int_0^{\infty} \alpha^b \frac{\alpha}{R(\emptyset)} e^{-\alpha^2/2R(\emptyset)}\, d\alpha \qquad \textbf{Eq. 3.28}$$

Let

$$z = \frac{\alpha^2}{2R(\emptyset)}$$

then

$$E(D) = \frac{N_p}{K} \int_0^{\infty} (2R(\emptyset))^{b/2}\, z^b\, e^{-z}\, dz$$

$$= \frac{N_p}{K} (2R(\emptyset))^{b/2}\, \Gamma\left(1 + \frac{b}{2}\right) \qquad \textbf{Eq. 3.29}$$

where $\Gamma(1 + b/2)$ is a gamma function which is defined as

$$\Gamma(b) = \int_0^{\infty} z^{b-1} e^{-z}\, dz \qquad \textbf{Eq. 3.30}$$

Eq. 3.29 can be expressed in terms of the moments of power spectral density G(w) as:

$$E(D) = \frac{T}{2\pi K} \left(\frac{m_2}{m_o}\right)^{1/2} (2m_o)^{b/2}\, \Gamma\left(1 + \frac{b}{2}\right) \qquad \textbf{Eq. 3.31}$$

Fatigue failure will occur when the expected damage equals unity. Eq. 3.31 is an important result and used for design purposes. It

implies that if the power spectral density function G(w) can be estimated at a critical location of a component from a Finite Element analysis and if G(w) is narrow band, then a life estimate can be calculated from G(w) for given material properties K and b. Hence, still at the design stage, by changing the geometry of the component or the structure, a new set of power spectral density plots can be calculated and an optimum life estimate can be achieved resulting in a considerable reduction in testing time. The method has been used in aircraft testing for some time[7], and has recently been extended to testing offshore structures[8, 9].

3.3.3 The Wide-Band Case:

Consider a stationary Gaussian process $\underline{x}(t)$ with zero mean value and variance σ_x^2, defined by Eq. 3.8. In terms of a standardized variable z with zero mean and unit variance, namely

$$z = \frac{x}{\sigma_x}$$

the peak probability density function w(z) which defines the probability that a peak will fall between z and z + dz is expressed as[3],

$$w(z) = \frac{c}{\sqrt{2\pi}} e^{-z^2/2c^2} + \gamma z e^{-z^2/2} \left[\tfrac{1}{2} + \mathrm{erf}(\gamma z/ c)\right] \quad \textbf{Eq. 3.32}$$

where γ is the irregularity factor defined by Eq. 3.2Ø, and

$$c = \sqrt{1 - \gamma^2}$$

and

$$\mathrm{erf}(y) = \frac{1}{\sqrt{2\pi}} \int_0^y e^{-t^2/2} dt$$

The shape of w(z) is determined by the irregularity factor, γ. If γ approaches unity, i.e. the narrow band case, then w(z) reduces to

a standard Rayleigh probability density function.

$$w(z) = ze^{-z^2/2} \qquad \textbf{Eq. 3.33}$$

If γ approaches zero, where the expected number of peaks per unit time is much larger than the expected number of zero crossings per unit time, then w(z) approaches a standard Gaussian probability density function:

$$w(z) = \frac{1}{\sqrt{2\pi}} e^{-z^2/2} \qquad \textbf{Eq. 3.34}$$

Note that, for the narrow band case, w(z) approaches a Rayleigh density function, although a Rayleigh density function is defined only for positive values of z, the general expression of Eq. 3.32 is valid for all values z.

The general form of w(z), Eq. 3.32, is something between a Gaussian and a Rayleigh probability density function, and is plotted in Fig. 3.4 as a function of z for 4 values of the dimensionless parameter γ, γ = .99, .74, .49 and .21.

However, having the peak probability density function w(z) does not make the fatigue damage estimation any easier for the wide band case. If the process is wide band, a time history of which is given in Fig. 3.1.d, it is not immediately obvious how to count fatigue stress cycles to be used with Miner's rule. It is assumed here that the rainflow method provides the answer to this problem, as it can identify cycles associated with closed hysteresis loops.

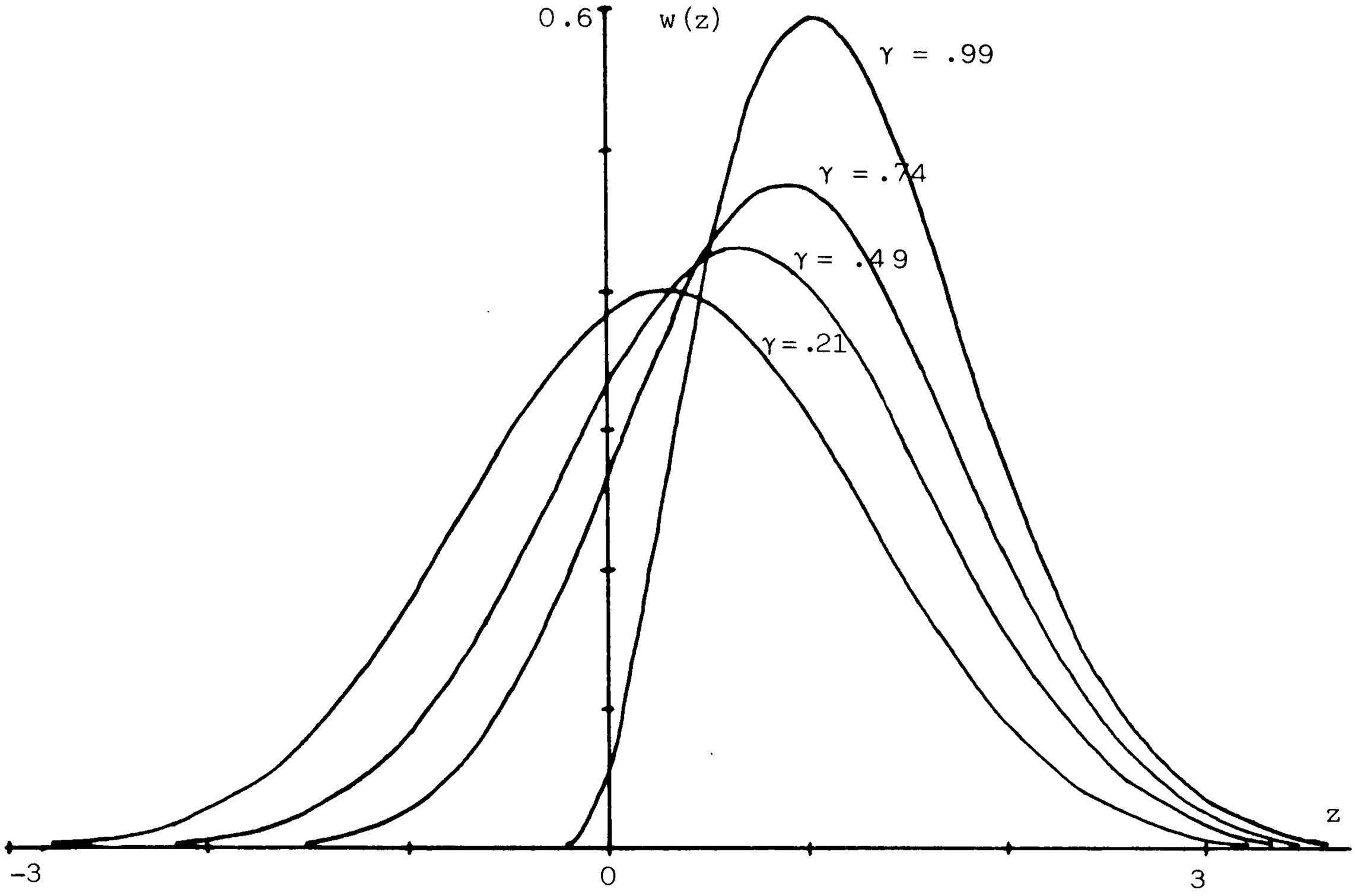

Fig. 3.4 Peak Density Total Density Function w(z) against the standardized variable z. (Eq. 3.32).

Because of the complexity of the rainflow count algorithm, it would be a very difficult task to derive the distribution of rainflow cycles from the spectral density function G(w). However, a Monte Carlo approach can be employed to generate a sample stress history $\underline{s}(t)$ from G(w) using FFT methods. Then the rainflow algorithm can be used on $\underline{s}(t)$ to extract the cycles and the probability density function of 'rainflow counted ranges' may be determined, which in turn may be used to calculate the fatigue damage by Eq. 3.27 for any given material constants K and b.

A similar approach has been employed by Wirsching et al[10, 11] to determine the probability density function of rainflow extracted ranges, and hence the fatigue damage, for a given power spectral density, G(w), by generating a random sample stress-time history $\underline{s}(t)$. In the first of these papers[10], the possibility of modelling the rainflow ranges of $\underline{s}(t)$ with a Weibull distribution function has been investigated. However, the simulation results showed that the density of $\underline{s}(t)$ in general is not Weibull. Despite this, the damage calculated by summing the contribution of individual rainflow cycles was compared with the damage calculated from the range density function assuming that it is Weibull. A correction factor which is a function of the irregularity factor γ, and the slope of S/N curve b, was suggested in conjunction with Weibull distribution.

In the second paper[11], no attempt was made to determine the probability density function of rainflow ranges. Instead, the fatigue damage under a wide band stationary process was compared with the fatigue damage of an equivalent narrow band process. Again a correction factor which is a function of γ and b, was proposed, this time in conjunction with a Rayleigh distribution having the same rms and the same expected rate of zero crossings as the wide band case. The correction factor, $\underline{C}$ in turn was treated as a random variable, Eq.3.35.

$$\underline{C}(b, \gamma) = 0.926-0.033b + (0.074 + 0.033b)(1-\sqrt{1-\gamma^2})^{1.587b-2.323} \qquad \text{Eq. 3.35}$$

3.4 Description of the Simulation:

3.4.1 General Procedure:

(i) For a given power spectral density G(w), calculate the zeroth second and fourth moments by using Eq. 3.7 i, ii, iii. Then calculate the rms or the standard deviation by Eq. 3.8, the expected rate of zero crossings by Eq. 3.15, the expected rate of peaks by Eq. 3.17, and the irregularity factor by Eq. 3.2Ø.

(ii) Generate a sample stress time history $\underline{s}(t)$ from G(w), by using inverse discrete Fourier transform (IDFT):

$$\underline{s}(k\Delta t) = \frac{\Delta w}{2\pi} \sum_{n=-N/2}^{N/2-1} \underline{F}(jn_{\Delta}w)\, e^{J2\pi kn/N} \qquad \textbf{Eq. 3.36}$$

where

$$k = Ø, 1, \ldots\ldots, N-1$$

$$\underline{F}\ (jn\Delta w) = \sqrt{G(n\Delta w)}\ e^{j\underline{\Phi}n},\ n = 1,\ N/2-1$$

and $\underline{\Phi}_n$ is a random phase angle uniformly distributed in the interval $[-\pi, \pi]$. N is the total number of samples and Δw and Δt are linked as:

$$N\Delta\, w\Delta t = 2\pi \qquad \textbf{Eq. 3.37}$$

Since $\underline{s}(k\Delta t)$ is expected to be a real function of time, the spectrum $\underline{F}(jn\Delta w)$ has to exhibit complex conjugate symmetry:

$$\underline{F}\ (jn\Delta w) = \underline{F}^*(-jn\Delta w),\ n = 1,\ 2,\ \ldots(N/2-1) \qquad \textbf{Eq. 3.38}$$

A further restriction on $\underline{F}(jn\Delta w)$,

$$\underline{F}\ (Ø) = Ø \qquad \textbf{Eq. 3.39}$$

ensures that the time history $\underline{s}(k\Delta t)$ has zero mean value.

(iii) Recalculate the rms from the stress time history $\underline{s}(k\Delta t)$

$$\sigma_s^2 = \frac{1}{N} \sum_{k=0}^{N-1} \underline{s}(k\Delta t)^2 \qquad \textbf{Eq. 3.4Ø}$$

and count the number of zero crossings and the number of peaks, and determine the irregularity factor. Compare these values against those calculated in step (i).

(iv) Repeat steps (ii) and (iii) 20 times in order to obtain a sufficiently long record, and call this record, one block of stress time history. Determine the amplitude probability density function for the block.

(v) Convert a block of stress time history to point process of peaks and troughs. Determine the peak and trough probability density functions.

(vi) Define 'an ordinary range' as the distance between successive peaks and troughs. Extract ordinary ranges, and apply a rainflow counting method to peaks and troughs to extract rainflow ranges. Determine the ordinary and rainflow range probability density functions.

(vii) Calculate the expected damage for various values of b by using rainflow counted ranges.

3.4.2 Simulation

The procedure described above is carried out on an RT-11 computer system which is constructed around a DIGITAL PDP-11 computer. A 1024-point FFT subroutine is used to obtain a sample stress-time history from a given power spectral density.

(i) A total of 7Ø different spectral densities are used. For the ease of comparison, the densities are shaped in such a way that they all have the same rms and the same expected rate of peaks, calculated by Eq. 3.8 and 3.17 respectively. The expected rate of peaks is chosen, arbitrarily, as 1Ø8 peaks per block so that there would be roughly 5 points between successive peaks and troughs yielding a 'smooth' stress-time history.

The two types of spectra used in this study are shown in Fig. 3.5. The rectangular bimodal spectrum, Fig. 3.5-a, is used extensively because of its simplicity to assume a wide range of values of the irregularity factor γ, having the same rms σ_x, and the same expected rate of peaks, μ, by adjusting the amplitudes and the frequency boundaries. The smooth spectrum in Fig. 3.5.b is a combination of two band pass filters, each having the analytical form:

$$|G_i(w)|^{1/2} = \frac{A}{\sqrt{1 + (f - f_i)^2/Q^2}} \qquad \textbf{Eq. 3.41}$$

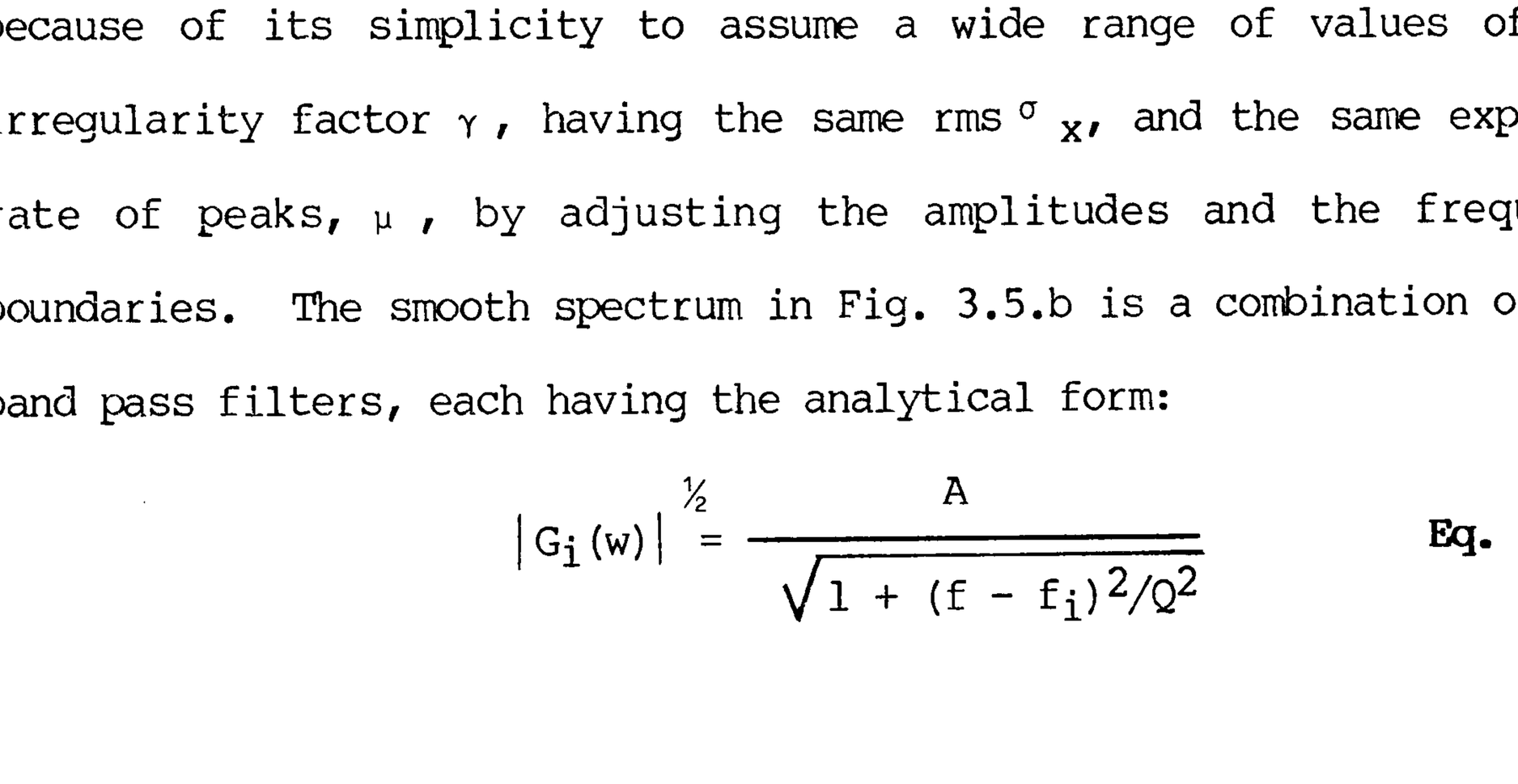

Fig. 3.5 Spectral Density Shapes

Initially, 14 smooth spectra and 14 rectangular spectra were used, covering a range of irregularity factors from .16 to .99 at fairly regular intervals. It is quite possible to find several spectral shapes having the same σ_x, μ and γ. A study of Eq. 3.7, 8, 16, 17 and 20 shows that the zeroth, second and fourth moments of the spectral densities must have the same values for each shape in order to have the same σ_x, μ and γ.

Despite the fact that the first moment of any spectral density of a real process $\underline{x}(t)$ is zero, let us define a single-sided first moment:

$$m_x = \frac{1}{\pi} \int_0^\infty wG(w)\ dw \qquad \textbf{Eq. 3.42}$$

Then the quantity m_x/m_o could be considered as the 'mean frequency' of the spectral density.

During the initial trials of fixing the spectrum parameters in Fig. 3.5 to have the same σ_x, μ and γ, it was soon observed that there is a link between the mean frequency of the spectrum and the fatigue damage calculated from the corresponding time domain history. In order to investigate this link further, 42 more spectra were chosen. They consist of 6 groups of 7 spectra, each spectrum of a group has the same σ_x, μ and γ, but different m_x.

The mean frequency of each spectrum was normalized by the expected rate of peaks to yield a dimensionless quantity, X_m,

$$X_m = \frac{m_x}{m_c \mu} \qquad \textbf{Eq. 3.43}$$

which could be considered as the 'relative mean' of the spectral density.

The spectral parameters described by Fig. 3.5.a and 3.5.b and Eq. 3.41 are listed in Table 3.1 for 70 spectra used in this study. The last two columns in Table 3.1 show the corresponding relative mean and irregularity factor, respectively, for each spectrum. Fig. 3.6.a shows a typical unimodal smooth spectrum, listed as Sp-2 in Table 3.1, and Fig. 3.6.b shows a bimodal spectrum, Sp-7. All the spectra have the same rms, 176.78, and have approximately the same expected rate of peaks, ~108.5 peaks per block.

(ii) Sample time histories (t) are generated as described in Section 3.4.1.ii. Fig. 3.7.(a), (b) and (c) shows 3 1024-point sample time histories at irregularity factors .99, .74 and .27, for Spectra 17, 24 and 28 respectively.

(iii) The mean and the rms of each sample time history $\underline{s}(t)$ are calculated. They are found to be 0.0 and 176.7, respectively, as expected.

(iv) The step (ii) is repeated 20 times and the sample time histories are conconated to give a sufficiently long record of stress time history, consisting 20480 sample points. This record is called one block. The number of zero crossings and the number of peaks are counted for each block, and they are found to be within less than .1% for most cases and within 5% for the worst case, of the values

calculated in step (i). Therefore the number of zero crossings and the number of peaks are assumed to be deterministic. Fig. 3.8 shows the amplitude probability density function of a typical block as compared with a Gaussian density function with zero mean and variance of 176.78. Regardless of the irregularity factor and the relative mean, all the amplitude probability density functions for all the spectra conform to the Gaussian density function with zero mean and σ_x.

(v) A block, as defined in step (iv), is then passed through a 'peak detector' subroutine, i.e. continuous time history is converted into the point process of peaks and troughs. Ordinary ranges and the rainflow ranges are extracted from the peak-trough history and stored for further analysis. Since the fatigue damage is assumed to be proportional with the b^{th} moment, where b is the slope of S-N curve, of the rainflow ranges density function, 1st, 2nd , 3rd, 6th and 9th moments are calculated and stored.

(vi)s Steps (ii) to (v) are repeated 10 times for each spectrum.

(vii) Steps (ii) to (vi) are repeated for each spectrum.

Table 3.1.

Smooth Spectra Parameters (Fig. 3.5b)

Sp	A_1	f_1	Q_1	A_2	f_2	Q_2	f_c	x_m	γ
1	32767	98.0	5.0	-	-	-	229	.908	.924
2	23580	90.0	10.0	-	-	-	210	.839	.869
3	22543	82.0	11.0	-	-	-	226	.775	.813
4	21683	74.0	12.0	-	-	-	233	.710	.757
5	20226	65.5	14.1	-	-	-	227	.644	.701
6	26333	40.5	5.0	18444	105	3.0	242	.567	.650
7	27019	30.0	5.0	20264	104	2.5	231	.493	.600
8	29204	32.0	5.0	17522	108	2.0	237	.450	.549
9	30202	30.0	5.0	15101	106	1.9	245	.403	.500
10	31527	29.0	5.0	10404	114	2.0	237	.360	.451
11	29680	25.0	6.0	7420	108	2.0	235	.311	.400
12	30402	20.0	6.0	6081	109	2.0	225	.257	.349
13	31091	19.8	6.0	-	-	-	236	.229	.300
14	32741	14.3	5.6	-	-	-	222	.182	.258

Rectangular Spectra Parameters (Fig. 3.5a)

Sp	A_1	f_1	p_1	A_2	f_2	p_2	x_m	γ
15	31800	2	17	3572	123	138	.092	.160
16	31500	2	17	3984	103	134	.109	.210
17	31000	2	17	5020	93	132	.137	.270
18	30000	2	17	5324	69	138	.183	.345
19	29000	2	17	7045	76	134	.236	.418
20	28000	2	17	11130	94	124	.293	.490
21	27000	2	17	12758	95	123	.342	.541
22	25000	2	17	10873	78	131	.420	.607
23	23000	2	17	12111	78	131	.501	.673
24	20000	2	17	13008	74	132	.604	.746
25	18000	2	17	16330	86	127	.688	.809
26	12000	2	17	13984	64	135	.791	.860
27	8000	2	17	16562	76	131	.890	.926
28	4000	2	17	30801	101	117	.981	.988

Table 3.1 (cont.)

Rectangular Spectra Parameters (Fig. 3.5a)

Sp.	A_1	f_1	p_1	A_2	f_2	p_2	x_m	γ
29	16000	2	15	32660	104	115	.795	.884
30	15850	2	14	21268	94	122	.802	.885
31	13700	2	17	18290	87	126	.809	.885
32	11100	2	22	16289	79	130	.819	.885
33	7840	2	40	15397	74	132	.831	.885
34	5440	2	62	14036	63	136	.839	.883
35	-	-	-	13492	49	138	.853	.885
36	23400	2	11	30150	104	115	.682	.815
37	17020	2	20	23930	100	118	.693	.815
38	14000	2	30	23130	100	119	.701	.814
39	12000	2	41	19140	95	123	.713	.815
40	11000	2	44	14664	80	131	.722	.815
41	9700	2	53	13296	71	135	.733	.815
42	7900	2	48	12158	49	139	.744	.814
43	24700	2	13	27482	104	115	.579	.745
44	18000	2	24	22276	101	118	.596	.744
45	17150	2	25	15081	87	127	.606	.746
46	15900	2	25	12140	66	135	.621	.747
47	12500	2	49	12826	80	133	.632	.746
48	11900	2	42	11156	55	139	.640	.746
49	-	-	-	10818	2	141	.648	.746
50	22480	2	19	23677	104	116	.495	.674
51	22300	2	19	17243	97	121	.499	.675
52	21700	2	19	12452	80	130	.508	.676
53	20900	2	19	10955	65	135	.518	.676
54	19700	2	19	10107	48	139	.526	.675
55	18700	2	19	9897	38	140	.533	.675
56	14800	2	31	9714	38	141	.546	.675
57	22000	2	23	21863	105	116	.423	.606
58	21000	2	25	14392	96	123	.429	.606
59	19820	2	28	13036	93	126	.436	.607
60	17980	2	34	11147	86	131	.448	.607
61	18000	2	32	9319	66	138	.450	.605
62	17090	2	32	8605	44	142	.460	.605
63	16000	2	35	8433	36	143	.468	.607
64	27200	2	17	13764	98	121	.334	.533
65	26900	2	17	10222	84	129	.341	.536
66	26400	2	17	8525	65	136	.346	.534
67	25980	2	17	8154	55	138	.352	.536
68	25580	2	17	7849	45	140	.354	.534
69	25000	2	17	7724	35	141	.360	.535
70	22200	2	20	7586	21	142	.370	.535

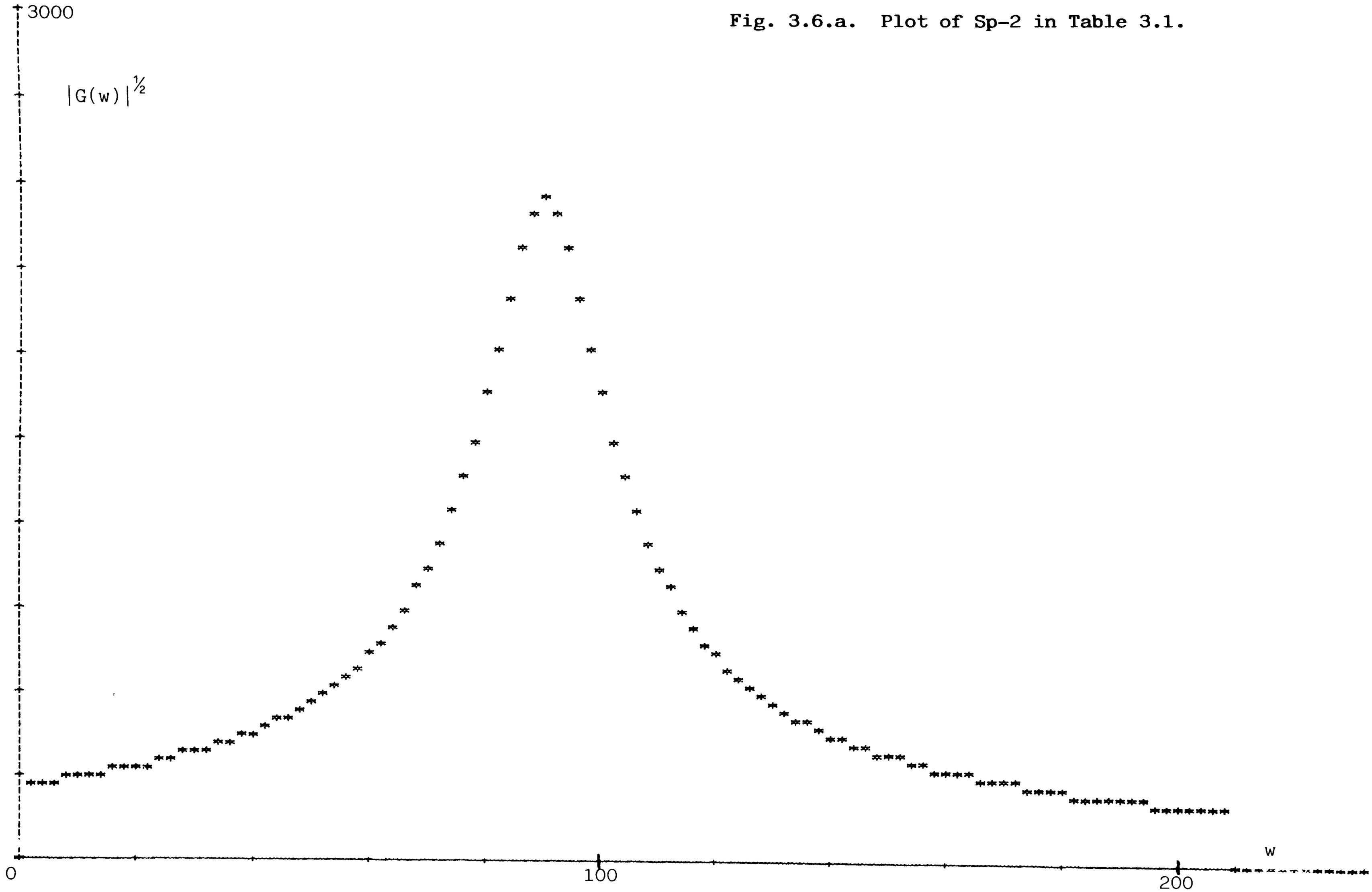

Fig. 3.6.a. Plot of Sp-2 in Table 3.1.

Fig. 3.6.b. Plot of Sp-7 in Table 3.1.

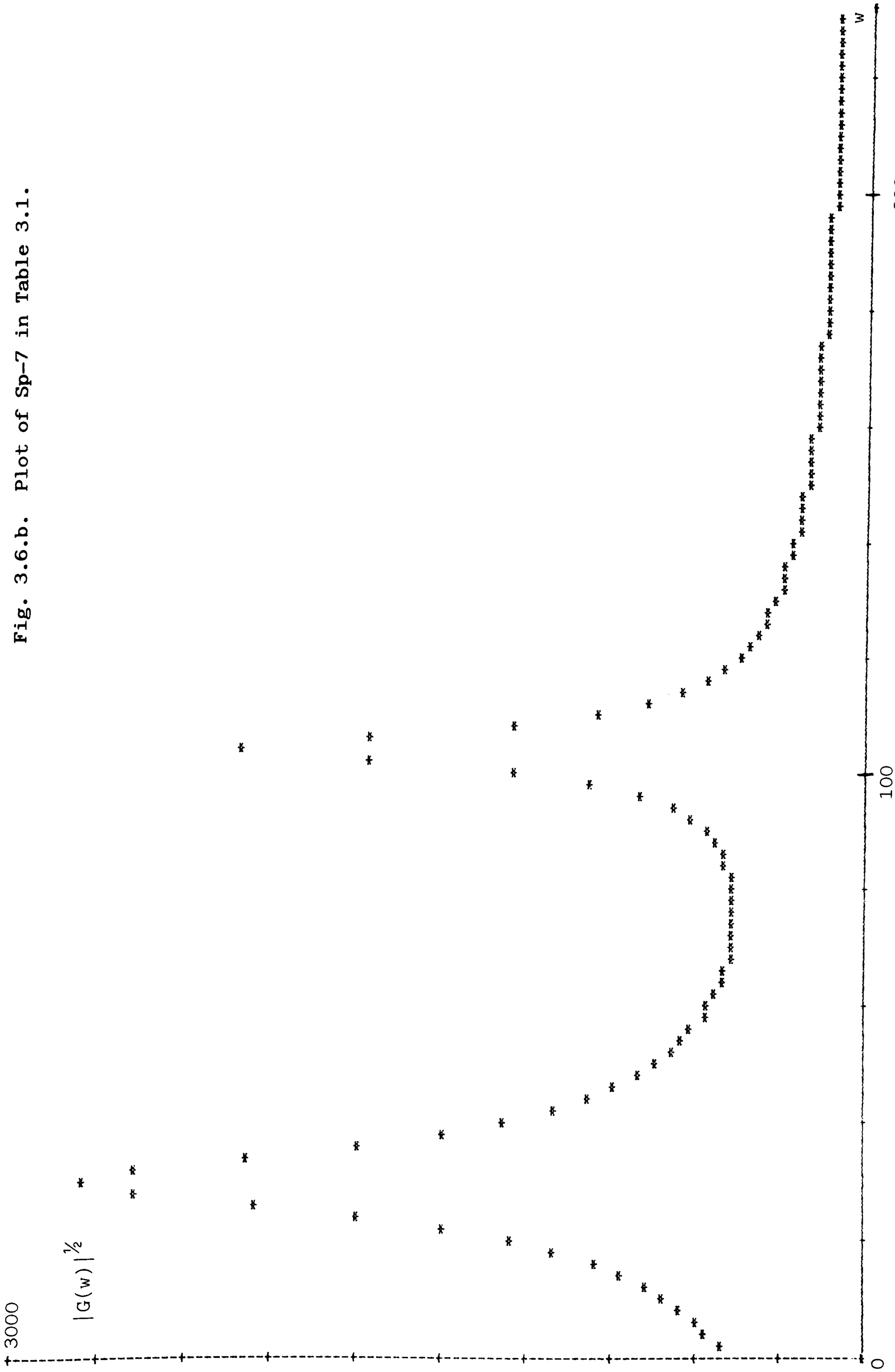

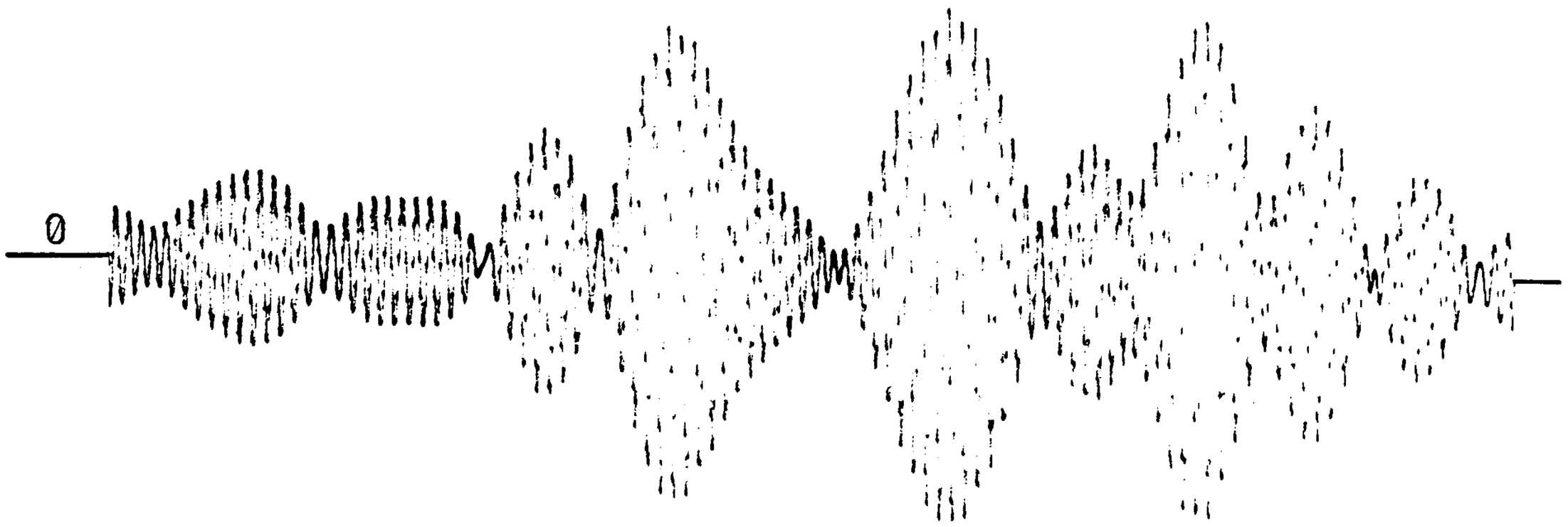

Fig. 3.7.a. Time History, γ = .99

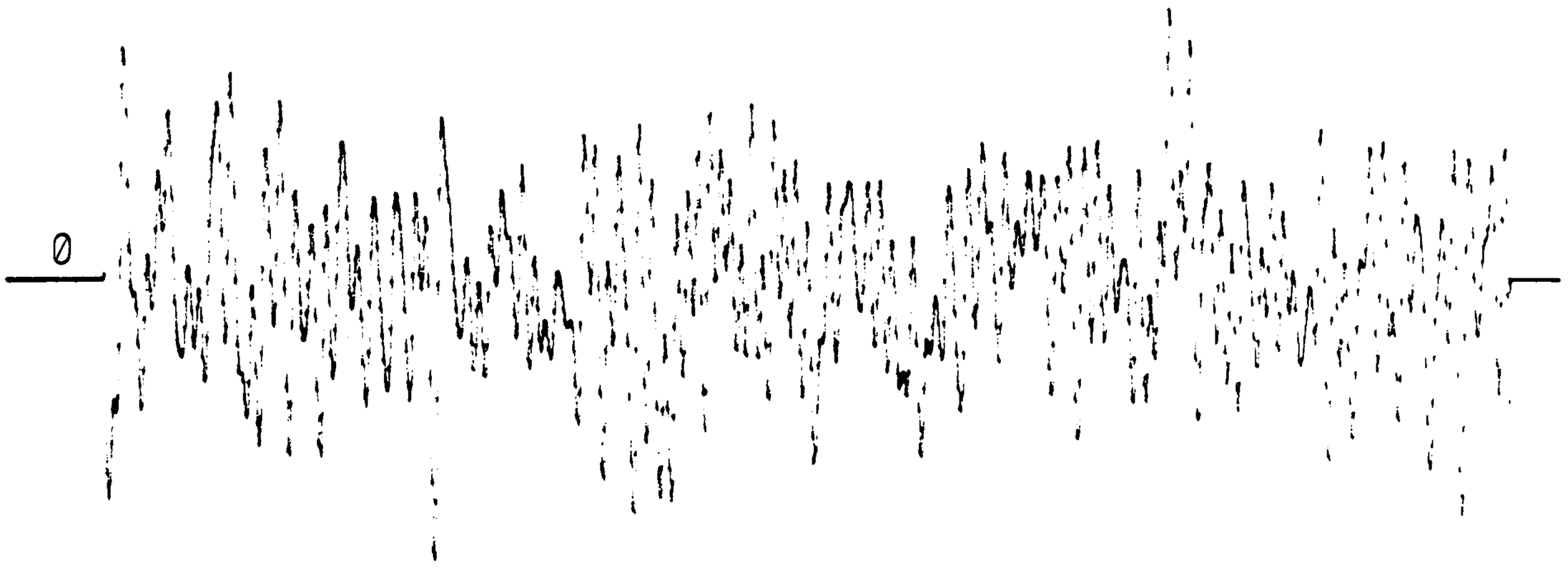

Fig. 3.7.b. Time History, γ = .74

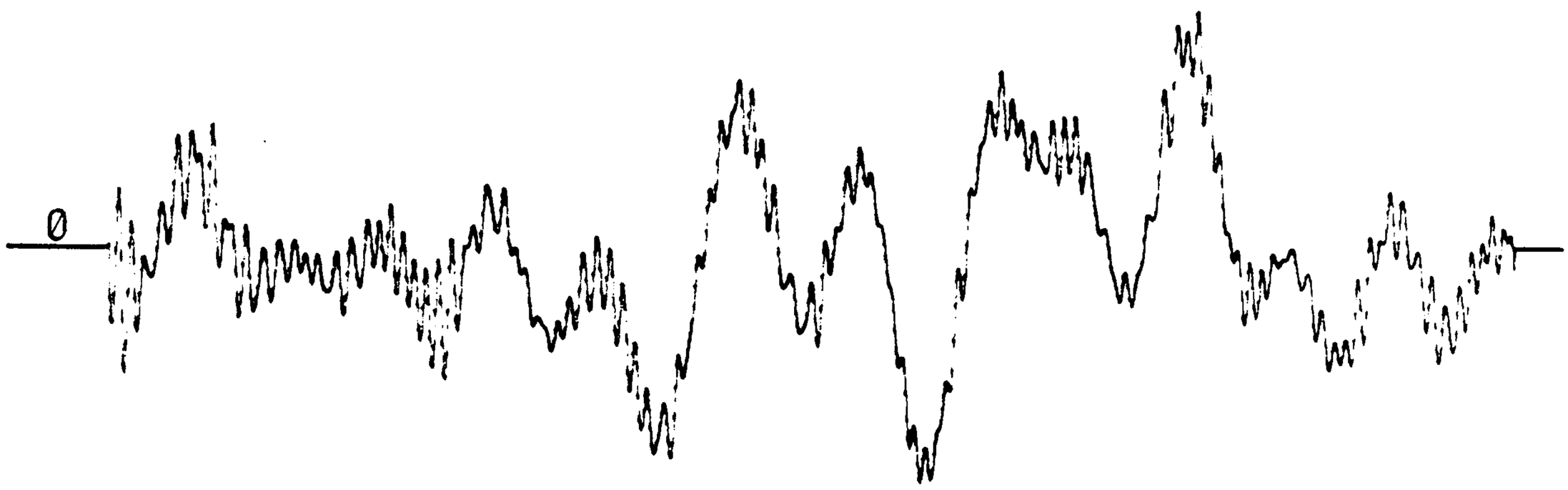

Fig. 3.7.c. Time History, γ = .27

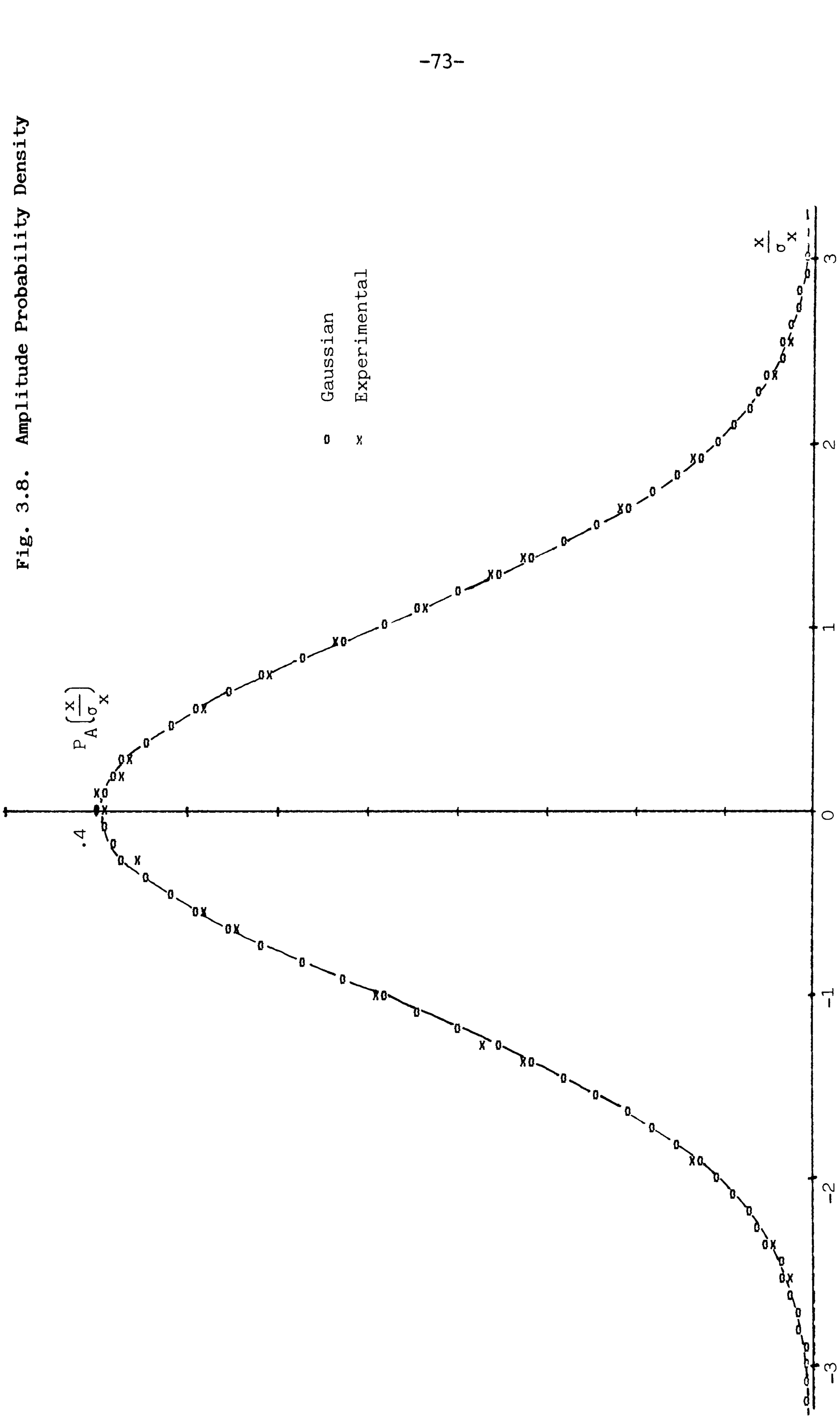

Fig. 3.8. Amplitude Probability Density

3.5 Results

Since the rms, σ_x, of the stress time histories is observed to be constant for all the spectra, the values of peaks and troughs are normalized by σ_x, and ordinary ranges and rainflow ranges are normalized by $2\sigma_x$.

In the ideal case of a narrow band power spectrum where the irregularity factor approaches unity, the distribution of both ordinary and rainflow ranges approaches the Rayleigh distribution. The fatigue damage calculations, in other words the moments of the rainflow ranges distribution, in section 3.4.2.(v) are normalized with the moments of the Rayleigh distribution. The Rayleigh distribution and its moments are:

$$f_R(x) = \frac{x}{\sigma_x^2} e^{-x^2/2\sigma_x^2} \qquad \textbf{Eq. 3.44}$$

$$M_R(b) = (\sqrt{2}\sigma_x)^b \Gamma\left(1 + \frac{b}{2}\right) \qquad \textbf{Eq. 3.45}$$

where Γ (.) is a Gamma function.

3.5.1. Peak-Trough Density Functions:

Although the distribution of peaks and troughs was not one of the objectives of this study, they are nevertheless investigated in the hope that they might shed some light on the distribution of ordinary ranges and particularly rainflow ranges. Another interesting point is to check the validity of Eq. 3.22 which defines the peak probability density function. Fig. 3.9 shows the simulation results and corresponding predicted results, by Eq. 3.32, of the peak density functions for 4 different irregularity factors, =.99, .74, .49 and .21

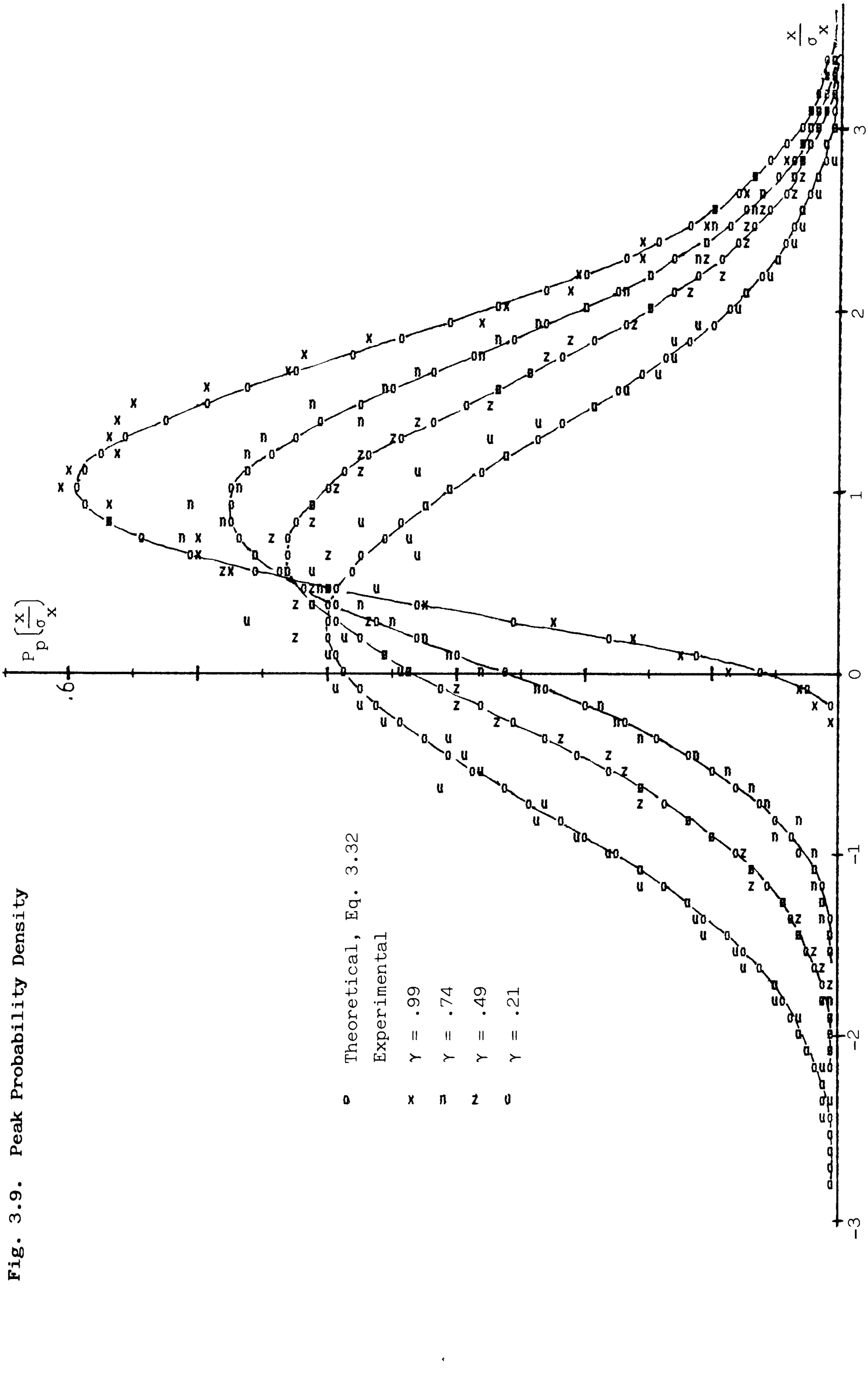

Fig. 3.9. Peak Probability Density

3.5.2. Ordinary-Range Density Functions:

Fig. 3.1Ø shows some examples of the ordinary-range density functions. Each plot of Fig. 3.1Ø represents a sample of approximately 43ØØØ ranges. Counting of the ranges is carried out with spacings of $\Delta x = Ø.Ø45\,\sigma_x$. Probability density function of ordinary-ranges is defined as:

$$P_{OR}\left(\frac{x}{2\sigma_x}\right)\Delta x = \frac{\text{No. of ranges in the interval } [x - \frac{\Delta x}{2},\ x + \frac{\Delta x}{2}]}{\text{Total no. of ranges}}$$

The probability densities are then smoothed by fitting a second-order polynomial (parabola) to successive 7 data points, and the mid-point is calculated from the parameters of the fitted polynomial. This is done for the clarity of representation of density functions.

Fig. 3.1Ø.i shows the probability density functions of ordinary-ranges for the smooth spectra with the irregularity factor varying from $\gamma = .3Ø$ to $\gamma = .92$. A cursory examination of these plots does not reveal much of the nature of density functions, particularly when $x < 2\sigma_x$. However 3.1Ø.ii, plot of density functions for the rectangular spectra reveals more about the link between the irregularity factors and corresponding density functions. The plot which corresponds to $\gamma = .99$ in Fig. 3.1Ø.ii is almost a perfect fit to a Rayleigh distribution with a Rayleigh parameter of $2\sigma_x$, as expected. As the irregularity factor γ decreases, the probability density functions keep their Rayleigh distribution shape except near the origin and peak at approximately $x = 2\sigma_x.\gamma$. In terms of a standardized variable z, where $z = x/2\sigma_x$, Fig. 3.1Ø.ii suggests the

Fig. 3.10.i. Ordinary-Range Density Functions (Smooth Spectra)

Y	Sp. No.
.92	1
.81	3
.70	5
.60	7
.50	9
.40	11
.30	13

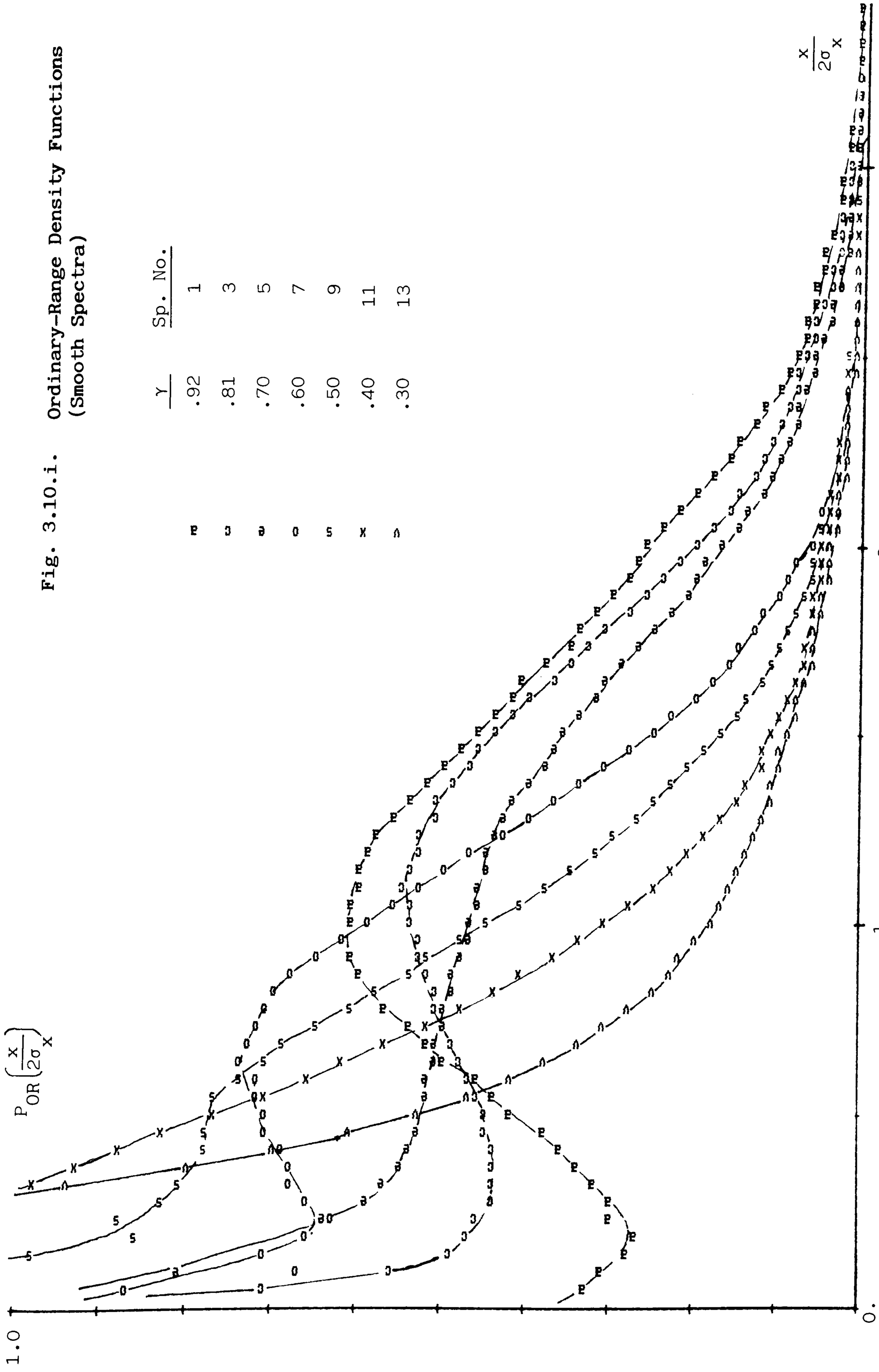

Fig. 3.10.ii. Ordinary Range Density Functions
(Rectangular Spectra)

γ	Sp. No.
.99	28
.86	26
.74	24
.61	22
.49	20
.34	18
.21	16

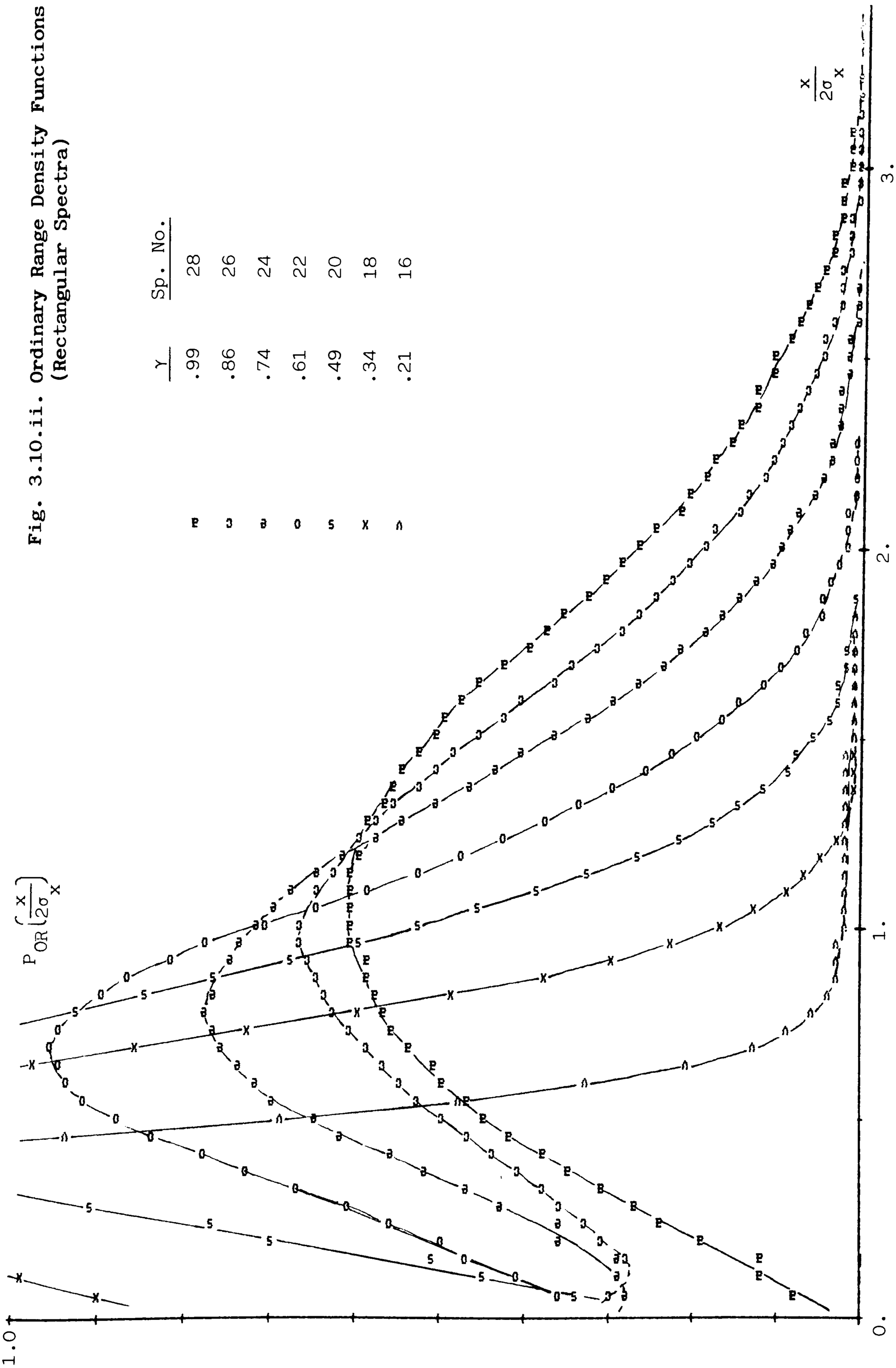

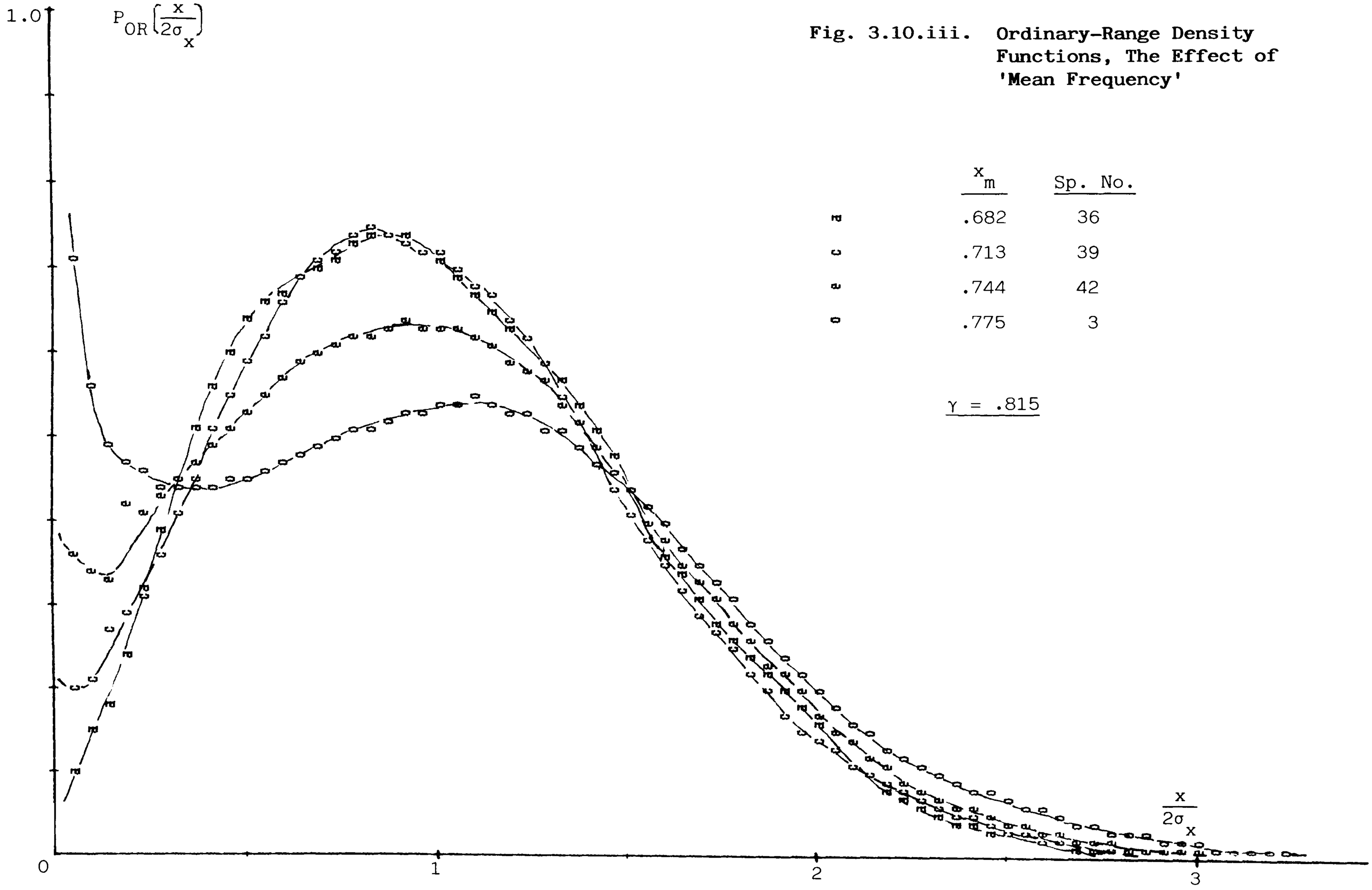

Fig. 3.10.iii. Ordinary-Range Density Functions, The Effect of 'Mean Frequency'

	x_m	Sp. No.
a	.682	36
c	.713	39
e	.744	42
o	.775	3

$\gamma = .815$

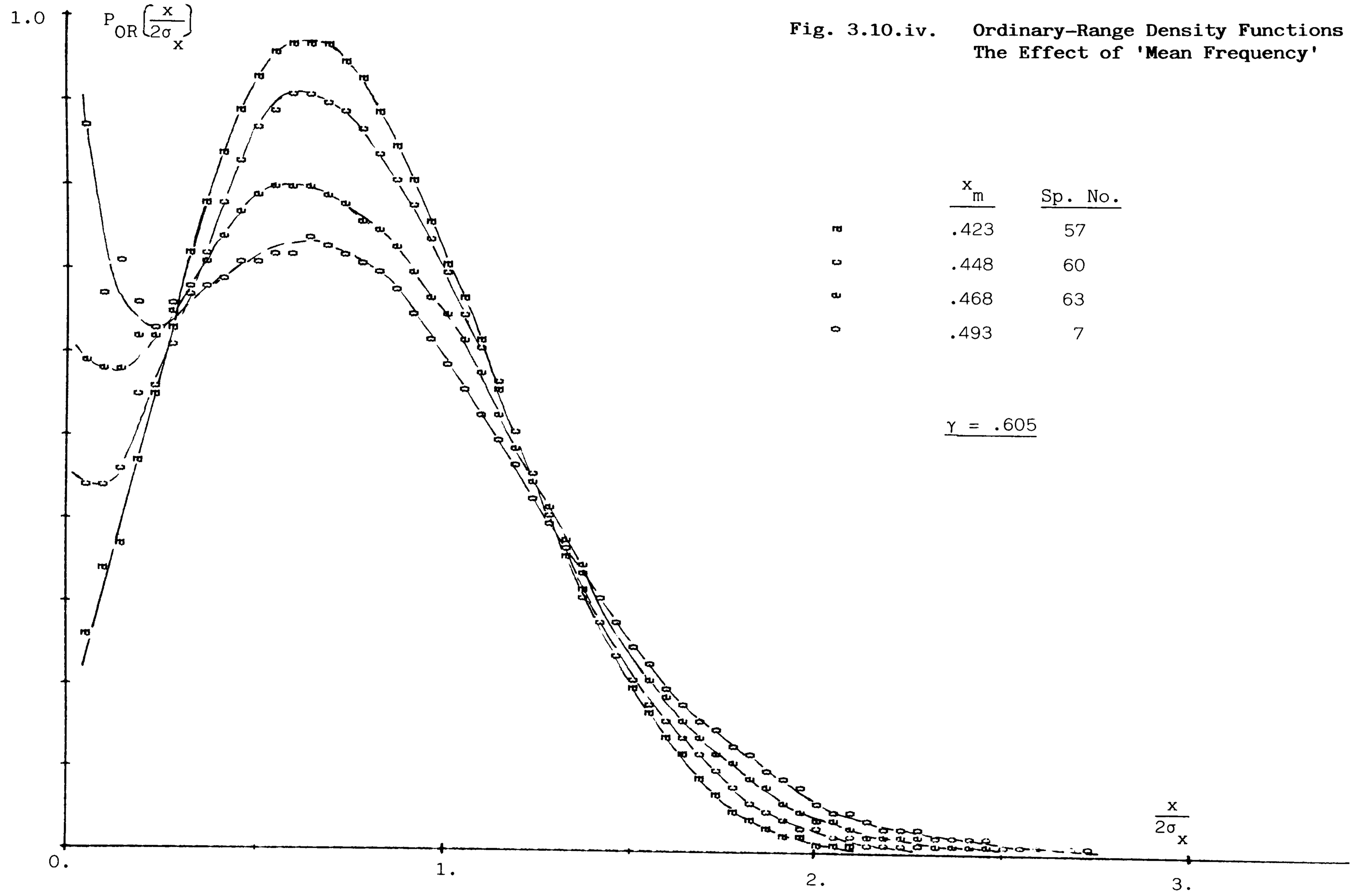

Fig. 3.10.iv. Ordinary-Range Density Functions
The Effect of 'Mean Frequency'

	x_m	Sp. No.
a	.423	57
c	.448	60
e	.468	63
o	.493	7

γ = .605

following equation between the irregularity factor and the corresponding probability density function:

$$P_{OR}(z) = \frac{z}{\gamma^2} e^{-z^2/2\gamma^2} \qquad \textbf{Eq. 3.46}$$

which is a Rayleigh distribution.

The basic difference between smooth and rectangular spectra is that the smooth spectra have greater 'mean frequency', x_m, values than the corresponding rectangular spectra x_m values for the same irregularity factors. The result of this difference on the range probability density functions is that, now looking back at Fig. 3.10.i again, higher densities for very small and very large ranges, and lower densities in the middle around $x/2\sigma_x = 1$.

The effect of mean frequency on the ordinary-range distribution is illustrated in Fig. 3.10.iii and Fig. 3.10iv. In each of these figures, the irregularity factor stays approximately constant, $\gamma = .815$ and .605 respectively, the mean frequency changes. When the mean frequency becomes the lowest, the corresponding density function approaches the Rayleigh distribution, as defined in Eq. 3.46, with a Rayleigh parameter of γ. As the mean frequency increases, the density near the origin increases, the peak around $x = 2\sigma_x$ decreases and also shifts to the right causing higher densities for large values of x.

In a similar study of J. R. Rice et al[5], the 'rise and fall' densities for stationary Gaussian random functions with rectangular power spectra are determined from the joint probability

density functions of x, $\dot{x}$ and $\ddot{x}$ with a 6-by-6 correlation matrix. In that study, it was observed that the rise and fall densities showed 'an unexpected hump' near the origin, and the authors were unable to say whether the hump was due to numerical inaccuracies or was inherent in the approximation developed. However, even if the densities near the origin could have been calculated accurately, which were claimed to be wildly fluctuating, it would still have been difficult to make a judgement on the nature of the hump, because the spacing of $\Delta x = .2\sigma_x$, at which the range densities were calculated, was too large to observe the behaviour of densities near the origin. Had a spacing of $\Delta x = .2\sigma_x$ been used in Fig. 3.10, the smooth variation of densities near the origin would have been seen as 'humps', too.

3.5.3. Rainflow-Range Density Functions:

Fig. 3.11 shows some examples of the rainflow-range probability density functions corresponding to the same cases in Fig. 3.10. As in the ordinary-range density functions, each plot of Fig. 3.10 represents a sample of approximately 43000 ranges and the counting of the rainflow ranges is carried out with spacings of $\Delta x = 0.045\sigma_x$. Probability density function of rainflow-ranges is defined as:

$$P_{RR}\left(\frac{x}{2\sigma_x}\right)\Delta x = \frac{\text{No. of ranges in the interval } [x - \frac{\Delta x}{2},\ x + \frac{\Delta x}{2}]}{\text{Total no. of ranges}}$$

Again, the probability densities are then smoothed by fitting a second-order polynomial to successive 7 data points.

Fig. 3.11.i and 11.ii show the probability density functions of

Fig. 3.11.i. Rainflow-Range Density Functions
(Smooth Spectra)

Sp. No.	γ
1	.92
3	.81
5	.70
7	.60
9	.50
11	.40
13	.30

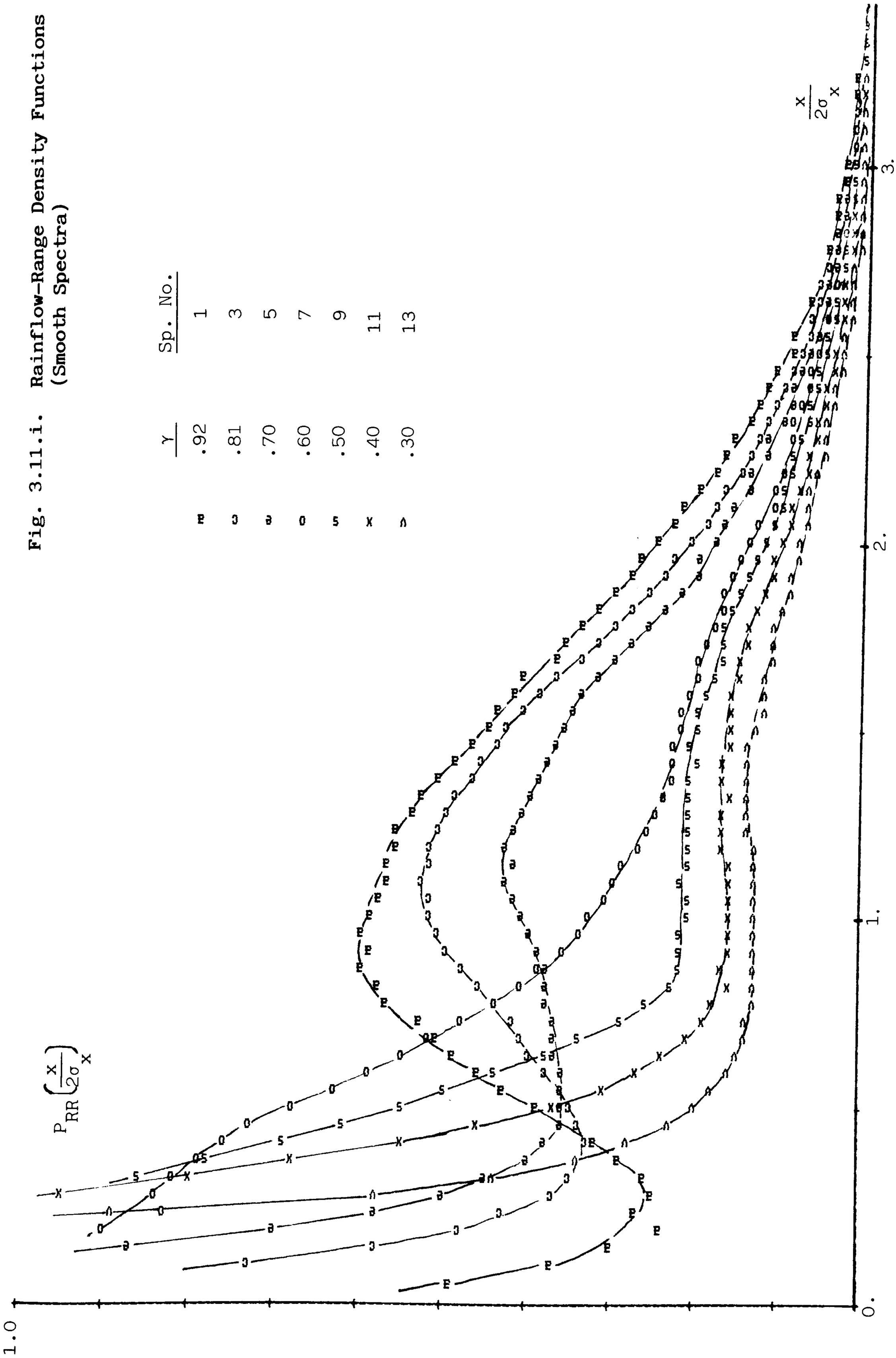

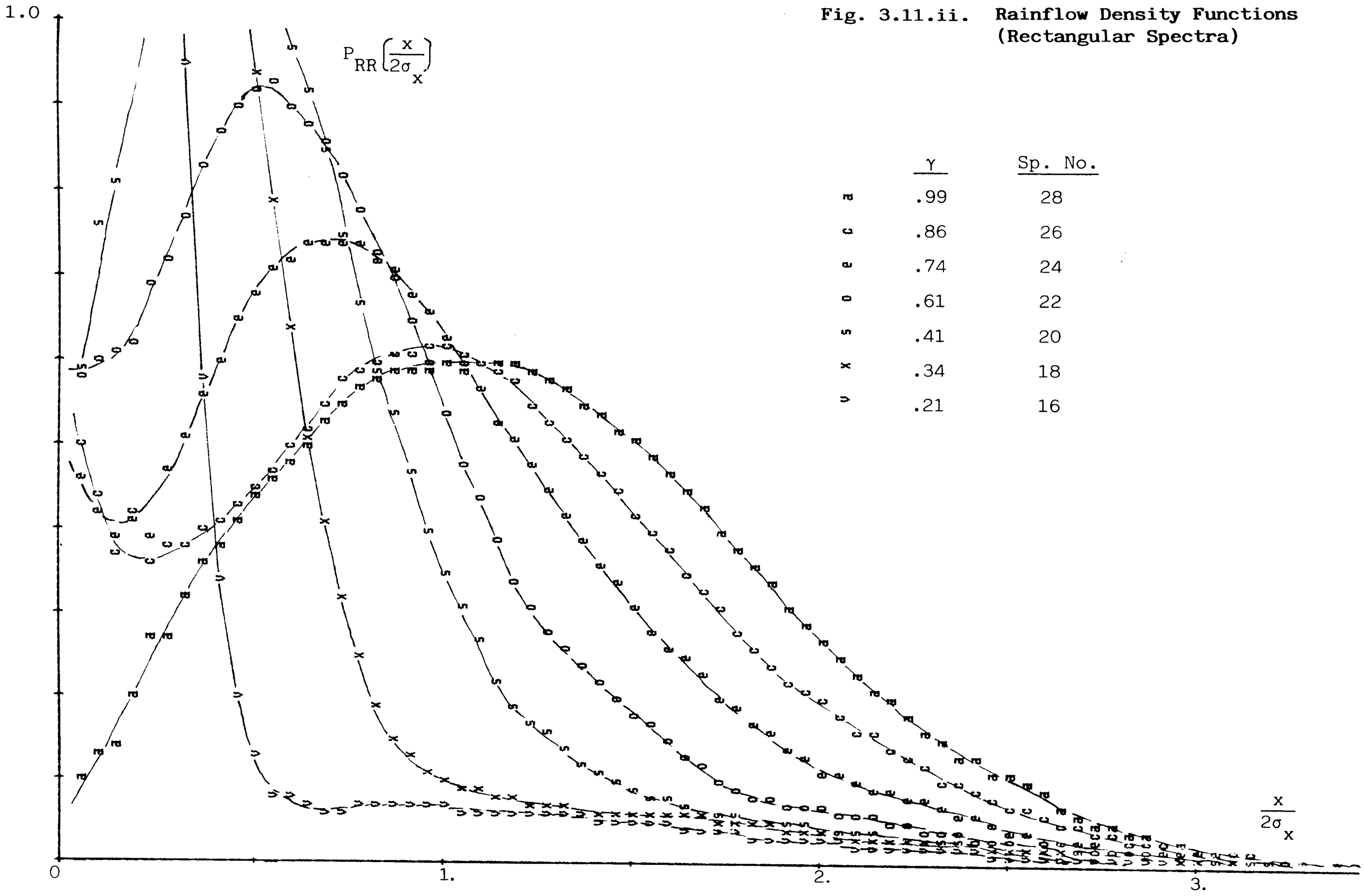

Fig. 3.11.ii. Rainflow Density Functions (Rectangular Spectra)

	γ	Sp. No.
a	.99	28
c	.86	26
e	.74	24
o	.61	22
s	.41	20
x	.34	18
v	.21	16

Fig. 3.11.iii. Rainflow-Range Density functions
The Effect of 'Mean Frequency'

	x_m	Sp. No.
a	.423	57
b	.448	60
c	.468	63
d	.493	7

$\gamma = .605$

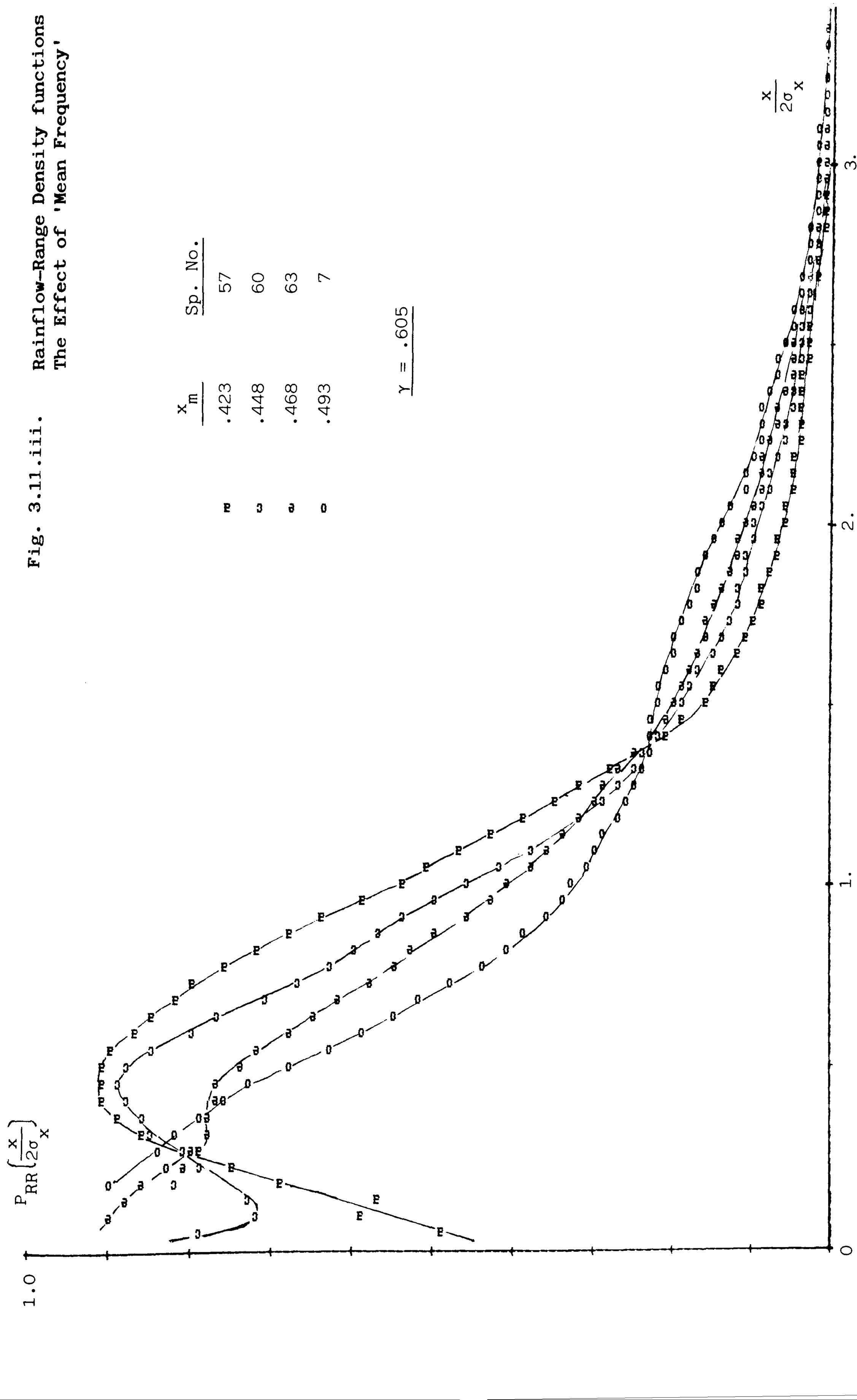

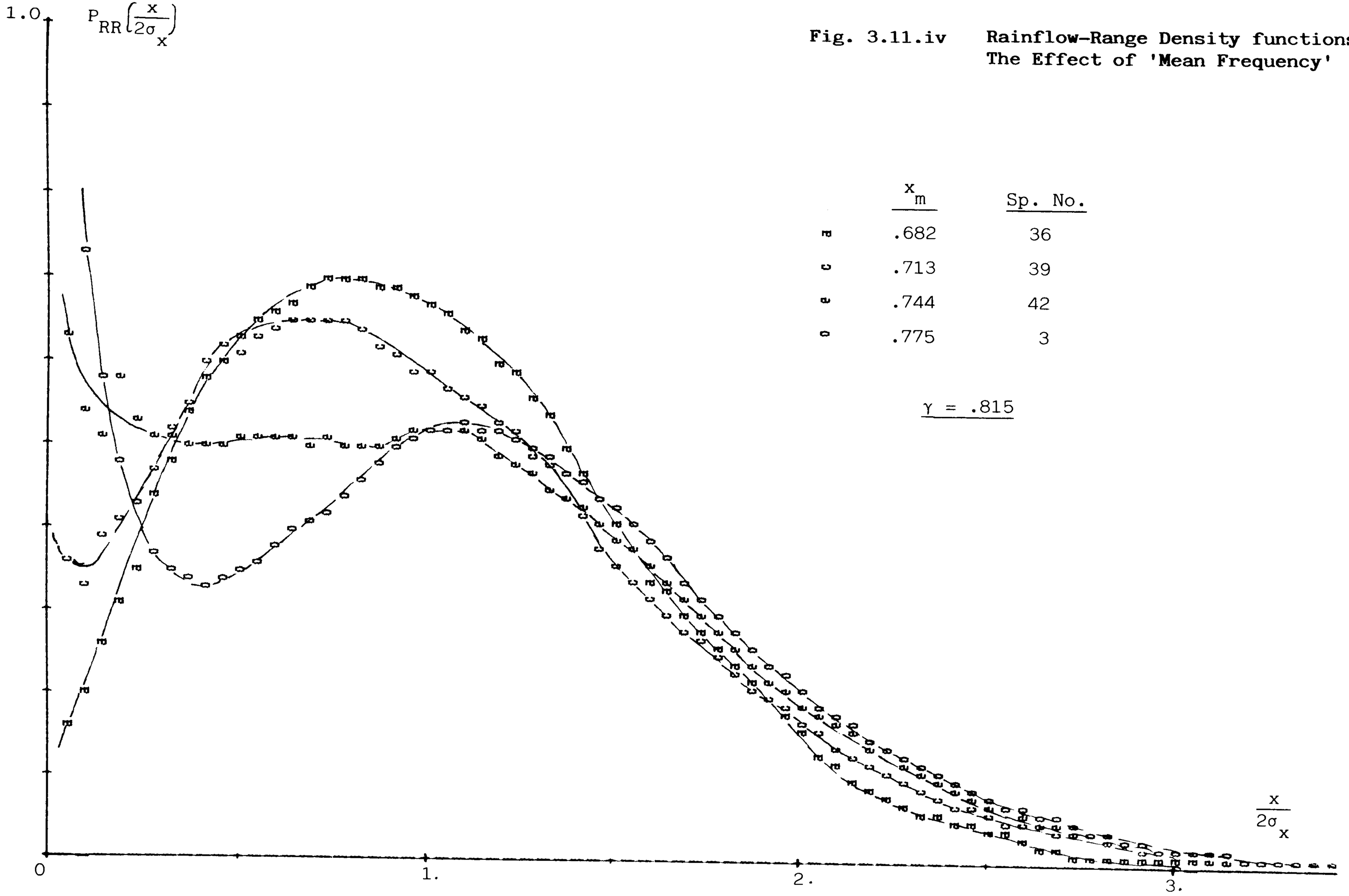

Fig. 3.11.iv **Rainflow-Range Density functions**
The Effect of 'Mean Frequency'

	x_m	Sp. No.
a	.682	36
c	.713	39
e	.744	42
o	.775	3

$\gamma = .815$

rainflow-ranges for the smooth and rectangular spectra respectively. A comparison of ordinary-range and rainflow-range densities indicates that, although both sets of plots appear to have the same shape, there are distinctive differences between the two densities corresponding to the same power spectrum. For the same irregularity factor and mean frequency, the density of rainflow-ranges is almost twice as much of its counterpart ordinary-range density near the origin. In the middle region where the densities peak, the rainflow-range density becomes smaller than the ordinary-range density. Another difference, the most important one from fatigue damage point of view, is that the rainflow range density becomes considerably higher than the ordinary-range density at higher ranges. For example, the ordinary-range densities approach zero at comparatively small ranges depending on the irregularity factor, as in Fig. 3.1Ø.ii, while the corresponding rainflow-range densities exhibit probabilities for comparatively large ranges even for small irregularity factors, Fig. 3.11.ii.

The above observation is consistent with the way in which the rainflow and ordinary ranges are counted. Small ranges BC and EF in Fig. 3.12 are interrupting larger ranges AD and DG respectively; while the ranges AB, BC, CD, DE, EF and FG are counted once only by the ordinary range method, the interrupting ranges BC and EF are counted twice, i.e. two ranges at the same level yielding two full cycles, BCB' and EFE', by the rainflow method, plus another full cycle ADG. Therefore, the rainflow method counts more ranges at small ranges, less at medium ranges, and more at high ranges than the ordinary range method does.

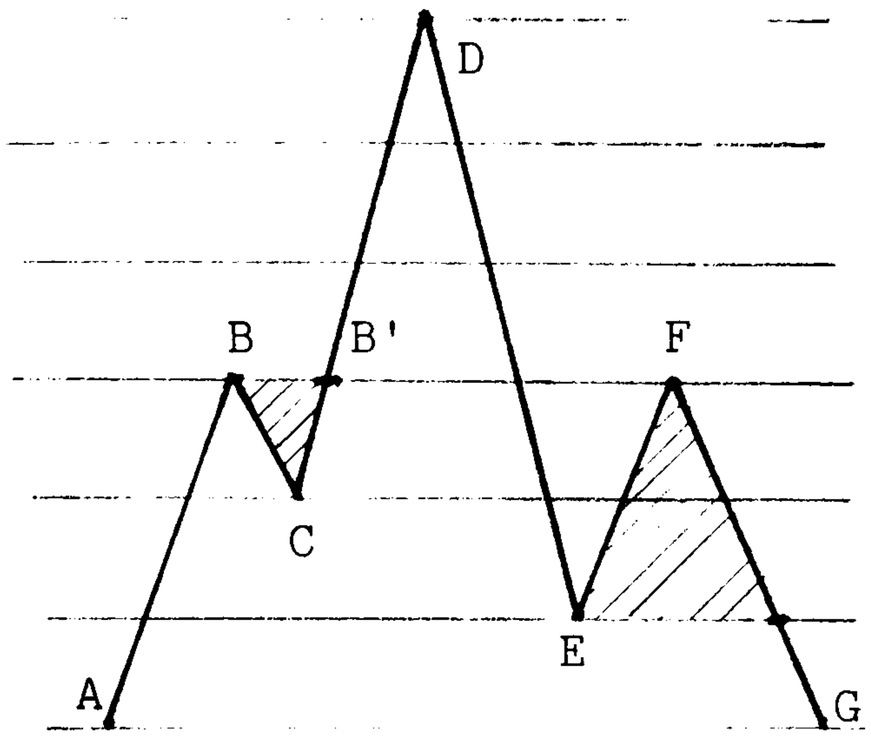

Level	Ordinary R	Rainflow R
1	1	2
2	1	2
3	2	-
4	1	-
5	1	-
6	-	2

Fig. 3.12 A comparison of rainflow and ordinary-range counting methods.

The effect of mean frequency on the rainflow-range distribution can be observed in Fig. 3.11.iii and 11.iv. Again in each of these figures the irregularity factor stays approximately constant, the mean frequency changes. As the mean frequency increases, the density of low and high ranges increases, the density of medium ranges decreases.

3.5.4. Moments

The moments of ordinary-range and rainflow range densities are calculated with the standardized variable $z = x/2\sigma_x$, and are normalized with the moments of the standard Rayleigh distribution. The normalized moments of ordinary-ranges are determined from:

$$M_{OR}(b) = \frac{\int_0^\infty z^b P_{OR}(z)\,dz}{\int_0^\infty z^b z e^{-z^2/2}\,dz} \qquad \textbf{Eq. 3.47}$$

and the moments of rainflow-ranges are determined from

$$M_{RR}(b) = \frac{\int_0^\infty z^b P_{RR}(z)\,dz}{\int_0^\infty z^b z e^{-z^2/2} dz} \qquad \textbf{Eq. 3.48}$$

The normalized moments corresponding to the ordinary-range and rainflow-range densities in Fig. 3.10 and Fig. 3.11 are calculated and plotted in Fig. 3.13 and Fig. 3.14. Fig. 3.13.i shows the normalized moments of ordinary ranges for the smooth spectra, and, 13-ii for the rectangular spectra, and Fig. 3.13.iii and 13.iv show the effect of mean frequency on the moments. The normalized mean of z, i.e. b = 1, is equal to the irregularity factor for all cases, regardless of the mean frequency. This is consistent with the calculation of 'average height of rise and fall' in[5]. However as the mean frequency increases, the rate at which the normalized moments approach zero decreases, as in Fig. 3.13.iii and 13.iv.

Fig. 3.14.i shows the normalized moments of rainflow-ranges for the smooth spectra, and 14.ii for the rectangular spectra. The effect of mean frequency on rainflow-range moments is illustrated in Fig. 3.14.iii and 14.iv. Again the normalized mean of rainflow ranges is equal to the irregularity factor, regardless of the mean frequency. However, the moments of rainflow ranges do not approach zero as in the case of ordinary ranges, but they approach a 'steady state' value which increases when the mean-frequency increases for the same irregularity factor.

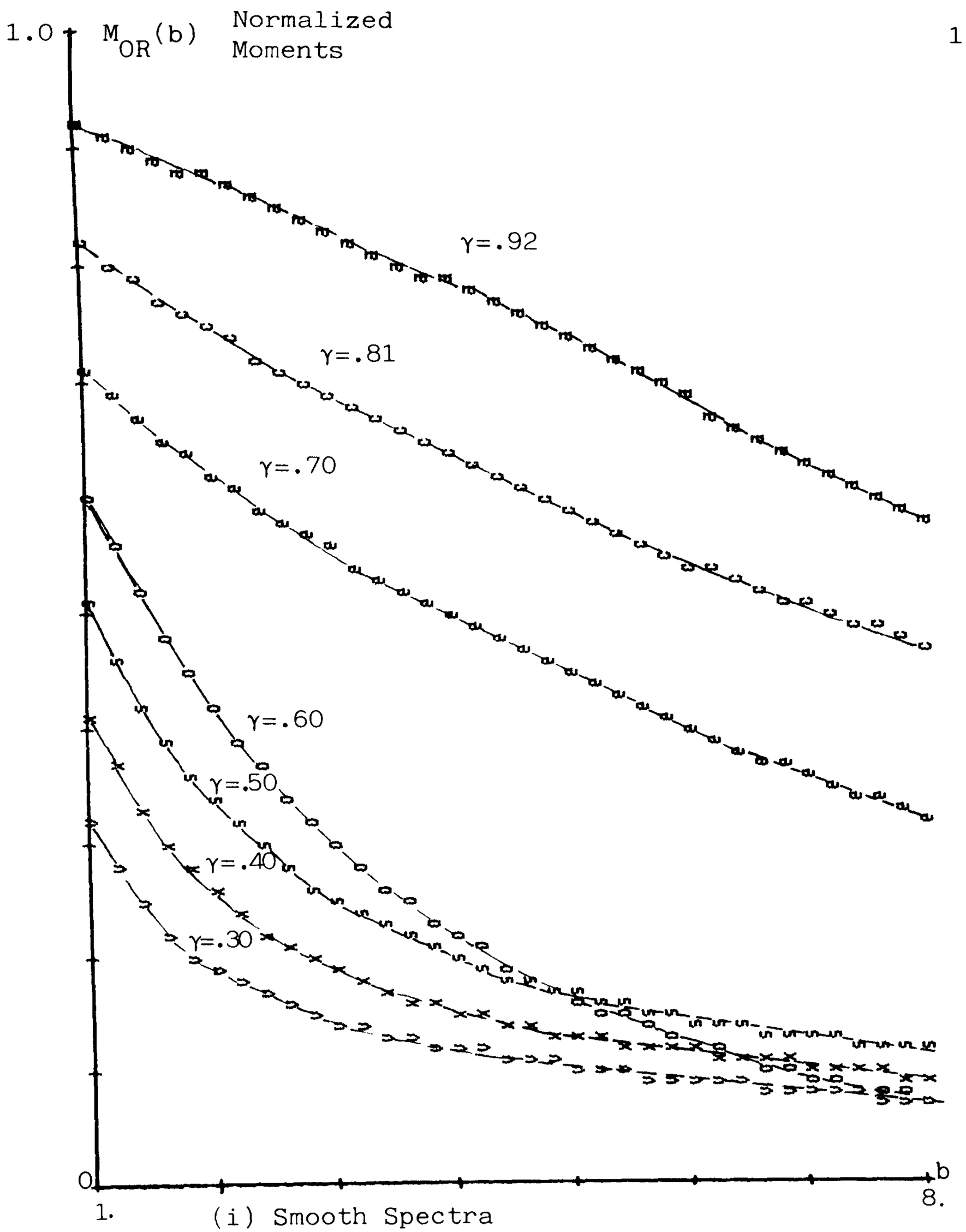

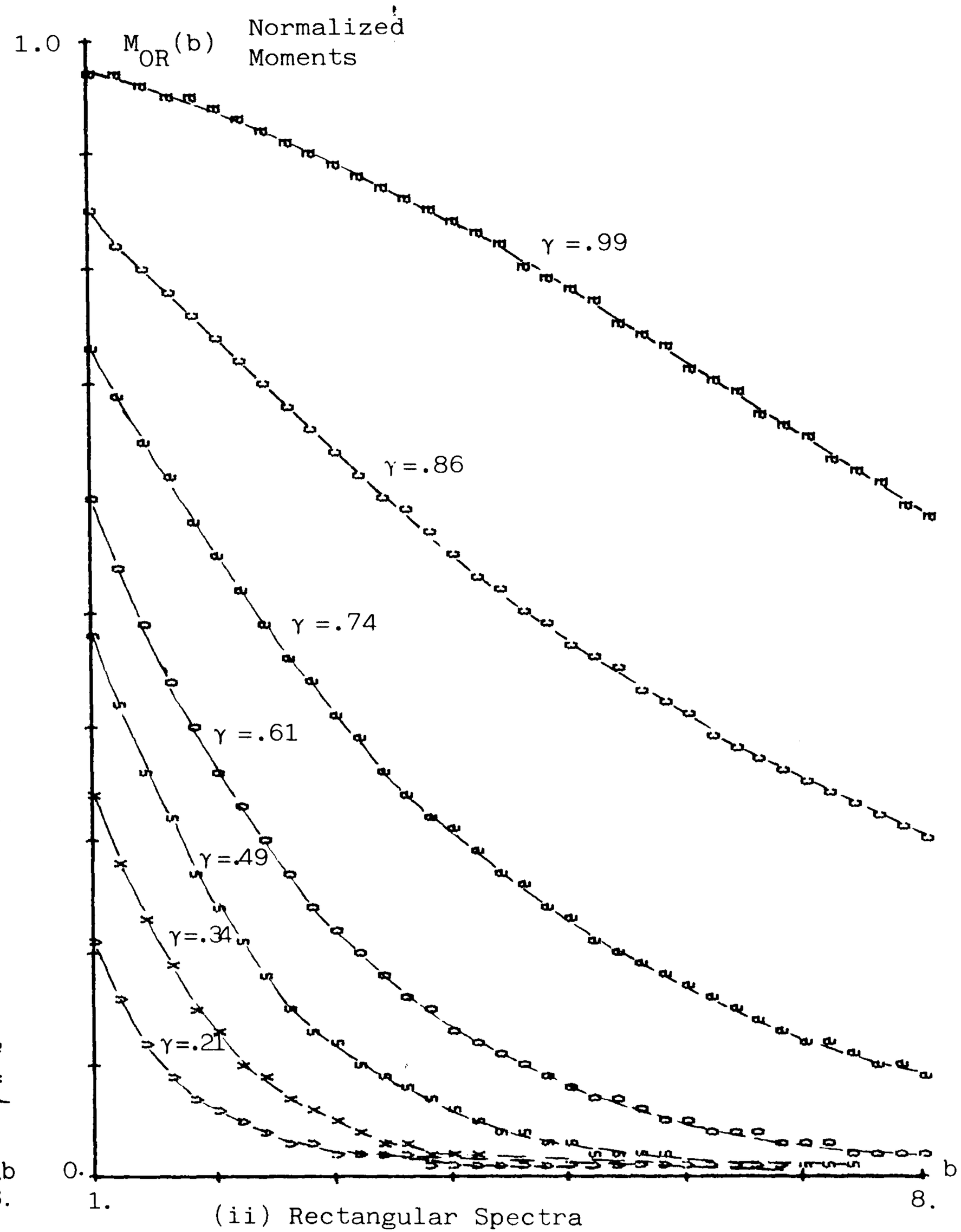

Fig. 3.13. Moments of Ordinary Range Distribution

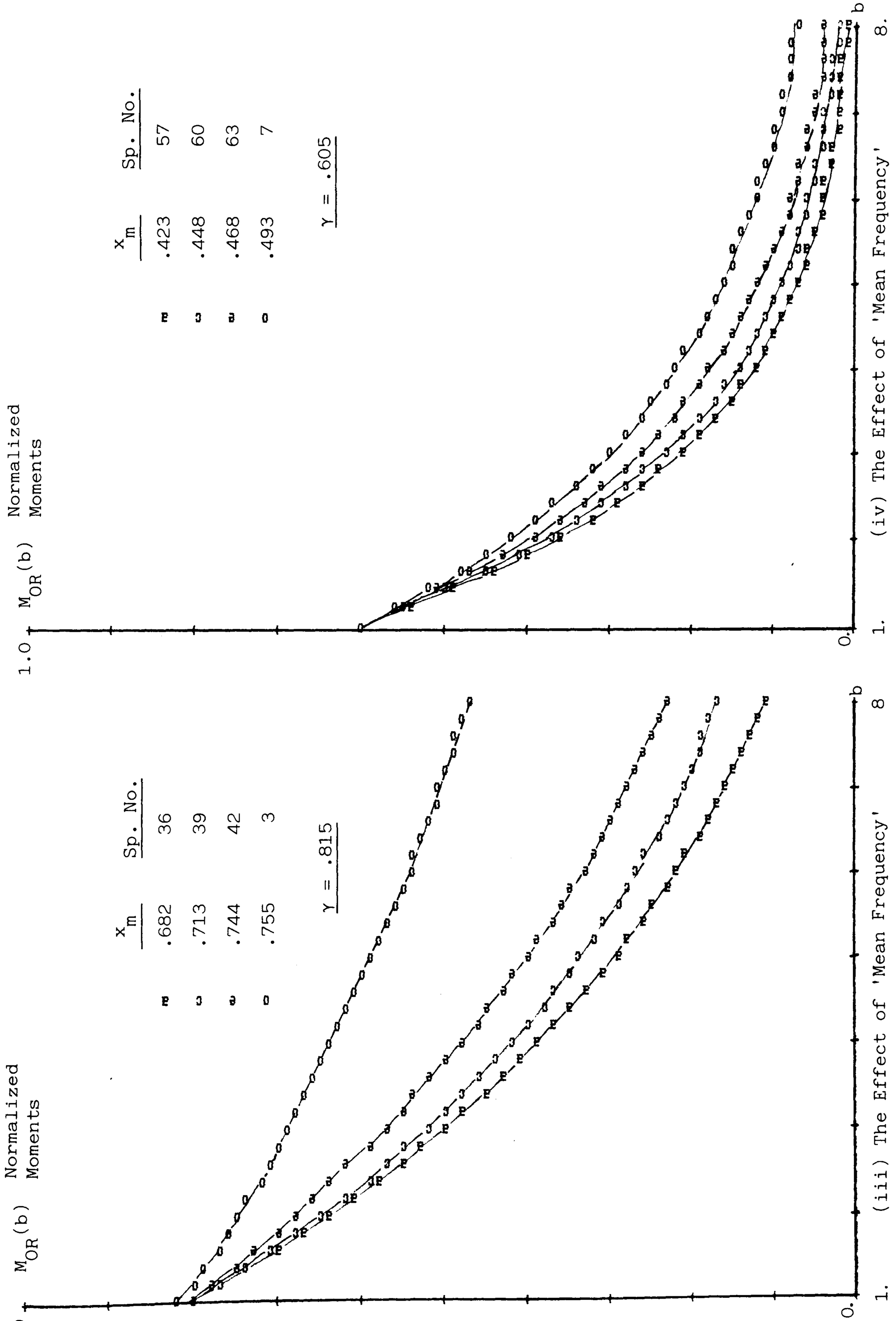

Fig. 3.13. (cont). Moments of Ordinary Range Distribution

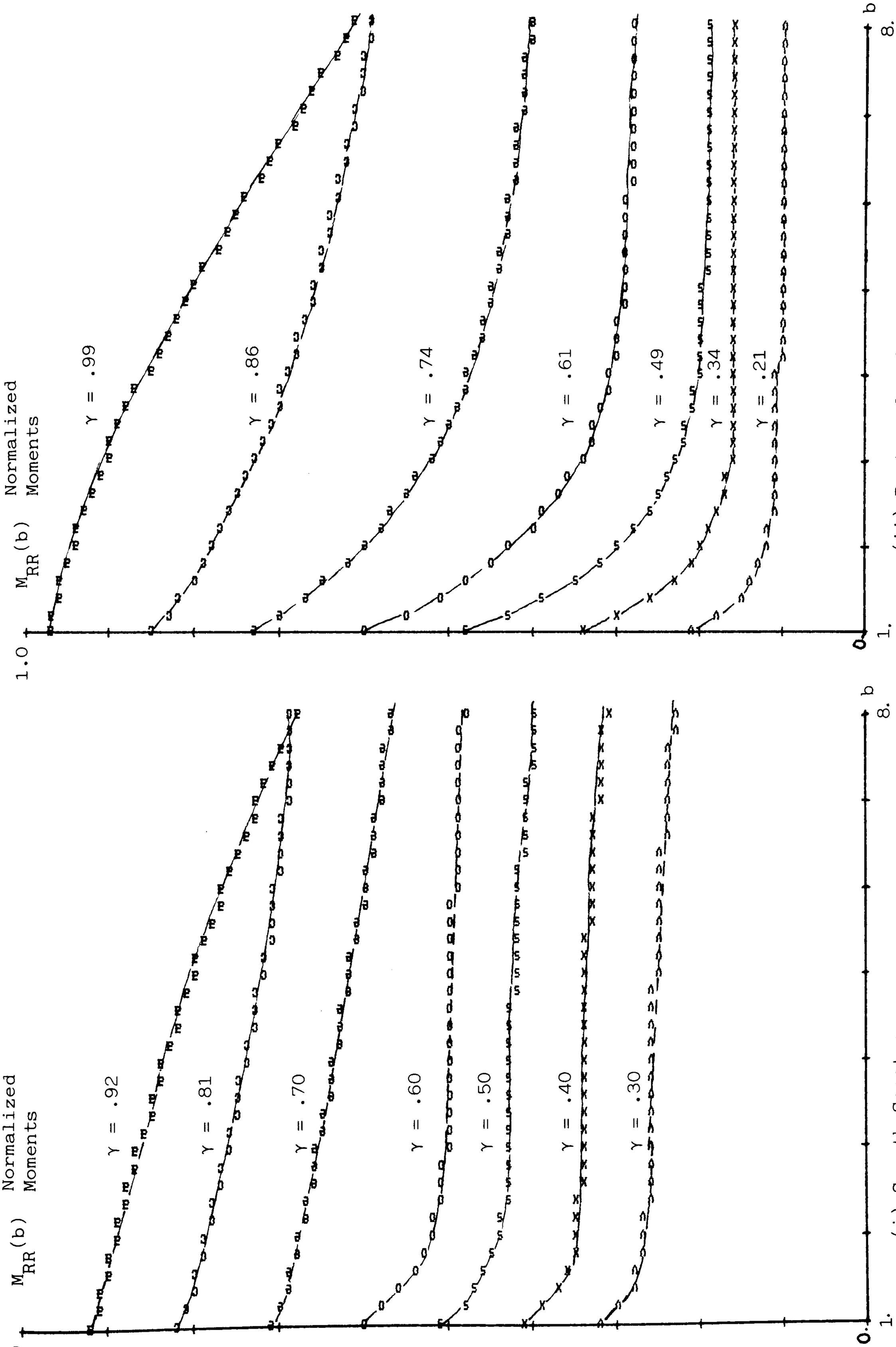

Fig. 3.14. Moments of

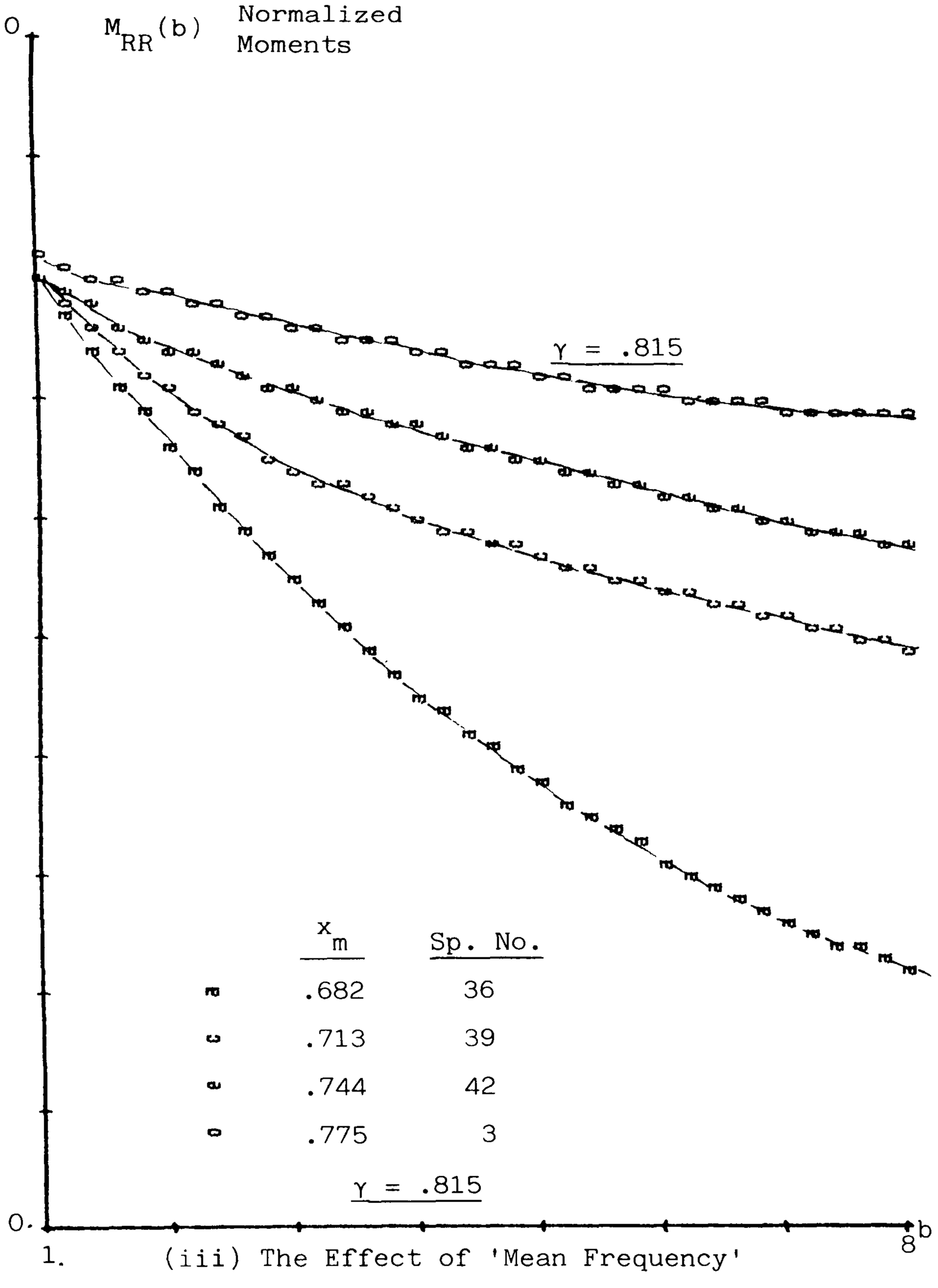

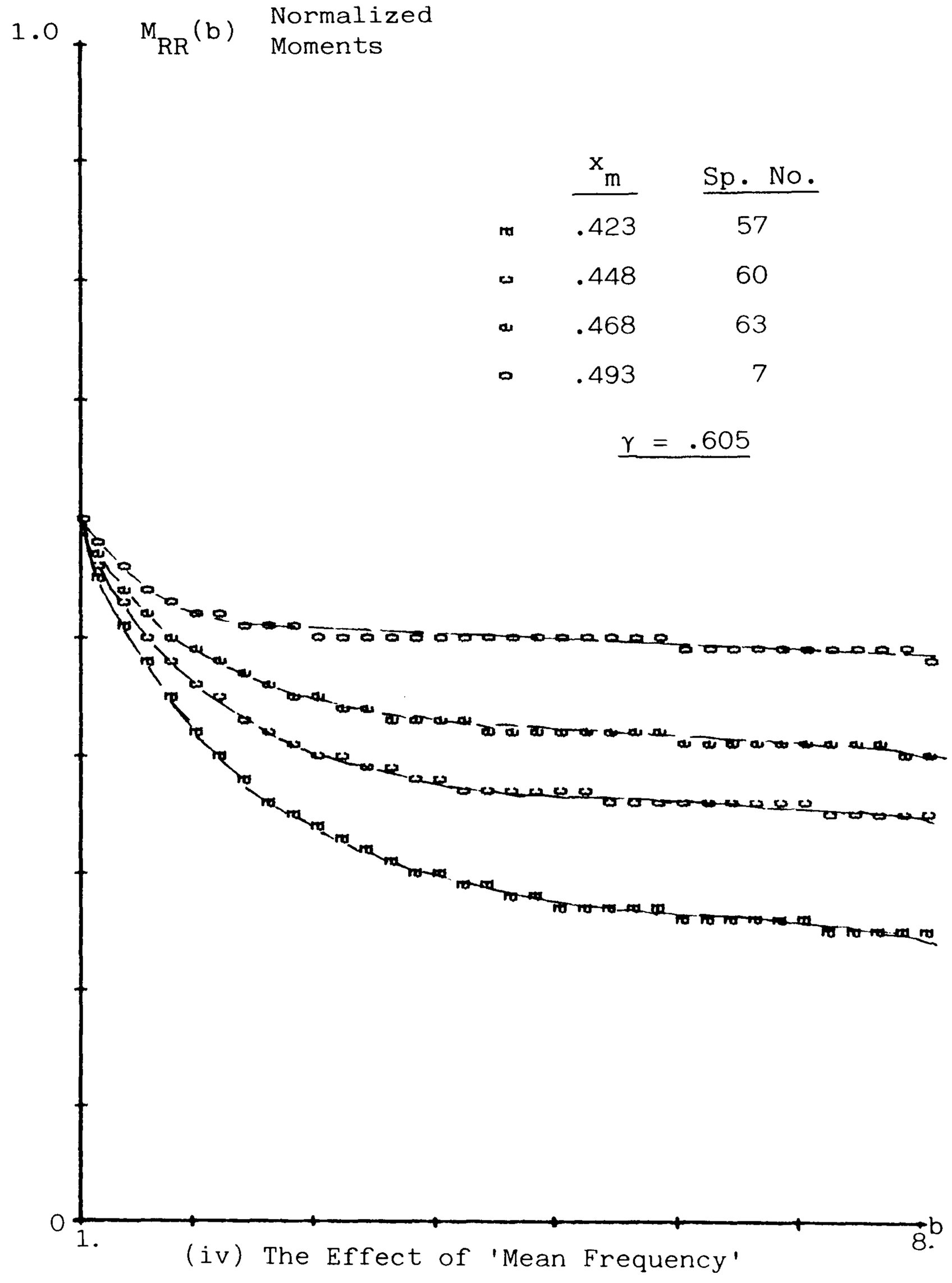

Fig. 3.14.(cont). Moments of Rainflow Range Distribution

3.6. Modelling

3.6.1. Model for Ordinary-Range Densities:

The behaviour of ordinary-range densities at small ranges, Fig. 3.1Ø, suggests an exponential decrease near the origin. The latter part of the densities features a Rayleigh function. Therefore the following closed-form equation, the sum of an exponential function and a Rayleigh function, is proposed as the ordinary-range probability density function:

$$P_{OR}(z) = c_1 \frac{1}{\tau} e^{-z/\tau} + c_2 \frac{z}{\alpha^2} e^{-z^2/2\alpha^2}, \quad z > \emptyset \qquad \textbf{Eq. 3.49}$$

where

$$c_1 + c_2 = 1$$

and τ, c_2 and α are functions of the irregularity factor γ, and the mean frequency x_m.

When the mean frequency, x_m, approaches a certain value, to the minimum value it can take for a given irregularity factor γ, the exponential term goes to zero, i.e. both c_1 and τ approach zero, c_2 becomes unity, and the density becomes a Rayleigh distribution with the Rayleigh parameter α equal to the irregularity factor γ. As the mean frequency, x_m, increases for the same irregularity factor, γ, the contribution of exponential term to the density increases, i.e. both c_1 and τ increase, c_2 decreases, and α increases causing higher densities at higher ranges.

The model parameters are found as the parameters which minimize a cost function. First, an error term, e_i, is defined:

$$e_i^2 = \frac{[P_{OR}(z_i) - \overline{P_{OR}}(z_i)]^2}{P_{OR}(z_i)} \qquad \textbf{Eq. 3.50}$$

where $P_{OR}(z_i)$ is the simulation result, and $\overline{P_{OR}}(z_i)$ is the proposed form, Eq. 3.49, of the ordinary-range density function at discrete intervals of z_i. Then the cost function is defined as the sum of error terms:

$$\text{cost} = N\sum_{i=1}^{n} e_i^2 \qquad \textbf{Eq. 3.51}$$

where N is the total no. of samples, and n is the number of intervals. The problem is now reduced to minimizing the cost function with 3 parameters, namely τ, c_2, α.

Various minimization techniques were employed to find the 3 parameters which give the best fit. Among these are the simplex method, direct search and gradient methods. Apart from numerous iterations involving time-consuming exponentiation and multiplication operations for 70 spectra, the major problem was that the search for parameters which minimize the cost function quite often converged to a local minimum instead of the global minimum. That is why various minimization methods were tried and searches were repeated starting at very different initial points in the parameter space and the best of minima was chosen, every fit eventually had to pass an 'eye test'.

The 3 model parameters for each of 70 densities are listed in Table 3.2. The last column in Table 3.2 shows the cost or the 'goodness of fit' indicator. The results confirm the observation made

earlier from density plots, that is when the mean frequency x_m takes the minimum value for a given irregularity factor, then the density becomes Rayleigh distribution with a Rayleigh parameter equal to the irregularity factor. As the mean frequency x_m increases, the contribution of the exponential term increases, in fact at lower irregularity factors it becomes so dominant that the density practically becomes an exponential density. As x_m increases, the Rayleigh parameter α increases, but c_2 decreases. Fig. 3.15 shows three typical examples of the simulation results with the proposed model outputs of the ordinary range densities. The plots also show the contribution of each type of densities, exponential and Rayleigh.

Fig. 3.16 shows the plot of 3 model parameters against the mean frequency x_m. The first step in determining the model parameters in terms of the irregularity factor, γ, and the mean frequency, x_m, was to find out the relationship between the minimum mean frequency, x_{min}, for a given irregularity factor. Fig. 3.17 shows the plot of the mean frequency against the irregularity factor. Although the minimum values shown in this plot are not necessarily to be the actual minimum, however they are the smallest to be found by trial-and-error method by altering the power spectra. Assuming these to be the minima, the following form for the minimum mean frequency is proposed:

$$x_{min} = \frac{\gamma (1 + \gamma^2)}{2} \qquad \text{Eq. 3.52}$$

The choice of this form is dictated by the observation of Fig. 3.17, that when γ approaches zero, x_m approaches $\gamma/2$, and when γ approaches unity, x_m approaches γ^2. However in the mid range, x_{min} calculated by Eq. 3.52 is sometimes greater than, although negligibly

small, the minimum values shown on the graph. An alternative form for the minimum mean frequency is:

$$x_{min} = \frac{\gamma}{1 + 1.25(1-\gamma)} \qquad \textbf{Eq. 3.53}$$

which is a better approximation.

Although a detailed examination of Fig. 3.16 indicates that the variation of parameters, particularly of c_2 and γ, is hyperbolic near $x_m = x_{min}$, however for the sake of simplicity, the variations are approximated by straight lines. Solid lines in Fig. 3.16 show the variation of parameters c_2, α, and τ with the mean frequency x_m at the same irregularity factor γ. The following forms of closed-form equations for the parameters in Eq. 3.49 are proposed:

$$c_1 = \frac{1}{\gamma^2}(x_m - x_{min}) \qquad \textbf{Eq. 3.54}$$

$$\tau = \emptyset.\emptyset 2 + \frac{2}{\gamma}(x_m - x_{min}) \qquad \textbf{Eq. 3.55}$$

$$c_2 = 1 - \frac{1}{\gamma^2}(x_m - x_{min}) \qquad \textbf{Eq. 3.56}$$

$$\alpha = \gamma + \frac{1}{\gamma}(x_m - x_{min}) \qquad \textbf{Eq. 3.57}$$

where x_{min} is defined by Eq. 3.52 or 53.

Despite its known invalidation, Eq. 3.52 is used to predict the model parameters listed in Table 3.3. However, in order to prevent c_1 having negative values on c_2 being greater than unity, the difference term $(x_m - x_{min})$ is squared first, then square-rooted, as it would have been done if these parameters were approximated by hyperbolas.

Table 3.2

Ordinary-Range Model Parameters
Best-Fit Parameters Obtained from the Simulation Results

Sp	τ	α	c_2	Cost
1	0.103	0.964	0.948	81.8
2	0.136	0.943	0.911	94.7
3	0.158	0.936	0.856	131.3
4	0.191	0.929	0.796	116.3
5	0.225	0.916	0.731	91.0
6	0.254	0.807	0.756	108.8
7	0.211	0.715	0.803	103.1
8	0.541	0.708	0.460	247.5
9	0.540	0.682	0.336	314.8
10	0.569	0.580	0.147	252.4
11	0.518	0.582	0.058	332.2
12	0.457	0.411	0.039	219.2
13	0.236	0.861	0.199	198.4
14	0.241	0.798	0.133	81.3
15	0.280	0.131	0.473	2895.3
16	0.273	0.212	0.597	441.7
17	0.278	0.285	0.752	87.9
18	0.108	0.371	0.899	21.6
19	0.079	0.435	0.941	42.8
20	0.050	0.493	0.981	39.1
21	0.048	0.541	0.982	77.2
22	0.081	0.616	0.963	80.0
23	0.085	0.681	0.965	70.4
24	0.087	0.757	0.966	67.1
25	0.065	0.808	0.984	57.9
26	0.117	0.880	0.956	84.5
27	0.101	0.933	0.973	48.9
28	0.034	0.978	0.996	117.9
29	0.032	0.877	0.997	106.2
30	0.053	0.877	0.992	43.0
31	0.063	0.880	0.986	46.4
32	0.086	0.888	0.976	46.4
33	0.108	0.898	0.965	69.5
34	0.141	0.910	0.949	105.9
35	0.159	0.923	0.937	112.9

Table 3.2 (cont.)

Ordinary-Range Model Parameters
Best-Fit Parameters Obtained from the Simulation Results

Sp.	τ	α	c_2	cost
36	0.032	0.809	0.997	109.8
37	0.049	0.807	0.992	100.2
38	0.057	0.807	0.991	84.3
39	0.074	0.814	0.982	63.3
40	0.104	0.829	0.964	68.4
41	0.130	0.841	0.947	72.5
42	0.175	0.860	0.924	109.0
43	0.036	0.740	0.996	107.2
44	0.050	0.740	0.991	133.7
45	0.066	0.747	0.980	68.3
46	0.104	0.768	0.954	91.4
47	0.121	0.771	0.950	57.6
48	0.163	0.790	0.921	96.8
49	0.172	0.799	0.909	74.6
50	0.058	0.673	0.989	137.7
51	0.040	0.671	0.989	62.2
52	0.078	0.683	0.973	64.5
53	0.104	0.697	0.951	86.2
54	0.129	0.710	0.926	86.9
55	0.144	0.718	0.916	83.4
56	0.176	0.728	0.898	67.8
57	0.064	0.608	0.984	144.7
58	0.068	0.610	0.975	66.1
59	0.085	0.614	0.970	48.5
60	0.107	0.629	0.948	43.6
61	0.138	0.642	0.920	49.9
62	0.185	0.661	0.885	40.4
63	0.201	0.672	0.865	19.2
64	0.045	0.533	0.986	88.8
65	0.059	0.542	0.975	64.8
66	0.094	0.554	0.945	82.1
67	0.108	0.564	0.929	88.8
68	0.134	0.570	0.910	77.5
69	0.133	0.577	0.904	66.4
70	0.152	0.585	0.886	31.1

Table 3.3

Ordinary-Range Model Parameters
from Closed-Form Eqs. 3.55, 56, and 57

Sp	τ	α	c_2
1	0.131	0.980	0.940
2	0.195	0.957	0.899
3	0.264	0.935	0.850
4	0.325	0.909	0.799
5	0.366	0.874	0.754
6	0.342	0.811	0.752
7	0.304	0.742	0.763
8	0.356	0.717	0.693
9	0.383	0.682	0.637
10	0.413	0.647	0.564
11	0.412	0.596	0.511
12	0.372	0.525	0.496
13	0.458	0.519	0.271
14	0.364	0.429	0.333
15	0.147	0.224	0.602
16	0.024	0.212	0.991
17	0.082	0.301	0.885
18	0.078	0.374	0.916
19	0.068	0.442	0.942
20	0.063	0.511	0.957
21	0.028	0.535	0.992
22	0.059	0.620	0.967
23	0.056	0.691	0.973
24	0.103	0.782	0.944
25	0.066	0.832	0.972
26	0.118	0.909	0.943
27	0.086	0.959	0.965
28	0.028	0.992	0.996
29	0.052	0.896	0.982
30	0.069	0.904	0.972
31	0.083	0.912	0.964
32	0.106	0.923	0.951
33	0.134	0.937	0.936
34	0.153	0.947	0.924
35	0.183	0.962	0.907

Table 3.3 (cont.)

Ordinary-Range Model Parameters
from Closed-Form Eqs. 3.55, 56, and 57

Sp	τ	α	c_2
36	0.047	0.823	0.983
37	0.074	0.837	0.966
38	0.094	0.847	0.955
39	0.124	0.862	0.936
40	0.148	0.874	0.921
41	0.173	0.887	0.905
42	0.201	0.900	0.888
43	0.039	0.749	0.987
44	0.083	0.771	0.957
45	0.109	0.785	0.940
46	0.149	0.805	0.913
47	0.180	0.820	0.892
48	0.203	0.831	0.877
49	0.223	0.842	0.863
50	0.048	0.684	0.979
51	0.061	0.691	0.969
52	0.088	0.704	0.949
53	0.116	0.718	0.928
54	0.140	0.730	0.910
55	0.162	0.741	0.894
56	0.201	0.760	0.865
57	0.069	0.624	0.959
58	0.090	0.635	0.942
59	0.112	0.646	0.923
60	0.153	0.666	0.889
61	0.160	0.670	0.883
62	0.193	0.687	0.856
63	0.220	0.700	0.833
64	0.040	0.540	0.981
65	0.024	0.532	0.996
66	0.045	0.543	0.976
67	0.069	0.554	0.954
68	0.075	0.558	0.948
69	0.097	0.569	0.927
70	0.137	0.588	0.890

Fig. 3.15.i. Ordinary-Range Density Function

Sp. No. = 1

γ = .92

x Simulation Result

0 Model Output

e Exponential Term

r Rayleigh Term

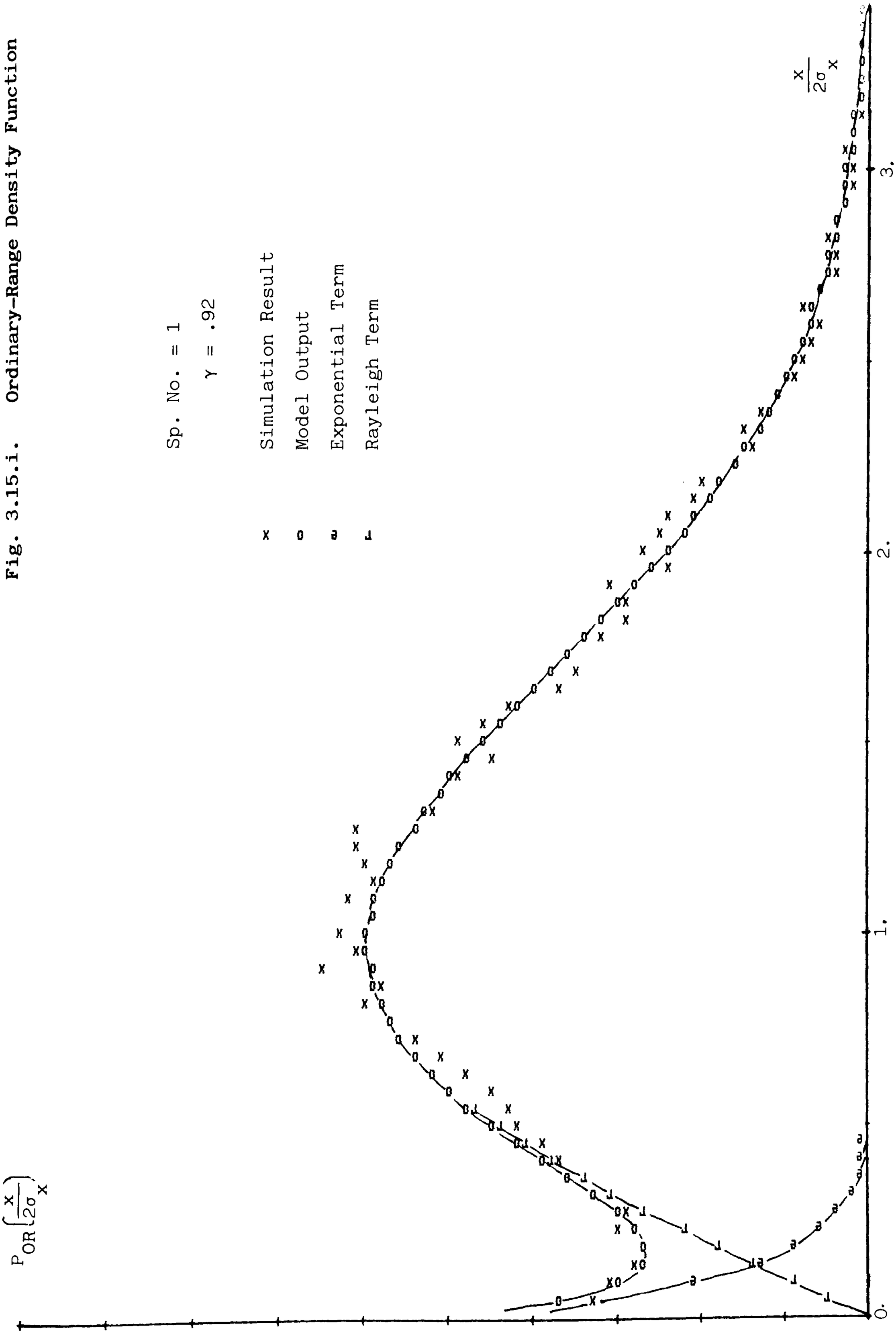

Fig. 3.15.ii. Ordinary Range Density Function

Sp. No. = 6

γ = .57

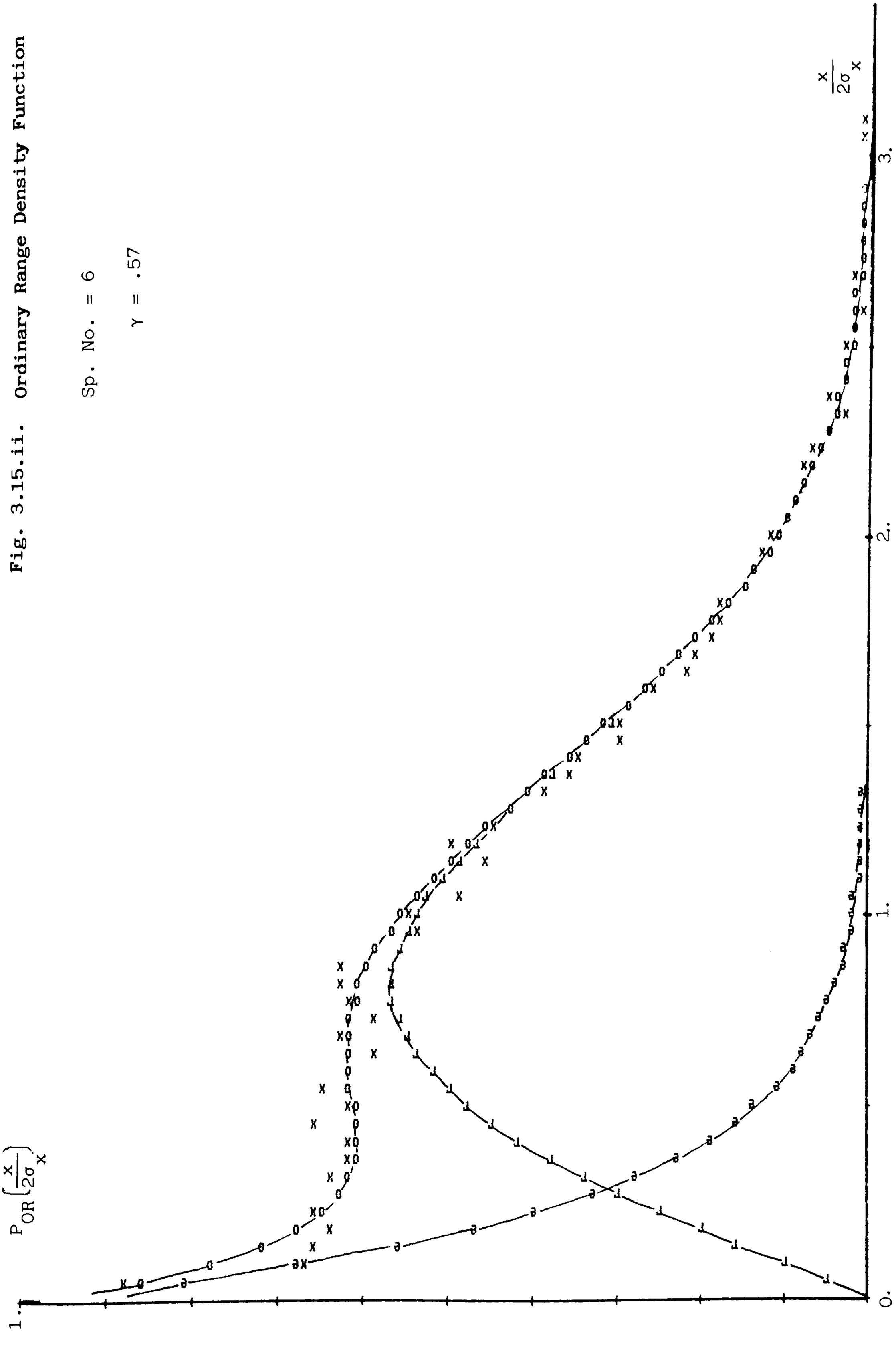

Fig. 3.15.iii. Ordinary-Range Density Function

Sp. No. = 65

γ = .53

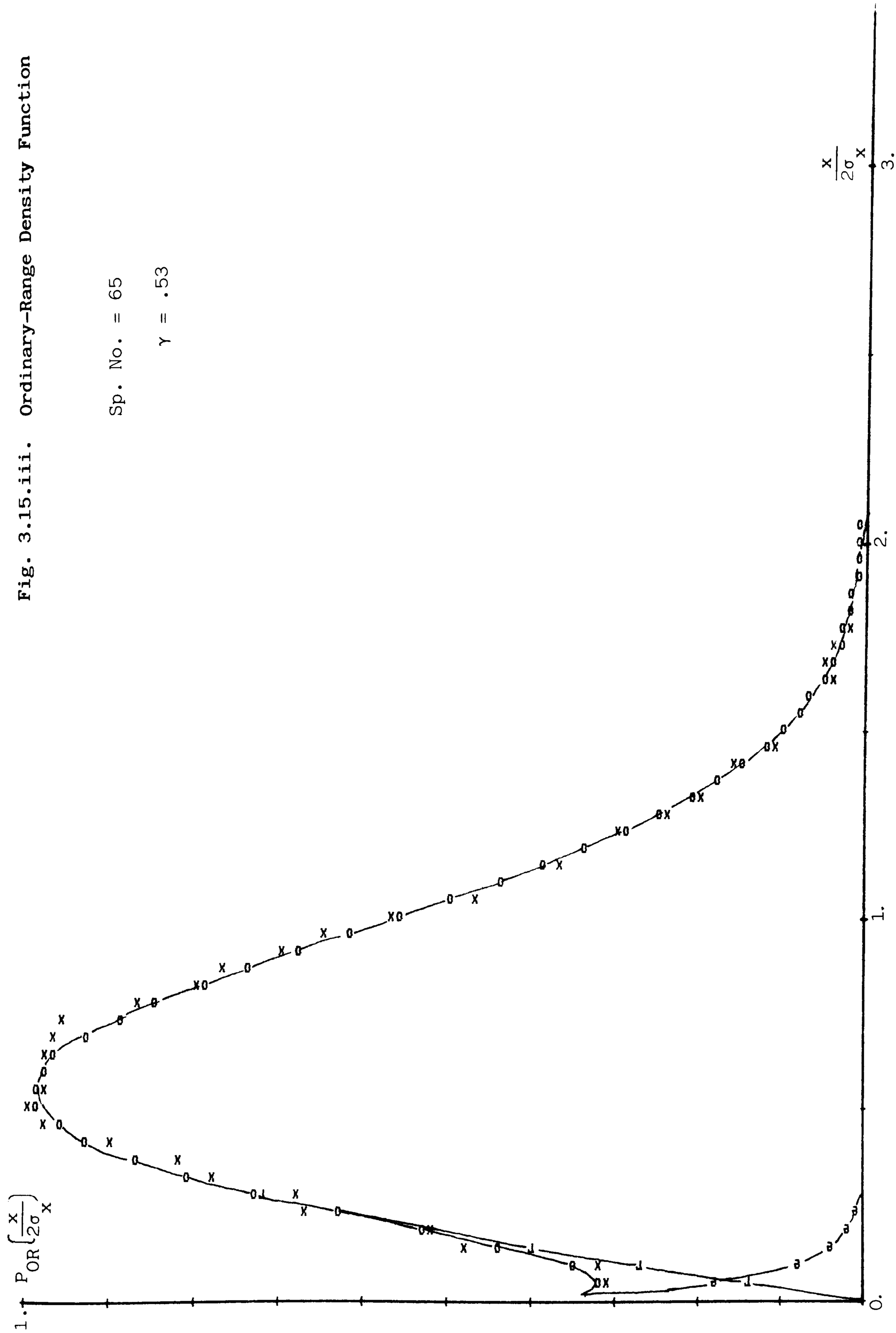

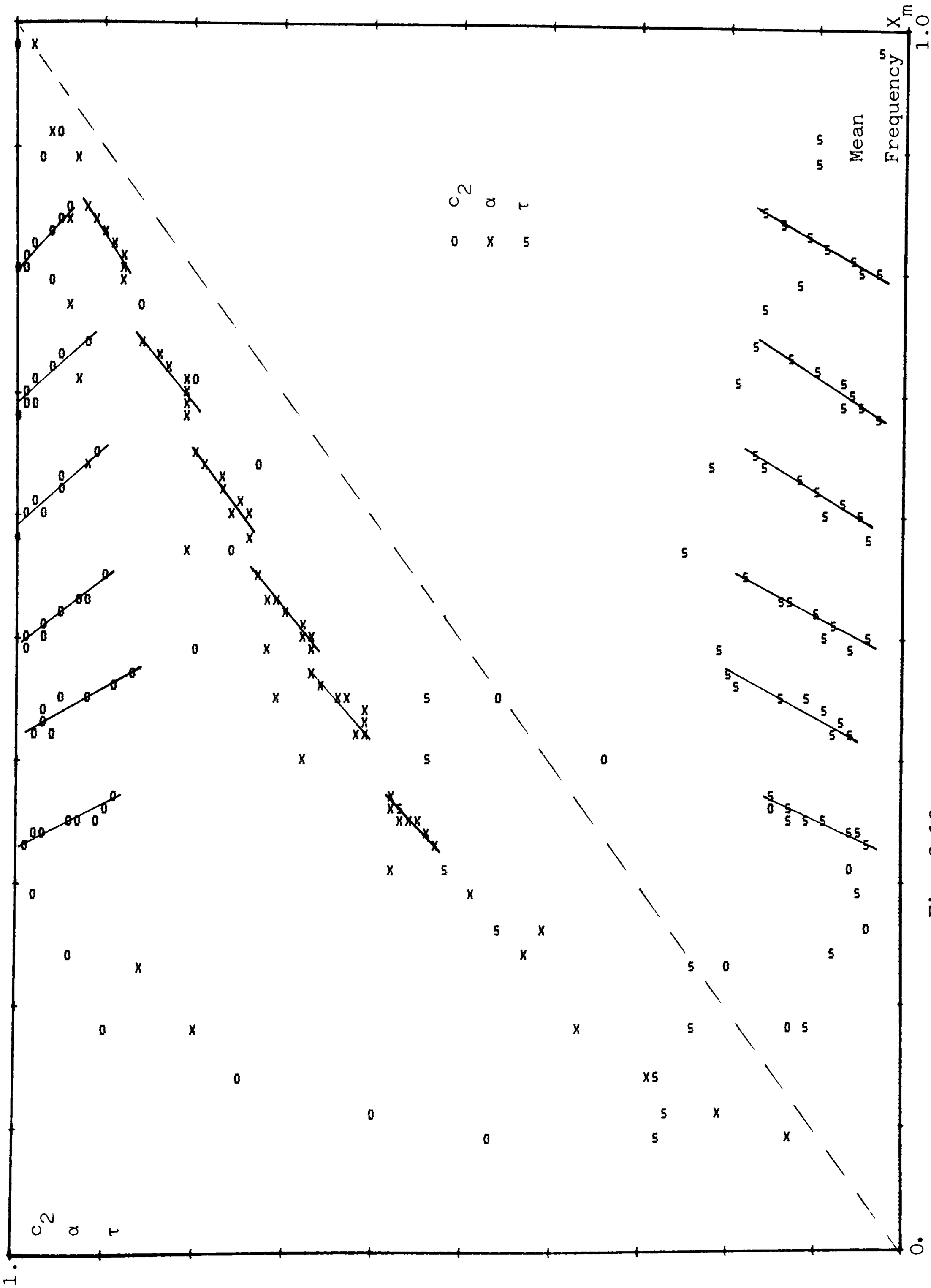

Fig. 3.16. τ, c_2, and α (Eq. 49) vs. Mean Frequency

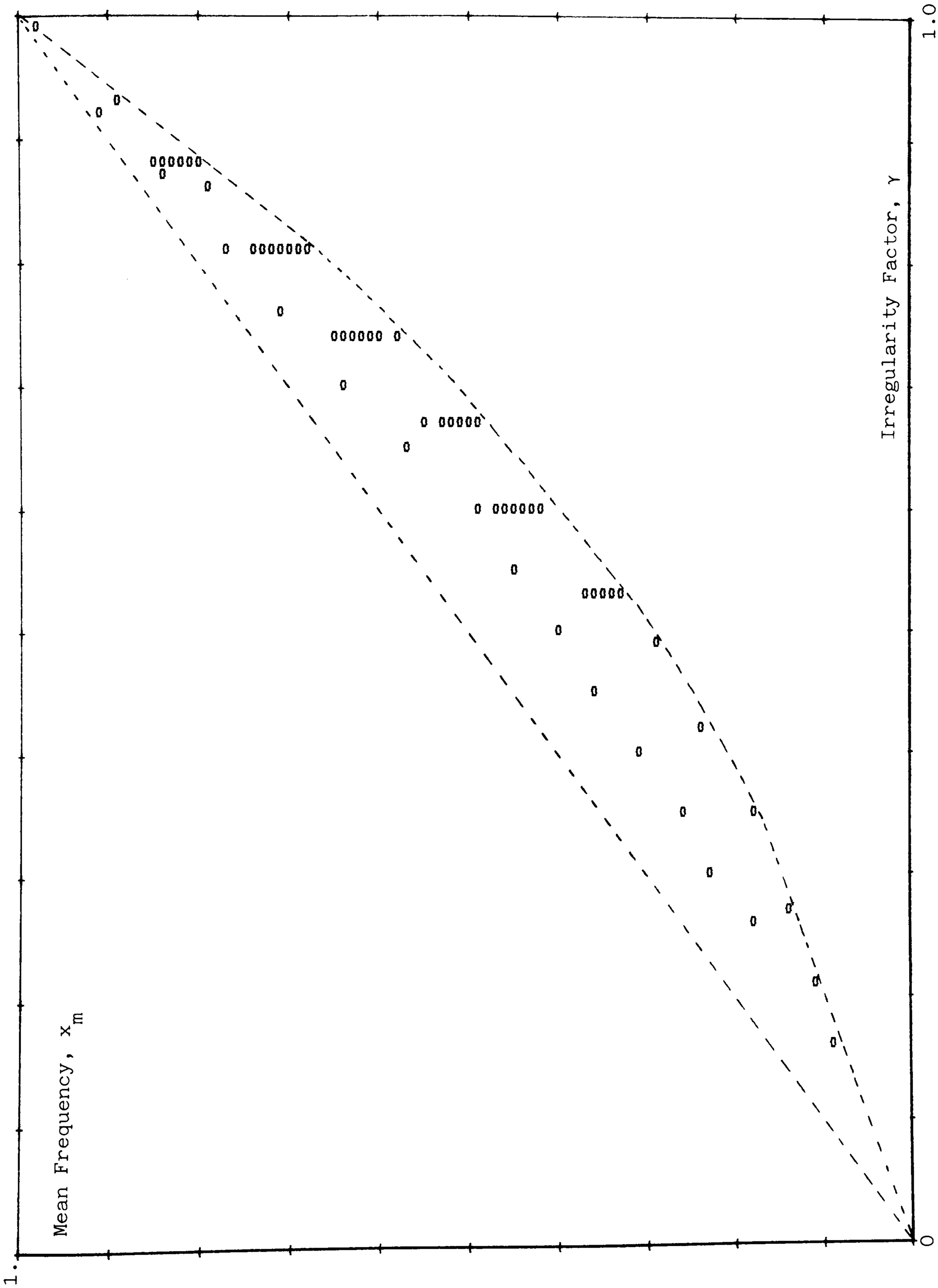

Fig. 3.17. Plot of Mean Frequency vs. Irregularity Factor

3.6.2 Model for Rainflow-Range Densities:

As in the case of ordinary-ranges, rainflow-range densities exhibit an exponential variation near the origin, as shown in Fig. 3.11. Again, the mid-range features a Rayleigh function. However, as indicated earlier, the rainflow-range densities do not trail off to zero as early as the ordinary-ranges do. Even for very low irregularity factors, the densities continue to exist for very large ranges. Also the observation that the moments of rainflow range densities normalized with the moments of a standard Rayleigh distribution approach steady-states for higher moments suggest the existence of a standard Rayleigh distribution to explain the high-range densities. Therefore the following closed-form equation, the sum of an exponential function, a Rayleigh function with variable Rayleigh parameter and a standard Rayleigh function, is proposed as the rainflow-range probability density function:

$$P_{RR}(z) = c_1 \frac{1}{\tau} e^{-z/\tau} + c_2 \frac{z}{\alpha^2} e^{-z^2/2\alpha^2} + c_3 z e^{-z^2/2} \qquad \textbf{Eq. 3.58}$$

where $c_1 + c_2 + c_3 = 1$

and τ, c_2, α and c_3 are functions of the irregularity factor γ, and the mean frequency x_m.

In order to find the model parameters an error term is defined similarly, as in the case of ordinary-ranges,:

$$e_i^2 = \frac{[P_{RR}(z_i) - \overline{P_{RR}}(z_i)]^2}{P_{RR}(z_i)} \qquad \textbf{Eq. 3.59}$$

where $P_{RR}(z_i)$ is the simulation result, and $\overline{P_{RR}}(z_i)$ is the proposed form, Eq. 3.58, of the rainflow-range density function at

discrete intervals of z_i. Then a cost function is defined as the sum of error terms:

$$\text{cost} = N\sum_{i=1}^{n} e_i^2$$

where N is the total no. of samples, and n is the no. of intervals.

The problem of finding 'best fit' parameters τ, c_2, α and c_3 which minimize the cost function was turned out to be somewhat more difficult than the minimizing the cost function for ordinary-ranges. First of all, there was no clear indication to the initial estimates for the model parameters. Secondly, addition of another parameter, c_3, increased the 'curse of dimensionality', by adding another dimension to the parameter search space and adding another exponential and multiplication operation to the iteration time. Lastly, but certainly not the least, the search converging to a local minimum instead of the global minimum became more problematical than the case for ordinary-ranges. It was quite possible to find very diverse values for the parameters yielding practically the same cost value and also passing the 'eye-test'. The problem became more acute when fitting parameters for high irregularity factors, when the effects of the standard and the variable Rayleigh functions became inseparable.

Again different minimization methods were employed and repeated starting at very different initial points in the parameter space and the best-fit model parameters are listed in Table 3.4, the last column showing the cost or the goodness of fit indicator. Fig. 3.18 shows three examples of simulation results with the proposed model outputs of the rainflow-range densities. The plots also show the contribution of the exponential and the variable Rayleigh terms.

To comment on the variation of parameters listed in Table 3.4 proved to be a difficult task because of the dispersity of parameter variations as shown in Fig. 3.19.i and 19.ii. It was an equally difficult task to express the model parameters in close-form in terms of the irregularity factor and the mean frequency. Again, the solid lines in Fig. 3.19 denote the mean frequencies having the same irregularity factor. Although the solid lines in Fig. 3.19.ii indicate a linear variation of both the variable and the standard Rayleigh scaling factors c_2 and c_3, and consequently the exponential turn scaleing factor c_1, there is however no clear indication to how τ and α vary with x_m.

In determining the model parameters for the rainflow-range densities, the help of normalized moments of rainflow-ranges is sought. Fig. 3.20 shows the normalized moments, 2nd, 4th and 6th moments, against the mean frequency, solid lines denoting x_m having the same irregularity factor. Although the solid lines for the 2nd moments have different slopes than the unity, they are remarkably close to the $y = x$ line. Therefore it is assumed that the 2nd moments are equal to x_m. The 1st normalized moments of rainflow-ranges, i.e. the normalized mean of the ranges, is found to be equal to the irregularity factor γ, regardless of variation of x_m.

Assuming that Eq.3.58 is to be the correct form for the rainflow-range probability density function, the moments are:

$$\bar{m}_{RR}(b) = \int_0^\infty z^b \, \bar{P}_{RR}(z)\,dz$$

or

To comment on the variation of parameters listed in Table 3.4 proved to be a difficult task because of the dispersity of parameter variations as shown in Fig. 3.19.i and 19.ii. It was an equally difficult task to express the model parameters in close-form in terms of the irregularity factor and the mean frequency. Again, the solid lines in Fig. 3.19 denote the mean frequencies having the same irregularity factor. Although the solid lines in Fig. 3.19.ii indicate a linear variation of both the variable and the standard Rayleigh scaling factors c_2 and c_3, and consequently the exponential term scaling factor c_1, there is however no clear indication to how τ and α vary with x_m.

In determining the model parameters for the rainflow-range densities, the help of normalized moments of rainflow-ranges is sought. Fig. 3.20 shows the normalized moments, 2nd, 4th and 6th moments, against the mean frequency, solid lines denoting x_m having the same irregularity factor. Although the solid lines for the 2nd moments have different slopes than the unity, they are remarkably close to the $y = x$ line. Therefore it is assumed that the 2nd moments are equal to x_m. The 1st normalized moments of rainflow-ranges, i.e. the normalized mean of the ranges, is found to be equal to the irregularity factor γ, regardless of variation of x_m.

Assuming that Eq.3.58 is to be the correct form for the rainflow-range probability density function, the moments are:

$$\bar{m}_{RR}(b) = \int_0^\infty z^b \, \bar{P}_{RR}(z)\,dz$$

or

$$\bar{m}_{RR}(b) = c_1\tau^b\,\Gamma(1+b) + c_2(\sqrt{2}\alpha)^b\,\Gamma(1+\frac{b}{2}) + c_3(\sqrt{2})^b\,\Gamma(1+\frac{b}{2}) \quad \textbf{Eq.3.60}$$

Then the moments normalized by the moments of the standard Rayleigh density become:

$$M_{RR}(b) = \frac{c_1\tau^b\,\Gamma(1+b)}{(\sqrt{2})^b\,\Gamma(1+\frac{b}{2})} + c_2\alpha^b + c_3 \quad \textbf{Eq. 3.61}$$

By writing the above observations in equation form, we have, for the Øth moment, i.e. the total probability:

$$c_1 + c_2 + c_3 = 1 \quad \textbf{Eq. 3.62}$$

for the 1st moment, i.e., the mean:

$$.8c_1\tau + c_2\alpha + c_3 = \gamma \quad \textbf{Eq. 3.63}$$

and for the 2nd moment:

$$c_1\tau^2 + c_2\alpha^2 + c_3 = x_m \quad \textbf{Eq. 3.64}$$

There are 3 equations for 5 unknowns, 2 more equations are needed. After a detailed study of Fig. 19.ii, it is assumed that c_1 takes the following form:

$$c_1 = \frac{2(x_m - \gamma^2)}{1 + \gamma^2} \quad \textbf{Eq. 3.65}$$

Two further assumptions are made based on the observations of c_1 and τ, the exponential scale and decay factors for both the ordinary-ranges and the rainflow ranges. The first of these assumptions is that

$.8c_1$ term in Eq. 3.63 is equal to c_1^2, and the second is that $c_1\tau^2$ term in Eq. 3.64 is negligible. Re-writing Eq. 3.62, 63 and 64 with these assumptions, we have:

$$c_2 + c_3 = 1 - c_1 \qquad \textbf{Eq. 3.66}$$

$$c_2\,\alpha + c_3 = \gamma - c_1^2 \qquad \textbf{Eq. 3.67}$$

$$c_2\,\alpha^2 + c_3 = x_m \qquad \textbf{Eq. 3.68}$$

Now the rest of parameters can be solved with the following steps:

$$\alpha = \frac{\gamma - x_m - c_1^2}{1 - \gamma - c_1 + c_1^2} \qquad \textbf{Eq. 3.69}$$

$$c_2 = \frac{1 - \gamma - c_1 + c_1^2}{1 -} \qquad \textbf{Eq. 3.7Ø}$$

$$c_3 = 1 - c_1 - c_2 \qquad \textbf{Eq. 3.71}$$

and finally,

$$\tau = 1.25(\gamma - c_3 - c_2\,\alpha)/c_1 \qquad \textbf{Eq. 3.72}$$

The above equations for α, c_2, c_3 and τ can be expressed in terms of and x_m only, by replacing one into another, however the terms do not always simplify and the equations get longer and slightly complicated by each replacement. The model parameters predicted by Eq. 3.65, 69, 7Ø, 71 and 72 are listed in Table 3.5.

Table 3.4

Rainflow-Range Model Parameters
Best-Fit Parameters Obtained from the Simulation Results

Sp	τ	α	c_2	c_3	cost
1	0.070	0.829	0.056	0.876	107.2
2	0.101	0.859	0.071	0.804	147.6
3	0.048	0.141	0.072	0.816	167.9
4	0.053	0.154	0.095	0.756	164.2
5	0.075	0.189	0.094	0.692	115.7
6	0.079	0.275	0.235	0.580	91.0
7	0.097	0.331	0.326	0.482	119.1
8	0.096	0.289	0.300	0.444	164.9
9	0.086	0.261	0.309	0.405	213.1
10	0.089	0.228	0.285	0.365	259.9
11	0.080	0.219	0.279	0.324	226.4
12	0.089	0.217	0.269	0.267	216.8
13	0.077	0.200	0.118	0.258	192.6
14	0.086	0.217	0.116	0.202	160.5
15	0.068	0.093	0.355	0.105	304.2
16	0.113	0.148	0.466	0.105	28.1
17	0.169	0.207	0.524	0.111	60.7
18	0.134	0.286	0.642	0.135	47.1
19	0.132	0.351	0.692	0.153	63.7
20	0.324	0.417	0.671	0.162	78.2
21	0.201	0.462	0.719	0.187	67.7
22	0.105	0.510	0.674	0.245	62.5
23	0.099	0.564	0.628	0.302	36.3
24	0.096	0.624	0.542	0.393	50.7
25	0.087	0.666	0.505	0.461	57.9
26	0.132	0.802	0.356	0.554	79.5
27	0.103	0.849	0.267	0.682	60.1
28	0.032	0.951	0.231	0.762	117.8
29	0.243	0.888	0.905	0.072	75.3
30	0.135	0.880	0.830	0.143	113.6
31	0.126	0.862	0.691	0.260	107.3
32	0.112	0.859	0.571	0.377	109.9
33	0.145	0.849	0.377	0.543	37.8
34	0.177	0.904	0.293	0.593	83.1
35	0.182	0.937	0.157	0.710	221.5

Table 3.4 (cont.)

Rainflow-Range Model Parameters
Best-Fit Parameters Obtained from the Simulation Results

Sp	τ	α	c_2	c_3	cost
36	0.442	0.820	0.921	0.034	46.0
37	0.267	0.792	0.741	0.205	35.6
38	0.262	0.701	0.550	0.368	47.5
39	0.277	0.664	0.370	0.538	49.7
40	0.163	0.634	0.311	0.597	56.0
41	0.185	0.651	0.241	0.631	82.1
42	0.270	0.820	0.171	0.626	78.8
43	0.261	0.702	0.783	0.164	60.3
44	0.208	0.687	0.637	0.288	36.4
45	0.120	0.594	0.520	0.425	92.9
46	0.130	0.616	0.449	0.451	52.6
47	0.181	0.538	0.326	0.547	95.1
48	0.256	0.624	0.247	0.545	46.8
49	0.244	0.606	0.196	0.581	83.9
50	0.267	0.611	0.722	0.192	45.1
51	0.245	0.591	0.667	0.258	61.3
52	0.126	0.555	0.607	0.326	51.4
53	0.124	0.577	0.569	0.329	63.0
54	0.149	0.590	0.496	0.354	77.3
55	0.186	0.606	0.434	0.377	75.7
56	0.205	0.531	0.324	0.463	70.0
57	0.269	0.510	0.676	0.230	76.1
58	0.248	0.500	0.592	0.276	45.5
59	0.211	0.487	0.520	0.310	66.8
60	0.208	0.467	0.487	0.347	41.7
61	0.166	0.463	0.473	0.359	49.2
62	0.193	0.470	0.398	0.381	78.2
63	0.195	0.458	0.347	0.405	47.8
64	0.258	0.464	0.715	0.173	60.1
65	0.165	0.453	0.709	0.196	112.8
66	0.109	0.455	0.680	0.207	91.8
67	0.116	0.466	0.649	0.213	124.6
68	0.148	0.476	0.605	0.217	150.5
69	0.158	0.483	0.568	0.230	158.9
70	0.172	0.459	0.500	0.268	131.3

Table 3.5

Rainflow-Range Model Parameters
from Closed-Form Eqs. 3.69, 70, 71 and 72

Sp	τ	α	c_2	c_3
1	0.073	0.605	0.054	0.888
2	0.119	0.473	0.085	0.820
3	0.171	0.288	0.097	0.767
4	0.219	0.161	0.118	0.707
5	0.256	0.112	0.153	0.642
6	0.254	0.222	0.242	0.555
7	0.245	0.282	0.338	0.466
8	0.285	0.173	0.333	0.440
9	0.307	0.116	0.356	0.398
10	0.325	0.065	0.381	0.358
11	0.324	0.055	0.431	0.309
12	0.302	0.072	0.504	0.255
13	0.319	0.011	0.515	0.229
14	0.270	0.051	0.604	0.180
15	0.163	0.070	0.781	0.089
16	0.156	0.125	0.778	0.097
17	0.148	0.191	0.773	0.108
18	0.143	0.269	0.757	0.128
19	0.129	0.351	0.754	0.142
20	0.107	0.439	0.768	0.146
21	0.118	0.468	0.721	0.184
22	0.110	0.539	0.694	0.218
23	0.083	0.632	0.721	0.213
24	0.090	0.682	0.606	0.322
25	0.050	0.785	0.708	0.252
26	0.073	0.780	0.385	0.557
27	0.044	0.863	0.290	0.674
28	0.005	0.984	0.476	0.520
29	0.029	0.868	0.737	0.240
30	0.039	0.857	0.628	0.341
31	0.048	0.843	0.528	0.433
32	0.062	0.811	0.384	0.566
33	0.079	0.748	0.240	0.697
34	0.091	0.677	0.162	0.765
35	0.110	0.497	0.079	0.833

Table 3.5 (cont.)

Rainflow-Range Model Parameters
from Closed-Form Eqs. 3.69, 70, 71 and 72

Sp	τ	α	c_2	c_3
36	0.038	0.796	0.784	0.185
37	0.055	0.781	0.674	0.282
38	0.067	0.766	0.594	0.352
39	0.086	0.733	0.472	0.460
40	0.100	0.698	0.385	0.535
41	0.116	0.648	0.301	0.607
42	0.133	0.575	0.224	0.670
43	0.052	0.720	0.788	0.171
44	0.078	0.696	0.663	0.275
45	0.094	0.675	0.587	0.338
46	0.118	0.633	0.476	0.429
47	0.136	0.591	0.398	0.493
48	0.150	0.553	0.346	0.535
49	0.162	0.512	0.302	0.569
50	0.079	0.633	0.737	0.200
51	0.087	0.625	0.709	0.222
52	0.102	0.608	0.650	0.268
53	0.119	0.587	0.592	0.313
54	0.133	0.566	0.542	0.352
55	0.145	0.543	0.498	0.386
56	0.167	0.496	0.425	0.441
57	0.115	0.534	0.678	0.229
58	0.127	0.520	0.644	0.255
59	0.139	0.505	0.608	0.281
60	0.162	0.471	0.543	0.327
61	0.165	0.465	0.533	0.335
62	0.184	0.431	0.483	0.370
63	0.199	0.401	0.445	0.397
64	0.104	0.480	0.757	0.160
65	0.117	0.469	0.726	0.181
66	0.127	0.458	0.699	0.199
67	0.139	0.445	0.669	0.220
68	0.143	0.442	0.660	0.225
69	0.154	0.428	0.633	0.244
70	0.175	0.400	0.583	0.277

Fig. 3.18.i. Rainflow-Range Probability Density Function

Sp. No: 1

$\gamma = .92$

x Simulation Result

o Model Output

e Exponential Term

r Rayleigh Term

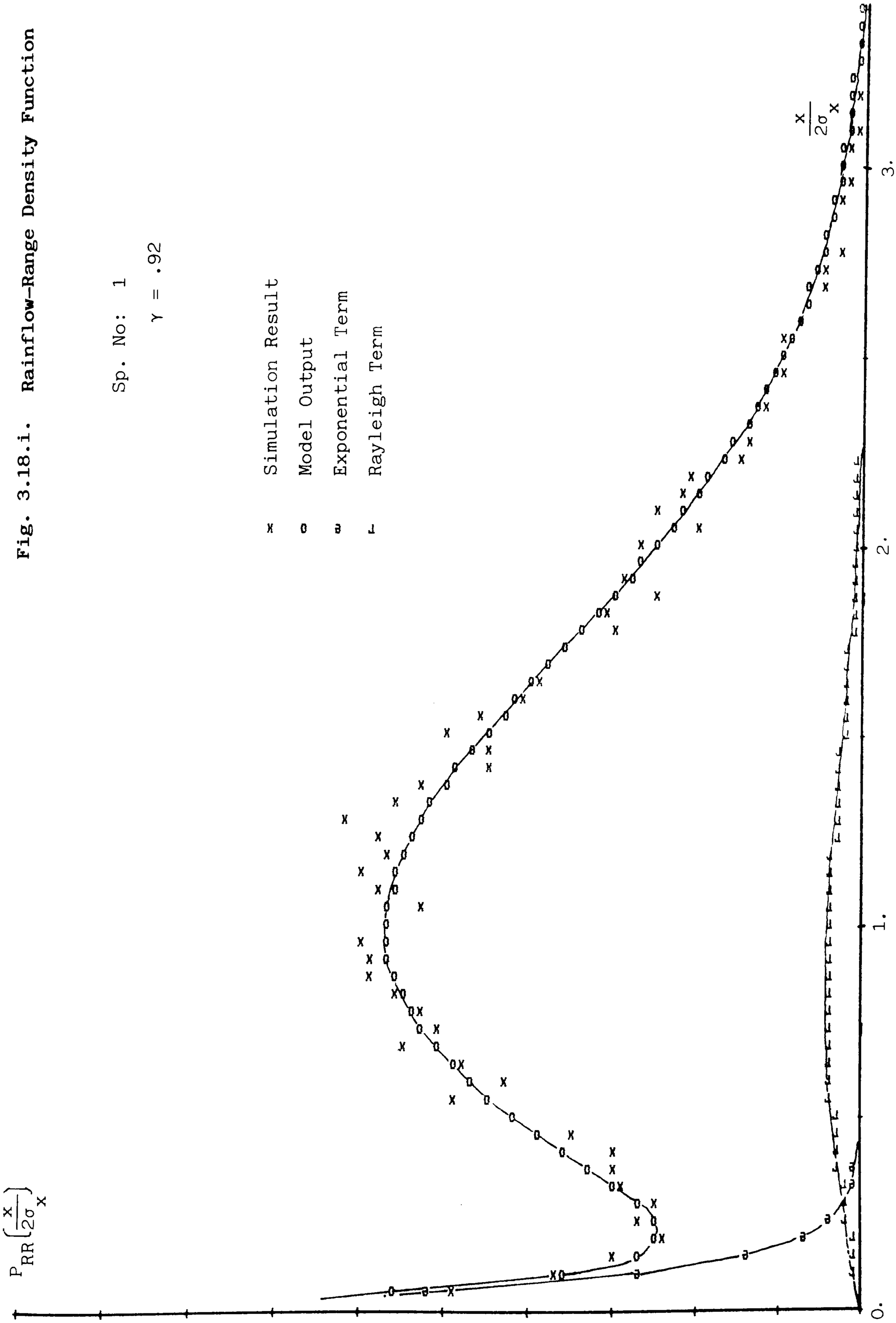

Fig. 3.18.ii. Rainflow Range Probability Density Function

Sp. No. = 6

γ = .57

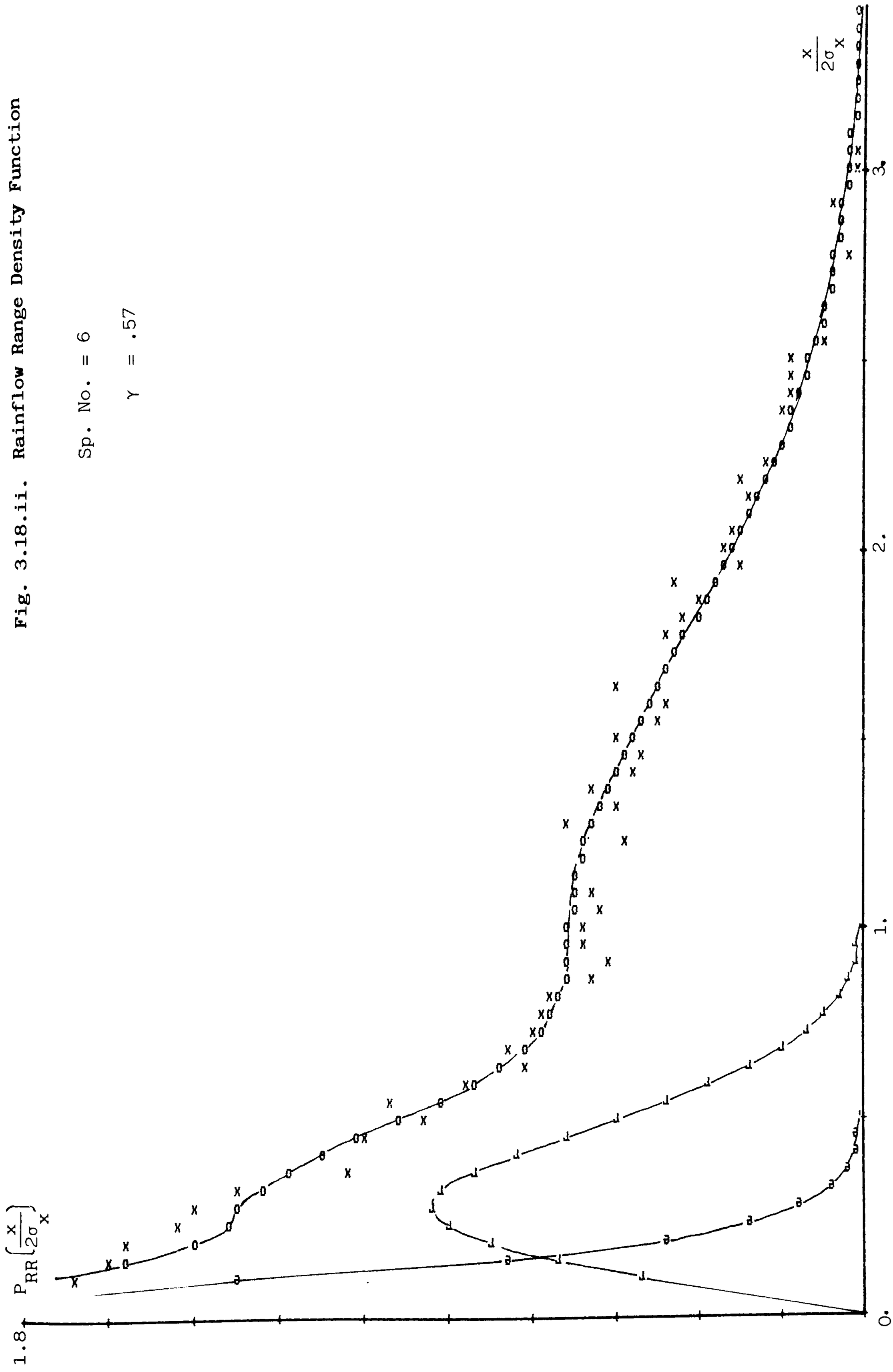

Fig. 3.18.iii. Rainflow Range Density Function

Sp. No. = 65

γ = .53

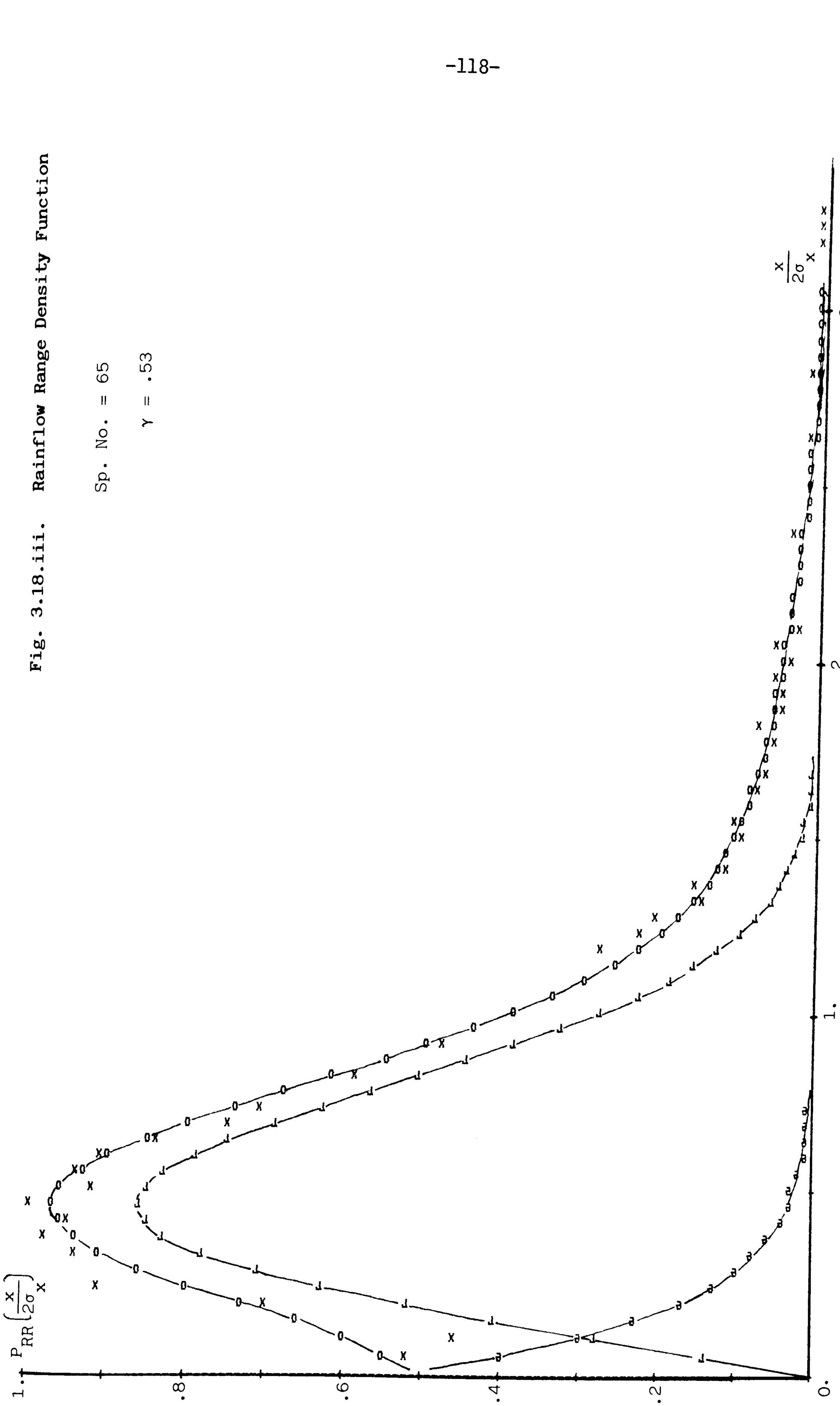

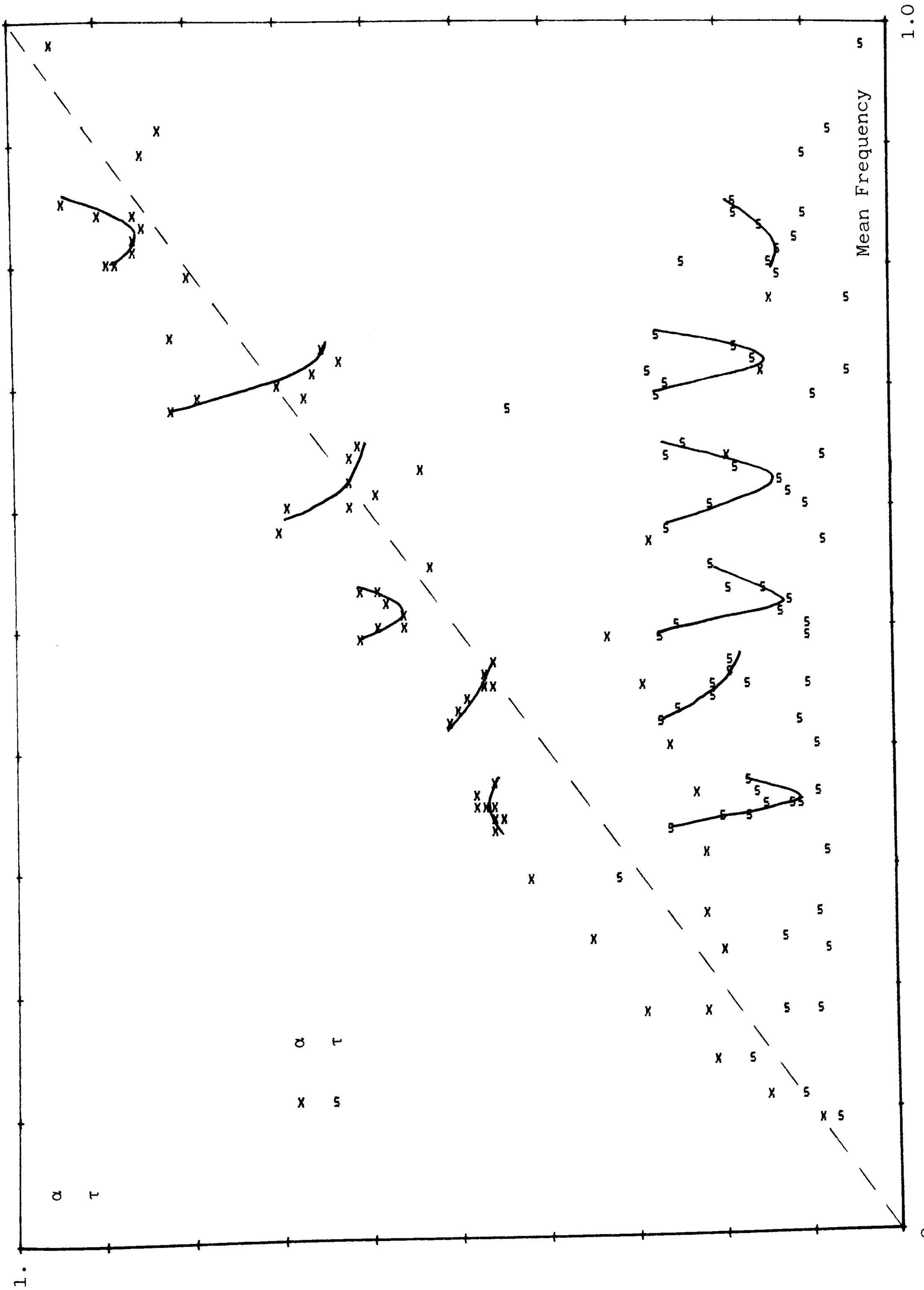

Fig. 3.19.i. Rainflow-Range Model Parameters τ and α vs. Mean Frequency

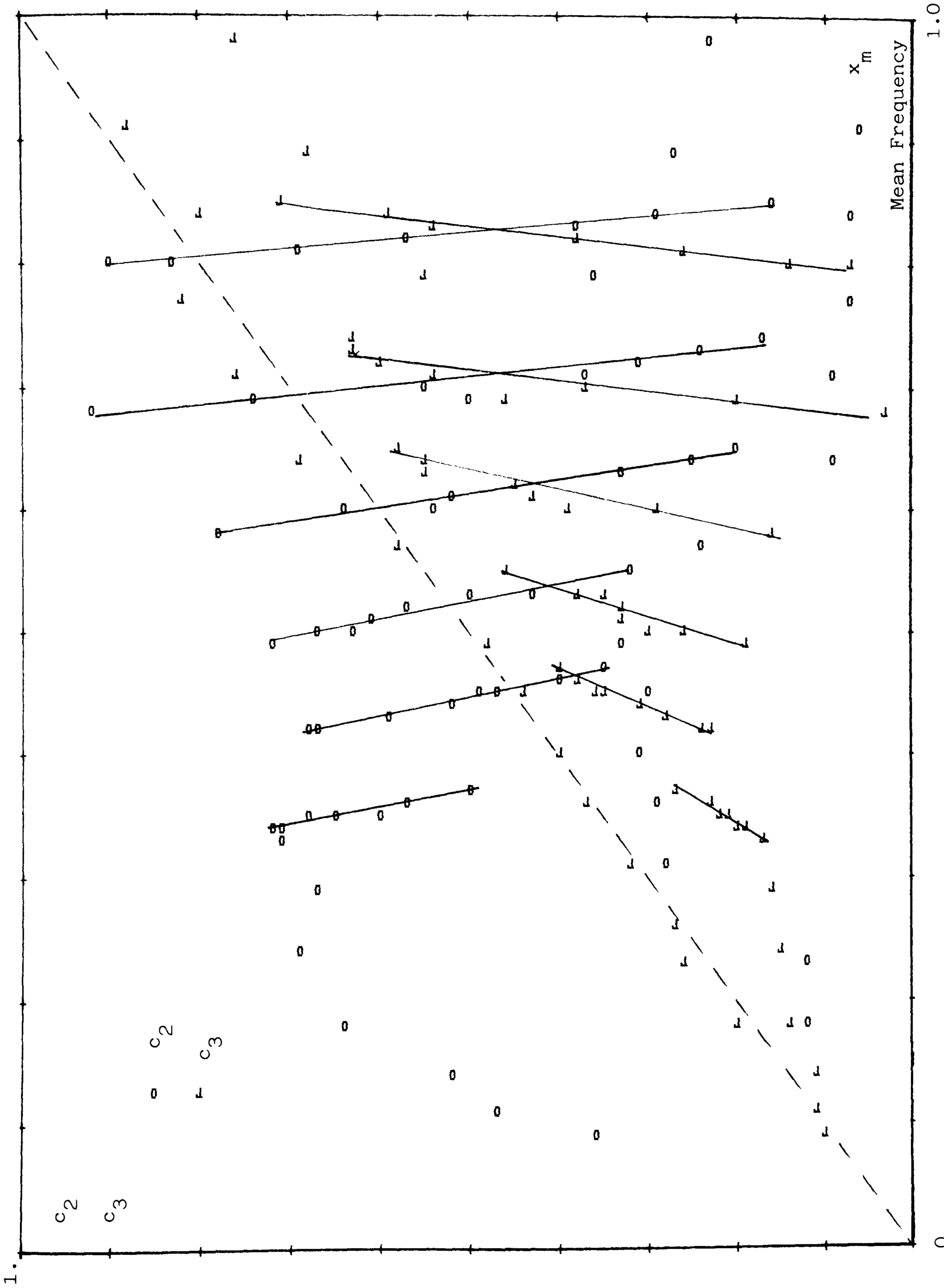

Fig. 3.19.ii. Rainflow-Range Model Parameters c_2 and c_3 vs. Mean Frequency

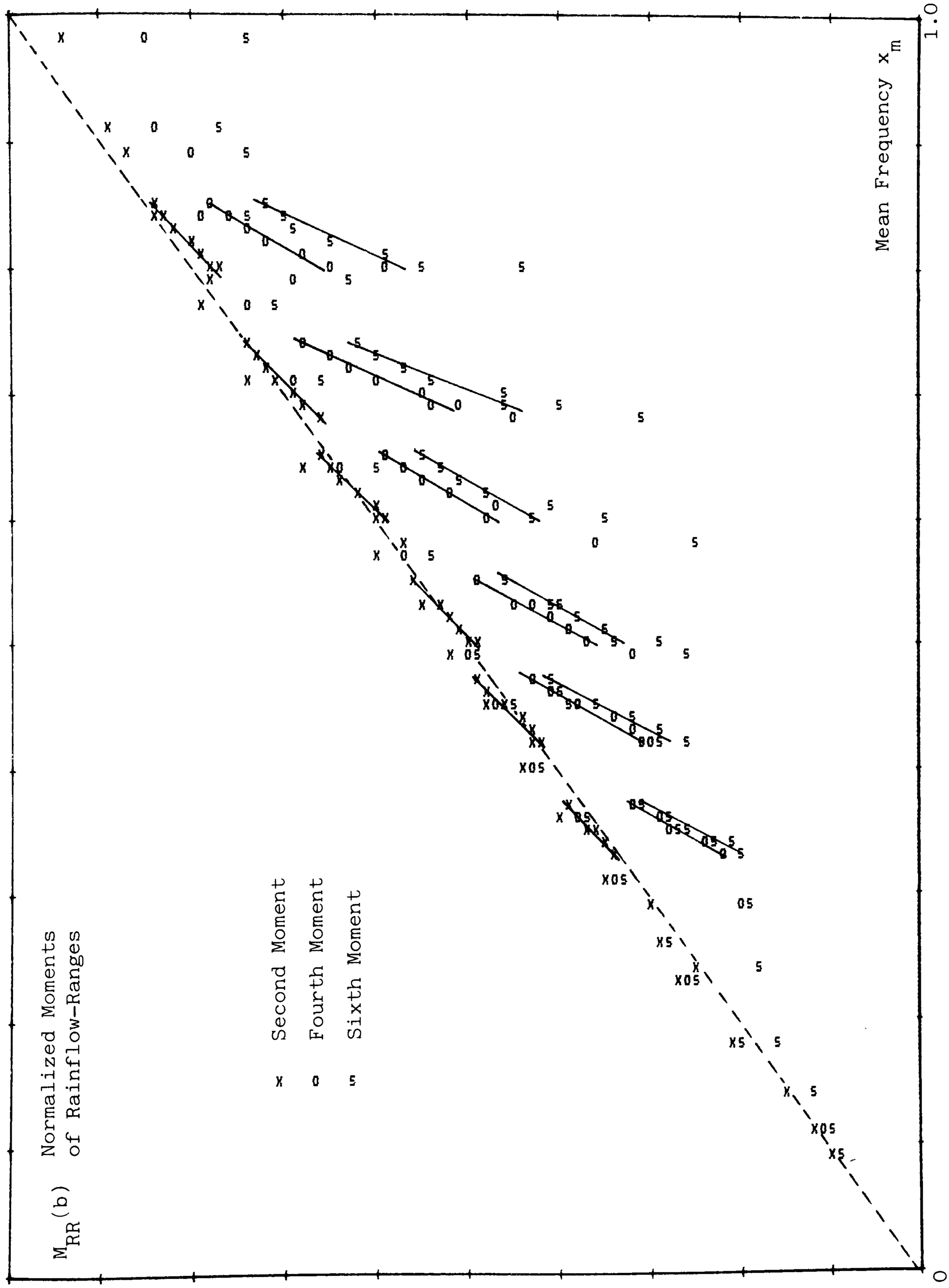

Fig. 3.20. Normalized Moments of Rainflow Ranges Against the Mean Frequency

3.7. Discussions:

First a word about the choice error terms in defining the cost functions. The first choice was a conventional one:

$$e_i^2 = [P(z_i) - \overline{P}(z_i)]^2$$

where $P(z_i)$ is the simulation result, and $\overline{P}(z_i)$ is the proposed model output. With this choice of error term, the model output for both ordinary and rainflow ranges, predicts the simulation results very accurately near the origin and the mid-range where the densities are high, but the prediction for high ranges is very poor. On the other hand, the prediction of high ranges is quite important, particularly from fatigue damage calculation point of view. As the moment gets higher, i.e. as the slope S/N curve, b, increases, the contribution of higher ranges to the moment, i.e. to the damage, increases.

$$e_i^2 = \left[\frac{P(z_i) - \overline{P}(z_i)}{\overline{P}(z_i)}\right]^2$$

With this choice, the problem is reversed. The model output predicts the simulation results admirably well for high ranges, but the prediction is quite poor near the origin where the densities are high, in the region where there are better 'quality' data. By normalizing the first error term with $\overline{P}(z_i)$, the weighing is shifted towards the low-probability high-range end.

The last choice of error term, for which the results reported in this study are based on, is:

$$e_i^2 = \frac{[P(z_i) - \overline{P}(z_i)]^2}{\overline{P}(z_i)}$$

This choice yields good agreement between the simulation results and the model outputs for all ranges. Although this form of error term was chosen for its own merit, it had the added advantage that the cost function calculated from these error terms is directly equal to the Pearson's Chi-Square statistic, χ^2,[12], with (n-1-r) degrees of freedom, where n is the number of intervals, and r is the number of model parameters. The number of intervals, n, is chosen such that the number of range occurrences in the last interval is 5. The number of model parameters, r, is 3 for the ordinary-ranges, 4 for the rainflow ranges; n varies from 70 to 140 for the ordinary ranges depending on the irregularity factor and the mean frequency, and from 140 to 150 for the rainflow-ranges. The corresponding 5 per cent rejection limit, i.e. the 95th percentile of the chi-square distribution with (n-1-r) degrees of freedom vary roughly from 90 to 170 for the ordinary ranges and from 170 to 180 for the rainflow-ranges. All the results listed in Table 3.2 and Table 3.4 are well within these limits except those for spectra from 8 to 16.

Another point of discussion is about the use of an exponential function to explain the variation of both ordinary and rainflow-ranges near the origin. The author had some reservations about employing an exponential function. Depending on the scale factor, and more importantly on the decay factor, the exponential term may continue to exhibit densities greater than the standard Rayleigh densities for large ranges. This is simply against the expectations. The limiting case for the peak, ordinary-range and rainflow-range densities is when the irregularity factor becomes unity, then all the densities converge

to the standard Rayleigh density. Therefore, the densities where the irregularity factor is less than unity are expected to exhibit lesser densities than the standard Rayleigh for high ranges. Despite this known defect, the exponential term kept its place simply because all the attempts to replace it with some other form has failed. Numerous combinations of Gaussian, Rayleigh, erf functions, and derivatives of Gaussian function have been tried in order to replace the exponential term, or sometimes the whole expression for the ranges, without much success.

A comparison of Table 3.2 and Table 3.3 indicate a good agreement between the best-fit parameters obtained from the simulation result for the ordinary-ranges and the parameters calculated from the proposed closed-form equations. The correlation is particularly good for the rectangular spectra, but not so good for the smooth spectra where the mean frequency takes quite high values for a given irregularity factor. This observation is partly expected, because the closed-form equations are derived by approximating a hyperbolic variation with a straight line where x_m takes values near the minimum it can take. Even with the straight line approximation the correlation of α and c_2 values between the two sets of results is quite good for the smooth spectra from 1-7. The worst correlation between the results are for spectra 8 to 16, those are also the cases where the cost function is the worst, well beyond the 5 per cent rejection limit of chi-square distribution. Therefore it is a difficult judgement to make whether the parameters estimated from the closed-form equations are out of place, or the parameters found by the minimization methods are

somehow not the 'best-fit', or simply the exponential plus Rayleigh function model is not valid for those spectra.

The comparison of Table 3.4 and Table 3.5, the lists of parameters for the rainflow-ranges requires some discretion. Considering the fact that there is no apparent relationship for the variation of and values with respect to x_m for the same irregularity factor, as shown in Fig. 3.19.i, it is not surprising to see very large differences between the two sets of results for these parameters. However, the values for scale factors c_2 and c_3 in both sets of parameters are very close to each other. The large discrepancies between the best-fit values and the estimated values for and may be explained by that when their corresponding scaling factors are very small, a small variation on the scaling factors causes very large change in the decay factors. It may also be that the parameters listed in Table 3.4 are not the 'best-fit' results, or even though they may be the result at the global minimum point in the parameter space, that point may not be the 'true' global minimum because of the peculiarities of error surface. After estimating the parameters in Table 3.5, some of the very different ones than the ones in Table 3.4 are tried on the simulation results, and the estimated parameters yield a reasonable approximate density.

One of the main objectives of this study, in fact the principal one, was to investigate 'the link between rainflow and the power spectral density'. In other words, it was to find an expression, hopefully a closed-form equation, for the moments of rainflow-range

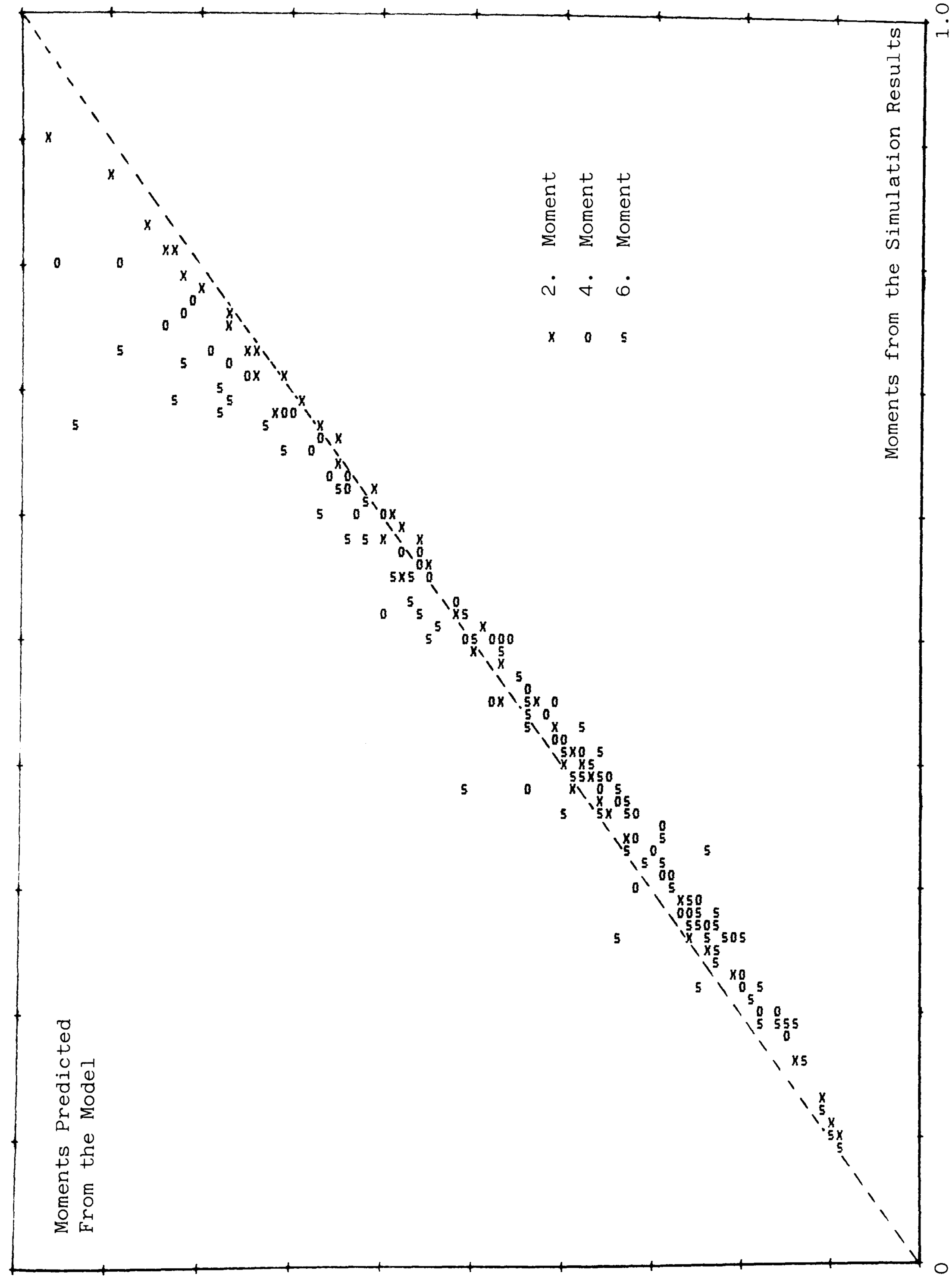

Fig. 3.21. Moments Predicted Against Moments Simulation Results

density function, which is directly proportional with the fatigue damage, in terms of some parameters of a given power spectral density. To this end, the aim is achieved remarkably well, as Fig. 3.21 illustrates the moments predicted by the proposed model against the moments actually calculated from the simulation results.

3.8 Summary and Conclusion:

For a given power spectral density, G(w) of a stationary Gaussian process, define the n^{th} moment of the spectral density, m_n:

$$m_n = \frac{1}{\pi}\int_0^\infty w^n G(w)\,dw$$

Then, the rms, σ_x:

$$\sigma_x = \sqrt{m_o}$$

The expected number of zero-crossings per unit time, λ_o:

$$\lambda_o = \sqrt{\frac{m_2}{m_o}}$$

The expected number of peaks per unit time, :

$$\mu = \sqrt{\frac{m_4}{m_2}}$$

The irregularity factor, :

$$\gamma = \frac{\lambda_o}{\mu} = \sqrt{\frac{m_2^2}{m_o m_4}}$$

The 'mean frequency', x_m:

$$x_m = \frac{m_1}{m_o}\sqrt{\frac{m_2}{m_4}}$$

Then, the instantaneous amplitude probability density function, in terms of a normalized variable $y = x/\sigma_x$, is a standard Gaussian:

$$P_A(y) = \frac{1}{\sqrt{2\pi}} e^{-y^2/2}$$

The peak probability density function:

$$P_P(y) = \frac{c}{\sqrt{2\pi}} e^{-y^2/2c^2} + \gamma y e^{-y^2/2} \left[\tfrac{1}{2} + \operatorname{erf}(\gamma y/c) \right]$$

where $$c = \sqrt{1 - \gamma^2}$$

The ordinary-range probability density function, P_{OR}, in terms of a normalized variable $z = x/2\sigma_x$, and for $z > 0$:

$$P_{OR}(z) = c_1 \frac{1}{\tau} e^{-z/\tau} + c_2 \frac{z}{\alpha^2} e^{-z^2/2\alpha^2}$$

where

$$c_1 = \frac{1}{\gamma^2} (x_m - x_{min})$$

$$\tau = 0.02 + \frac{2}{\gamma} (x_m - x_{min})$$

$$c_2 = 1 - \frac{1}{\gamma^2} (x_m - x_{min})$$

$$\alpha = \gamma + \frac{1}{\gamma} (x_m - x_{min})$$

and

$$x_{min} = \frac{\gamma(1 + \gamma^2)}{2}$$

The moments of ordinary-ranges, $m_{OR}(b)$:

$$m_{OR}(b) = c_1 \tau^b \Gamma(1 + b) + c_2 (\sqrt{2}\alpha)^b \Gamma\left(1 + \frac{b}{2}\right)$$

The normalized moments of ordinary-ranges, $M_{OR}(b)$

$$M_{OR}(b) = c_1 \left(\frac{\tau}{\sqrt{2}}\right)^b \frac{\Gamma(1+b)}{\Gamma\left(1+\frac{b}{2}\right)} + c_2 \alpha^b$$

For $b > 2.$, the normalized moments can be approximated:

$$M_{OR}(b) \simeq c_2 \alpha^b$$

The rainflow-range probability density function, P_{RR}, in terms of a normalized variable $z = x/2\sigma_x$, and for $z > 0$:

$$P_{RR}(z) = c_1 \frac{1}{\tau} e^{-z/\tau} + c_2 \frac{z}{\alpha^2} e^{-z^2/2\alpha^2} + c_3 \, z e^{-z^2/2}$$

where

$$c_1 = \frac{2(x_m - \gamma^2)}{1 + \gamma^2}$$

$$\alpha = \frac{\gamma - x_m - c_1^2}{1 - \gamma - c_1 + c_1^2}$$

$$c_2 = \frac{1 - \gamma - c_1 + c_1^2}{1 - \alpha}$$

$$c_3 = 1 - c_1 - c_2$$

$$\tau = 1.25(\gamma - c_3 - c_2)/c_1$$

The moments of rainflow-ranges, $m_{RR}(b)$:

$$m_{RR}(b) = c_1 \tau^b \Gamma(1 + b) + c_2(\sqrt{2}\alpha)^b \Gamma\left(1 + \frac{b}{2}\right) + c_3(\sqrt{2})^b \Gamma\left(1 + \frac{b}{2}\right)$$

The normalized moments of rainflow ranges, $M_{RR}(b)$:

$$M_{RR}(b) = c_1 \left(\frac{\tau}{\sqrt{2}}\right)^b \frac{\Gamma(1 + b)}{\Gamma\left(1 + \frac{b}{2}\right)} + c_2 \alpha^b + c_3$$

For $b > 2.$, the normalized moments can be approximated:

$$M_{RR}(b) \simeq c_2 \alpha^b + c_3$$

A link between fatigue life estimation based on rainflow counted ranges and measured or calculated power spectral density is proposed. The link is presented in the form of a probability density function of rainflow ranges for a given power spectral density. If a power spectral density plot at a critical location of a component or a structure can be measured or calculated, the terms needed for a fatigue life estimation can then be calculated from the moments of the power spectral density. These terms are rms, expected number of peaks and zero crossings, irregularity factor and mean frequency. Parameters of the proposed model for the distribution of rainflow ranges are determined using only the irregularity factor and the mean frequency.

The importance of presenting the link in terms of a probability density function is in that once the probability density function of rainflow counted ranges is determined, then a life estimation can be made with any form of S/N data. The usage is not restricted to a straight line representation of S/N data on a log-log scale only. In general, the expected damage per unit time, E(D), is calculated as:

$$E(D) = \mu \int_0^\infty \frac{1}{N(x)} P_{RR}(x)\, dx$$

where N(x) is the relation between the number of loading cycles to failure, N, at the load or stress range x. $NS^b = K$ or $N = K/S^b$ is only a special case, N(x) may be a smooth curve with continuous change of slope, or it may contain a cut-off point, an endurance limit. However, before applying this method of life prediction, the basic assumption, that the loading experienced at the critical location is a

stationary Gaussian process, must be verified.

From a parallel study, a method for determining the ordinary-range probability density function for a given power spectral density is also presented. Although the distribution of ordinary-ranges is not important from the fatigue point of view, it is hoped that ordinary-range probability density functions may be useful in other areas of engineering.

REFERENCES FOR CHAPTER 3

1. Papoulis, A. "Probability, Random Variables, and Stochastic Processes", McGraw-Hill, Inc., New York, 1965.

2. Bendat, J. C. "Principles and Applications of Random Noise Theory", John Wiley, New York, 1958.

3. Bendat, J. C. "Probability Functions for Random Noise", NASA Report on Contract NAS-5--459Ø.

4. Rice, S. O. "Mathematical Analysis of Random Noise", papers on Noise and Stochastic Processes, ed. N. Wax, Dover, New York, 1954.

5. Rice, J. R., Beer, F. P. "On the Distribution of Rises and Falls in a Continuous Random Process", Journal of Basic Engineering, Trans. ASME, June 1965, pp. 398-4Ø4.

6. Sjostrom, S. "On Random Load Analysis", Pure and Applied Mathematics and Physics, Trans. of the Royal Instn. of Tech., Stockholm, Sweden, No. 181, 1961.

7. Kirkby, W. T., Edwards, P. R. "A Method of Fatigue Life Prediction Using Data Obtained Under Random Loading Conditions", RAE TR 66Ø23, Royal Aircraft Establishment, Farnborough, 1966.

8. Williams, A. K., Rinne, J. E. "Fatigue Analysis of Steel Offshore Structures", Proc. Instn. of Civil Engineers, Part 1, Vol. 6Ø, Nov. 1976, pp. 635-654.

9. Hallam, N. G. "Fatigue Analysis of Offshore Oil Platforms", paper presented to SEECD '78, 'Applications of Computers in Fatigue', Soc. of Environmental Engineers, April 1978.

1Ø. Wirsching, P. H., Shehata, A. M. "Fatigue Under Wide Band Random Stresses Using the Rainflow Method", Journal of Engineering Materials and Technology, Trans. ASME, July 1977, pp. 2Ø5-211.

11. Wirsching, P. H., Light, M. C. "Fatigue Under Wide Band Random Stresses", Journal of the Structural Division, Proc. ASCE, Vol. 1Ø6, No. ST7, July 198Ø, pp. 1593-16Ø7.

12. Lindgren, B. W. "Statistical Theory", Macmillan Publishing Co. Inc., New York, 1968.

CHAPTER 4

AN OVERVIEW OF FATIGUE DAMAGE CALCULATIONS

In machines and structures made of engineering metals, cyclic loading and the resulting metal fatigue often necessitate predictions of service life. The life of any specimen, subjected to any type of loading cycle, is the sum of the number of cycles required to initiate and develop a macrocrack, and the number of cycles required for the macrocrack to grow across the specimen cross-section.

Most fatigue properties are obtained from constant amplitude cyclic tests of smooth specimens, whereas machine components and structural members are rarely of uniform section and they are subjected in service to cyclic loadings of varying amplitude, the variation in level following either a regular or random pattern. To design a component for a finite life, it is necessary to have a method of predicting service fatigue life of the component for a given geometry, from smooth specimen constant amplitude test data. The investigation of fatigue under varying loads has come to be known as the study of "cumulative damage", because of the early interest in how fatigue damage at various load levels accumulated.

It has been observed[1, 2, 3] that, for very sharply notched parts, the fatigue life is governed by the crack growth after an early crack initiation. Small, smooth laboratory specimens, on the other hand, spend most of their lives in crack initiation. For the

intermediary cases, both the crack initiation and propagation phases are significant. The partition between crack initiation life and crack propagation life is found to depend on the material and the geometry of the specimen, on the stress level and on the stress ratio[1, 4].

The traditional methods based on nominal stress and elastic stress concentration factors usually predict life to total failure, and recent local stress-strain methods are used to predict crack initiation life. With the appearance of a fatigue crack, fracture mechanics concepts become appropriate for predicting the subsequent crack propagation life from the crack growth data.

4.1 Nominal Stress Methods

In general the results of constant amplitude nominal stress tests on notched specimens give an S/N curve of similar form to that for plain specimens[1, 3, 4, 5]. The S/N curve for notched specimens is displaced to the left and can cross over that for plain specimens at very short endurances, as in Figure 4.1., somewhere in the region of 100-1000 cycles.

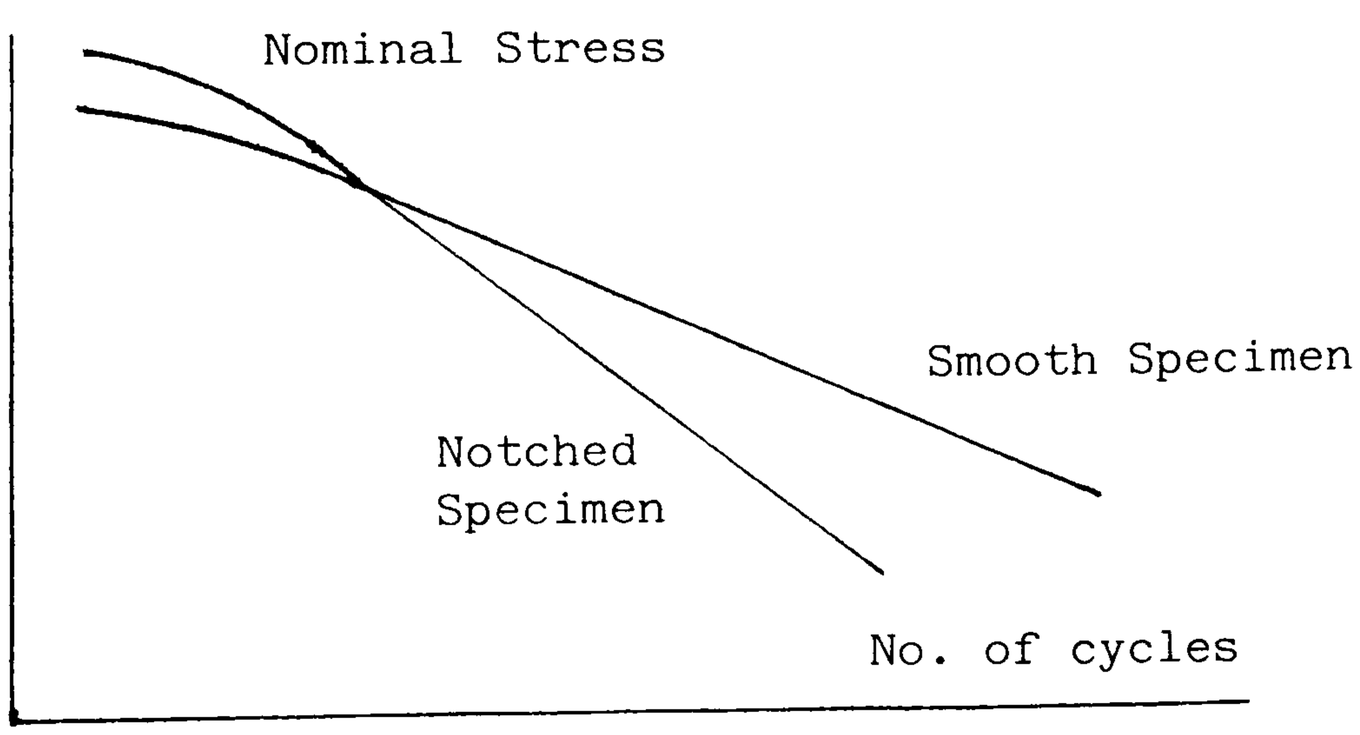

Figure 4.1 Schematic S/N curves for smooth and notched specimens.

The following three nominal stress methods differ only in the way in which the notched specimen S/N curve is related to the plain specimen S/N curve.

4.1.1. Nominal Stress Method I

This method assumes[6] the following relation between the smooth and notched specimen S/N curves. Both are straight lines on a log-log plot. Both have the same fatigue strength at cycle 1. At 1 million cycles the notched specimen fatigue strength is that of the smooth specimen's divided by K_t, the theoretical stress concentration factor. This is shown schematically in Figure 4.2.

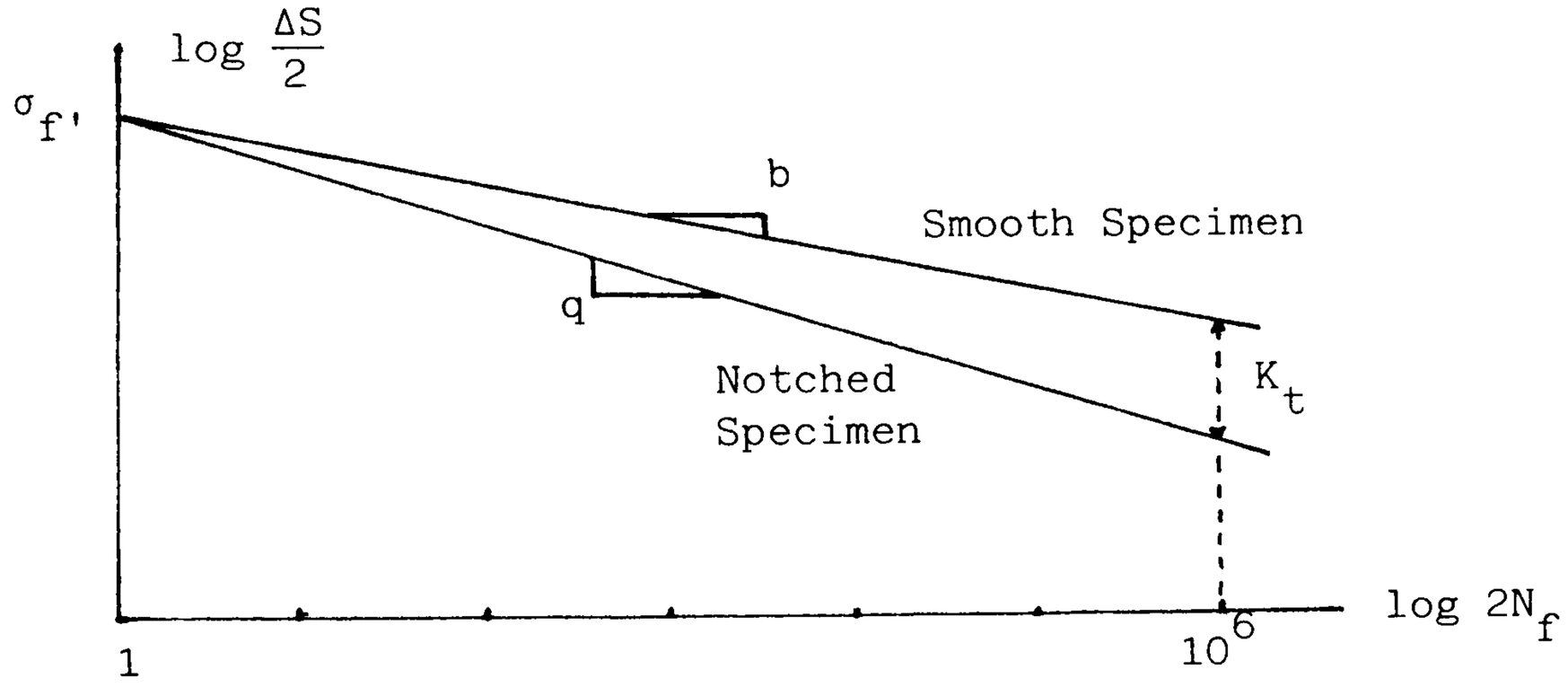

Figure 4.2 Estimated notched S/N curve from a smooth specimen S/N curve.

S/N curve for the smooth specimen:

$$\log \frac{\Delta S}{2} = b \log (2N_f) + \log \sigma_f' \qquad \textbf{Eq. 4.1}$$

or

$$\frac{\Delta S}{2\sigma_f'} = (2N_f)^b \qquad \textbf{Eq. 4.2}$$

where σ_f' is the fatigue strength coefficient

b is the fatigue strength exponent

S/N curve for the notched specimen:

$$\log \frac{\Delta S}{2} = q \log (2N_f) + \log \sigma_f' \qquad \textbf{Eq. 4.3}$$

or

$$\frac{\Delta S}{2\sigma_f'} = (2N_f)^q \qquad \textbf{Eq. 4.4}$$

where

$$q = b - \frac{\log K_t}{6}$$

The operations required to estimate the crack initiation life under variable amplitude loads are:

i) Count load ranges by the rainflow method

ii) Calculate nominal stress ranges dividing load ranges by the cross-section area

iii) Calculate damage for each stress range from the estimated S/N curve. Eq. 4.4 may be written in the form:

$$\frac{1}{2N_i} = D_i = \left(\frac{\Delta S}{2\sigma_f'}\right)^{-1/q} \qquad \textbf{Eq. 4.5}$$

iv) Add damages in the block using Miner's rule, Eq. 2.1

4.1.2 Nominal Stress Method II

The first method does not consider the case where the S/N curve

for notched specimens may cross that for smooth specimens. This method in this section and the following one take account of notch strengthening at short lives. This method assumes[6] a similar relation between the smooth and notch specimen S/N curves as in Method I. Both are straight lines on a log-log plot. At 1 million cycles the notched specimen fatigue strength is that of smooth specimens divided by K_t. However they have the same fatigue strength at 1000 cycles, instead of at cycle 1, as in Method I. In other words, at cycle 1, the notched specimen strength is K_t times the smooth specimen strength.

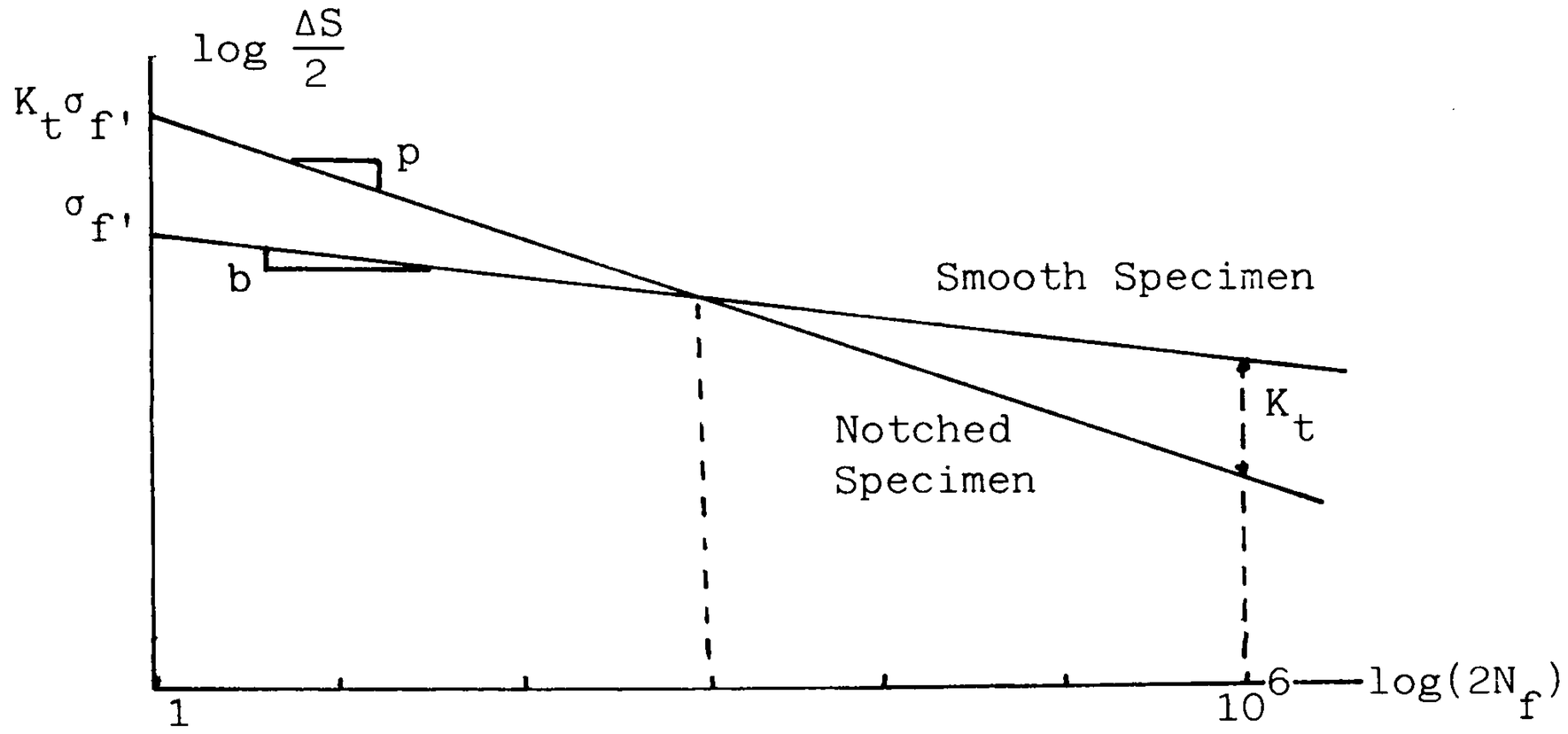

Figure 4.3 Nominal Stress Method II, estimated S/N curve.

S/N curve for the notched specimen, Figure 4.3.:

$$\log \frac{\Delta S}{2} = p \log (2N_f) + \log (K_t \ \sigma_f') \qquad \textbf{Eq. 4.6}$$

or

$$\frac{\Delta S}{2 \ K_t \ \sigma_f'} = (2N_f)^p \qquad \textbf{Eq. 4.7}$$

where

$$p = b - \frac{\log K_t}{3}$$

The operations required to estimate the crack initiation life

are the same as the ones described previously with one exception. The following equation is used to calculate the damage in place of Eq. 4.5.

$$D_i = \left(\frac{\Delta S}{2 K_t \sigma_f'}\right) -1/p \qquad \textbf{Eq. 4.8}$$

4.1.3 Nominal Stress Method III

This method is very similar to Method II. The only difference is that the notched specimen S/N curve crosses that for smooth specimen at cycle 100 instead of 1000, Figure 4.4.

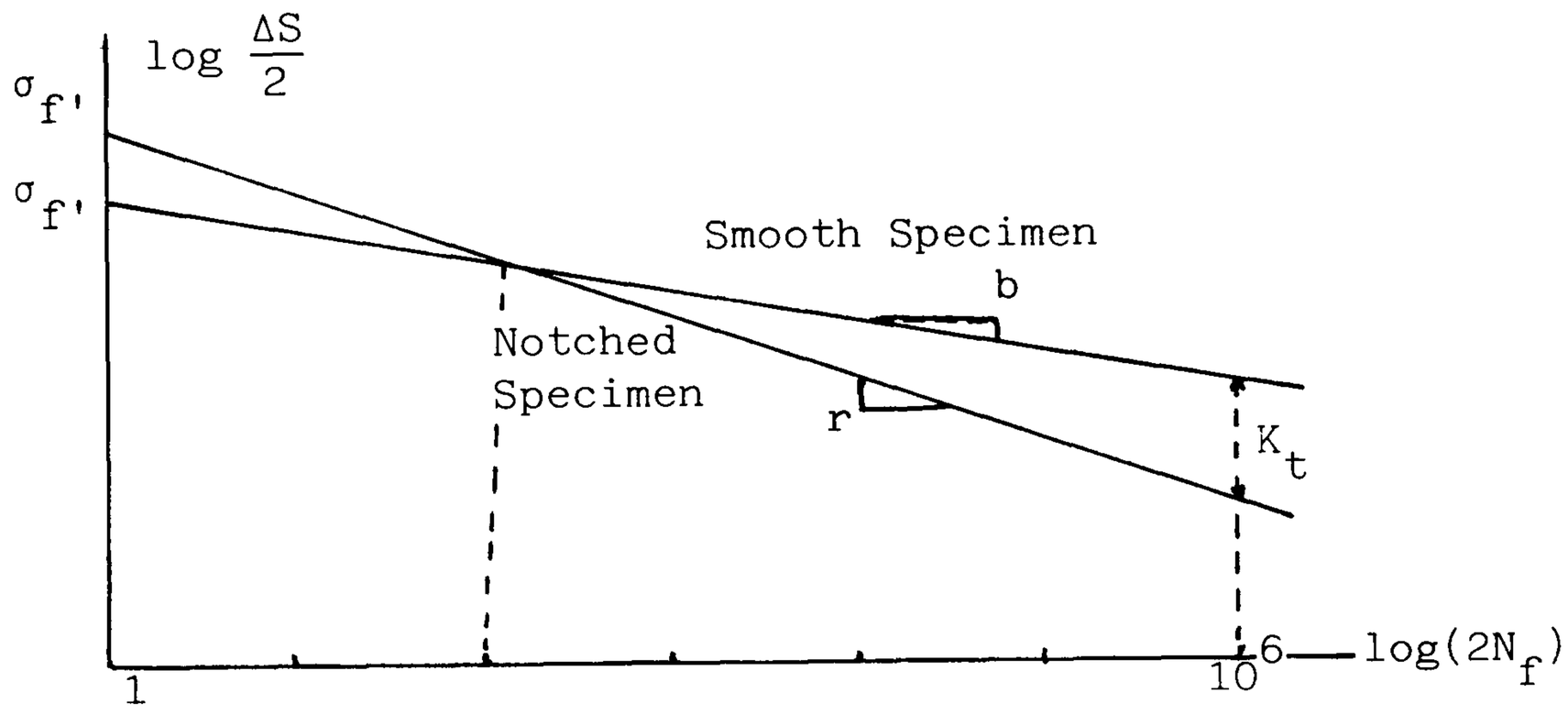

Figure 4.4 Nominal Stress Method III, estimated S/N curve.

In this case, S/N curve for the notched specimen:

$$\log \frac{\Delta S}{2} = r \log (2N_f) + \log (\sqrt{K_t}\ \sigma_f') \qquad \textbf{Eq. 4.9}$$

or

$$\frac{\Delta S}{2\sqrt{K_t}\ \sigma_f'} = (2N_f)^r \qquad \textbf{Eq. 4.10}$$

where

$$r = b - \frac{\log K_t}{4}$$

the damage becomes:

$$D_i = \left(\frac{\Delta S}{2\sqrt{K_t}\ \sigma_f'} \right) -1/r \qquad \textbf{Eq. 4.11}$$

Obviously these three methods are fairly crude. If necessary they could be improved by ad hoc tests on notched specimens. The cross-over life and the life at which the reduction in fatigue strength of the notched specimen is in proportion to the theoretical stress concentration factor, may be modified. A fatigue notch factor K_f may be used instead of the theoretical stress concentration factor K_t. However all these refinements require a prior knowledge of the material.

4.2 Local Stress-Strain Methods

Fatigue failures in metallic structures are generally due to the initiation of cracks at notches or other stress raisers where local stresses reach levels at which inelastic material deformation and finite fatigue life occur. On the other hand, it is seldom possible to actually measure stresses or strains where the fatigue damage will occur at a critical location. Hence designers have increasingly been forced to the utilization of analyses which transform nominal load histories on components into terms of local stresses and strains at the critical locations. This approach has two principal advantages. First, life predictions for a wide variety of situations may be made from a limited amount of small, smooth specimen test data, and such information is becoming increasingly available through the published literature. Second, it provides a basis for considering various material behaviour related interaction effects.

In the following sections, the basic elements of the local strain approach are considered. These are cyclic stress-strain properties, stress-strain hysteresis loop curves, strain-life material properties, and a notch analysis. In a later section, this information will be combined into specific life prediction procedures.

4.2.1. Cyclic Stress-Strain Curve

It is well known that cyclic loading of metals in the inelastic range changes their stress-strain response. Most engineering metals exhibit cyclic hardening or softening depending upon their particular metallurgical state. Normally, a constant or steady state response is achieved after a number of cycles which is generally small in proportion to that required for crack initiation. This steady-state response is characterized by the cyclic stress-strain curve which is the locus of tips of the stable hysteresis loops at different completely reversed, constant amplitude, controlled strain tests, Figure 4.5.

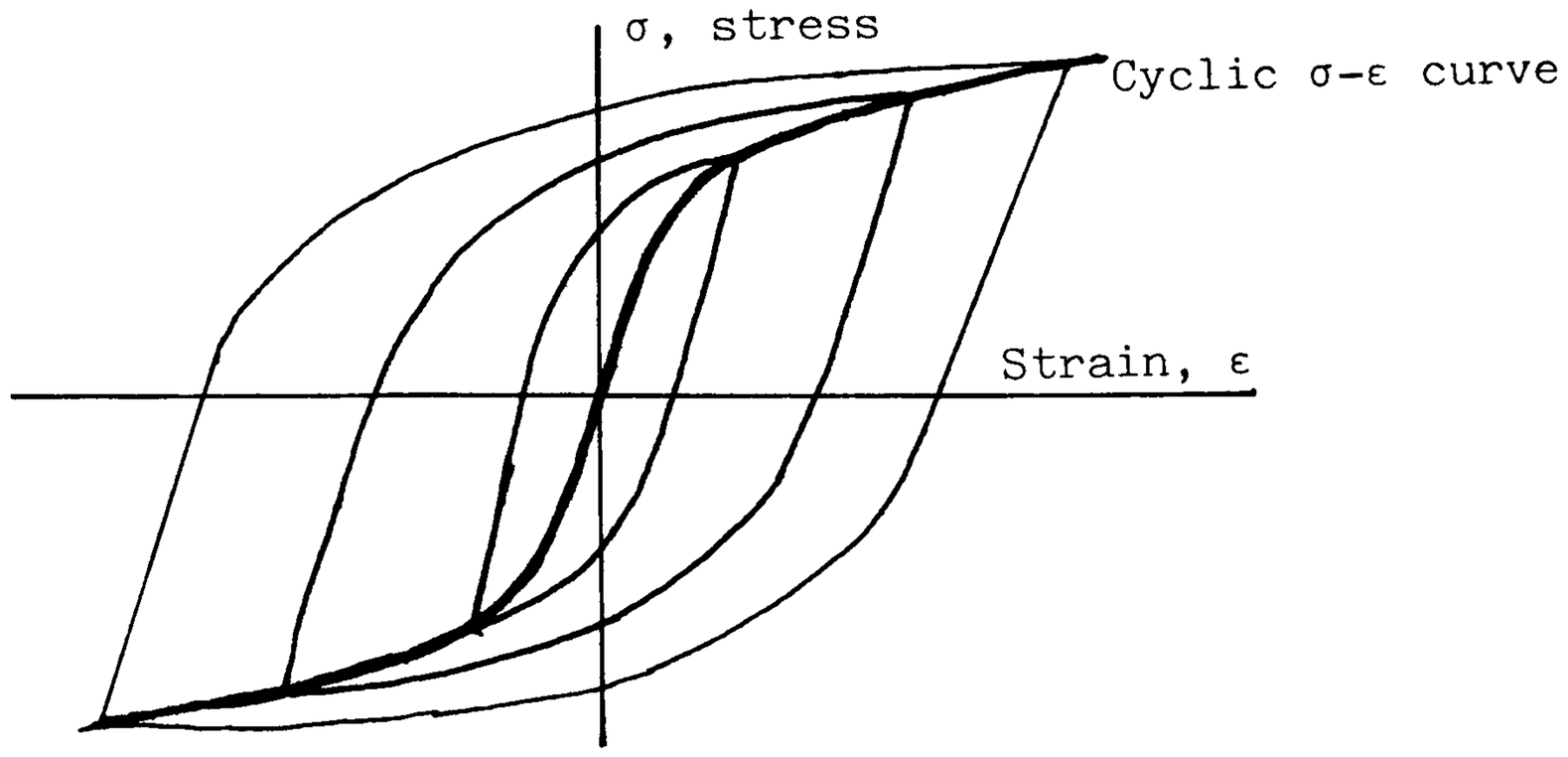

Figure 4.5 Cyclic stress-strain curve determined from a set of stable hysteresis loops.

There are several experimental techniques for determining the cyclic stress-strain curve of metals. These include using companion specimens, multiple and incremental step strain tests, monotonic tension after cyclic straining, and analysis of individual hysteresis loops[7]. During a constant amplitude controlled strain test, after the initial rapid hardening or softening is complete so that the stress-strain behaviour is approximately stable, a stress-strain hysteresis loop as in Figure 4.6 is formed. Usually, hysteresis loops taken at half the fatigue life may be used to approximate the behaviour during most of the life.

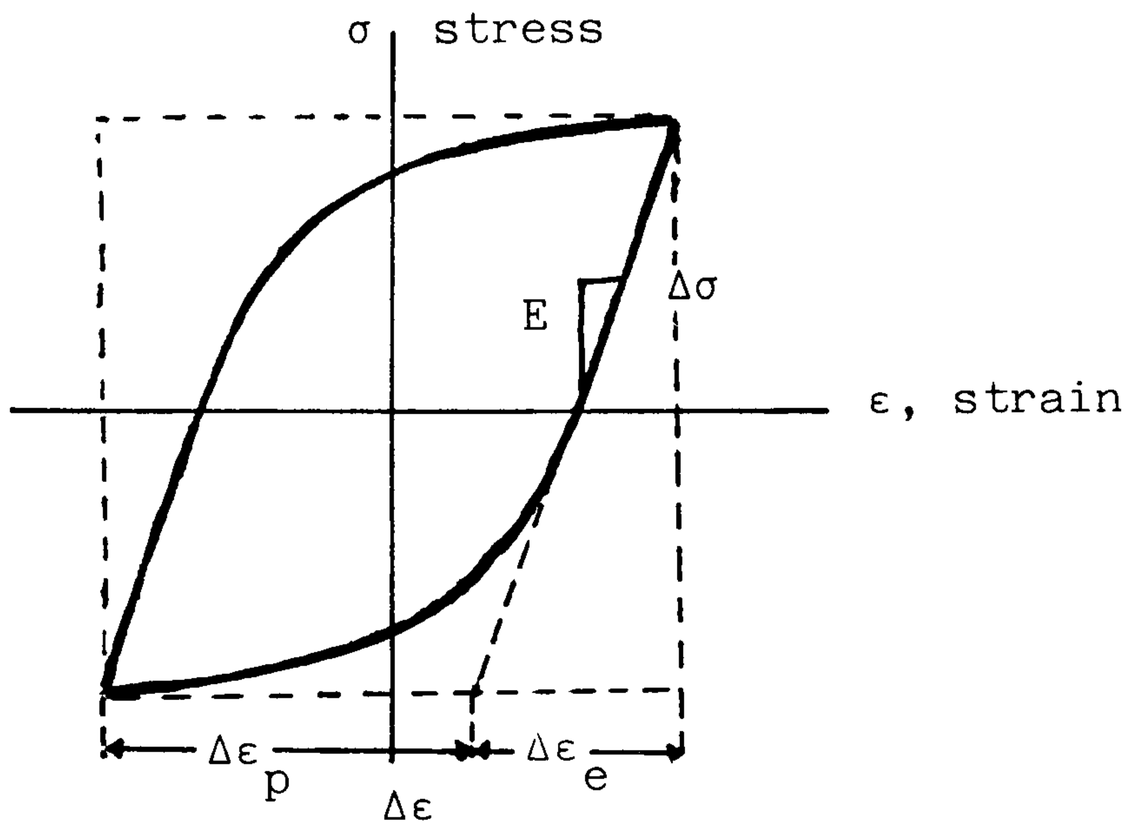

Figure 4.6 Stress-strain hysteresis loop.

To obtain a mathematical relationship describing the cyclic stress-strain curve, the total strain range $\Delta\varepsilon$ in Figure 4.6 is divided into elastic and plastic components, $\Delta\varepsilon_e$ and $\Delta\varepsilon_p$ respectively. Amplitudes, or half ranges, of these quantities are usually employed.

$$\frac{\Delta\varepsilon}{2} = \frac{\Delta\varepsilon_e}{2} + \frac{\Delta\varepsilon_p}{2} \qquad \textbf{Eq. 4.12}$$

and

$$\frac{\Delta\epsilon_e}{2} = \frac{\Delta\sigma}{2E} \qquad \text{Eq. 4 13}$$

where $\Delta\sigma$ is the stress range and E is the elastic or Young's modulus. If the plastic strain is extracted and a log-log plot is made of stress versus plastic strain, a straight line usually results, which implies a power function of the form:

$$\frac{\Delta\epsilon_p}{2} = \left(\frac{\Delta\sigma}{2K'}\right)1/n' \qquad \text{Eq. 4.14}$$

where K′ is the cyclic strength coefficient and n′ is the cyclic strain hardening exponent. Combining Eqs. 4.13 and 4.14 into 4.12 gives a relationship for total strain in terms of stress

$$\frac{\Delta\epsilon}{2} = \frac{\Delta\epsilon}{2E} + \left(\frac{\Delta\sigma}{2K'}\right)1/n' \qquad \text{Eq. 4.15}$$

4.2.2 Simulation of Stress-Strain Hysteresis Loops

During irregular variation of strain with time. as in Figure 4.7, the stress-strain behaviour appears complex, but with the assumptions and rules described in the paragraphs that follow, it is possible to predict the stress-strain response corresponding to an irregular loading.

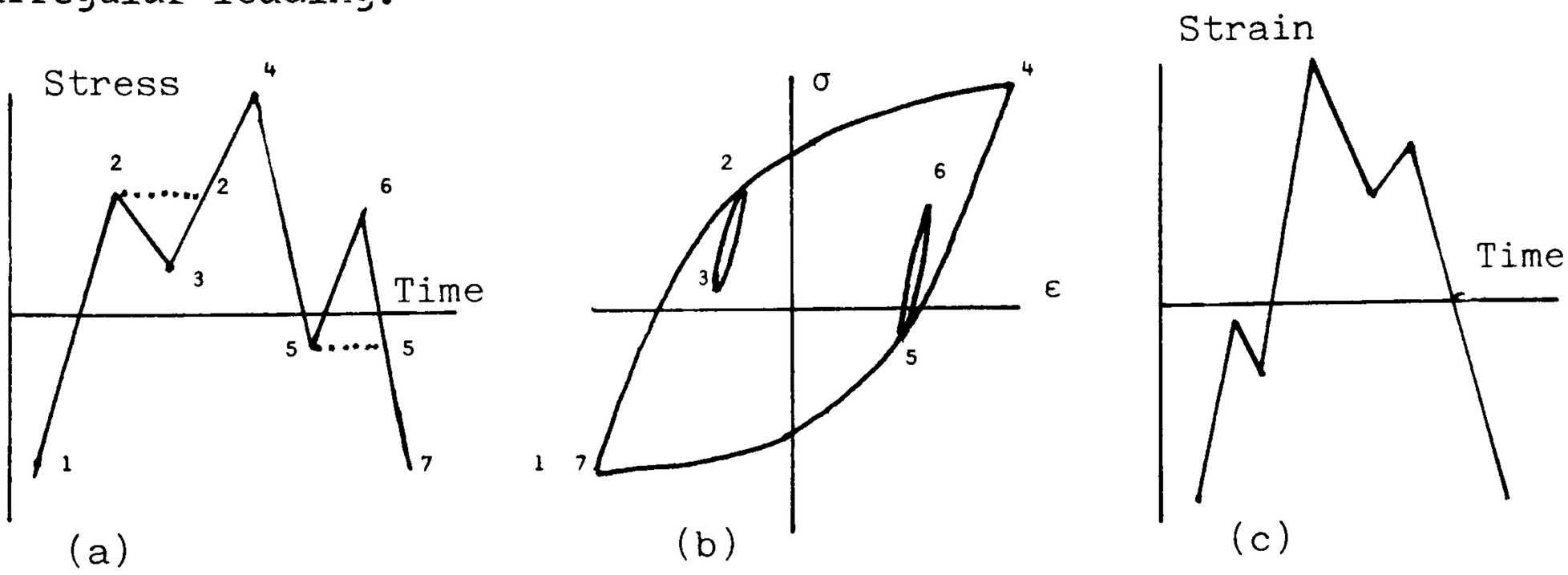

Figure 4.7 Stress and strain against time and corresponding hysteresis loops.

i) The material behaviour will be approximated by assuming that cyclic hardening or softening is complete and also that other transient deformation behaviour, such as creep or mean stress relaxation is of no importance.

ii) During stable cycling, the stress-strain path followed from tip to tip of any hysteresis loop has approximately the shape of the cyclic stress-strain curve of the material, but twice as large in both coordinates[8, 9, 10]. This rule follows the definition of the cyclic stress-strain curve which is the locus of stable, fully reversed loop tips. Thus all stable hysteresis loop traces for a given metal follow a unique curve which may be mathematically described by expanding the cyclic stress-strain curve with a scale factor of two, and shifting its origin and rotating the axes 180° every time the strain excursion changes its direction.

iii) When a strain excursion next reaches a value at which the direction of straining was previously reversed, for example points 2′ and 5′ of Figure 4.7, a stress-strain hysteresis loop is closed. The stress-strain path beyond this point is the same as if the interruption had not occurred, no matter how many interruptions there are. Furthermore, once a strain excursion forms a closed loop, this excursion does not affect the subsequent behaviour. This rule has been called a "memory effect" in material behaviour; the material remembers the stress-strain path it was following when interrupted and resumes this path when the interruption is over[9, 10].

iv) These forementioned rules are based on experimental observations for unnotched axial test specimens[7, 9, 10]. Hence, in a strict sense, they apply only to a uniaxial state of stress.

4.2.3 Notch Analysis

In dealing with complex geometrics, it is necessary to relate nominal loads and stresses to the local stress-strain response at the critical locations in a structure. This necessitates using the load history, stress-strain relationship described in the preceding section, in conjunction with an elastic-plastic mechanics analysis of the notched component.

In theory, sophisticated elastic-plastic analysis techniques such as finite elements could be applied on a reversal-by-reversal basis during an irregular load history. However, this would be expensive and time consuming for histories containing more than a few load reversals. On the other hand, a finite element analysis may be employed to calculate the stresses and strains at the root of a notch in a specific component at a given load level. By repeating the same procedure at different load levels, the load versus notch strain calibration curves may be obtained[11]. These curves can also be determined experimentally by strain gauge measurements in the notch during completely reversed cyclic loading[12]. For the load-strain calibrations, an equation of the following form was found to fit the experimental data:

$$\frac{\Delta\epsilon}{2} = \frac{P}{c_1} + \left(\frac{P}{c_2}\right)1/d \qquad \textbf{Eq. 4.16}$$

where $\Delta\epsilon$ is the local strain, P is the applied load and c_1, c_2 and d are material constants.

Experimental or theoretical load versus notch strain calibration curves are seldom available and they are applicable to a particular material and component geometry. Thus, alternative means of obtaining a load-strain curve must be considered. One of the most popular forms of notch analysis was originally developed by Neuber for nonlinear deformation at the notch root and subsequently extended to fatigue applications[13]. During plastic deformation, the geometric mean of the stress and strain concentration factors, K_σ and K_ϵ respectively, is postulated to remain equal to the theoretical stress concentration factor, K_t.

$$K_t = (K_\sigma\ K_\epsilon)^{1/2} \qquad \textbf{Eq. 4.17}$$

Expressed in terms of ranges, Eq. 4.17 can be rewritten as:

$$K_t = \left(\frac{\Delta\sigma}{\Delta S}\ \frac{\Delta\epsilon}{\Delta e}\right)^{1/2} \qquad \textbf{Eq. 4.18}$$

where $\Delta\sigma$ and $\Delta\epsilon$ are local, ΔS and Δe are nominal stress and strain ranges. Given the further assumption of nominal elasticity,

$$\Delta S = E.\Delta e \qquad \textbf{Eq. 4.19}$$

and combining and rearranging Eqs. 3.18 and 3.19 leads to:

$$K_t\ \Delta S = (\Delta\sigma.\Delta\epsilon.E)^{1/2} \qquad \textbf{Eq. 4.20}$$

Since nominal stress is proportional to load, Eq. 4.20 provides, when used in conjunction with Eq. 4.15, a relationship between applied load and local notch strain, for a given K_t.

Eq. 4.20 is of the form of a hyperbola and defines the control condition at a notch root as shown in Figure 4.8. For simulations, the material is allowed to deform along its cyclic stress-strain curve, in a manner described in the previous section, until it intersects the control hyperbola, thus satisfying the required equality. This construction is then carried out for each reversal in the history.

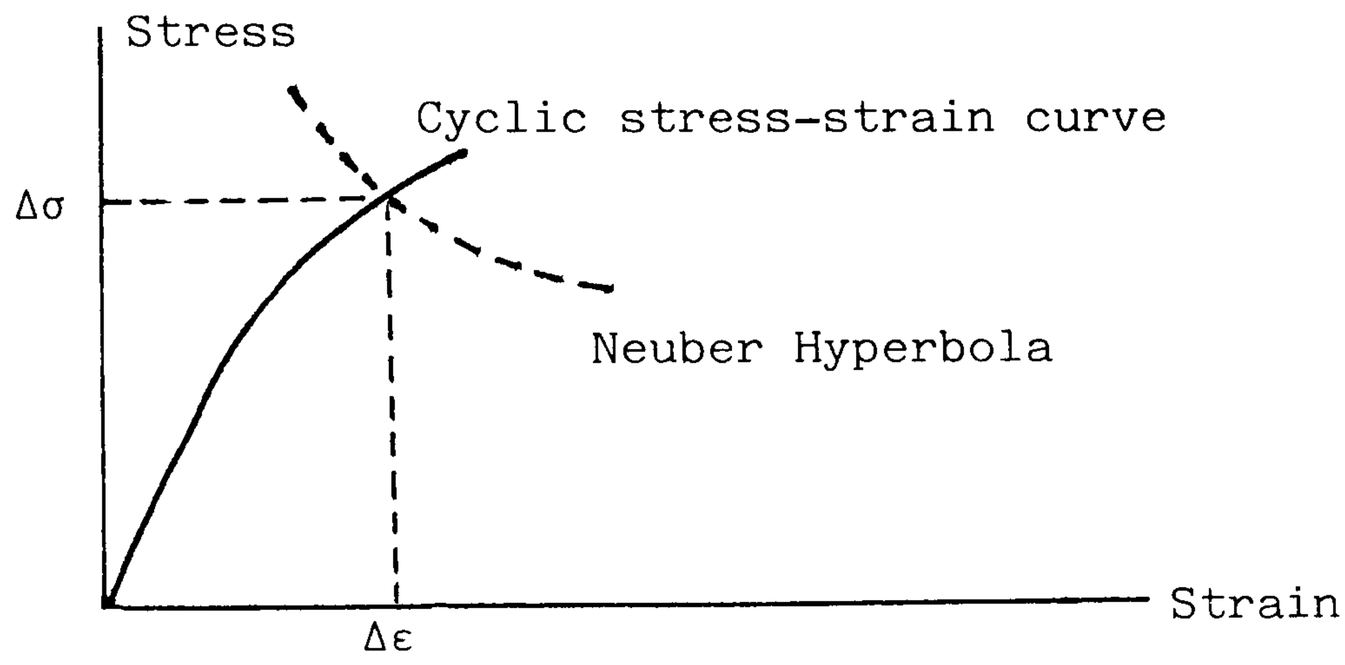

Figure 4.8 Construction for determining notch root stress and strain.

As in the nominal stress methods, the theoretical stress concentration factor, K_t, may be replaced by the fatigue notch factor, K_f. K_f is defined as the ratio of the fatigue strength for an unnotched specimen to the nominal fatigue strength of a notched specimen at the same life, generally measured at a long life[5]. Determination of K_f by means other than extensive fatigue testing has led to the following expression due to Peterson[14].

$$K_f = 1 + \frac{K_t - 1}{1 + a/r} \qquad \textbf{Eq. 4.21}$$

where r is the notch root radius and a is a material constant which in turn has to be determined from fatigue tests at long life.

The stress concentration factor, K_t, is defined as the ratio of maximum local stress to the nominal stress based on minimum cross-section area, and can be calculated from the geometry of the notch alone. It is not a function of material properties. However the definition of K_f implies that K_f depends on the material properties and the notch geometry. Even for a given material and geometry, it is not a constant but a function of life or stress level at which a comparison has to be made.

Eq. 4.21 indicates that K_f is always less or equal to K_t, the higher the value of K_t the greater the difference becomes. Obviously if life is estimated by applying K_t to un-notched test results the estimates will be very approximate, fortunately, on the conservative side if a measured or calculated value of K_f can be found they will be more accurate.

4.2.4 Cyclic Strain-Life Properties

Fatigue resistance of metals can be characterized by strain-life curves that are determined from smooth specimens tested in completely reversed strain control. If elastic and plastic strains are separated and plotted against number of cycles on log-log coordinates, as in Figure 4.9, straight lines usually result.

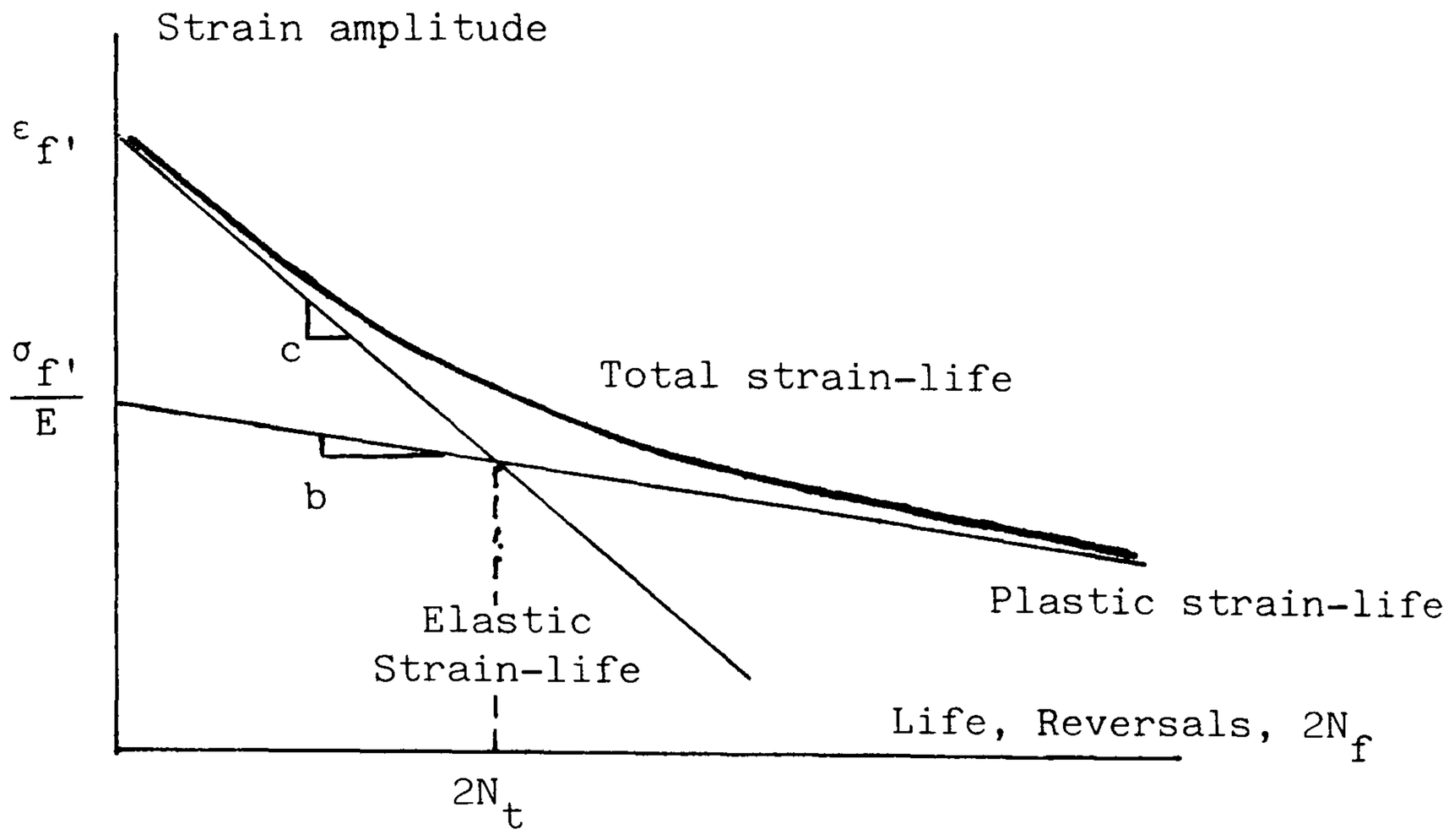

Figure 4.9 Strain-life curve

The equation for the plastic strain-life relationship can be written as:

$$\frac{\Delta\varepsilon_p}{2} = \varepsilon_{f'} (2N_f)^c \qquad \textbf{Eq. 4.22}$$

where $\varepsilon_{f'}$ is the fatigue ductility coefficient, the intercept of the log $(\Delta\varepsilon p/2)$ versus log $(2N_f)$ plot at $2N_f = 1$.

and c is the ductility exponent, the slop of the log $(\Delta\varepsilon p/2)$ versus log $(2N_f)$ plot.

The elastic strain-life relationship is simply the stress-life relationship divided by the modulus of elasticity, E.

$$\frac{\Delta\varepsilon_e}{2} = \frac{\sigma_{f'}}{E} (2N_f)^b \qquad \textbf{Eq. 4.23}$$

4.3 Various Cumulative Damage Calculations by Using Local Stress-Strain Approach

The basic elements of the local stress-strain approach to the fatigue crack initiation are discussed in the previous section. Various life prediction procedures may now be assembled from the ingredients presented above. These are, in summary:

(i) Cyclic stress-strain relationship

$$\frac{\Delta\epsilon}{2} = \frac{\Delta\sigma}{2} + \left(\frac{\Delta\sigma}{2K'}\right)^{1/n'} \qquad \textbf{Eq. 4.15}$$

(ii) Nominal stress-local notch strain relationship

either (a) load-strain calibration

$$\frac{\Delta\epsilon}{2} = \frac{P}{c_1} + \left(\frac{P}{c_2}\right)^{1/d} \qquad \textbf{Eq. 4.16}$$

or (b) Neuber's rule

$$K_t\Delta S = (\Delta\sigma\Delta\epsilon E)^{1/2} \qquad \textbf{Eq. 4.20}$$

(iii) Strain-life relationship

$$\frac{\Delta\epsilon}{2} = \frac{\sigma_f'}{E}(2N_f)^b + \epsilon_f'(2N_f)^c \qquad \textbf{Eq. 4.24}$$

While differing in details, all the methods discussed below employ the same basic steps. These are as follows:

i) Begin analysis of the repeating load history at the most extreme point. This ensures all the hysteresis loops are closed. Calculate the notch stress and strain values at this point by using either a load-strain calibration curve or the Neuber's rule and the

where σ_f' is the fatigue strength coefficient, the intercept of the $\log(\Delta\epsilon_e/2)$ versus $\log(2N_f)$ plot at $2N_f = 1$ divided by E,

and b is the fatigue strength exponent, the slope of the $\log(\Delta\epsilon_e/2)$ versus $\log(2N_f)$ plot.

Then, the equation describing the total strain-life relationship becomes:

$$\frac{\Delta\epsilon}{2} = \frac{\sigma_f'}{E}(2N_f)^b + \epsilon_f'(2N_f)^c \qquad \textbf{Eq. 4.24}$$

These properties, b, σ_f', c and ϵ_f' determining strain-life relationship, and K' and n' for the cyclic stress-strain curve are generally called cyclic properties as apposed to monotonic material properties. Hence (') in $\sigma_f'.\epsilon_f'$, K' and n' is used to differentiate these cyclic properties from their counterpart monotonic properties. Although it appears that there are six different cyclic material constants, only four of these constants are unique. By manipulating Eq. 4.13, 4.14, 4.22 and 4.23, it can be shown that n' and K' can be determined as:

$$n' = \frac{b}{c} \qquad \textbf{Eq. 4.25}$$

and

$$K' = \frac{\sigma_f'}{(\epsilon_f')^{n'}} \qquad \textbf{Eq. 4.26}$$

However, in practice, three separate data fits for Eqs. 4.15, 4.22 and 4.23 are usually made, so that the mutual consistency of these six constants is often only approximate.

cyclic stress-strain relationship.

ii) For the next point on the load history, calculate the new notch stress and strain values by following the cyclic stress-strain curve and stopping when the nominal stress-local notch strain relationship is satisfied.

iii) Determine whether a hysteresis loop is closed by either Wetzel's counting method or rainflow method.

iv) For each closed hysteresis loop, calculate the corresponding cyclic life, N_f, from the strain-life relationship.

v) Sum the inverse of cyclic lives according to the Miner's rule.

vi) Then, the prediction of number of blocks to crack initiation is made as the inverse of the sum of damages accumulated for the block.

The differences between the methods arise mainly in 3 areas: The first is how to relate the load to the local stresses and strains, i.e. whether to use a load-strain calibration equation obtained experimentally or calculated by using a Finite Element analysis of the given specimen, Eq. 4.16, or to employ Neuber's rule to calculate the local stress and strain for a given load level, Eq. 4.20.

Once the local strain is calculated, the second area of differences is how to relate the local strain or stress to the life,

$2N_f$ in Eq. 4.24. The obvious choice is, a direct approach, to solve Eq. 4.24 in terms of $(2N_f)$ for a given local strain $\Delta\varepsilon$. Admittedly, due to the non-linear nature of Eq. 4.24, the life cannot be calculated directly, an iterative solution, for example Newton-Raphson method, is needed; despite this slight drawback, it is still surprising to note that this direct approach is rarely used in the life estimation methods published in the open literature. The most common way of calculating the life for a given strain is the method developed by Landgraf[15]. Once the local stress and strain are calculated, the partition of Eq. 4.15 is used to calculate the elastic and plastic components of the local strain:

$$\frac{\Delta\varepsilon_e}{2} = \frac{\Delta\sigma}{2E}$$

$$\frac{\Delta\varepsilon_p}{2} = \left(\frac{\Delta\sigma}{2K'}\right)^{1/n'}$$

The strain-life relationship of Eq. 4.24 is also partitioned for the elastic and plastic components of the local strain:

$$\frac{\Delta\varepsilon_e}{2} = \frac{\sigma_f'}{E}(2N_f)^b$$

$$\frac{\Delta\varepsilon_p}{2} = \varepsilon_f'(2N_f)^c$$

Then the ratio of plastic to elastic strain becomes:

$$\frac{\Delta\varepsilon_p}{\Delta\varepsilon_e} = \frac{\varepsilon_f' E}{\sigma_f'}(2N_f)^{c-b}$$

Or, in terms of damage per reversal:

$$\frac{1}{2N_f} = \left(\frac{\sigma_f'}{E\varepsilon_f'}\frac{\Delta\varepsilon_p}{\Delta\varepsilon_e}\right)^{\frac{-1}{c-b}} \qquad \textbf{Fig. 4.27}$$

Since the material properties and the elastic and plastic strains on

the right-hand side of Eq. 4.27 are all known, the damage per reversal can be calculated directly without resorting to iterative techniques.

Another common approach to solving the reciprocal life found in the literature makes use of the product of local stress and strain, ($\Delta\epsilon . \Delta\epsilon$). Since the elastic strain is directly proportional with the local stress, multiplying Eq. 4.23 with Eq. 4.24 yields:

$$\frac{\Delta\epsilon}{2} \cdot \frac{\Delta\epsilon}{2} = \frac{(\sigma_f')^2}{E} (2N_f)^{2b} + \sigma_f' \epsilon_f' (2N_f)^{c+b} \qquad \textbf{Eq. 4.28}$$

This form of life expression is particularly useful if Neuber's rule is to be used to determine the local stress and strain. Then there is no need to calculate the local stress and strain, because the left-hand side of Eq. 4.28 can be expressed in terms of the nominal stress, hence the load, directly, by making use of Eq. 4.20:

$$\left(\frac{\Delta S}{2} K_f\right)^2 \frac{1}{E} = \frac{(\sigma_f')^2}{E} (2N_f)^{2b} + \sigma_f' \epsilon_f' (2N_f)^{c+b} \qquad \textbf{Eq. 4.29}$$

Eq. 4.29 is then solved iteratively for reciprocal life to determine the damage per reversal, without actually determining the local stress and strain.

Going back to Eq. 4.27, the choice of the plastic to elastic strain ratio in terms of life seems somewhat arbitrary. It is equally

possible to write an equation for the product of the elastic and plastic strains in terms of life:

$$\frac{\Delta\epsilon_e}{2} \cdot \frac{\Delta\epsilon_p}{2} = \frac{\sigma_f'}{E} \epsilon_f' (2N_f)^{c+b}$$

$$\frac{1}{2N_f} = \left(\frac{E}{\sigma_f'\epsilon_f'} \frac{\Delta\epsilon_e}{2} \frac{\Delta\epsilon_p}{2}\right)^{\frac{-1}{c+b}} \qquad \text{Eq. 4.30}$$

Although the choice of the product of the elastic and plastic strains also seems arbitrary, there is some justification for this choice. If a cyclically loaded material exhibited a perfectly linear elastic relation between stress and strain, then there would be no energy conversion and the material would be resistant to fatigue failure. The energy necessary to cause fatigue failure is intimately related to hysteresis energy[16].

The area inside the hysteresis loop, A_H, shown in Fig. 4.6, is

$$A_H = \Delta\epsilon\,\Delta\sigma - 2\int_0^{\Delta\sigma}\left[\frac{\sigma}{E} + \left(\frac{\sigma}{K'}\right)^{1/n'}\right] d\sigma$$

Replacing $\Delta\epsilon$ by Eq. 4.15 and taking the integral:

$$A_H = \frac{1 - n'}{1 + n'} \Delta\sigma\left(\frac{\Delta\sigma}{K'}\right) 1/n'$$

or

$$A_H = \frac{1 - n'}{1 + n'} \quad E\,\Delta\epsilon_e\Delta\epsilon_p$$

Hence the area inside the hysteresis loop is directly proportional with the product of the elastic and plastic strain, and if the hysteresis energy is any measure of fatigue damage, then there is justification for using the product, $^{\Delta\epsilon}e^{\Delta\epsilon}p$, as a damage index.

In deriving the last three methods for calculating the life, there is an intrinsic assumption made, that the strain equations Eq. 4.15 and Eq. 4.24, governing the cyclic stress-strain relationship and the strain-life relationship respectively, can be separated into two parts for the elastic and plastic strain, and that the corresponding parts are equal:

$$\frac{\Delta\epsilon_e}{2} = \frac{\Delta\sigma}{2E} = \frac{\sigma_f'}{E}(2N_f)^b$$

$$\frac{\Delta\epsilon_p}{2} = \left(\frac{\Delta\sigma}{2K'}\right)^{1/n'} = \epsilon_f'(2N_f)^c$$

If indeed this is the case, then there is no need to use any product or ratio terms, the reciprocal of life can be calculated simply as:

$$\frac{1}{2N_f} = \left(\frac{E}{\sigma_f'}\frac{\Delta\epsilon_e}{2}\right)^{-1/b} \qquad \textbf{4.31}$$

$$\frac{1}{2N_f} = \left(\frac{1}{\epsilon_f'}\frac{\Delta\epsilon_p}{2}\right)^{-1/c} \qquad \textbf{4.32}$$

This assumption also necessitates that there should be only 4 independent material constants, not 6 as Eq. 4.15 and Eq. 4.24 suggest. K' and n' can then be expressed in terms of σ_f', ϵ_f', b, and c

$$K' = \frac{\sigma_f'}{(\epsilon_f')^{b/c}}$$

and

$$n' = \frac{b}{c}$$

Another corollary for this assumption is that all the 6 equations, Eq. 4.24, 27, 29, 3Ø, 31 and 32, for the reciprocal life should give one and the same result. However, in practice, three separate data fits are usually made, one for the cyclic stress-strain data to determine K' and n', one for plastic strain-life for $^{\varepsilon}{}_{f}'$ and c, and another for elastic strain-life for $^{\sigma}{}_{f}'$ and b. Hence the mutual consistency of these 6 constants is often only approximate, and the 6 equations for the calculation of the reciprocal life may give different results.

The third area of differences between various fatigue damage estimation methods, a controversial area, is how to account for mean stress effects. It is well established that mean tensile stresses have a detrimental effect on the overall fatigue life of components, and mean compressive stresses have a beneficial effect. The controversy is about dividing the effect of mean stresses into the crack initiation and crack propagation stages.[17]. However constant amplitude test results on laboratory test specimens have resulted in several empirical relationships[18, 19, 2Ø].

A commonly used mean stress correction is due to Morrow[18].

$$\frac{\Delta\varepsilon_{eff}}{2} = \frac{\Delta\sigma/2}{1 - \sigma_m/\sigma_f'} \qquad \textbf{Eq. 4.33}$$

where $\Delta\sigma_{eff}/2$ is effective local stress amplitude expected to cause damage in the same number of cycles as the actual combination of mean and amplitude, σ_m and $\Delta\sigma/2$. Then the strain-life relationship becomes:

$$\frac{\Delta\varepsilon}{2} = \frac{\sigma_{f'} - \sigma_m}{E} (2N_f)^b + \varepsilon_{f'}(2N_f)^c \qquad \textbf{Eq. 4.34}$$

Another mean stress correction in regular use is the Smith-Watson Topper parameter[19]:

$$\frac{\Delta\sigma_{eff}}{2} = \sqrt{\frac{\Delta\sigma}{2}\left(\frac{\Delta\sigma}{2} + \sigma_m\right)} \qquad \textbf{Eq. 4.35}$$

A common use of this correction is a modification of Eq. 4.28. Since $\Delta\sigma/2$ is the amplitude and σ_m is the mean of the local stress, the sum gives the peak stress on the maximum stress, σ_{max}, for a given hysteresis loop. Then the Eq. 4.28 becomes:

$$\sigma_{max}\frac{\Delta\varepsilon}{2} = \frac{(\sigma_{f'})^2}{E}(2N_f)^{2b} + \sigma_{f'}\varepsilon_{f'}(2N_f)^{c+b} \qquad \textbf{Eq. 4.36}$$

4.4 Discussion

With 2 ways of calculating the local stress and strain for a given load, and 6 ways of determining the life for the local stress, and/or strain, and 3 ways - one without the mean - of incorporating the mean stress effects, the choices are quite numerous. Considering that there are also at least 3 ways of cycle counting in regular use, Range-Pair, Wetzel's and Rainflow methods, the number of combinations of these options would be awesomely too many to an initiate in the area of the local stress-strain approach to the fatigue damage calculations.

However, the situation is not as complicated as it looks. To start with, there are not 3 choices for the cycle counting. As

demonstrated in Chapter 2, as far as identifying and extracting closed stress-strain hysteresis loops is concerned, all the 3 methods give identical results, provided that the repeating history starts at the most extreme point. If a mean stress correction is required, then extracting the closed loops from the load history would not be enough, because for the mean stress correction, the amplitude, and the mean or the maximum point of the local stress are required, not of the load. Hence the exact location of the local stress displacement is needed, not just its amplitude. Although the closed loops extracted from the load history are linked one-to-one with the local hysteresis loops, and the amplitudes of local stress and strain can be directly calculated from the load, however in order to find the mean local stress, the tips of the local stress-strain hysteresis loops must be at all times defined. Therefore a cycle counting method which can extract closed loops in sequence is needed. The range-pair method, as in its presented form in Chapter 2, is incapable of doing so. Both Wetzel's method and the third version, the pattern classification, of rainflow do extract closed loops in sequence and keep up with the 'memory effects' of materials. Since discrete elements are used in Wetzel's method, some rounding errors necessarily occur. They can be minimized by using more elements at the expense of computer storage and execution time. Hence to extract closed-loop cycles for crack initiation life calculations, the pattern classifying rainflow method is recommended for its simplicity, efficiency and ease of use.

Secondly, there is an apparent paradox in that there are 6 different ways of relating the local strain and/or stress to the life,

$2N_f$. If the assumption made in deriving the 6 equations, Eq. 4.24, 27, 29, 3Ø, 31 and 32, is correct, i.e. that the elastic and plastic strain parts of the cyclic stress-strain relationship and the strain-life relationship, Eq. 4.15 and 4.24 respectively, can be separated and are equal, then all 6 equations must give the same result, <u>any</u> one of them may be used. If the assumption is not correct, then there cannot be 6 different equations. In this case, only the strain-life relationship, Eq. 4.24, can be used. The reason for this apparent paradox is that the cyclic stress-strain relationship and the strain-life relationship are <u>not</u> laws of nature, both of them, as the name implies, are relationships which explain a set of experimental results best. The material properties determined from data fits are not constants, they are average values which reflect the change in the material properties during a cyclic loading. Therefore the mutual consistency of the material properties is only approximate. If, at the end of data fits to experimental results, Eq. 4.25 and 4.26 hold, i.e. the two parameters can be expressed in terms of the other four, then all the 6 equations for the life are valid, but they all give the same result, so any one of them may be employed. If the values of n' and K' determined from the local stress-strain data fit are considerably different than the values calculated from σ_f', b, ε_f', and c, then the validity of the assumption is questionable, so is the validity of 6 different equations which are based on this assumption. Therefore, the original strain-life relationship, Eq. 4.24 should be used in this case, because it is the result of a direct fit to the experimental data, there is no equation manipulation involved causing extra uncertainties.

Dowling et al[20] single out the cyclic stress-strain curve as the most important concept in the local strain approach for making life estimates. However, if the mean stress correction is not required, or considered to be negligible, and if the applied load-local strain calibration curve is available, then the cyclic stress-strain curve is not necessary for making life estimates, the life can be directly calculated from the strain-life relationship. If the load-strain curve is not available, then the Neuber's rule must be used to find the local stress and strain for a given load, then the cyclic stress-strain curve becomes necessary and important. There are several ways of obtaining the cyclic stress-strain curves of metals[7]. If the curve as a result of a constant amplitude controlled strain test is available, then this should be preferred, because the same strain values are used to determine the strain-life curve. Then the stress-strain and strain-life curves are directly linked by using the same strain values.

If rainflow is used as the cycle counting, and the strain-life relationship in its original form without any manipulation is used to link the local strain to the life, then the number of choices to calculate fatigue life estimates is considerably reduced. The options left are which nominal stress-local notch strain relationship to use, and whether to include the mean stress corrections or not. If the load-strain calibration curve is not available, then one is left with the Neuber's rule. If it is available, then both methods may be used for comparison purposes. The same argument goes for the choice of the mean stress correction. Life estimates with and without the mean

stress correction can be made to establish the importance of the mean stress effect for the particular situation of interest. Considering that the two equations, Eq. 4.34 and 4.35, for the mean stress correction are empirical relations to explain certain experiments, the validity and compatibility of these equations should be checked for the material type, specimen geometry and the loading type under consideration.

So far, all the comments made, the conclusions drawn are based on the basic equations and their manipulations. In the next chapter some numerical examples are given. In order to put the subsequent discussion in proper perspective, the life estimations are made with the well-documented, extensive test data[21], on which a considerable number of fatigue life estimates are based[22]. The purpose of the following exercise is not to produce yet another set of predictions, but rather to highlight the points discussed in this chapter. Particular attention will be paid to the influence of the material fatigue properties on the crack-initiation life estimates.

REFERENCES FOR CHAPTER 4

1. Fuchs, H. O., Stephens, R. I., "Metal Fatigue in Engineering", J. Wiley and Sons, New York 1980.

2. Dowling, N. E., "Notched Member Fatigue Life Predictions Combining Crack Initiation and Propagation", Fatigue of Engineering Materials and Structures, Vol. 2, pp 129-138, 1979.

3. Frost, N. E., Marsh, K. J., Pook, L. P., "Metal Fatigue", Oxford University Press, 1974.

4. Haibach, E., "Fatigue Data for Design Applications", Proc. of Fatigue '81 SEE Conf. held at Warwick University, England, March 1981.

5. Osgood, C. C. "Fatigue Design", Pergamon Press, Second Edition, 1982.

6. Nelson, D. V., Fuchs, H. O., " Predictions of Cumulative Damage Using Condensed Load Histories", SAE Paper No: 750045.

7. Landgraf, R. W., Morrow, J., Endo, T., "Determination of the Cyclic Stress-Strain Curve", JMLSA, Vol. 4, No. 1, March 1969.

8. Dowling, N. E., "Fatigue Failure Predictions for Complicated Stress-Strain Histories", Journal of Materials, JMLSA, Vol. 7, No. 1, March 1972.

9. Wetzel, R. M., "A Method of Fatigue Damage Analysis", Ph.D. Thesis, Waterloo University, Canada, 1971.

10. Martin, J. F., Topper, T. H., Sinclair, G. M., "Computer Based Simulation of Cyclic Stress-Strain Behaviour with applications to Fatigue", Materials Research and Standards, MTRSA, Vol. 11, No. 2.

11. Barron, G. E., "A Finite Element and Cumulative Damage Analysis of a Keyhole Test Specimen", SAE Paper 750041.

12. Landgraf, R. W., Richards, F. D., LaPointe, N. R., "Fatigue Life Predictions for a Notched Member Under Complex Load Histories", SAE Paper 750040.

13. Conle, A., Nowack, H., "Verification of a Neuber-based Notch Analysis by the Companion-Specimen Method", Experimental Mechanics, Feb. 1977.

14. Peterson, R. E., "Analytic Approach to Stress Concentration Effect in Fatigue of Aircraft Materials". Proc. of the Symposium on Fatigue of Aircraft Structures, pp. 273-279 WADC Technical Report 59-507, August 1959.

15. Landgraf, R. W., "Cumulative Fatigue Damage Under Complex Strain Histories", ASTM STP 519, 1973.

16. Feltner, C. E., Morrow, J. D., "Microplastic Strain Hysteresis Energy as a Criterion for Fatigue Fracture", Journal of Basic Engineering, Trans. of ASME, March 1961.

17. Sherratt, F., Eaton, D., "Fatigue Life Estimation by Local Stress'Strain Methods", Journal of Soc. of Environmental Engineers, Sept. 1983.

18. Morrow, J., "Fatigue Properties of Metals", Fatigue Design Handbook, SAE, 1968.

19. Smith, K. N., Watson, P., and Topper, T. H., "A Stress-Strain Function for the Fatigue of Metals", Journal of Materials, ASTM, Vol. 5, No. 4, Dec. 1970.

20. Dowling, N. E., Brose, W. R. Wilson, W. K., "Notched Member Fatigue Life Predictions by Local Strain Approach", Paper presented at SAE Automotive Engineering Congress and Exposition, Detroit, Feb. 1975.

21. Tucker, L., Bussa, S., "The SAE Cumulative Damage Test Program", SAE Paper 750038.

22. "Fatigue Under Complex Loading: Analyses and Experiments", Editor: Wetzel, R. M., SAE publication, 1977.

CHAPTER 5

A SENSITIVITY ANALYSIS OF FATIGUE DAMAGE CALCULATIONS

5.1 Introduction

The fatigue life predictions made in this chapter are based on the results of the extensive research coordinated by the Society of Automotive Engineers (SAE) Fatigue Design and Evaluation Committee. Three different types of load histories were applied to notched test specimens, machined from two steels, Man-Ten and RQC-100. Tests were conducted at several load levels for each history. The load spectra consist of a Transmission history, 1705 reversals long, mainly tensile, a combination of variable excitation with many large excursions from the mean; a Suspension history, 2506 reversals, mainly compressive, a combination of random excitation with occasional large excursions from the mean; and a Bracket history, 5936 reversals, with near zero mean, approximately narrow-band type vibration. A complete description of the test programme is found in Ref.[1].

The aim of the following life predictions is not to produce 'better' life estimates for the test results, it is to gain insight into the potential variability of prediction methods, to highlight the significance, utility and implication of various alternatives. Predictions based on a load-life curve and nominal stresses will be discussed first. Then the three areas where the local strain approaches differ, as discussed in Chapter 4.3, will be investigated

numerically, with a particular emphasis on the way in which the local stress and strain is linked to the life. The question of how sensitive the prediction methods might be to variations in cyclic properties will also be evaluated.

TABLE 5.1

'Old' and 'New' Sets of Material Properties

for MAN-TEN and RQC-100

	Property	MAN-TEN		RQC-100	
		Old	New	Old	New
	Cyclic stress-strain relationship				
E	Elastic modulus, ksi	29500	29500	29500	29500
K'	Cyclic strength coef. ksi	173.	160.	201.	167.
n'	Cyclic strain hrd. expn.	.168	.193	.148	.100
	Load-strain calibration				
c_1	, kips	-	1410.	-	1410.
c_2	, kips	-	66.7	-	65.5
d			.39	-	.31
	Strain-life relationship				
σ_f'	Cyclic fatigue strength coef.ksi.	170.	133.	167.	168.
b	Cyclic fatigue strength expn.	-0.12	-0.095	-0.073	-0.075
ε_f'	Cyclic fatigue ductility coef.	0.90	0.26	0.62	1.06
c	Cyclic fatigue ductility expn.	-0.60	-0.47	-0.67	-0.75
	The SAE notched specimen				
K_f	Fatigue notch factor	-	2.88	-	2.88
	Load-life relationship				
w	Notched specimen load coef., kips	-	83.4	-	101.4
z	Notched specimen load expn.	-	.23	-	.23

5.2 Load-Life Estimations:

The same SAE report[1] also includes constant amplitude load versus cycles to crack initiation data for the SAE notched specimen. Straight lines, on a log-log scale, are fitted to these data which have the form:

$$\frac{\Delta P}{2} = w(2N_f)^z \qquad \textbf{Eq. 5.1}$$

where $\Delta P/2$ is the load amplitude, and w and z are fitting constants. The values for w and z are listed in Table 5.1 alongside with the other material fatigue properties of the two steels.

A simple, the simplest of all, life calculation was made with these load-life data fits. Cycles were extracted by a direct application of rainflow to the load histories; the life, $2N_f$, for each load range, ΔP, was calculated from Eq. 5.1, and the reciprocal lives were added linearly according to Miner's rule to obtain the 'damage per block', for one block of a load history. Finally, the reciprocal of this quantity was used as the life estimate, in terms of 'number of blocks to crack initiation'.

The calculated fatigue lives which resulted are summarized in Table 5.2 alongside with the experimental lives from Ref.[1]. The predicted lives are compared in Fig. 5.1 with the experimental data. The solid line in Fig. 5.1, and in the following similar plots, represent perfect agreement between predicted and experimental lives, the dashed lines represent a factor-of-three scatter band. Points

Table 5.2.

Variable Amplitude Fatigue Life Estimations
Load-Life and Nominal Stress Methods

Material : MAN-TEN

Load (Kips)	Exprm. life (blocks)	Predicted Lives L-L	NS-1	NS-2	NS-3
Transmission					
16.0	8.4				
16.0	12.5	11.7	0.7	12.1	3.8
16.0	12.8				
8.0	74.0				
8.0	154.0	261.9	35.0	184.9	97.3
8.0	420.0				
3.5	3755.0				
3.5	4270.0	10667	3996	4789	4609
3.5	5800.0				
Suspension					
16.0	-				
16.0	7.7	36.7	2.6	32.2	12.6
16.0	28.0				
9.0	162.0				
9.0	208.0	484.0	70.5	310.2	184.0
9.0	430.0				
6.0	1410.0				
6.0	1750.0	2982	720	1530	1220
6.0	2240.0				
Bracket					
16.0	1.5				
16.0	2.0	1.6	0.1	1.6	0.5
16.0	2.6				
8.0	11.5				
8.0	20.8	35.7	5.2	24.3	13.4
8.0	23.0				
3.5	270.0				
3.5	510.0	1454	597	630	637
3.5	1588.0				

Table 5.2. (cont.)

Variable Amplitude Fatigue Life Estimations
Load-Life and Nominal Stress Methods

Material : RQC-100

Load (Kips)	Exprm. life (blocks)	Predicted Lives L-L	NS-1	NS-2	NS-3
Transmission					
16.0	22.2				
16.0	23.5	52.7	5.1	63.4	24.1
16.0	29.9				
8.0	269.0				
8.0	374.0	1428.8	448.6	1225.5	854.7
8.0	460.0				
3.5	57000				
3.5	88000	73216	94459	41907	60218
3.5	88000				
Suspension					
16.0	19.9				
16.0	24.4	176.3	21.7	187.7	87.1
16.0	64.0				
9.0	-				
9.0	1710	2730	890	2193	1684
9.0	-				
6.0	-				
6.0	48000	18820	12395	12401	13575
6.0	-				
Bracket					
16.0	3.3				
16.0	4.2	7.3	0.8	8.5	3.5
16.0	5.1				
8.0	47.0				
8.0	87.5	198.9	70.0	164.5	122.5
8.0	113.0				
3.5	2673				
3.5	2673	10190	14739	5626	8632
3.5	5020				

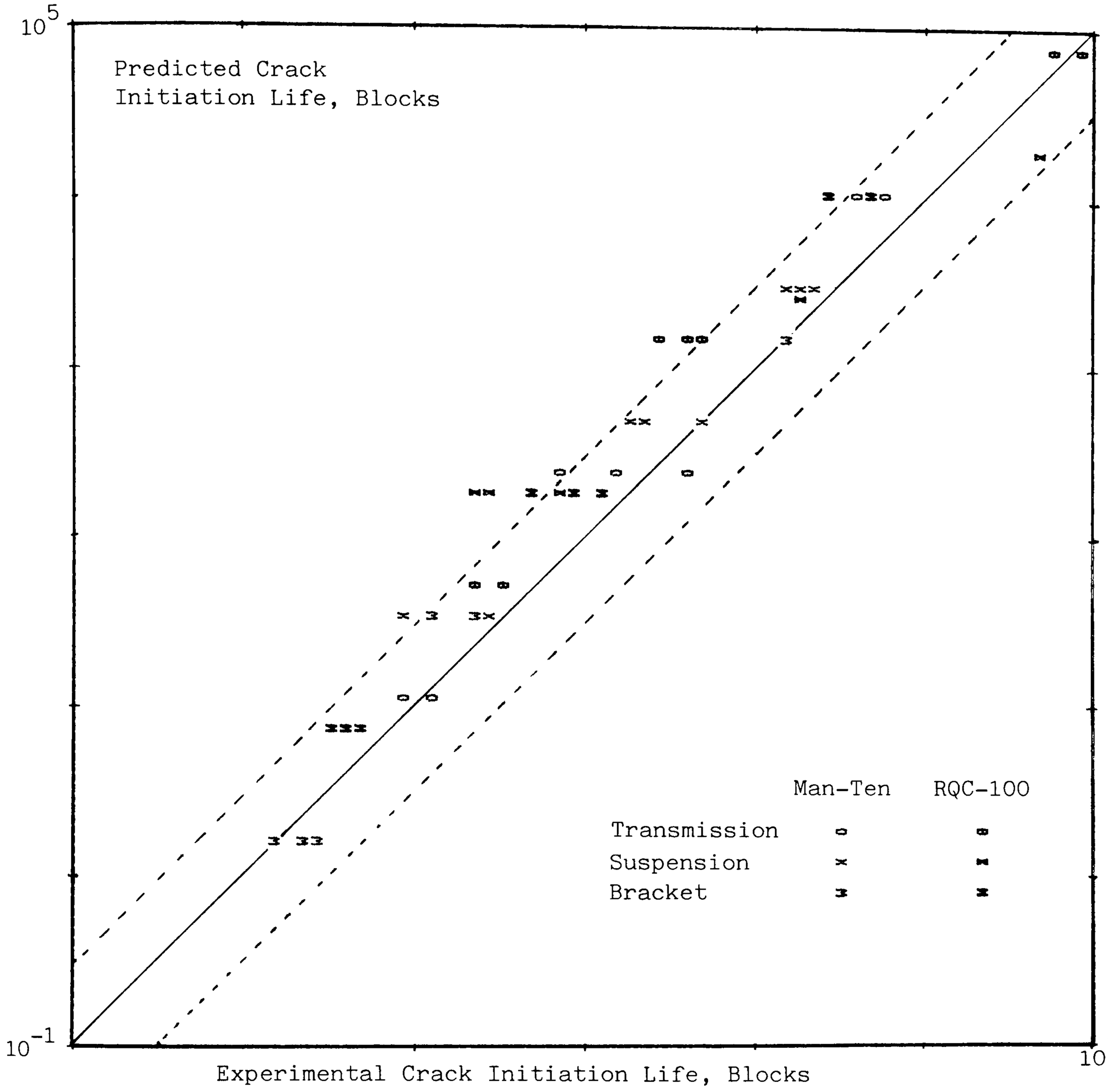

Fig. 5.1. Life calculations based on constant amplitude load-life data for the notched SAE spectrum

falling below the solid line indicate a conservative estimate, and those above a non-conservative estimate.

Reasonable results are obtained by this method, with the calculations tending to be non-conservative, particularly for RQC-100 at intermediate lives. However, most of the predictions are within the factor-of-three scatter band. Obviously, life calculations based on load do not have the capability of handling local mean stress effects because there is no notch analysis, leading to the determination of local stress and strain, involved in this method. However, the same deficiency of the load-life method, i.e. that there is no local stress-strain analysis, is also its strength. The load-life data is determined from the tests where the actual component itself is being tested. Manufacturing variables such as surface finish and residual stresses are accounted for in the test data. In life calculations, no assumption other than Miner's liner damage rule and rainflow counting is made. Thus, the reasonable success of calculations just made was possible not only because the mean stress effects were unimportant in the SAE tests, but also because the life was directly linked to the load that the component itself experiences.

5.3 Nominal Stress Methods

Nominal stress methods are discussed in Chapter 4.1. Life calculations based on these methods were made. Rainflow counted load ranges were converted to nominal stress ranges at the notch root by multiplying the applied load by a constant. This assumes that nominal stresses are always elastic. Damage for each stress range was

calculated from a notched S/N curve estimated from smooth σ-N data. The foll owing life expressions were used in these calculations:

Method 1

$$\frac{\Delta S}{2\sigma_f'} = (2N_f)^q \qquad \textbf{Eq. 5.2}$$

where

$$q = b - \frac{\log K_f}{6}$$

Method 2

$$\frac{1}{K_f}\frac{\Delta S}{2\sigma_f'} = (2N_f)^p \qquad \textbf{Eq. 5.3}$$

where

$$p = b - \frac{\log K_f}{3}$$

Method 3

$$\frac{1}{\sqrt{K_f}}\frac{\Delta S}{2\sigma_f'} = (2N_f)^r \qquad \textbf{Eq. 5.4}$$

$$r = b - \frac{\log K_f}{4}$$

Damage was summed as the inverse of $2N_f$ for each stress range ΔS in a given load block.

The estimated fatigue lives by these methods are summarized in Table 5.2 and plotted in Fig. 5.2, 3 and 4. Nominal Stress Method 1 overestimates the damage for short and intermediate lives, particularly for Man-Ten. It calculates as much as an order of magnitude too much damage for Man-Ten at the highest load levels for all the three histories. Nominal Stress Method 2 corrects the tendency of the Method 1 to be overly conservative at short and intermediate lives. For all the three histories and both metals, virtually all the predictions are within the factor-of-three scatter band, with the predictions tending

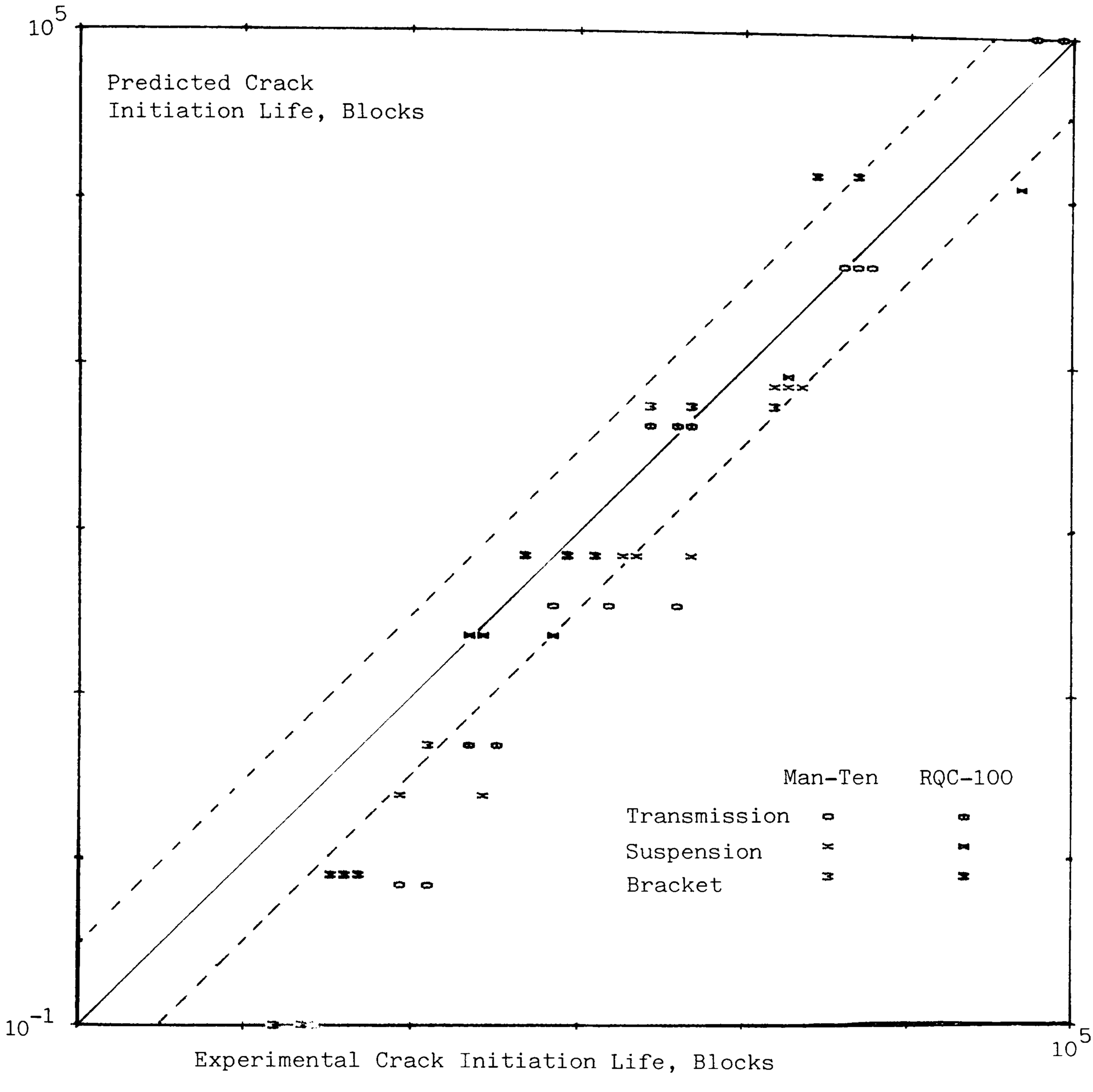

Fig. 5.2. Life calculations based on Nominal Stress 1

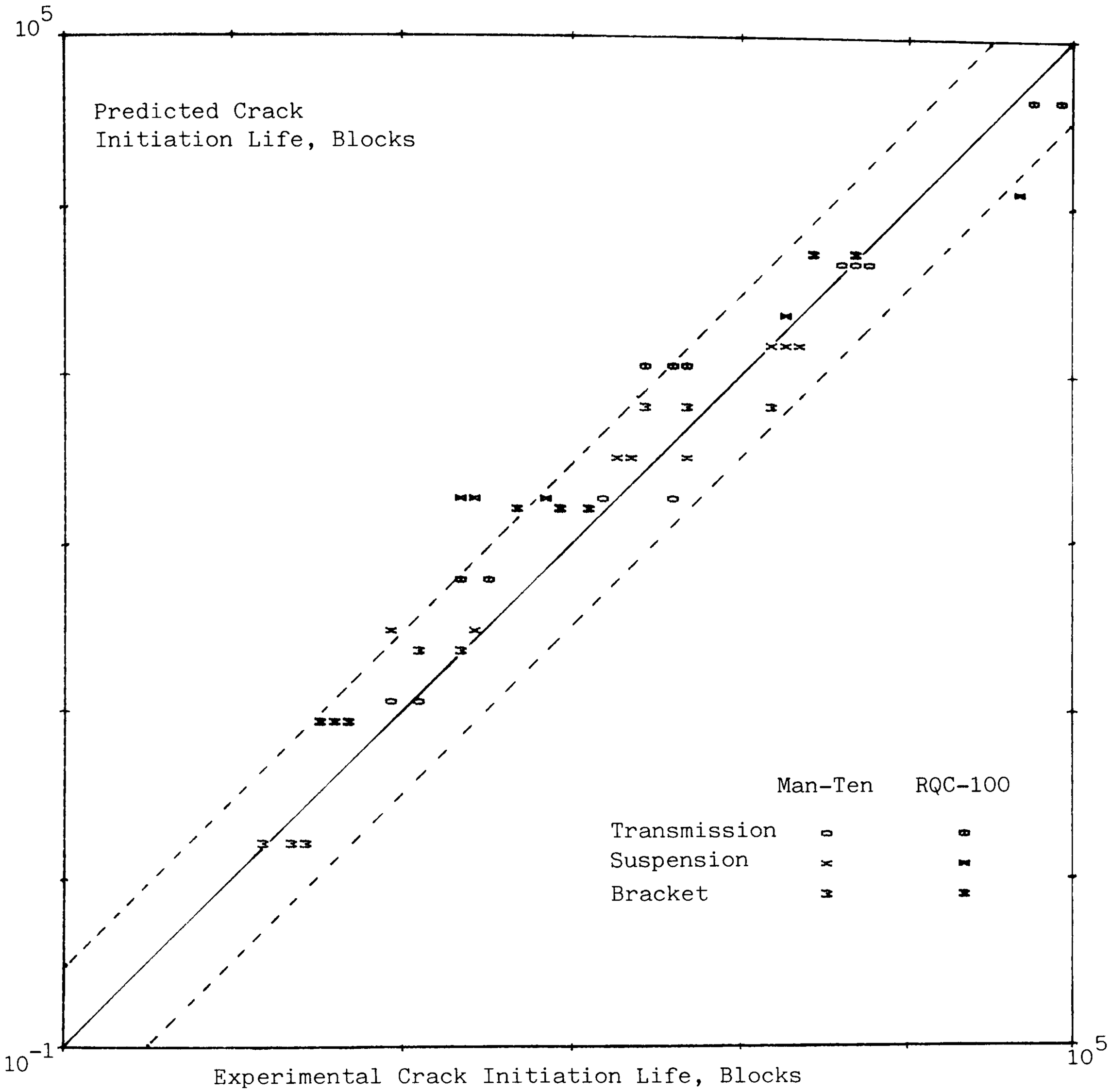

Fig. 5.3. Life calculations based on Nominal Stress 2

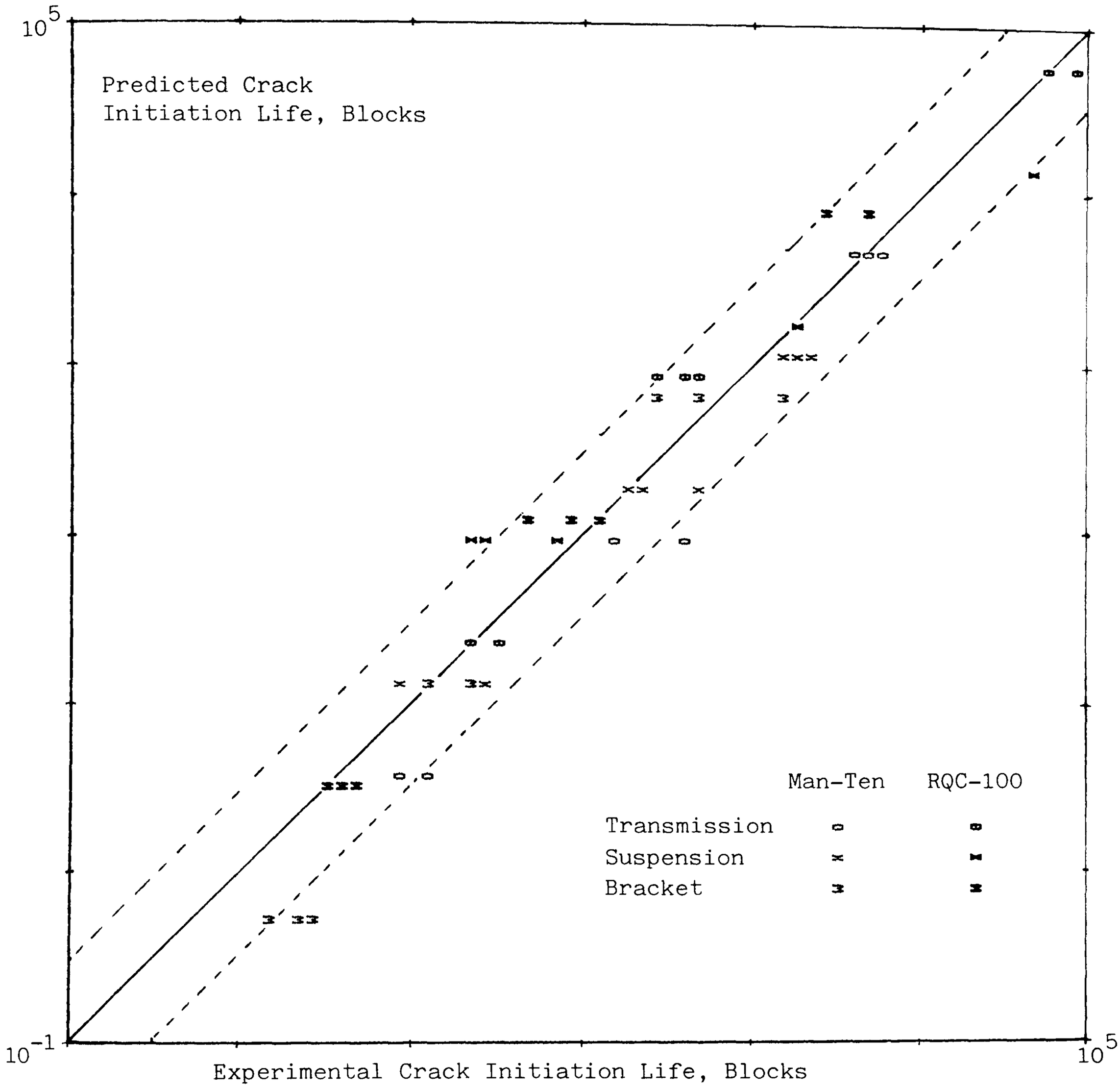

Fig. 5.4. Life calculations based on Nominal Stress 3

to be slightly non-conservative for RQC-100. The results predicted by Nominal Stress Method 3 are between the values predicted by Methods 1 and 2 at each load level, as expected. Again almost all the predictions are within the scatter band, this time with slightly conservative predictions for Man-Ten.

As in the load-life method, Nominal Stress Methods are incapable of accounting for the mean stress effects since no local stress at the notch root is calculated. Even if it were possible to account for the mean stresses, the effect would probably be far less significant than the effect of the choice of approximation to the notched S/N data from the smooth σ-N data.

5.4 Local Stress-Strain Methods:

In order to highlight the advantages and usefulness of the local strain approach, and identify the possible sources of error, the three areas, discussed in Chapter 4.3, where the local strain approaches differ are examined separately. The three areas are, (a) the way in which the local stress and/or strain is linked to the life, (b) the way in which the local strain is determined for a given load level, and (c) the way in which the mean stress effect is accounted for.

Assume that the local stress and strain are known, $\Delta\varepsilon$, $\Delta\varepsilon$, and that the elastic and plastic parts of the local strain can be separated and calculated, $\Delta\varepsilon_e$, $\Delta\varepsilon_p$. Then the 6 ways of relating the local

stress and/or strain to the life are:

Method 1:

$$\frac{\Delta\epsilon}{2} = \frac{\sigma_f'}{E}(2N_f)^b + \epsilon_f'(2N_f)^c \qquad \textbf{Eq. 5.5.}$$

Solve the strain-life relationship iteratively for the reciprocal life.

Method 2:

$$\frac{1}{2N_f} = \left(\frac{\sigma_f'}{E\epsilon_f'}\frac{\Delta\epsilon_p}{\Delta\epsilon_e}\right) - \frac{1}{c-b} \qquad \textbf{Eq. 5.6}$$

Method 3:

$$\frac{1}{2N_f} = \left(\frac{E}{\sigma_f'\epsilon_f'}\frac{\Delta\epsilon_p}{2}\frac{\Delta\epsilon_e}{2}\right) - \frac{1}{c+b} \qquad \textbf{Eq. 5.7}$$

Method 4:

$$\frac{\Delta\sigma}{2}\frac{\Delta\epsilon}{2} = \frac{(\sigma_f')^2}{E}(2N_f)^{2b} + \sigma_f'\epsilon_f'(2N_f)^{c+b} \qquad \textbf{Eq. 5.8}$$

Solve Eq. 5.8 iteratively for the reciprocal life.

Method 5:

$$\frac{1}{2N_f} = \left(\frac{E}{\sigma_f'}\frac{\Delta\epsilon_e}{2}\right) - \frac{1}{b} \qquad \textbf{Eq. 5.9}$$

Method 6:

$$\frac{1}{2N_f} = \left(\frac{1}{\epsilon_f'}\frac{\Delta\epsilon_p}{2}\right) - \frac{1}{c} \qquad \textbf{Eq. 5.10}$$

5.4.1 Load-Strain Analysis:

As a first step towards examining the relevant importance of each area where the local strain approaches differ, the mean stress effect was disregarded, the local strain for each load range was calculated from the load-strain calibration curve, and the corresponding damage for each local strain range was calculated by the

6 methods above. The load-strain calibration curve is given in the following form:

$$\frac{\Delta\varepsilon}{2} = \frac{\Delta P}{2c_1} + \left(\frac{\Delta P}{2c_2}\right)^{1/d} \qquad \textbf{Eq. 5.11}$$

where $\Delta\varepsilon/2$ and $\Delta P/2$ are the local strain and applied load amplitudes respectively, and c_1, c_2 and d are fitting constants.

Since the effect of mean stresses was neglected, there was no need to calculate the exact locations of cyclic stress-strain hysteresis loops, only the amplitudes of local stress and strain were necessary and sufficient. There, load ranges corresponding to closed hysteresis loops were extracted by applying rainflow to the load histories and the local strain range for each load range was calculated from Eq. 5.11. Once the local strain range was determined, the local stress was calculated from the cyclic stress-strain curve:

$$\frac{\Delta\varepsilon}{2} = \frac{\Delta\sigma}{2E} + \left(\frac{\Delta\sigma}{2K'}\right)^{1/n'} \qquad \textbf{Eq. 5.12}$$

For a given $\Delta\varepsilon$, Eq. 5.12 was solved iteratively for $\Delta\sigma$. Then the elastic and plastic parts of the local strain were assumed to be:

$$\frac{\Delta\varepsilon_e}{2} = \frac{\Delta\sigma}{2E} \qquad \textbf{Eq. 5.13}$$

and

$$\frac{\Delta\varepsilon_p}{2} = \left(\frac{\Delta\sigma}{2K'}\right)^{1/n'} \qquad \textbf{Eq. 5.14}$$

Finally, the corresponding damages were evaluated by each method with their respective equations, Eq. 5.5 to Eq. 5.10, and the damage terms summed according to Miner's rule.

The values of the constants for Eq. 5.11, and also the fatigue

and cyclic stress-strain constants needed for Eq. 5.12 and Eq. 5.5 were obtained from Refs.[1] and [2]. These values are listed in Table 5.1. "New" material properties were used in the life calculations in this section. The calculated fatigue lives are listed in Table 5.3.

The predicted lives are not going to be compared with the experimental lives at this stage, instead the lives predicted by the 6 methods for each load level, history and material are compared with each other. An examination of values in Table 5.3 row by row, i.e. the comparison of the life calculations for the same load level, history and material show that all the 6 methods calculate practically the same life, particularly for RQC-100. The predictions made by the 6 methods for RQC-100 are all within less than 1% of each other. Although not very significant in terms of fatigue calculations, there are noticeable differences in the life predictions made for Man-Ten. The largest difference is between Methods 2 and 5 at short lives. Method 2 overestimates the damage, 1.5 times as much, compared to Method 5, at short lives. At long lives, the roles are reversed, Method 5 overestimates the damage compared to Method 2, with much reduced ratio. The lives calculated by the other 4 methods are very close, all within 5% of each other.

As stated in Chap. 4.3, if the assumptions made in obtaining the 6 equations for life are correct, i.e. the elastic and plastic parts of the stress-strain and strain-life relationships can be separated and that the corresponding parts are equal, then there must be only 4 independent material constants, not 6 as the stress-strain

and strain-life relationships suggest, K' and n' can then be expressed in terms of σ_f', ε_f', b, and c. Furthermore, then all the predictions by the 6 methods must give one and the same result. Cyclic stress-strain properties calculated from cyclic fatigue properties are:

$$n' = \frac{b}{c} \text{ and } K' = \frac{\sigma_f'}{(\varepsilon_f')^{b/c}}$$

for Man-Ten

$$n' = \frac{-0.085}{-0.47} = 0.202$$

$$K' = \frac{133.}{0.26^{0.202}} = 174.63$$

for RQC-100

$$n' = \frac{-0.075}{-0.75} = 0.100$$

$$K' = \frac{168.}{1.06^{0.1}} = 167.02$$

Calculated values of K' and n' for RQC-100 are practically the same as the values listed in Table 5.1 and the life predictions for RQC-100by the 6 methods are practically the same, as expected. Calculated values of K' and n' for Man-Ten are slightly but noticeably different than the values listed in Table 5.1, 174. against 160., and 0.202 against 0.193, and the life predictions for Man-Ten by the 6 methods using the values in Table 5.1 reflect these differences. The lives for the same load level and history are close but not the same, the differences being more noticeable at short lives where the life is largely dictated by the plastic strain, where K' and n' become dominant in determining the total strain.

5.4.2 Neuber's Analysis

The next step in the evaluation of local strain methods was to use Neuber's notch analysis to calculate the local stress and strain for a given load level. This was done in order to highlight the difference between the two notch analysis methods. As in the previous calculations, the effect of mean stresses was ignored. Rainflow counted load ranges were converted to the nominal stresses by multiplying the applied load by a constant, assuming nominal elasticity. The local stress and strain at the notch root are related to the nominal stress by Neuber's rule:

$$\frac{\Delta\sigma}{2}\,\frac{\Delta\epsilon}{2} = \frac{1}{E}\left(K_f\,\frac{\Delta S}{2}\right)^2 \qquad \textbf{Eq. 5.15}$$

A fatigue notch factor, K_f, the value of which is listed in Table 5.1, was used in place of the stress concentration factor, K_t. Replacing $\Delta\epsilon/2$ in Eq. 5.15 by Eq. 5.12 gives:

$$\frac{1}{E}\left(K_f\,\frac{\Delta S}{2}\right)^2 = \frac{\Delta\sigma}{2}\,\frac{\Delta\sigma}{2E} + \left(\frac{\Delta\sigma}{2K'}\right)^{1/n'} \qquad \textbf{Eq. 5.16}$$

Eq. 5.16 was solved iteratively for the local stress, $\Delta\sigma$, for each nominal stress range, ΔS, calculated from rainflow counted load range. Once the local stress was determined, the elastic and plastic strains were calculated, using Eq. 5.13 and 14. Then the reciprocal lives were calculated by the 6 methods using their respective equations, Eq. 5.5 to Eq. 5.10 and the damage terms added linearly.

The predicted lives, using the 'new' material properties, are listed in Table 5.4. Naturally, the same trend is observed, with

regard to evaluating the damage by different methods. Life predictions for RQC-100 by the 6 methods are practically the same, while predictions for Man-Ten differ slightly but noticeably, particularly at short lives, for the same load level and history.

A comparison of Table 5.3 with 5.4 show the effect of calculating the local strain by the two notch analysis methods. Lives calculated using the load-strain curves are approximately twice longer than the lives obtained from Neuber's rule at short lives. In other words, Neuber's rule is a factor of 2 more conservative than the corresponding load-strain analysis at short lives. At intermediate lives, Neuber's rule is still more conservative, but with a reduced factor. At long lives both analyses predict almost the same result, Neuber's rule tending to be less conservative than the load-strain calibration curve.

The load-strain calibration curves, used to obtain the prediction in Table 5.3, are the results of experimental data[3] for the specimen tested. Another load-strain curve can be obtained directly from Neuber's rule. At a given load, Eq. 5.16 is solved iteratively for the local stress, and the local strain is found from Eq. 5.12. Experimental and Neuber's rule load-strain calibration curves for both materials are compared in Fig. 5.5. Then the above observation becomes obvious for, simply, Neuber's rule overestimates the local strain for the specimen and materials used in the SAE test programme.

Table 5.3.

Variable Amplitude Fatigue Life Estimations

Load-Strain Analysis, 'New' Material Properties

Load (kips)	M-1	M-2	M-3	M-4	M-6	M-6
			Material : MAN-TEN			
Transmission						
16.0	11.3	10.3	11.7	11.9	15.0	11.1
8.0	241.2	229.7	243.1	247.9	271.2	237.7
3.5	17624	16914	18159	17296	16720	18458
Suspension						
16.0	35.4	32.9	36.4	37.0	44.0	35.0
9.0	496.5	477.4	502.5	508.6	552.7	492.5
6.0	3578	3554	3603	3603	3688	3584
Bracket						
16.0	1.5	1.4	1.5	1.6	2.0	1.5
8.0	32.7	31.5	32.9	33.5	35.9	32.3
3.5	2897	3175	3026	2838	2742	3085
			Material : RQC-100			
Transmission						
16.0	14.4	14.4	14.4	14.4	14.5	14.4
8.0	261.7	261.5	261.6	261.8	262.1	261.6
3.5	704754	703323	703598	704795	704828	703472
Suspension						
16.0	46.0	46.0	46.0	46.0	46.1	46.0
9.0	588.3	587.8	588.0	588.5	589.0	587.9
6.0	9868	9855	9859	9871	9877	9858
Bracket						
16.0	1.7	1.7	1.7	1.7	1.7	1.7
8.0	44.6	44.6	44.6	44.6	44.7	44.6
3.5	91859	91686	91722	91871	91882	91706

Table 5.4.

Variable Amplitude Fatigue Life Estimations

Neuber Analysis, 'New' Material Properties

Load (kips)	M-1	M-2	M-3	M-4	M-6	M-6
			Material : MAN-TEN			
Transmission						
16.0	5.3	4.8	5.5	5.6	7.3	5.2
8.0	111.5	104.5	113.2	115.7	131.9	109.6
3.5	12922	13585	13199	12747	12437	13353
Suspension						
16.0	16.7	15.3	17.3	17.6	21.9	16.5
9.0	236.6	222.9	240.6	245.1	278.5	233.4
6.0	1956	1900	1967	1989	2098	1940
Bracket						
16.0	0.7	0.6	0.7	0.7	0.9	0.7
8.0	15.8	14.9	16.0	16.3	18.2	15.6
3.5	2185	2333	2256	2153	2102	2287
			Material : RQC-100			
Transmission						
16.0	7.4	7.4	7.4	7.4	7.4	7.4
8.0	185.3	185.2	185.3	185.4	185.6	185.3
3.5	842160	840458	840783	842206	842242	840635
Suspension						
16.0	25.0	25.0	25.0	25.0	25.0	25.0
9.0	402.8	402.6	402.7	403.0	403.4	402.6
6.0	9144	9134	9137	9147	9153	9135
Bracket						
16.0	0.9	0.9	0.9	0.9	0.9	0.9
8.0	32.8	32.8	32.8	32.8	32.9	32.8
3.5	106842	106639	106680	106853	106866	106662

Table 5.5.

Variable Amplitude Fatigue Life Estimations

Neuber Analysis, 'Old' Material Properties

Load (kips)	M-1	M-2	M-3	M-4	M-5	M-6
			Material : MAN-TEN			
Transmission						
16.0	12.2	18.2	11.1	9.8	4.1	13.6
8.0	156.8	295.1	158.0	117.1	44.7	202.9
3.5	7557	39656	16427	5391	2770	23386
Suspension						
16.0	31.0	53.2	30.8	23.9	9.8	38.4
9.0	310.1	638.5	338.9	231.6	92.5	437.1
6.0	1891	5057	2447	1361	560	3274
Bracket						
16.0	1.5	2.2	1.4	1.2	0.5	1.7
8.0	20.3	41.4	21.5	14.9	5.7	28.0
3.5	1159	6861	2814	847	458	4025
			Material : RQC-100			
Transmission						
16.0	6.7	5.4	6.8	7.6	16.0	6.1
8.0	166.9	87.7	133.9	238.0	717.0	111.0
3.5	931886	25290	59039	1237643	1655785	40538
Suspension						
16.0	22.7	16.2	21.6	26.8	60.5	19.0
9.0	365.5	194.4	295.8	508.3	1506.3	245.7
6.0	7848	1942	3443	12535	32116	2672
Bracket						
16.0	0.8	0.6	0.8	1.0	2.2	0.7
8.0	29.3	13.2	20.9	42.3	122.8	17.1
3.5	104548	4270	9864	154329	238704	6815

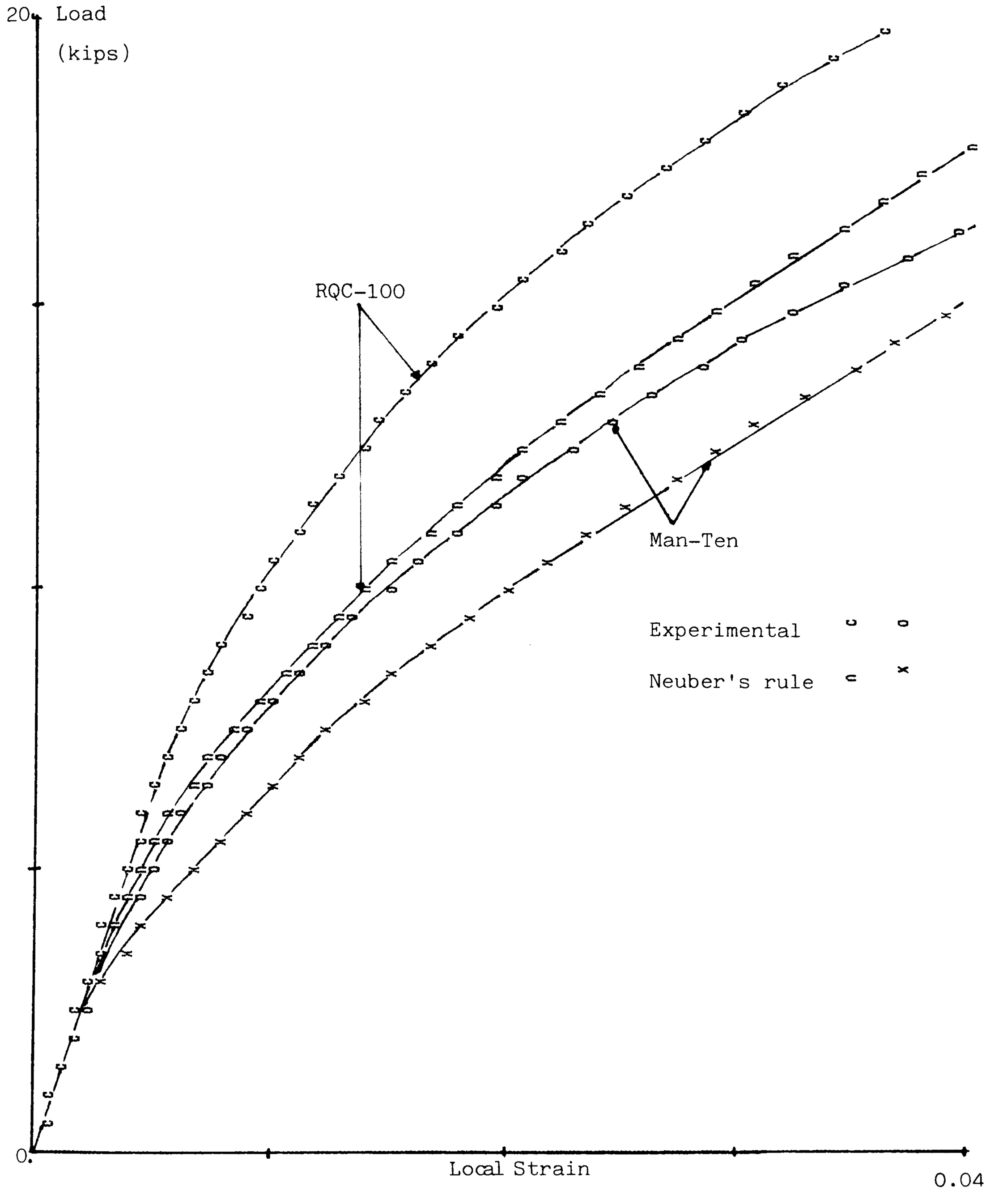

Fig. 5.5 Experimental and Neuber's rule load-strain curves

5.4.3 Neuber's Analysis, 'Old Properties'

Another set of life calculations was made employing Neuber's rule exactly the same way as in Section 5.4.2 with the only difference that the 'old' set of material properties listed in Table 5.1 was used. The predicted lives are listed in Table 5.5.

When the cyclic stress-strain properties, K' and n', are calculated from the cyclic fatigue properties, σ_f', b, ε_f' and c, they would give

for Man-Ten

$$n' = \frac{-0.12}{-0.60} = 0.200$$

$$K' = \frac{170.}{0.90^{0.2}} = 173.62$$

for RQC-100

$$n' = \frac{-0.073}{-0.67} = 0.109$$

$$K' = \frac{167.}{0.62^{0.109}} = 175.93$$

These calculated values of K' and n' for both sets of materials are very different than the values listed in Table 5.1 under the 'old' heading, 173.6 vs 173. and 0.200 vs 0.168 for Man-Ten, and 175.9 vs 201. and 0.109 vs 0.148 for RQC-100. Obviously, the life calculations made by the 6 methods reflect these differences. The most affected two methods are Methods 2 and 5, always giving extreme results. If the life predictions made by Method 1 is chosen as the base line to compare the other predictions, then for Man-Ten Method 2 predicts

grossly unconservative lives, particularly at long lives a factor of 5-6 too unconservative, while Method 5 predicts roughly a factor of 3 too conservative lives. For RQC-100, again Methods 2 and 5 always give extreme results, however, this time in the opposite directions and with differences more expanded.

In order to highlight the differences between the methods further, which yield 6 different life predictions for the same set of material properties and the same load history, a new set of life predictions were made using the 6 methods, this time, assuming a simple, constant amplitude loading. This was done to avoid confusion due to differing length of load histories and the load severity variation within each load history used in the earlier predictions.

The calculated lives for constant amplitude loading by Methods 2 to 6 are plotted against the lives calculated by Method 1, the base line calculations, and shown in Figs. 5.6 and 5.7. This time the predicted lives are in terms of number of reversals, not number of blocks of load history. The dashed lines in these figures represent perfect agreement between Method 1 and the rest of the methods. The transition lives are also indicated in these figures, kind of landmarks, to help examining the variation of methods in different regions of life. A transition fatigue life, $2N_t$, is defined as the number of reversals at which the local elastic strain equals to the local plastic strain:

$$\frac{\sigma_f'}{E}(2N_t)^b = \varepsilon_f'(2N_t)^c$$

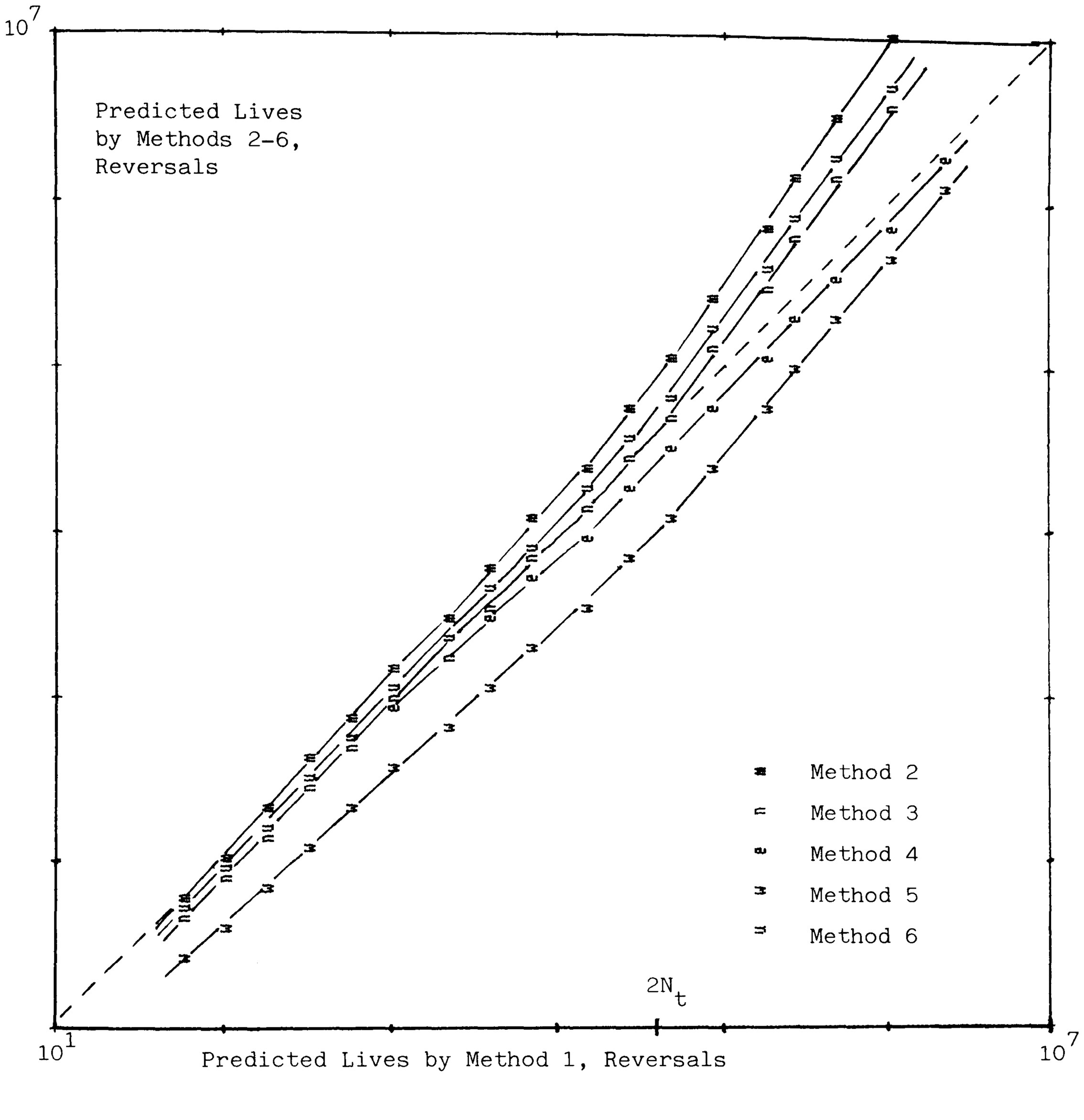

Fig. 5.6. Comparison of predictions by Method 2-6 and base-line predictions for constant amplitude loadings, for MAN-TEN

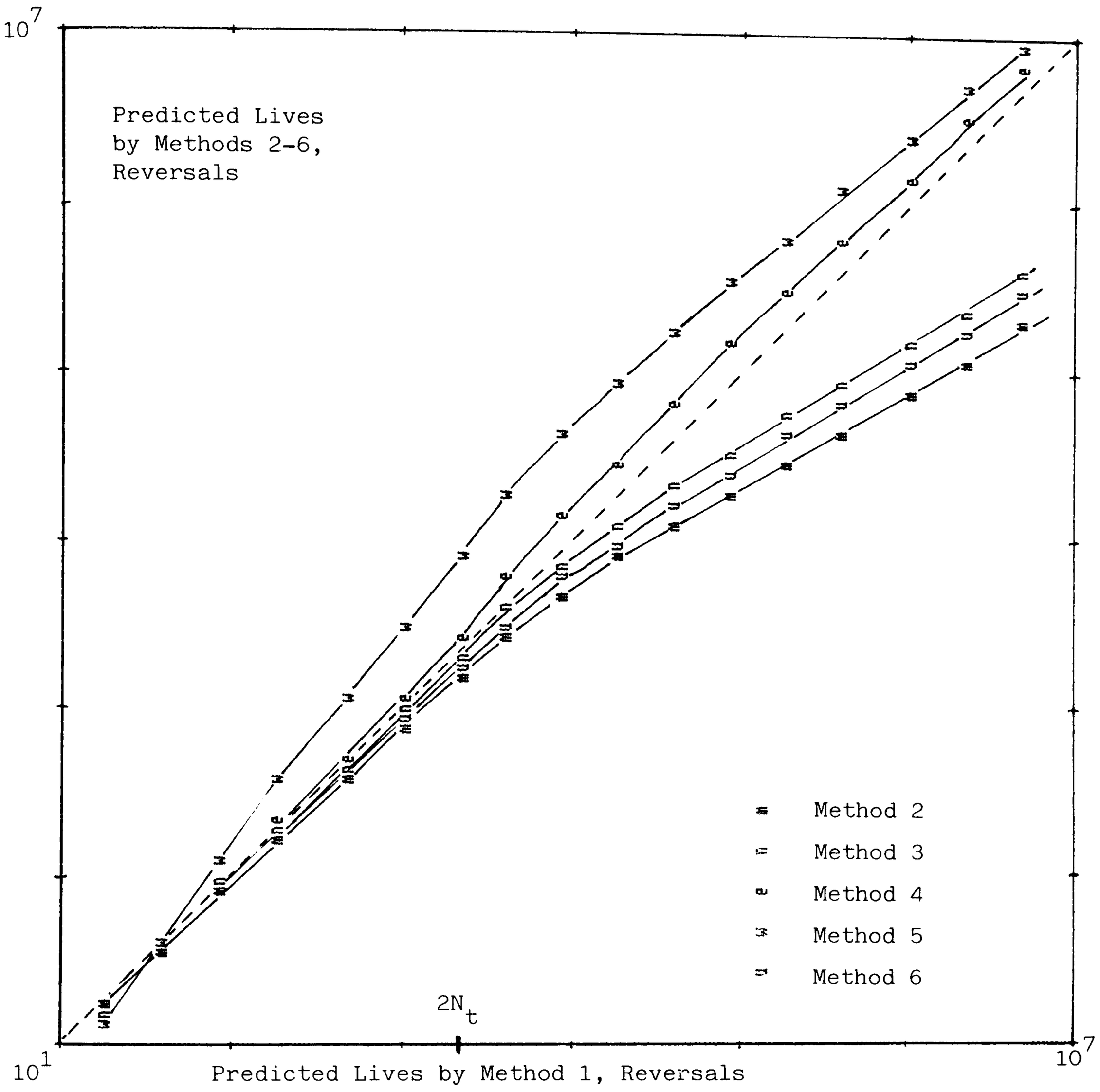

Fig. 5.7. Comparison of predictions by Method 2-6 and base-line predictions for constant amplitude loadings, for RQC-100

or

$$2N_t = \left(\frac{\sigma_f'}{E\epsilon_f'}\right)^{\frac{1}{c-b}}$$

The transition lives for Man-Ten and RQC-100, from the 'old' set of material properties, are 37000 and 2600 reversals, respectively.

The observations made for the life predictions for the block histories in Table 5.5 can now be re-observed in Figs. 5.6 and 5.7 in a more comprehensible and demonstrative way. For Man-Ten, Method 5 predicts roughly a factor of 3 too conservative lives than the base line predictions at short and intermediate lives; the predictions approach the perfect agreement line at long lives with the worst agreement at the transition life. Methods 2, 3 and 6 show the same tendency in varying degrees, that they all predict the same lives as the base line, almost a perfect agreement, up to the transition life; then they all start diverging from the perfect agreement line, with varying slopes. Obviously, the agreement gets worse as the life increases, a decade after the transition life Method 2 predicts an order of magnitude too non-conservative lives than the base line. Method 1 gives the nearest results to the base line calculations. It starts with good agreement at short lives, the agreement becomes the worst at the transition life, but only a factor of 1.4 conservative, and it again approaches to the base line at long lives.

The variation of life predictions for RQC-100 follows exactly the same pattern as the predictions for Man-Ten with only one difference, the methods previously predicting conservative lives compared to the base line now predict non-conservative lives, and vice

versa. Naturally, the transition life is different, and the scale of variations is different, but all the methods exhibit the same distinct tendency to overestimate or underestimate lives as in the case for Man-Ten. Again Method 4 is the nearest to the base line.

Note that the differences between the predictions with the 6 methods for the same material and load are due to the inconsistency of K' and n' values calculated from σ_f', b, ϵ_f' and c and K' and n' values given in the 'old' material data. If two sets of K' and n' values were equal, then all the methods would yield the same fatigue life for the same material and load, as they did, in Table 5.4; nearly the same for Man-Ten and inseparably close for RQC-100. This clearly suggests that the response of a method to a material property change is not the same for all the methods. In the following section, the sensitivity of the prediction methods to variations in the cyclic material properties is investigated.

5.5 Sensitivity of Prediction Methods to Material Properties

In order to investigate the sensitivity of the prediction methods systematically and quantitatively, a sensitivity term, $^{\eta}x$, is introduced as an indication of how a life prediction by a method changes in response to a variation in the property, x, in question. The steps to calculate the sensitivity terms are as follows: For each method,

i) Calculate the life, $2N_f$, for a given level of load, using the listed material properties in Table 5.1.

ii) Increase the material property in question, x, by a small amount, Δx. 1% of the original value was chosen for Δx in this study. While keeping the rest of properties the same, calculate the life, $2N_{f+}$, for the same load level.

iii) Decrease x by Δx, and calculate $2N_{f-}$.

iv) The sensitivity term, η_x, for x, can now be defined as:

$$\eta_x = \frac{2N_{f+} - 2N_{f-}}{2N_f} \quad \frac{x}{2\Delta x} \qquad \textbf{Eq. 5.17}$$

Defined in this way, the sensitivity term can be viewed as the "normalized discrete partial differentiation of the life, $2N_f$, with respect to the property in question, x". A more practical interpretation of this definition is that η_x is a measure of rate of percentage change in the life, $2N_f$, in response to 1 percent change in the property, x, while the rest of the properties stay the same.

Sensitivity terms for each cyclic material property, σ_f', b, ε_f', c, K' and n', and also for the fatigue notch factor, K_f, were calculated at different load levels, covering a range from very short lives to very long lives, for both Man-Ten and RQC-100. Again a constant amplitude loading was used, to avoid the confusion due to the varying length of service histories used in the earlier predictions, and also due to the variation in the load severity within each service history. "New" material properties were used. The sensitivity terms for each material property were plotted against the life, $2N_f$, for the 6 methods, and are shown in Figs. 5.8 to 5.12 for RQC-100. The scale and the length of both axes in these plots are kept the same to make comparisons easier with y-axis, the sensitivity axis linear; x-axis, the life-axis logarithmic scale.

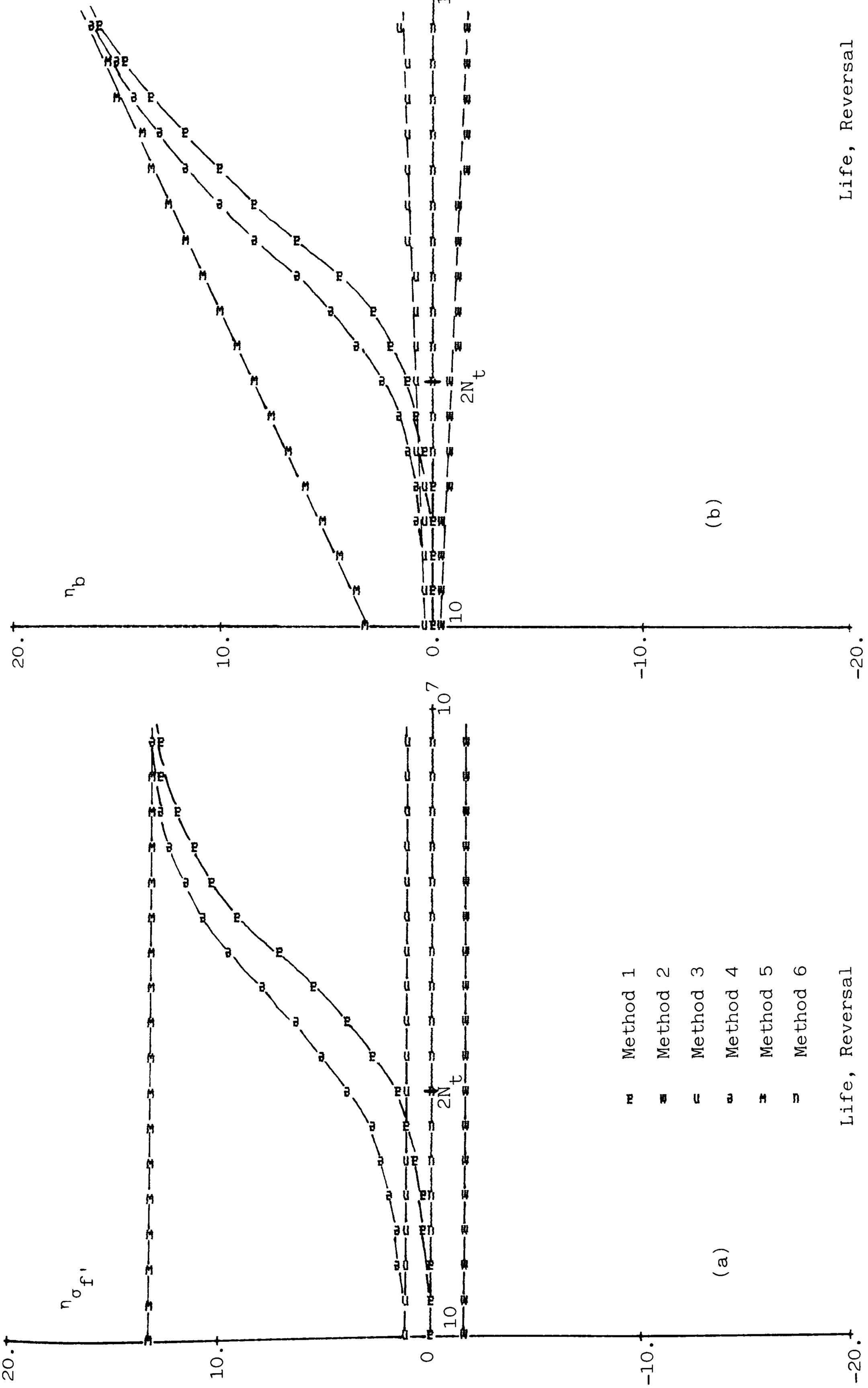

Fig. 5.8. Variation of the sensitivity terms for (a) σ_f (b) b

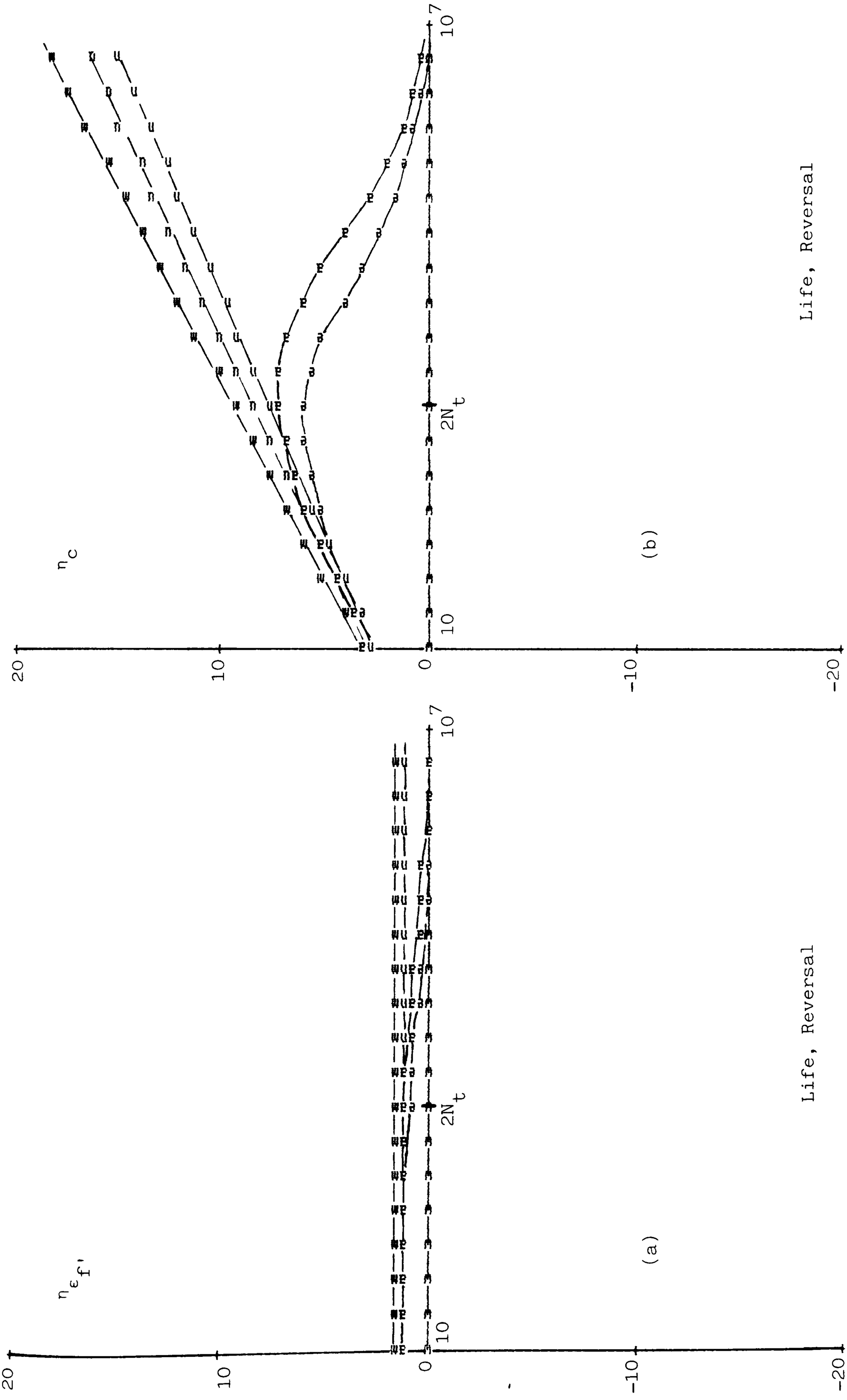

Fig. 5.9. Variation of the sensitivity terms for (a) $\epsilon_{f'}$, (b) c

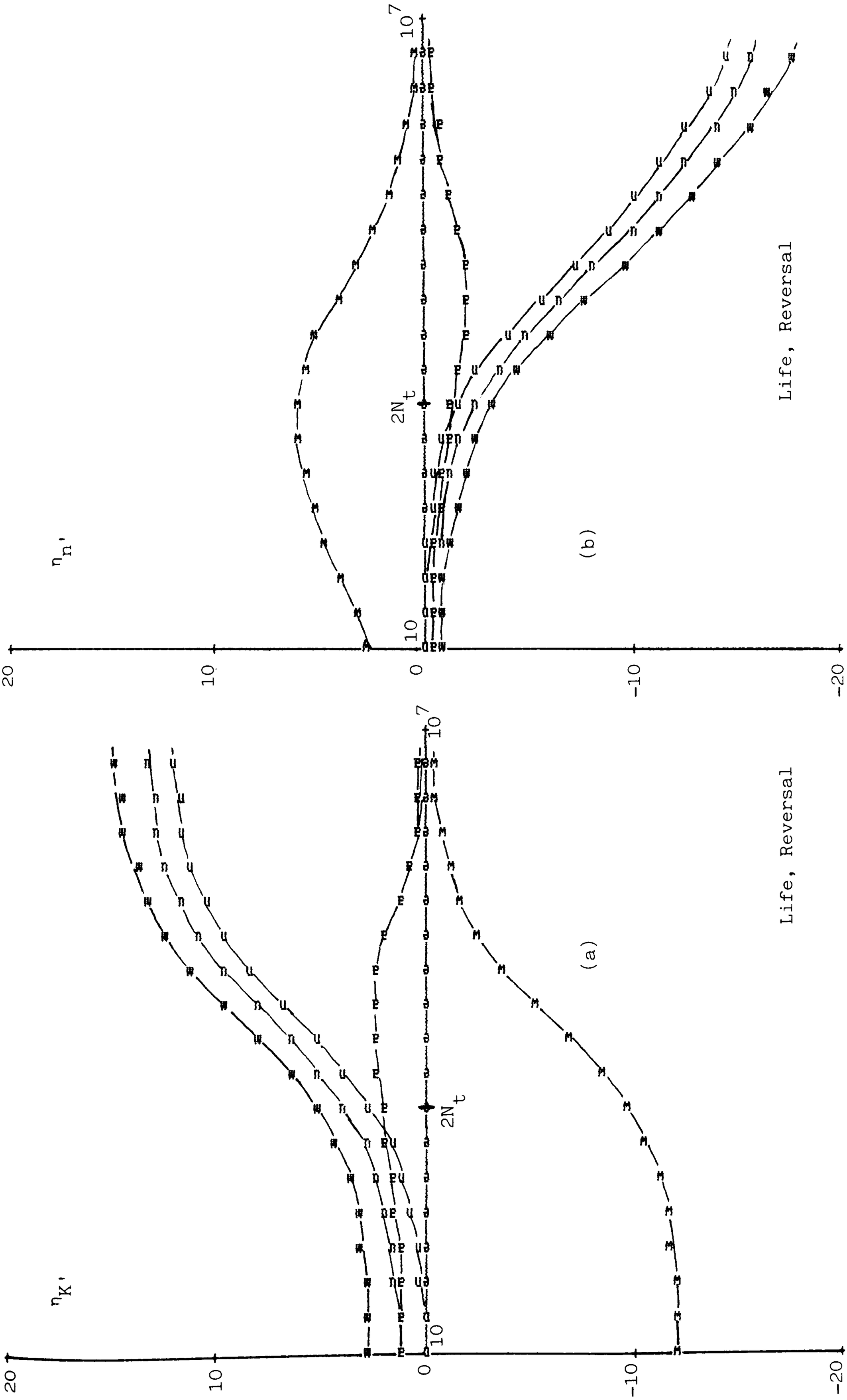

Fig. 5.10. Variation of the sensitivity terms for (a) K' (b) n'

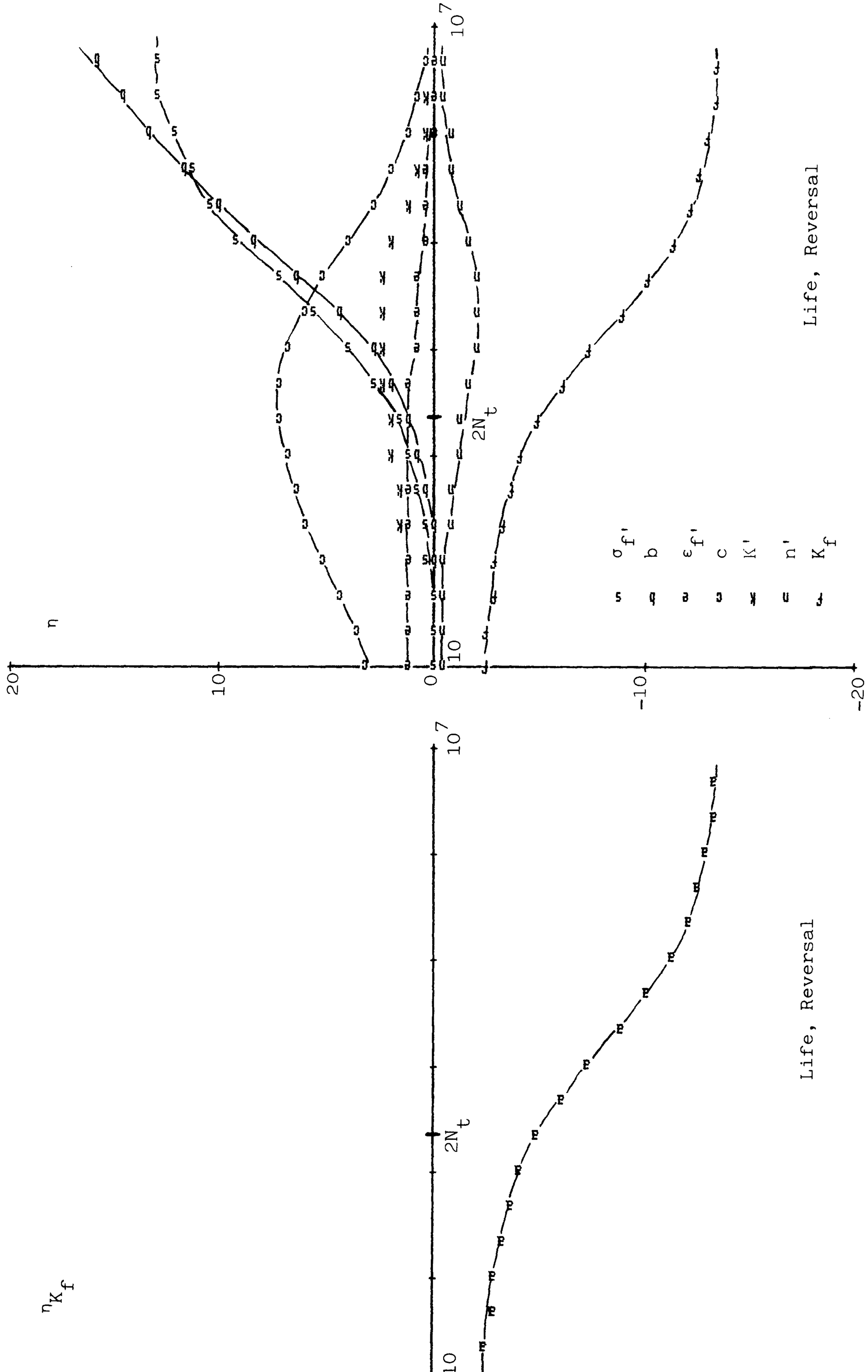

Fig. 5.11. Sensitivity to Fatigue Notch Factor, K_f

Fig. 5.12. Sensitivity of Method 1 to all the properties

Before discussing how the 6 methods respond to changes in the material properties, it may be pertinent to remind briefly how the 6 methods calculate the life. In all methods, the local stress, the local elastic and plastic strains are determined using Neuber's rule for a given load level. Then Method 1 calculates the life from the complete strain-life curve using the total strain. Method 2 makes use of the ratio of the plastic to elastic strain, whereas Method 3 uses the product of the elastic and plastic strain. Method 5 uses only the elastic strain part of the total strain-life curve, Method 6 employs only the plastic part. Method 4 makes use of the product of the local stress and total strain, as a result the cyclic stress-strain curve is by-passed, and the life is directly linked to the applied load by Neuber's rule, as explained in Chapter 4.3 and Eq. 4.29. With these points in mind, the variation of the sensitivity terms calculated by the 6 methods is discussed for pairs of related material properties, with Method 1 as the base line.

Fatigue strength (elastic strain-life) properties, σ_f' and b,

Fig. 5.8: $^{n}\sigma_f'$ of Method 1, i.e. the sensitivity of Method 1 to a variation in σ_f', starts out from zero at short lives, implying that this method is insensitive to a change in σ_f', that whatever the change in σ_f' might be, it does not affect the final life prediction at short lives. $^{n}\sigma_f'$ of Method 1 exhibits a gradual increase around the transition life, followed by a relatively sharp increase at intermediate lives, then a gradual approach to a steadystate value at very long lives. At long lives, Method 1 becomes highly sensitive to a change in σ_f', i.e. a small change in σ_f' would cause a fairly

large change in the life prediction by Method 1. If a numerical example is necessary, it is safe to say that for lives longer than 10^6 reversals, a 1-percent-increase in σ_f' would cause approximately a 12-percent-increase in the life predicted by Method 1. The reason for this apparent reluctancy in giving a numerical example is that any n_x of any method is a measure of <u>average</u> rate of percentage change in life due to 1-percent change in the property x, at a particular x. It is not necessarily a proportionality constant between the predicted life change and the change in the property. For example, the statement, that, for lives longer than 10^6 reversals, a 4-percent-increase in σ_f' would cause approximately a 48-percent-increase in the life predicted by Method 1, may not be true. Indeed, it is not true; from the actual calculations, a 4-percent-increase in σ_f' would cause not 48, but approximately 65-percent increase in life.

$n_{\sigma_f'}$ of Method 4 follows a similar pattern to that of Method 1, i.e. Method 4 is also fairly insensitive to σ_f' at short lives and becomes very sensitive at long lives, gradually approaching to the same steady-state level as Method 1, but more sensitive than Method 1 for all lives. Method 6, which uses the plastic strain only, does not depend on the elastic strain-life properties, therefore $n_{\sigma_f'}$ for Method 6 is zero for all lives, as expected. Methods 2 and 3 display relatively low, constant level of sensitivity for the whole life spectrum. However, having a negative sign for $n_{\sigma_f'}$, Method 2 predicts a decreased life for an increase in σ_f', contrary to the expectation. Method 5, which uses the elastic strain only, shows a

constant, but the highest level of sensitivity to a change in σ_f'; it is indeed this level that $\eta_{\sigma_f'}$, of Methods 1 and 4 approach at the steady state. A high level of sensitivity to σ_f' at short lives, meaning that a small change in σ_f' would cause a large change in the predicted life by Method 5, is also against the expectation, because at short lives, the life is governed mainly by the plastic strain, the contribution of the elastic strain is negligible, as Method 1 predicted.

η_b, the sensitivity in response to a change in b, follows a similar pattern to that of σ_f' for all methods, constants in the previous case becoming lines for this case. Method 5 is again the most sensitive of all to b at all lives, however it is not constant this time; the sensitivity depends on the life, it increases linearly with the life. η_b of Method 1, the base line, starts out from zero at short lives, meaning that the life predictions by Method 1 does not depend on b at short lives, then increases relatively sharply at intermediate lives and gradually approaches to the asymptote determined by Method 5 at long lives. η_b of Method 4 follows the same pattern as Method 1, with somewhat more sensitivity. Method 6 altogether, and Methods 2 and 3 are relatively insensitive to variation in b for all lives.

Fatigue ductility (plastic strain-life) properties, ϵ_f' and c,

Fig. 5.9:

All the methods are relatively insensitive to variation in

$^{\varepsilon}f'$ for all lives. Method 5, which uses the elastic strain only, does not depend on the plastic strain-life properties, therefore $^{n}\varepsilon_{f}'$ and ^{n}c of Method 5 are zero for all lives. Surprisingly, Method 2, which uses the ratio of the plastic to elastic strain, displays the highest, but still relatively low, level of sensitivity for all lives, even more than Method 6, which uses the plastic strain only, does. Methods 1 and 4 again display similar behaviour, they start with a constant, fairly low level of sensitivity, after the transition life, the sensitivity starts decreasing, gradually dropping to zero at long lives.

^{n}c, the sensitivity in response to a change in c, of Method 1 starts out as a straight line at short lives, with the asymptotic line determined by Method 6, reaches its peak value around the transition life, then gradually starts decreasing, and approaches zero at long lives. ^{n}c of Method 4 follows the same pattern with a slightly reduced sensitivity for all lives c of the other 3 methods, Methods 2, 3 and 6 are straight lines with varying positive slopes indicating that a small change in the plastic strain property c would cause a large change in the life prediction at long lives where the life is dominated mainly by the elastic strain. The behaviour of Methods 2, 3 and 6 is again contrary to expectations at long lives.

Cyclic stress-strain properties, K' and n', Fig. 5.10:

$^{n}K'$ of Method 1 starts with a constant value at short lives, increases very slowly reaching the maximum value not at the transion

life, but almost a decade later, then gradually decreases and approaches zero at long lives. $^{n}K'$ of Methods, 2, 3 and 6 display an S-shape variation, they all start with a constant value at short lives, gradually increasing at intermediate lives, and reaching a high level of steady-state sensitivity at long lives. $^{n}K'$ of Method 5 also displays an S-shape variation, it starts with a high level, but negative, of sensitivity at short lives, increases at intermediate lives meaning that the magnitude of the sensitivity decreases, and approaches zero at long lives. The behaviour of Method 5, which uses the elastic strain only, is contrary to expectations on two accounts, one is the sign of the variation which is negative meaning that an increase in K' would cause a decrease in the life predicted by Method 5. The other is the magnitude of the variation at short lives, indicating that a small change in K' would cause a large change in the predicted life. The behaviour of Methods, 2, 3 and 6 is again contrary to expectations at long lives.

$^{n}n'$ of Method 1 follows a similar pattern to $^{n}K'$ but with a negative sign. The variations of $^{n}n'$ for the other 4 methods still display S-shape curve as in the previous case for $^{n}K'$, with signs reversed and the steady-state levels at short and long lives becoming asymptotic lines. Method 4 by-passes the use of the cyclic stress-strain relationship, $^{n}K'$ and $^{n}n'$ of Method 4 are zero, as expected.

Fatigue Notch Factor, K_f, Fig. 5.11:

Although it is not a material property, the sensitivity of the

life prediction methods to the fatigue notch factor is also investigated. For once, all the 6 methods are affected to the same degree by a change in K_f throughout the life spectrum. The negative sign indicates that an increase in K_f would cause a decrease in the life predicted, all the methods are very sensitive to a change in K_f at long lives. Although the sensitivity at short lives is relatively small in this plot, however, compared to the sensitivity to the material properties at short lives, the sensitivity of life predictions to K_f is considerably high even at short lives.

Sensitivity of Method 1, Fig. 5.12:

Finally, the sensitivity of Method 1 to all the material properties and the fatigue notch factor is summarized in Fig. 5.12.

General Comments:

Although the sensitivity variations of the methods using only the materials properties of RQC-100 are shown in Figs. 5.8 to 5.12, the sensitivity calculations using the properties of Man-Ten exhibit the same pattern to that of RQC-100. The differences between the two sets of sensitivity plots are the location of the transition life and the scale of the plots, for the obvious reason that the magnitudes of the properties for the two materials are quite different. However, the sensitivity plots for both materials display the same shape, the same trend for all the methods, therefore the sensitivity plots for Man-Ten are not included. Indeed, the subject under scrutiny in this study is

not the material properties, but the behaviour of the life prediction methods in response to a change in the material properties.

Of the 6 methods investigated, only Method 1 behaves in the way that is expected from a life prediction method which conforms to the experimentally observed data, Method 4 coming a close second. The differences between Methods 1 and 4 are that Method 4 does not depend on K' and n', therefore the sensitivity of Method 4 to these properties is zero while Method 1 exhibits some low level, but distinct, sensitivity, and that the sensitivity of Method 4 to the other properties is either slightly higher or lower than that of Method 1, but follows the same pattern. The difference between Method 1 and the other 4 methods is not just a slight difference in magnitude of sensitivities, but a difference of attitudes. The sensitivity of Method 5 to all the properties consistently disagrees with that of Method 1 at short and intermediate lives, with the difference getting smaller at long lives. In fact, Method 5 becomes a limiting case of Method 1 at long lives. The sensitivity of Methods 2, 3, and 6 to all the properties consistently disagrees with that of Method 1 at intermediate and long lives, with difference getting progressively worse at long lives, and getting smaller at short lives. This time, it is Method 6 which becomes the limiting case of Method 1 at short lives.

The concepts, "contrary to expectations", "disagreement in attitude" may be explained best with an example. Suppose the fatigue strength exponent, b, is slightly increase from b_1 to b_2, while keeping the other properties constant. The effect of this change on

the strain-life curve is illustrated in Fig. 5.13. Since the other parameters are kept constant, there would not be any change in the total strain calculated with the new set of properties. However, there would be a change in the life predicted from the new strain-life curve, this change, an increase, would be negligibly small at high strain values, in other words, at short lives, and considerably large at long lives. The sensitivity of Methods 1 to b conforms to this observation, as shown in Fig. 5.8.b, so does Method 4. However, from the same figure, Method 5 predicts a considerable increase in the life even at short lives and Methods 2, 3 and 6 predict a negligible change in the life even at long lives. Method 2 displays even a further disagreement that an increase in b would cause a decrease in the predicted life.

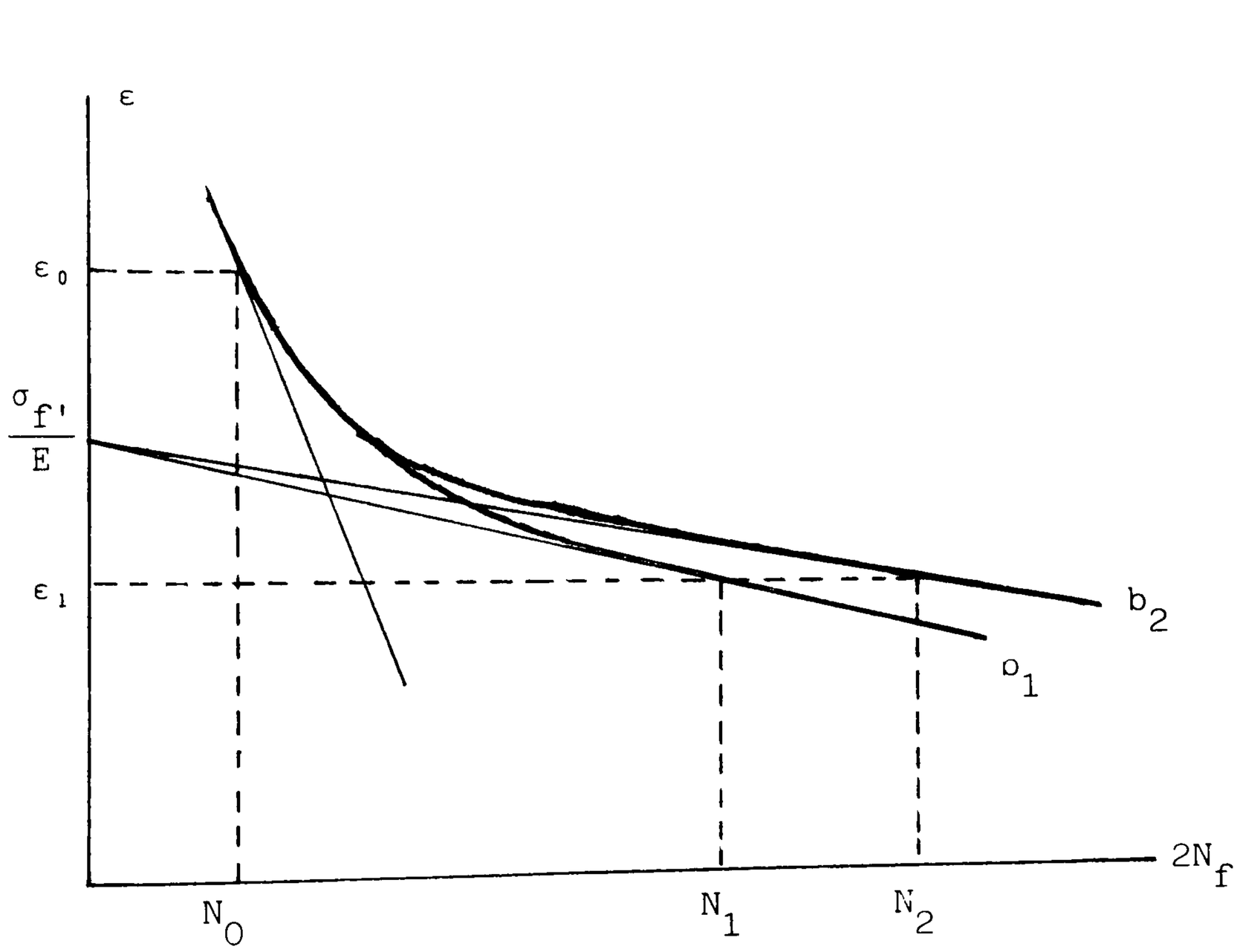

Fig. 5.13 The effect of b on the fatigue life.

Note that there is an intrinsic assumption in the sensitivity calculations presented in this section, that all the 6 material properties are independent. The fact that whether K' and n' values are consistent with σ_f', b, ϵ_f' and c, i.e. the two of them can be calculated from the other four, has no relevance on the sensitivity calculations. The consistency of the material properties affects only the absolute predictions by the 6 methods at which the sensitivity calculations are made, not the sensitivity itself. Those lives may be the same, as indeed the same for RQC-100, see Table 5.4, but the different methods show different sensitivity for the same property at the same life. The reason for the difference in sensitivities is the assumption that there are 6 independent material properties and the effect of each property on the predicted life is different for each method. Furthermore, if the set of material properties is not consistent, then the methods would predict very different lives in accordance to their sensitivity to the properties; life predictions using the 'old' sets of data for Man-Ten and RQC, Figs. 5.6 and 5.7, clearly illustrate this argument. As indicated by the sensitivity analysis, the disagreement between Method 5 and Method 1 is worse at short and intermediate lives, and Methods, 2, 3 and 6 predict very different results than Method 1 after the transition life, the difference progressively getting worse at long lives.

Had there been only 4 independent properties, then not only all the methods would predict the same life for the same conditions they would also show the same sensitivity to changes in material properties. In fact, all the methods would then exhibit exactly the same sensitivity as Method 4 which by-passes the use of K' and n'.

There are two immediate conclusions that emerge from the sensitivity analysis. The first is that if there is any doubt about the consistency of the material properties, then do use Method 1 at all times and do not use the other methods, as Method 1 employs the most direct approach, predicts lives using the observed test data without any further assumptions than the assumptions already made about the form of the cyclic stress-strain and the strain-life relationships. The other methods make further assumptions as discussed in Chapter 4, consequently they behave "contrary to expectations", as explained earlier.

The first conclusion might seem quite trivial, however considering the popularity of some of the methods other than Method 1[2, 3, 4, 5, 6, 7] the importance of the conclusion about the use of Method 1 can be understood. Admittedly, the life predictions made by all the methods using the 'new' set of material properties would practically give the same result, as shown in Table 5.3 and 5.4, they might give very different results if the consistency of the parameters is not achieved, as in the life predictions using the 'old' set, Table 5.5 and Figs. 5.6 and 5.7.

The second conclusion of the study of sensitivity is about the determination of material properties, and it is in the form of a proposal. Fig. 5.12 shows the sensitivity of Method 1 to all the material properties, from this plot it is quite clear that the sensitivity of Method 1 to the cyclic stress-strain relationship properties, K' and n', is relatively low compared to the sensitivity to

the other properties. Method 4 does not use K' and n', yet it gives the closest results to Method 1 in terms of sensitivity and actual predicted lives for both 'old' and 'new' set of data. Finally, a cursory examination of the published material data indicate that most of the listed values for K' and n' are very close to the estimated values from the other material properties, having a good degree of consistency. Therefore, the proposal is to re-evaluate the material properties and re-examine the way the material properties are determined, with a view to achieving perfect consistency. Then all the 6 methods would give the same result eliminating the need to change in-house software that a user already has, which employs one of the methods other than Method 1.

5.6 Determination of the Fatigue Data

An important factor to consider regarding the cyclic material properties is that they are not unique, they are the parameters of relationships which explain the experimental data best. Therefore the cyclic material properties depend on not only the experimental data, but also the specific way the fatigue relationships are fitted to the test data. Quite often, separate sets of data are produced for similar materials or those of the same specification, and the cyclic properties are recalculated, as in the case of 'old' and 'new' sets of properties for Man-Ten and RQC-100. As an example to show that the material properties are not unique, that apparently very different values of the properties may explain the same relationship, the life predictions by Method 1, the base line calculations, using the 'old' properties are

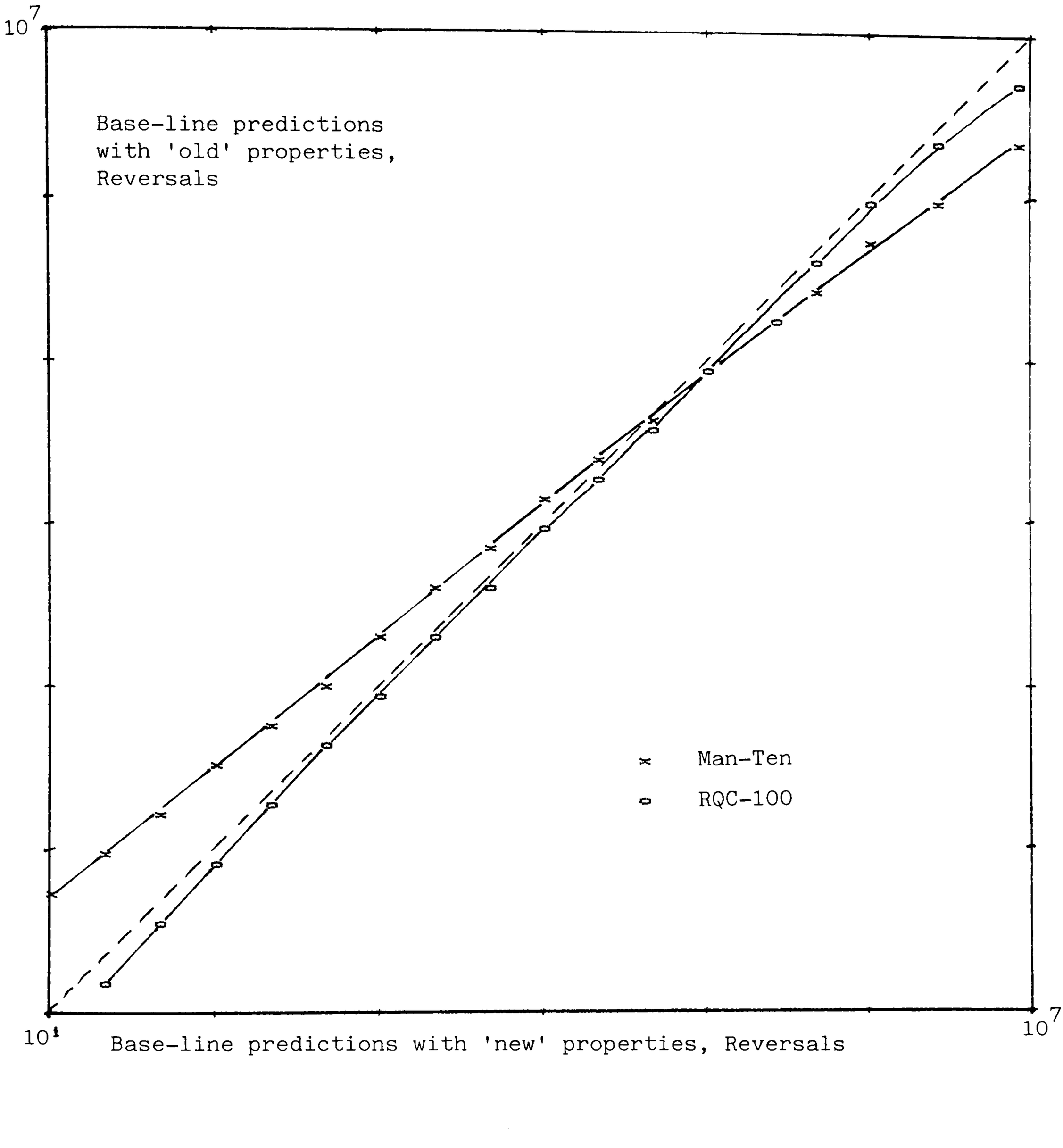

Fig. 5.14. Comparison of base line predictions for 'new' and 'old' material properties

plotted against the predictions using the 'new' values, in Fig. 5.14, again the dashed line indicating a perfect agreement. As seen from the figure, the predictions using the 'old' and the 'new' set of properties for RQC-100 are almost in perfect agreement throughout the life spectrum. On the other hand, the predictions for Man-Ten differ considerably, almost a factor of 5 at very short and very long lives, indicating that the 'new' set is substantially different than the 'old' one.

A widely accepted way of determining the cyclic fatigue properties is to analyse the data obtained from axial tests carried out on smooth specimens in fully reversed strain control[8]. These data consist of measurements taken from a stable stress-strain hysteresis loop recorded at about half the specimen life. The parameters directly measured are stress amplitude $\Delta\sigma/2$, total strain amplitude $\Delta\epsilon/2$, and the number of reversals to failure. Then the elastic and plastic parts of the total strain, $\Delta\epsilon_e/2$ and $\Delta\epsilon_p/2$, are determined from the recorded hysteresis loop. Values for σ_f' and b are calculated from the elastic strain-life data by linear regression on a log-log scale. Similarly, ϵ_f' and c are calculated from the plastic strain-life data, and K' and n' from stress-plastic strain data, by linear regression. The cycle properties calculated this way may or may not show the consistency required for the validity of Methods 2 to 6. However if the following procedure is adopted, the consistency of the parameters can be obtained.

Instead of separating the cyclic curves into elastic and

plastic parts, and fitting a straight line to the decomposed data, the original measured data, i.e. stress amplitude, strain amplitude and reversals, may be used directly to obtain the parameters of the stress-strain and the strain-life relationship by least-square curve fitting methods. The form of the cyclic relationships is not changed, for the stress-strain curve:

$$\frac{\Delta\varepsilon}{2} = \frac{\Delta\sigma}{2E} + \left(\frac{\Delta\sigma}{2K'}\right)^{1/n'} \qquad \textbf{Eq. 5.18}$$

and for the strain-life curve:

$$\frac{\Delta\varepsilon}{2} = \frac{\sigma f'}{E}(2N_f)^b + \varepsilon_{f'}(2N_f)^c \qquad \textbf{Eq. 5.19}$$

Assuming that K' and n' are not independent and can be derived from the other properties as:

$$n' = \frac{b}{c} \qquad \textbf{Eq. 5.20}$$

$$K' = \frac{\sigma_{f'}}{(\varepsilon_{f'})^{b/c}} \qquad \textbf{Eq. 5.21}$$

Putting Eq. 5.20 and 5.21 into Eq. 5.18

$$\frac{\Delta\varepsilon}{2} = \frac{\Delta\sigma}{2E} + \varepsilon_{f'}\left(\frac{\Delta\sigma}{2\sigma_{f'}}\right)^{c/b} \qquad \textbf{Eq. 5.22}$$

There are two equations, Eq. 5.22, which corresponds to the measured stress-strain data, and Eq. 5.19 to the strain-life data, and there are four parameters to be determined. Then the parameters can be found by a simultaneous fitting of curves, Eq. 5.22 and 5.19 to the measured data. The simultaneous fitting of curves this way does not complicate the procedure too much, because in both curves, represented by Eq. 5.22 and 5.19, y-axis is in terms of strain, then error-square terms for both curves may be added directly, reducing the problem to single curve

fitting. Complications arise not from the simultaneous fitting, but from the 'curve fitting' itself. Unless the set of data to be analyzed contains a large number of results, the parameters can only be determined statistically within wide confidence limits. The method of least squares does not necessarily lead to the physically most acceptable line, particularly concerning the position where the curve changes from a relatively steep slope to a flat slope. If there are only a few test results over a narrow range of strain values, various curves, i.e. different sets of parameters, may be equally satisfactory, though they may be quite different when extrapolated. An extra condition for the best-fit parameters in the simultaneous fitting is that the set of parameters should satisfy a 'goodness of fit' test for both curves.

If a satisfactory set of parameters can be found within reasonable confidence limits, then this set is the most desirable one not only because all the methods would then predict the same result so that any one of them could be used, but also because this set represents a direct link between the stress-strain-life curves and experimentally measured quantities. If, however, a satisfactory set of parameters, which fits the experimental results equally well for both curves, cannot be found, then obviously separate fittings are necessary using 6 independent parameters. In this case, it is the author's contention that two separate curve fittings should be carried out using Eqs. 5.18 and 5.19 in their full forms and the directly measured experimental data, not three fittings using the elastic and plastic parts of both the equations and the measured data. Also in this case,

where there are 6 independent parameters, only Method 1 should be used for fatigue life predictions.

5.7 The Effect of Mean Stress

This is the third area where the local strain approaches differ, as explained in Chapter 4.3. Having isolated the effect of linking the applied load to the local stress and strain in two different ways, and the effect of linking the local stress and strain to the life in six different methods on the predicted lives, it is now possible to investigate the influence of mean stress on the predicted lives. The rainflow cycle counting technique used in the earlier predictions was modified to allow for mean stress effects. Working through the load histories reversal by reversal, the exact values for the local stress and strain were calculated and stored. Whenever a closed hysteresis loop was detected, the mean stress and the maximum stress for each closed loop were calculated to be used with a mean-stress-corrected equation. The two equations accommodating mean stress effects used in this study are:

1. Morrow[9]

$$\frac{\Delta\epsilon}{2} = \frac{\sigma_f' - \sigma_m}{E} (2N_f)^b + \epsilon_f'(2N_f)^c \qquad \textbf{Eq. 5.23}$$

2. Smith-Watson-Topper[7]

$$\sigma_{max} \frac{\Delta\epsilon}{2} = \frac{(\sigma_f')^2}{E} (2N_f)^{2b} + \sigma_f'\epsilon_f'(2N_f)^{b+c} \qquad \textbf{Eq. 5.24}$$

where σ_m and σ_{max} are the mean and maximum value of the local stress for each closed loop.

Before the actual calculations, the behaviour of these two equations can be predicted from the sensitivity analysis presented earlier. Morrow correction can be viewed as the base line Method 1 equation with a dynamic variation in fatigue strength coefficient σ_f'. From the sensitivity plots for σ_f', Fig. 5.8.a, it is seen that Method 1 is quite insensitive to variations in σ_f' at short lives, then gradually becomes more sensitive at intermediate lives, and very sensitive at long lives. The equation for Smith-Watson-Topper correction is the same as the equation for Method 4, Eq. 5.8, with the modification that the stress amplitude, $\Delta\sigma/2$, is replaced by the maximum stress, σ_{max}. Although this modification does not mean simply a change in σ_f' as in Morrow correction, nevertheless a similar sensitivity displayed by Method 4 to a change in σ_f' is expected, which is also very similar to that of Method 1. In other words, mean stress corrections, if there are any, would be negligibly small at short lives, and quite considerable at long lives.

The predicted lives for the SAE histories with and without the mean stress corrections are summarized in Table 5.6. The predicted lives without the mean stress correction, i.e. the base line calculations, are compared in Fig. 5.15 with the experimental lives, and the comparison of the predicted lives using Smith-Watson-Topper mean stress correction is shown in Fig. 5.16. Although comparisons with the experimental results are given, the principal aim of this study is to examine the behaviour of methods themselves, therefore more importance is attached to relative comparisons than the absolute values of life predictions.

Table 5.6.

Variable Amplitude Fatigue Life Estimations

Mean Stress Effect

Material : MAN-TEN

Load (Kips)	Exprm. life (blocks)	Predicted Lives: No Mean Stress	Morrow	Smith Watson Topper
Transmission				
16.0	8.4			
16.0	12.5	11.4	10.5	10.4
16.0	12.8			
8.0	74.0			
8.0	154.0	238.8	202.1	178.2
8.0	420.0			
3.5	3755			
3.5	4270	16620	10794	7606
3.5	5800			
Suspension				
16.0	-			
16.0	7.7	40.1	40.5	40.7
16.0	28.0			
9.0	162.0			
9.0	208.0	510.5	542.9	557.3
9.0	430.0			
6.0	1410			
6.0	1750	3616	5480	7103
6.0	2240			
Bracket				
16.0	1.5			
16.0	2.0	1.5	1.5	1.5
16.0	2.6			
8.0	11.5			
8.0	20.8	33.1	34.2	34.7
8.0	23.0			
3.5	270			
3.5	510	2727	3096	3415
3.5	1588			

Table 5.6. (cont.)

Variable Amplitude Fatigue Life Estimations

Mean Stress Effect

Material : RQC-100

Load (Kips)	Exprm. life (blocks)	Predicted Lives No Mean Stress	Morrow	Smith Watson Topper
Transmission				
16.0	22.2			
16.0	23.5	14.5	9.7	10.4
16.0	29.9			
8.0	269.0			
8.0	374.0	260.6	153.7	153.4
8.0	460.0			
3.5	57000			
3.5	88000	701510	207614	120956
3.5	88000			
Suspension				
16.0	19.9			
16.0	24.4	46.8	58.7	58.8
16.0	64.0			
9.0	-			
9.0	1710.0	585.9	1161.3	1255.0
9.0	-			
6.0	-			
6.0	48000	9892	24699	33484
6.0	-			
Bracket				
16.0	3.3			
16.0	4.2	1.7	1.8	1.8
16.0	5.1			
8.0	47.0			
8.0	87.5	44.4	50.2	50.4
8.0	113.0			
3.5	-			
3.5	2673	90748	137603	173512
3.5	5020			

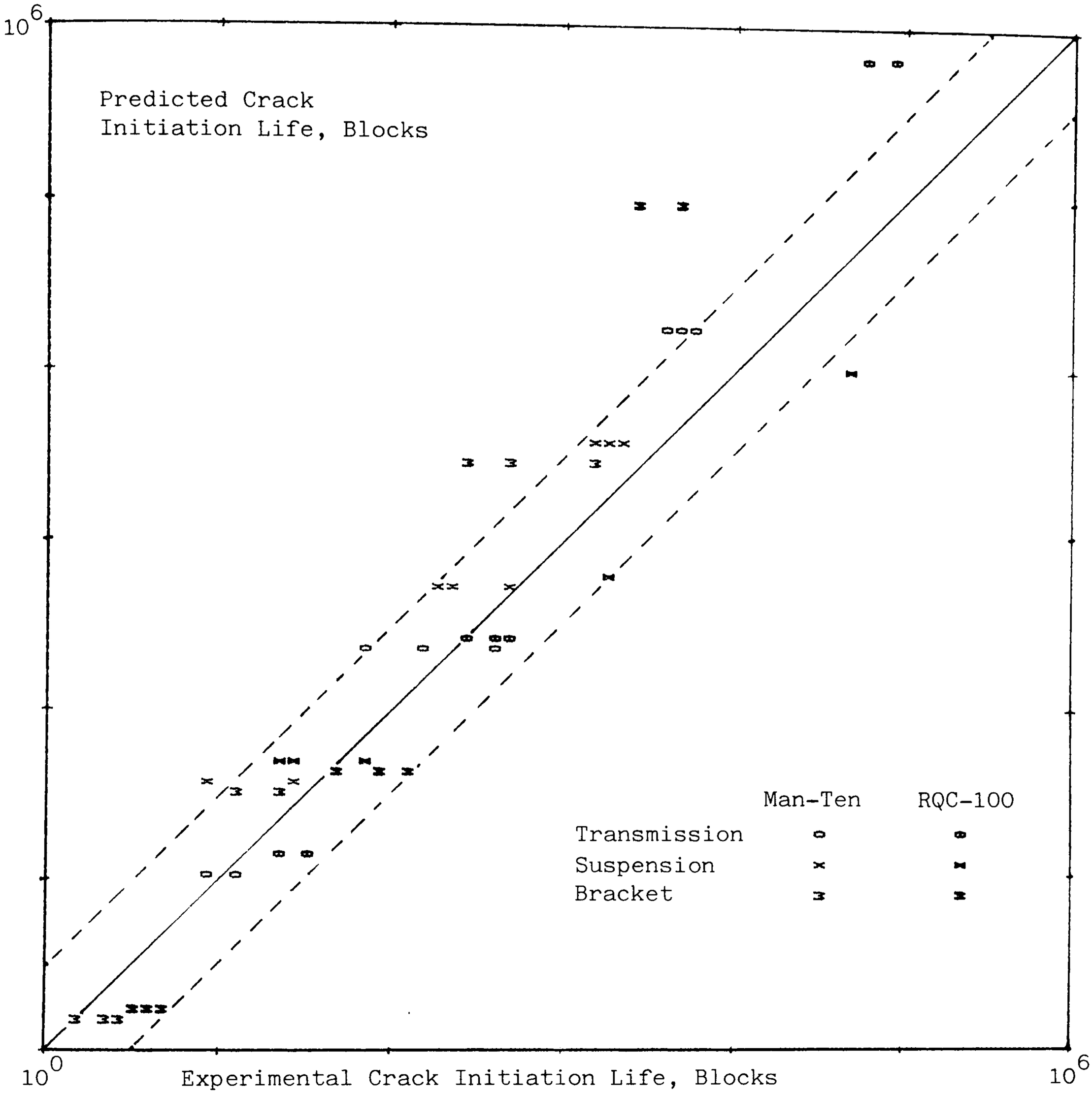

Fig. 5.15. Life calculations based on local strain approach, using load-strain curve, without mean stress correction

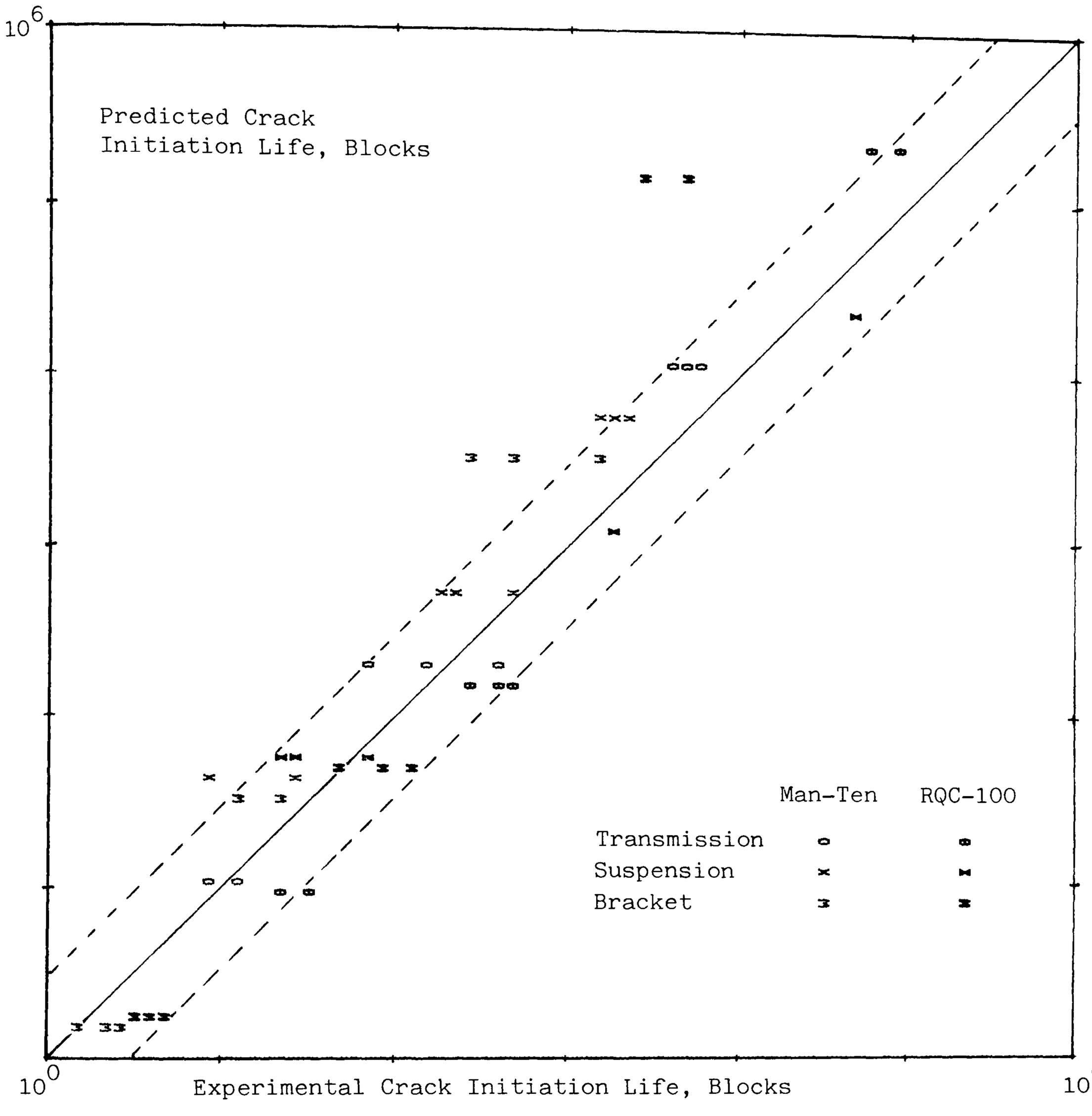

Fig. 5.16. Life calculations based on local strain approach, using load-strain curve, with Smith-Watson-Topper mean stress correction

The predicted lives with and without mean stress correction, in Table 5.6, are consistent with the inference of the sensitivity analysis and with the nature of load histories. At short lives, the effect of mean stress is hardly noticeable. The difference between the predicted lives with and without mean stress correction becomes considerable at intermediate lives and very significant at long lives, differing as much as a factor of 6, with Smith-Watson-Topper method accounting for the mean stress more than Morrow method does, particularly at long lives. The direction of changes in the predicted lives with the mean stress correction is consistent with the tensile bias of the transmission history, the compressive bias of the suspension history, and the slight compressive bias of the bracket history.

5.8 Discussion

Reasonable life predictions are obtained from calculations based on load-life data from notched components. Despite its simplicity and its inability to account for mean stress effects, the reasonable success of this method is due to the fact that the load-life data is obtained from tests where the actual component itself is being tested. However, the same reason makes this approach prohibitively expensive, because for every design change, material or geometry, the new component must be fabricated and tested.

Reasonable life predictions may also be obtained from Nominal Stress methods. However the main point to remember is that the

derivation of notched specimen S/N curve from the smooth specimen S/N curve is quite arbitrary. The choice of the cross-over life and the life at which the reduction in fatigue strength of the notched specimen is in proportion to the theoretical stress concentration factor heavily depends on the material and the geometry of the specimen.

The local strain approach avoids the drawbacks of load-life and nominal stress methods. For a given set of material properties, life estimates may be made for any number of different component geometries or load histories. This is a major advantage for components still in the design stage or components which cannot conveniently be tested. The needed material properties may be obtained by testing small laboratory specimens, and such information is increasingly more available through the published literature.

The three major categories where the local strain approaches differ are examined and assessed in detail in this chapter, and relevant discussion is included where necessary. In this section, some general comments are made which are drawn from the analysis presented in this chapter.

The question of how to link the applied load to the local strain seems a relatively unimportant one for the components used in the tests conducted by SAE. Neuber's rule appears to overestimate the local strain compared to the value obtained from the load-strain calibration curve. As a result, Neuber's rule predicts more conservative lives than the predictions based on the load-strain curve, with the difference worse at short lives, about a factor of 2, still relatively

small in terms of fatigue lives. The choice of notch root analysis depends on the form of data available. If a load-strain curve obtained from a finite element analysis or experimental strain measurements is available, then this approach has the advantage of eliminating the need for an estimation of the fatigue notch factor. If the load-strain curve is not available, then Neuber's rule will suffice. If both are available, then two sets of calculations will increase confidence in the predictions. However, additional information is needed before the conclusion, that "Neuber's rule overestimates the local strain", is extended to other materials and geometries with complete confidence.

The question of how to link the local stress and strain, once they are calculated, to the life is found to be a very important one, far outweighing the other questions. If a set of material properties is consistent, i.e. two of them can be expressed in terms of the other four, then all the 6 methods will give exactly the same life predictions, as the predictions using the 'new' set of material properties show. If, however, the set of material properties is not consistent, then all the methods will predict different lives, the difference between the lives becoming as high as a factor of 60 at long lives, as the calculations using the 'old' set of material properties demonstrate.

An important finding of this investigation is that Method 1, which calculates the life directly from the strain-life curve for a given local strain, must be preferred to the other methods. Whereas this conclusion seems so obvious and trivial, the reason for the

existence and popular use of other methods might be historical. When the concepts of local stress-strain fatigue analysis was introduced in the early 1970s, computers were not as widely available as today, and the 'execution time' and the cost of running a computer program might have been important considerations. The strain-life relationship is a nonlinear equation, solving such a relation for reciprocal life at a given strain level requires the use of an iterative method, for example Newton-Raphson method. Each iteration for this particular relationship requires four time-consuming exponentiation operations, and the solution of reciprocal life at a given strain level needs at least 2-3 or more iterations depending on the error tolerance and the initial estimate. Methods 2, 3, 5 and 6 calculate reciprocal lives without resort to an iterative methods, with one exponentiation operation. Considering the length of load histories, the longest 6000 reversals, with methods not requiring an iterative solution, savings in the execution time are quite considerable. However this is achieved at the expense of accuracy, as this study shows. This study highlights the dangers of manipulating or extending the relationships beyond their originally intended purpose, without verifying the assumptions made.

If the proposed procedure of determining the material properties is adopted, i.e. assuming that there are only 4 independent properties, these properties are determined by simultaneous curve fittings to stress-strain, strain-life data, and if a satisfactory set of material properties which explains both curves equally well can be found, then the assumptions made in deriving Methods 2 to 6 are verified, and any one of the methods may be employed, since they all give the same result.

The sensitivity analysis of Method 1 to variations in the material properties indicate that life predictions are relatively insensitive to variations in cyclic properties at short lives. At short and intermediate lives, life calculations are influenced most by changes in the fatigue ductility exponent, c, and the fatigue notch factor, K_f. At long lives life predictions become very sensitive to variations in the fatigue strength properties, σ_f' and b, and K_f. Life predictions are relatively insensitive to changes in the fatigue ductility coefficient, ε_f', and the cyclic stress-strain properties, K' and n', compared to the other properties at all lives.

The question of how to account for the mean stress effects is left unanswered. The <u>effect</u> of mean stress on life prediction using two different correction rules is illustrated, but the question of 'how' is left to the user. Both mean stress correction rules suggest that the effect of mean stress on the predicted lives depends on the bias of the particular load history, tensile or compressive, and the fatigue strength coefficient, σ_f'. However, the sensitivity analysis shows that little or no effect of mean stress is expected at short lives, up to the transition life of the material, regardless of the bias of the load history. At long lives, the effect of mean stress is expected to be incisive, predicting shorter lives for a tensile history and longer lives for a compressive history than the lives predicted without the mean stress correction for the same history. Actual predictions using the two rules for correction confirm the observations made from the sensitivity analysis, with Smith-Watson-Topper rule heightening the effect of mean stress somewhat more than Morrow rule.

Unfortunately there are only a few experimental results at long lives in the SAE test programme, which makes any pragmatic comparison very difficult. Additional information, in the form of more experimental results, is needed before passing any judgement on the effectiveness of the two mean stress correction rules. However, even if this information is forthcoming, reaching a conclusion with complete confidence may prove to be difficult, particularly for random load histories.

As the two correction rules themselves suggest, the effect of mean stress, if any, for any load history becomes noticeable, observable at long lives. This is also the region of life where the largest scatter in the experimental lives is expected. Where an order of magnitude scatter in life is not unusual, it would indeed be a very difficult task to differentiate and isolate the effect of mean stress from the scatter. As the sensitivity analysis illustrates, this is also the region of life where the fatigue life estimation methods are most susceptible to variations in the material properties, mainly the fatigue strength properties, σ_f' and b, and the fatigue notch factor, K_f. Another difficulty in assessing the effect of mean stress is related to the ambiguity of defining a 'crack length' at which the initiation process stops, the crack propagation, fracture mechanics takes over. Whether an observed phenomenon, for example a reduction in life due to mean tensile stresses, happened in the initiation period or in the propagation period would heavily depend on the choice of crack length, and is open to interpretation.

There are many other aspects of fatigue life calculation left out in this study, some of them are thought to be not so important, and some are beyond the scope of this investigation. An example of the first category is the transient cyclic stress-strain behaviour of a material, namely work hardening or softening. The whole concept of fatigue life calculations using a local strain approach is based on the assumption that the transient behaviour that the material undergoes will have run its course early in the life of a component, and the stable stresses and strains will prevail during most of the fatigue life. Besides, by taking a measurement of an hysteresis loop at approximately half-life of a specimen in determining the cyclic properties, the effect of transient behaviour on the fatigue life is already reflected in the fatigue data to some extent. If the effect of transient behaviour is known to be important, additional material information is needed to account for the effect. Additional information is also needed to account for the effect of environment on fatigue life, or the effect of any special cases, for example periodic overstraining. However extra care should be taken in incorporating any additional information into the fatigue damage analysis. Any modification to basic fatigue relationships and the assumptions made must be verified.

The second category of subjects that are left out covers a much larger area. Obviously, the total fatigue life covers the period starting from the existence of a detectable crack to the final fracture, which is the subject area of fracture mechanics. A similar study may be carried out for the crack propagation period. Existing

models for the crack growth may be examined systematically and tested numerically in an effort to sort out as to importance and relevance of various alternatives, to verify the assumptions made in deriving them, and to see the sensitivity of crack growth predictions to the variations in the model parameters.

Although this has nothing to do with the fatigue life calculation methods as such, a careful assessment of the load spectrum is as important to calculate fatigue life as any other points discussed in this chapter, if not more. Predicting the expected loads is a very crucial factor in fatigue life estimations, whether for crack initiation or crack propagation. This is particularly true for service histories where 5% of the total history seems to be doing 90% of the total damage, calculated by the crack initiation methods, like suspension and transmission histories in the SAE programme. Where omission or addition of a few large load cycles changes the whole complexion, the damage content of the history; measuring and predicting the service history becomes very important. Statistical methods and/or frequency domain techniques may be appropriate to evaluate service load records.

5.9 Conclusion

The load-life method gives good predictions, but relies on component data which may be expensive to obtain. Nominal stress methods may give good results depending on the choice of deriving notched specimen S/N curve from the smooth specimen data, a priori knowledge about the material and geometry is necessary. The local strain

approach offers an attractive solution for any number of component geometries or load histories using only smooth specimen data.

All the local strain methods differing only in the way in which the local stress and strain is related to the life will predict exactly the same life, if the set of 6 material properties is 'consistent'. If not, the difference between the predictions by the methods may be much more than an order of magnitude at long lives, depending on the level of inconsistency. This is due to invalidation of the assumptions which the methods are based on when the set is not consistent. The methods, then, not only differ in their absolute predictions, they also differ in their response to variations in material properties. The methods which use elastic or plastic strain only, or, the ratio or the product of elastic and plastic strain behave against expectations in their response to material variations. Method 1 should be used in this case.

Life predictions using Method 1 are sensitive to variations mainly in K_f and c at short lives, and σ_f', b and K_f at long lives. At intermediate lives σ_f', b, c, and K_f have roughly equal effect on the life predictions. Predictions are relatively insensitive to variation in ε_f', K' and n', implying that these parameters may be determined within wider confidence limits. Starting from this point, a new procedure of determining the material properties is proposed. If both stress-strain and strain-life curves can be fit to experimental results with only 4 independent parameters, namely, σ_f', b, ε_f' and c, then the assumptions which some life predictions are based on are validated.

The effect of mean stress is expected to be incisive at long lives. Both mean stress correction rules are consistent with the inference of the sensitivity analysis and with the bias of load histories. However, a conclusion regarding the effectiveness of these rules is not reached due to lack of experimental data at long lives.

REFERENCES FOR CHAPTER 5

1. Bussa, S. L., Tucker, L. E. "The SAE Cumulative Fatigue Damage Test Program", SAE Paper 750038.

2. Nelson, D. V., Fuchs, H. O. "Predictions of Cumulative Fatigue Damage Using Condensed Load Histories", SAE Paper 750045.

3. Landgraf, R. W., Richards, F. D., LaPointe, N. R., "Fatigue Life Predictions for a Notched Member Under Complex Load Histories", SAE Paper 750040.

4. "Fatigue Under Complex Loading: Analyses and Experiments" Editor: Wetzel, R. M., SAE publication 1977.

5. Dowling, N. E., Brose, W. R., Wilson, W. K., "Notched Member Fatigue Life Predictions by the Local Strain Approach", paper presented at SAE Automative Engineering Congress and Exposition, Detroit, Feb. 1975; also included in Ref.[4].

6. Landgraf, R. W., "Cumulative Fatigue Damage Under Complex Strain Histories", ASTM STP 519, 1973, pp. 212-227.

7. Smith, K. N., Watson, P., Topper, T. H., "A Stress-Strain Function for the Fatigue of Metals", Journal of Materials, JMLSA, Vol. 5, No. 4, Dec. 1970, pp. 767-778.

8. Kemp, S. D., "The Development and Use of a Materials Databank as an Aid to Product Development", proceedings of an International Conference held at the City University, London, 28-30 March 1983.

9. Morrow, J., "Fatigue Properties of Metals", Fatigue Design Handbook, SAE, 1968.

CHAPTER 6

CONCLUSION

AND

SOME SUGGESTIONS FOR FUTURE RESEARCH

The increasing use of computers in fatigue testing and analysis has led to considerable improvements especially for variable amplitude situations. Fatigue life estimation methods for the crack initiation and crack propagation stages, by the local strain approach and fracture mechanics, respectively, have been developed to a high degree of sophistication as a result of inexpensive but powerful computer systems enabling life predictions on a cycle-by-cycle basis, for a wide range of materials, components and service histories. However, there is no unique method or universally accepted procedure for predicting fatigue performance, each of these approaches exists in several modifications. A need therefore exists for a critical and numerical analysis of life prediction methods. In this study, the various stages in the methods to calculate crack initiation life are examined systematically.

Most contemporary fatigue life predictions consist of three steps, (i) reducing the service history into discrete cycles, (ii) associating a finite amount of damage with each cycle, (iii) and summing the damage cumulatively for each cycle counted. The three recent cycle counting techniques are described in detail in Chapter 2. Although they differ in algorithm, for a given block of load history, if the block starts and ends at an extreme point, then they all give an

identical cycle count. The third version, the pattern classification procedure, of the rainflow method is found to be simple to understand and easy to computerize requiring only one or two comparisons for each point of the load history. The rainflow method extract cycles in a manner which is consistent with the stress-strain behaviour of materials, therefore is best suited for the use of calculating the crack initiation life in conjunction with the local strain approach. If, however, the purpose of cycle counting is other than calculating the crack initiation life, the rainflow method may not be the best choice. For example, in crack propagation models, fatigue cracks are assumed to grow only under tensile loading, therefore either the load history has to be modified or the rainflow method.

Another area where the rainflow method is in obvious error is the service history re-generation and simulation. The rainflow method identifies the largest cycle, defined by the maximum peak and the minimum trough, and treats the others as interruptions. If a rainflow-counted peak-trough or range-mean matrix is used to simulate a load history, then at one point in the history the largest range will be generated which may never happen in a real service history. Other cycle counting methods, for example ordinary range-mean counting or frequency domain methods, may be more appropriate for data reduction and history reconstruction.

The frequency domain analysis of signals is well established in other fields of engineering. Given a set of dynamic input forces, a Finite Element program will predict power spectral density plots at any

point on a component or structure. In Chapter 3, a link is presented between the life estimation based on rainflow-counted ranges and the power spectral density of a stationary and ergodic random process. A procedure is outlined to determine the probability density functions of rainflow-ranges from a power spectral density function. Once the density of rain-flow ranges is determined, life predictions are not restricted to a straight line S/N data only; S/N data may take any form.

An obvious application area of such an approach is the life prediction of an offshore platform, where it is impractical to test the full-scale structure in the laboratory, also where the sheer number of cycles that the structure is expected to survive makes the use of a cycle-by-cycle counting almost an impossibility. If the various sea states can be approximated as stationary processes, and if the power spectral density at critical locations can be determined, then a life prediction based on rainflow ranges can be made for such structures.

Although the correlation between the probability densities obtained from the simulation results and the predicted densities by the proposed model is poor at short ranges, the correlation is quite good at intermediate to high ranges. This is partly intentional, because the contribution of short ranges to the overall fatigue damage is negligible, and the error term chosen in this study is geared towards fitting the model parameters for the intermediate and high ranges. Obviously, the way the model parameters are determined may be improved, if necessary the model itself may be modified to fit the simulation

results at all values of ranges. However, the presented model, as it stands, is capable of predicting the moments of rainflow-ranges quite accurately for a wide range of irregularity factors and moment power terms. In other words, life predictions can be made for any given S/N curve and power spectral density, provided the loading is a stationary Gaussian process.

From a parallel study, a model for the probability density functions of the ordinary ranges is also presented. Although no immediate application of this model is envisaged, it is hoped that it may be used in other fields of engineering, for example in characterizing surfaces in the manufacturing technology.

The second step in fatigue life predictions, i.e. the step of associating a finite amount of damage with each cycle counted, is examined in detail in Chapters 4 and 5. Various local strain methods of predicting fatigue crack initiation life available in the literature are analysed and classified systematically. The local strain methods differ from each other broadly in three areas, (i) how the local stress and strain are determined for a given load level, (ii) how the local stress and strain are linked to the smooth specimen strain-life data, (iii) and how the mean stress effect is accounted for.

Predictions made by these methods are compared with the published test data; however predictions are compared mostly within themselves in order to establish the differences between methods. A sensitivity analysis is carried out to examine how sensitive various

methods are to changes in the material properties. Results indicate that although accurate determination of the load-strain relationship is very important, life calculations are relatively insensitive to the way in which the relationship is determined, i.e. whether the load-strain relationship is obtained from Neuber's rule with a fatigue notch factor or from a finite element analysis.

The most significant difference in life predictions is observed for the methods differing only in the way in which the local stress and strain is linked to the life. If the cyclic stress-strain properties of the material calculated from the experimental results are different from the values estimated from the material strain-life properties, i.e., the set of material properties is not consistent, then the difference between the predictions made by these methods may be much more than an order of magnitude. A factor of 60 difference between the predictions is observed at long lives.

The difference between the life calculations made by the methods which use the same set of material properties is due to invalidation of the assumptions on which the methods are based when the set is not consistent. A new procedure of determining the material properties which will produce a consistent set is proposed. Considering that the life predictions are relatively insensitive to the cyclic stress-strain properties, if both stress-strain and strain-life curves can be fitted to experimental results using only the cyclic fatigue properties, then the assumptions on which some life prediction methods are based are validated, and any one of them can then be used.

However, if the consistency cannot be achieved, then the base line method which uses the basic relationships without any further assumptions should be employed for life predictions.

A natural extension of the work presented in this thesis is to the life predictions for the crack propagation stage. This study demonstrates the need for a critical and numerical re-analysis of existing crack growth models. A similar comparative study is needed to sort out the importance and relevance of various models which are available in establishing a specific procedure to calculate the crack propagation life, and the sensitivity of calculations to crack growth model parameters.